

DIFFERENTIAL VERY-LONG-BASELINE INTERFEROMETRY TECHNIQUES
FOR PRECISE ORBIT DETERMINATION
OF A GEOSYNCHRONOUS SATELLITE

BY

TADASHI SHIOMI

MAY 1986

KASHIMA SPACE RESEARCH CENTER
RADIO RESEARCH LABORATORY
IBARAKI, JAPAN

DIFFERENTIAL VERY-LONG-BASELINE INTERFEROMETRY TECHNIQUES
FOR PRECISE ORBIT DETERMINATION
OF A GEOSYNCHRONOUS SATELLITE

BY

TADASHI SHIOMI

MAY 1986

KASHIMA SPACE RESEARCH CENTER
RADIO RESEARCH LABORATORY
IBARAKI, JAPAN

DOC
1986
13
電気系

ABSTRACT

A method of differential very-long-baseline interferometry (DVLBI) for a precise orbit determination of a geosynchronous satellite is analyzed and proved by experiments. Taking advantages of a very-long-baseline interferometry (VLBI) as a passive and precise observation system, we successfully applied it to tracking a geosynchronous satellite aiming at highly accurate orbit determination. The effective exclusion of systematic observation errors became possible by a differential method using quasars as reference radio sources.

A DVLBI experiment with inter-continental baselines successfully achieved a satellite position accuracy of a few meters, which is higher than that obtained by conventional radio tracking methods by more than 1-order.

Covariance analyses show that a DVLBI applied to satellite signals with wide bandwidth in dual frequencies can perform a position accuracy of better than 1 m for a geosynchronous satellite.

The DVLBI techniques are useful not only for tracking spacecrafts in various orbits, but also for developing differential observation systems for navigation, geodesy and radio monitoring.

ACKNOWLEDGEMENT

I am greatly indebted to my thesis supervisor, Prof. Iwane Kimura for his constant guidance and advice to the work.

Many people have been sources of encouragement and helpful technical discussions. Among them are Dr. Nobuyuki Kawano and the staff of Radio Astronomy Applications Section (VLBI research and development group), Radio Research Laboratory. Dr. Nobuyuki Kawano has been constantly encouraging me with valuable advice and suggestions. The VLBI group supported me in the experiments and in the development of the data reduction software.

I am especially grateful to the staff of Satellite Control Section, RRL, where I worked for many years, for supporting me in every phase of the work with valuable discussion and reliable operations in the experiments.

The experiments reported here would not have been possible without the support and cooperation not only of many sections of RRL but also of Jet Propulsion Laboratory, California Institute of Technology. Special thanks are due to Dr. G.M. Resch, Dr. F.F. Donovan and Dr. J.S. Border, who originally suggested the RRL-JPL joint experiment. I wish to thank

Dr.J.S.Border for his close cooperation in the data analysis of the joint experiment while I stayed at JPL.

I extend my thanks and appreciation especially to Dr. Noboru Wakai, Director General and Mr. Ken-Ichi Tsukamoto, Director of Planning and Technical Consulting Division, both of RRL, for supporting and encouraging me throughout the work.

CONTENTS

Chap. 1	Introduction.....	1
	References.....	8
Chap. 2	Accuracy of Orbit Determination and Information Contents of Tracking Data.....	10
2.1	Orbit Determination.....	10
2.1.1	Orbital Motion of Spacecraft.....	10
2.1.2	Spacecraft Orbital Measurements.....	16
2.1.3	Orbit Determination.....	23
2.2	Accuracy of Orbit Determination.....	29
2.2.1	Covariance Analysis and Simulations.....	29
2.2.2	Bias Errors and Model Parameter Errors.....	34
2.2.3	Evaluation of Observation Residuals.....	37
2.3	Sensitivity and Information Contents of Observations.....	39
2.3.1	Sensitivity and Observability.....	39
2.3.2	Information Contents of Observations.....	45
	References.....	50
Chap. 3	VLBI Methods for Tracking Geosynchronous Satellites.....	53
3.1	Introduction to VLBI.....	53
3.1.1	General Concept and Brief History of VLBI.....	53
3.1.2	Applications of VLBI for Tracking Spacecraft ..	56
3.2	VLBI Data Processing.....	59
3.2.1	Signal Analysis of VLBI.....	59
3.2.2	Derivation of VLBI Observables.....	66

3.3	Tracking a Geosynchronous Satellite by DVLBI Method.....	80
3.3.1	Principle of DVLBI Method.....	80
3.3.2	Sensitivity of DVLBI Observable.....	82
3.3.3	DVLBI as Tracking Method for Geosynchronous Satellite.....	87
3.4	Errors in DVLBI Delay Observable.....	94
3.4.1	VLBI Hardware System Errors.....	94
3.4.2	Propagation Media Errors.....	96
3.4.3	Geometric Errors.....	101
	References.....	106
Chap. 4	CS Tracking Experiment by DVLBI and Range and Angle Measurements.....	110
4.1	Introduction.....	110
4.2	System of Experiment.....	113
4.2.1	Range and Angle Measurement System.....	113
4.2.2	K-II VLBI System.....	116
4.2.3	Observation Strategy.....	119
4.3	Sensitivity and Accuracy of Observables.....	124
4.3.1	Sensitivity of Range, Azimuth Angle and DVLBI Observables.....	124
4.3.2	Accuracy of Range, Azimuth Angle and DVLBI Observables.....	132
4.4	DVLBI Data Processing.....	141
4.4.1	Method and Results of Delay Estimation.....	141
4.4.2	Estimation of System Delay.....	149

4.5	Orbit Determination and Accuracy Analysis.....	152
4.5.1	Orbit Determination.....	152
4.5.2	Accuracy Analysis.....	155
4.6	Conclusion.....	161
	References.....	163
Chap. 5	RRL-JPL DVLBI Experiment to Track a Geosynchronous Satellite.....	165
5.1	Introduction.....	165
5.2	System of Experiment.....	166
5.2.1	Earth Stations and VLBI System.....	166
5.2.2	Geosynchronous Satellite and Its Signal.....	171
5.2.3	Quasars and Observation Window.....	174
5.3	Observation Strategy.....	174
5.3.1	Sensitivity of Delay Observables.....	174
5.3.2	Observation Model and Errors.....	179
5.3.3	Observation Schedule.....	184
5.4	Data Processing.....	188
5.4.1	Derivation of Delay and Delay Rate Observables.....	188
5.4.2	Pre-Processing of Raw VLBI Observables.....	193
5.5	Orbit Determination.....	213
5.5.1	Satellite Dynamic Model.....	213
5.5.2	Precise Orbit Determination with DVLBI Delay Observables.....	216
5.6	Conclusion.....	227
	References.....	228

Chap. 6	Applications.....	229
6.1	Tracking of Satellites in Various Orbits.....	229
6.2	Differential Tracking Methods with Navigation Satellite System.....	232
6.3	Radio Monitoring by Interferometric Methods.....	238
	References.....	243
Chap. 7	Conclusion.....	245
Appendix A	Development of Precise Orbit Determination Program for DVLBI (DVODP).....	249
Appendix B	Reweighting the Observables.....	253
Appendix C	Alternative Estimation of Large Dimensional Parameters.....	255
Appendix D	Sensitivity of DVLBI Delay Observable to Keplerian Orbital Elements of a Geosynchronous Satellite.....	261
Appendix E	Nondynamic Analysis of the Position Estimation Accuracy of a Geosynchronous Satellite.....	264

CHAPTER 1 INTRODUCTION

Over thousands of spacecrafts are orbiting in not only near earth but also in geosynchronous orbits these days⁽¹⁾⁽²⁾. In order to accomplish each spacecraft mission, one of the most fundamental requirements is to determine the spacecraft orbit with sufficient accuracy using various tracking (or orbital measurement) methods. The requirement on the accuracy is getting higher and higher as human activities and mission goals in space become more and more complexed and sophisticated. From a practical viewpoint, other requirements are growing to reduce the cost and burden of tracking operations at earth stations by, for example, attaining sufficient tracking data in short observation spans.

Satellites especially in the geosynchronous orbit have been and will be also used as crucial components of space systems, for example, for navigations of other spacecrafts or mobile stations on the earth's surface and for space VLBI (Very-Long-Baseline Interferometry)⁽³⁾ where a satellite itself becomes an observation platform of the VLBI. In those systems, satellites positions are required to be determined very precisely. For example, the Tracking and Data Relay Satellite System (TDRSS)⁽⁴⁾⁽⁵⁾ of the USA uses two geosynchronous satellites, approximately 130 degrees apart in longitude, and

track low orbit satellites around the earth and to relay telecommunication data between such satellites and a mission control station on the earth. In this system it is essentially important to determine the TDRS's position as accurate as possible, as if it is an earth station with the height of the geosynchronous orbit to support some kind of earth observation satellites. For example, the satellite for the Ocean Topography Experiment (TOPEX)⁽⁶⁾, which may be tracked by the TDRS, should be determined with an altitude accuracy of less than 10 cm. This means that the TDRS orbital position should be determined with an accuracy of about less than a few meters to satisfy the requirement. Satellite systems which use geosynchronous satellites for navigations of airplanes, ships and small mobile stations on the ground also require the accuracy of meter-order in the position of the satellites.

One of the most widely used tracking methods for geosynchronous satellites is a ranging method which measures the distance between a tracking station and a satellite by a propagation time of ranging tones or pseudo-noise PCM codes which modulate a carrier transmitted from the tracking station and retransmitted from the satellite. Usually more than two, distantly located tracking stations are required, in which each station should have up-link capability (or active-radio capability in the sense that signal transmissions from the earth stations are necessary) and calibration facility. The

resolution of less than a meter in range measurements has been attained, but it is not easy to obtain absolute range observables with that accuracy because of various errors due to propagation media effects and equipment delays both at the earth stations and on the satellite. Actually, the most highly attained accuracy of the position of a geosynchronous satellite is about several tens of meters so far⁽⁷⁾.

Furthermore, in such "active" methods, the operations at earth stations should be coordinated so that the transmitting signals do not make any conflicts on the satellite nor any interferences to other space telecommunication links.

On the other hand, from the viewpoint of the effective usages of radio frequencies and satellite orbits in space, it is internationally requested⁽⁸⁾ to monitor space radio stations which uses various radio waves under the more and more crowded radio environment in space. In the monitoring of space radio stations, it is fundamentally recommended that a monitoring station has a capability to track any space radio station (that is, spacecraft) and identify it by "passive" methods (or receive-only methods). Because, the monitoring should be carried out independently to the operations of spacecrafts and it is not welcomed to transmit other, especially strong, radio waves, such as radar signals, for the purpose.

We can use antennas which have narrow beams to detect the incident angles of the radio waves from spacecrafts⁽⁹⁾, but we

cannot always expect high accuracies of the observations because of the limitations of antenna beam, insufficient signal strength and propagation media effects. Sometimes optical observation methods can be used⁽¹⁰⁾, but they are easily affected by weather conditions and the observations are limited to the period when the reflected light is detectable against the background optical brightness of the sky.

We study on and develop "passive" tracking methods which only receive signals from spacecrafts or, more generally, radio sources and attain required effective observables with respect to the orbits or the positions and velocities of the radio sources. We especially notice a modern interferometric method, very-long-baseline interferometry (VLBI), whose techniques have recently been developed drastically and its high capabilities have been proved in astrometry, astronomy and geodesy⁽¹¹⁾⁽¹²⁾. Some of those VLBI techniques have also been applied in the deep space navigation fields especially by groups in JPL⁽¹³⁾.

VLBI has many advantages if it is successfully used for tracking geosynchronous satellites. Because the VLBI is a passive method which needs no uplink capabilities and it can observe any kind of radio wave (even noise emissions from an on-board transponder) transmitted or emitted from a spacecraft. By using highly stable atomic frequency standards at observation stations, the observed signal can be integrated for about 10 minutes to lead to a high signal-to-noise ratio,

which means that we can obtain highly precise VLBI observables, for example, a delay observable with an accuracy of several centi-meters even when the radio wave is fairly weak. On the other hand, the data reduction processes are complexed and time-consuming so far. In addition to it, the VLBI observables usually contain various systematic errors because of system noises, propagation media effects, system equipment delays and clock errors.

A differential VLBI (DVLBI) technique⁽¹⁴⁾ can remove common bias errors in adjacent VLBI observations between a spacecraft and a natural radio sources (usually we use extra-galactic radio sources with precisely known angular position). It means that VLBI becomes a self-calibrated tracking system by a differential technique. It would be ideal to use reference radio sources which are seen very nearly to the objective satellites and to use long orthogonal baseline vectors. In actual situations, however, those conditions are not always satisfied nor the angular positions of such reference radio sources are error-free. Therefore, it is important to optimize tracking geometry, quasar selection, and observation schedule, or sometimes to combine different types of tracking methods under a given actual condition.

The purposes of our study are twofold; one is to theoretically develop a new interferometric technique, DVLBI, which can be used to track a satellite in the geosynchronous

orbit to determine the orbit very precisely as well as to analyze errors and observabilities for various tracking strategies. The other is to experimentally prove the above technique and discuss applications of them to orbit determination of satellites in other orbits and to differential measurement systems for geodesy and radio monitoring systems from both the earth and space.

In Chap. 2 we review orbit calculation and determination systems, then analyze the relation between observations and orbit determination accuracy. Though this is one of old subjects in navigation technology it is useful to review the problem to develop the VLBI techniques. Particularly, we develop a concept of information contents of tracking data⁽¹⁵⁾. It is effectively used to evaluate the usefulness of various tracking methods and to optimize them.

In Chap. 3 we analyze the VLBI and DVLBI methods applied to navigations on geosynchronous satellites in some detail.

Chap. 4 is devoted to description on our experiment⁽¹⁴⁾ where a real-time VLBI system was used to track a Japan's Experimental Communication Satellite (CS) by a DVLBI method. The obtained DVLBI observables were added to conventional range and angle data to lead an orbit determination with an accuracy of 200 m in terms of the satellite position.

In Chap. 5 we describe in detail the RRL-JPL joint experiment⁽¹⁶⁾⁽¹⁷⁾, where intercontinental baselines were used

to track a communication satellite (DSCS II, USA) located above the Pacific Ocean. In this experiment, we successfully proved the advantages of the DVLBI method by attaining an accuracy of a few meters in satellite position determination.

Chap. 6 is for applications of DVLBI methods not only to navigation of satellites in other orbits than the geosynchronous one, but also to passive radio monitoring in ground and space communication systems. Differential observation methods with navigation satellites are also discussed aiming at applications to navigation and geodesy.

Chap. 7 gives conclusion.

References

- (1) Reynolds, R. C., N. H. Fischer and E. E. Rice, Man-made debris in low earth orbit -- A threat to future space operations, J. Spacecraft, 20, 3, 1983, pp. 279-285.
- (2) Morgan, W. L., Geosynchronous satellite list: 1983, J. British Interplanet. Society, 36, 1983, pp. 377-382.
- (3) Wu, S. C., Error estimation for Δ VLBI angle and angle rate measurements over baselines between a ground station and a geosynchronous orbiter, TDA Progress Report 42-71, JPL, 1982.
- (4) Schneider, W. C. and A. A. Garman, Tracking and Data Relay Satellite System: NASA's new spacecraft data acquisition system, IAF-79-F-274, IAF'79, Sep. 1979.
- (5) Fang, B. T., Satellite-to-satellite tracking orbit determination, J. Guidance and Control, 2, 1, Jan-Feb. 1979.
- (6) Jet Propulsion Laboratory 1982 Annual Report, JPL, 1982.
- (7) Argentiero, P. and F. Loveless, Orbit determination with the Tracking Data Relay Satellite System, X-932-76-185, GSFC NASA, 1977.
- (8) WARC 1979 Final Acts, Article 20--International Monitoring, ITU, 1979.
- (9) Arimoto, Y., T. Shiomi, T. Nishigaki, S. Kawase and H. Murakami, Orbit control of a Communication Satellite based on one-station tracking, 13th International Symp. on Space

Technology and Science, Tokyo, 1982.

(10) King-Hele, D. G., The value of photographic observations in improving the accuracy of satellite orbits, J. British Interplanet. Society, 35, 1982, pp. 355-362.

(11) Whitney, A. R., Precision geodesy and astrometry via Very-Long-Baseline Interferometry, Doctoral Thesis, MIT, 1974.

(12) Ma, C., Very Long Baseline Interferometry applied to polar motion, relativity and geodesy, NASA Technical Memorandum 79582, 1978.

(13) Hidebrand, C. E., J. S. Border, F. F. Donovan, S. G. Finley, B. Moultrie and L. J. Skjerve, Progress in the application of VLBI to interplanetary navigation, Conference on VLBI Techniques, Toulouse, France, 1982.

(14) Shiomi, T., S. Kozono, Y. Arimoto, S. Nagai and M. Isogai, Precise orbit determination of a geosynchronous satellite by Δ VLBI method, J. Radio Res. Labs., 31, 133, 1984, pp. 111-132.

(15) Bucy, R. S. and P. D. Joseph, "Filtering for stochastic processes with applications to guidance", Interscience Publ., John Wiley & Sons, Inc., 1968.

(16) Shiomi, T., Analysis on Δ VLBI navigation on a geosynchronous spacecraft, JPL Engineering Memorandum 314-314, July 1984.

(17) Border, J. S. and F. F. Donovan, Jr., Geosynchronous orbiter tracking by VLBI: Demonstration design, AIAA/AAS Astrodynamics Conference, AIAA-84-2050, 1984.

CHAPTER 2 ACCURACY OF ORBIT DETERMINATION AND INFORMATION
 CONTENTS OF TRACKING DATA

2.1 Orbit Determination

2.1.1 Orbital Motion of Spacecraft

The equation of motion of a spacecraft may generally be written with an inertial coordinate system in the form

$$\ddot{\underline{r}} = \underline{f} (\underline{r}, \dot{\underline{r}}, t, \underline{p}_{sc}) \quad (2.1)$$

where

\underline{r} : spacecraft position vector from the central body

$\dot{\underline{r}}$: spacecraft velocity vector

$\ddot{\underline{r}}$: spacecraft acceleration vector

t : time variable

\underline{p}_{sc} : vector of dynamic parameters

A uniform time, such as the solar system barycentric dynamical time (TDB or ET, ephemeris time), is usually used as the time variable in ephemeris calculation not only of satellites but also of the moon and planets. In the case of a satellite orbiting around the earth, the right-hand side of Eq.(2.1) is written as

$$\begin{aligned} \underline{f} (\underline{r}, \dot{\underline{r}}, t, \underline{p}_{sc}) = & \underline{f}_g (\underline{r}, t, \underline{p}_g) + \underline{f}_b (\underline{r}, t, \underline{p}_b) \\ & + \underline{f}_d (\underline{r}, \dot{\underline{r}}, t, \underline{p}_d) + \underline{f}_r (\underline{r}, t, \underline{p}_r) \\ & + \underline{f}_T (t, \underline{p}_T) + \underline{f}_R (t, \underline{p}_R) \end{aligned} \quad (2.2)$$

where

\underline{f}_g : acceleration by the earth's gravitation
 including the nonspheric effects
 \underline{f}_b : acceleration by bodies including the sun
 and the moon
 \underline{f}_d : atmospheric drag effect
 \underline{f}_r : solar radiation pressure effect
 \underline{f}_T : acceleration by thrust of the spacecraft
 \underline{f}_R : random acceleration due to gas leaks from
 the reaction control systems of the spacecraft
 or to other unmodeled effects

$P_g, P_b, P_d, P_r, P_T, P_R$

: dynamic parameters pertaining to the above
 accelerations

There are also the effect of tidal variation of the earth's
 gravitational field, the earth's albedo effect, and
 gravitational effects by some other planets, on a satellite
 motion. But they are very small and negligible in almost all
 earth orbiting satellites including geosynchronous one which we
 have a major concern.

Earth's Gravitational Acceleration

In the case of a spacecraft orbiting around the earth, the
 first term in Eq.(2.2) has the major effect. It is usually
 written as

$$\underline{f}_g (\underline{r}, t, p_g) = \left(\frac{\partial U}{\partial \underline{r}} \right)^T \quad (2.3)$$

where U is the generalized potential function of the earth and is written as

$$U = \frac{\mu}{r} \left\{ 1 + \sum_{n=1}^{\infty} \sum_{m=0}^n \left(\frac{R_E}{r} \right)^n P_n^m (\sin \phi) \right. \\ \left. \times (C_{nm} \cos m\lambda + S_{nm} \sin m\lambda) \right\} \quad (2.4)$$

where

μ : gravitational constant of the earth

r, ϕ, λ : radius, latitude and longitude of spacecraft relative to the earth

R_E : mean equatorial radius of the earth

$P_n^m (\sin \phi)$: associated Legendre function of the first kind

C_{nm} and S_{nm} : tesseral harmonic coefficients

Usually the zonal harmonic coefficient J_n is defined as

$$J_n = - C_{n0} \quad (2.5)$$

which represents the potential characteristics that depend only on spacecraft latitude (ϕ). Since the harmonic coefficients C_{nm} and S_{nm} are caused by the nonspherocity of the earth, they become much smaller at the higher orders than the second (J_2 or C_{20}). In the case of a geosynchronous satellite, however, high order tesseral coefficients have significant effect due to

resonance effect of the satellite's synchronous motion to the earth's rotation.

Point-Mass Gravitational Acceleration by Bodies in the Solar System

The acceleration \underline{f}_b which is caused by bodies such as moon, sun and so on (which are treated as point masses) is written as

$$\underline{f}_b(\underline{r}, t, \underline{p}_b) = \sum_{k=1}^n \mu_k \left\{ \frac{\underline{r}_k - \underline{r}}{\|\underline{r}_k - \underline{r}\|^3} - \frac{\underline{r}_k}{\|\underline{r}_k\|^3} \right\} \quad (2.6)$$

where

k : number of bodies considered

μ_k : gravitational constant of the body k

\underline{r}_k : vector from the central body to the k -th body

The second term in the right hand side of Eq.(2.6) reflects the k -th body's gravity effect on the central body. In the case of a satellite around the earth, it is usually sufficient to include the effects of the moon and the sun.

Atmospheric Drag

The contribution of atmospheric drag to the acceleration of the satellite is generally given by

$$\underline{f}_d(\underline{r}, \dot{\underline{r}}, t, \underline{p}_d) = -\frac{C_{DA}}{2m} \rho \underline{V}_R \underline{V}_R \quad (2.7)$$

where

C_D : aerodynamic drag coefficient of the satellite

A : effective cross-sectional area of the
satellite

m : satellite mass

ρ : density of the atmosphere at the satellite
position

$$\underline{v}_R = \dot{\underline{r}} - \underline{\omega}_E \times \underline{r}$$

: relative velocity of the satellite to the
atmosphere rotating with the earth

$\underline{\omega}_E$: angular velocity vector of the earth

The effect of the atmospheric drag is significant in the case
of a near-earth satellite.

Solar Radiation Pressure

The solar radiation pressure acceleration \underline{f}_r is given as

$$\underline{f}_r(\underline{r}, t, \underline{p}_r) = \gamma P_s \frac{\tau A}{m} \underline{R}_s \quad (2.8)$$

where

γ : eclipse factor; $\gamma = 1$ in sunlight, $\gamma = 0$ in shadow

P_s : solar radiation pressure at the satellite
position

τ : reflectivity coefficient

A : reference area

\underline{R}_s : unit vector in the direction from the sun to the
satellite

The solar radiation pressure effect becomes more significant in the case of a satellite of which the orbit is higher and has larger area reflecting the sunlight. It is, however, not always easy to make a precise model of the solar radiation pressure. Because not only the attitude of a satellite with respect to the sunlight is not constant, but also the solar radiation pressure sometimes has components which are not parallel to \underline{R}_s due to a complexed structure of the satellite.

Acceleration by Spacecraft Thrust

The acceleration \underline{f}_T by thrust of a spacecraft should be included because a spacecraft usually has subsystems to control its orbit and attitude. The thrust produced by reaction control equipment (gas-jet thruster, ion engine, and so on) in occasions of orbit and attitude maneuvers is given using an impulsive or a continuous thrust model with parameters p_T .

Random Acceleration

The remaining acceleration \underline{f}_R represents random accelerations (or process noise) which are difficult to be described by deterministic models. Accelerations by gas leaks from a reaction control subsystem (which uses gas-jet thrusters) sometimes becomes significant in the case of a spacecraft which goes through deep space in a very long voyage⁽¹⁾.

When we actually calculate the spacecraft motion we should

evaluate each term in a given orbital condition in order to include every significant terms and to neglect meaningless terms. It is of course important to make accurate dynamic models pertaining to each terms and to evaluate the effects of the errors in those dynamic parameters.

Eq.(2.1) can be numerically integrated (special perturbation method⁽²⁾⁽³⁾) from an initial orbital condition of a spacecraft ($\underline{r}_0, \dot{\underline{r}}_0, t_0$), or it can also be solved analytically with a perturbative method (general perturbation method⁽⁴⁾⁽⁵⁾). Generally speaking, the numerical integration methods can easily include various perturbative accelerations which can be modeled, but they need large size of computer programs and much computing time. On the other hand, the general perturbation methods are fast in calculation time and effective in the case of spacecraft which do not require highly accurate orbital managements.

2.1.2 Spacecraft Orbital Measurements

The orbital motion of a spacecraft can be measured by various methods such as range measurements, range-rate measurements, viewing angle measurements, optical measurements, radar measurements, differential range (or VLBI) measurements and so on. All of those measurements supply geometrical information of a spacecraft position with respect to a specified station where the tracking equipment exists, or

supply information of the satellite's velocity vector. The observation equations are generally written in the form

$$\underline{z} (t) = \underline{g} (\underline{r}, \dot{\underline{r}}, t, \underline{p}_{\text{Obs}}) + \underline{n} \quad (2.9)$$

where

$\underline{z} (t)$: vector consisting of orbital measurement data or orbital observables at time t

\underline{g} : model of the observables

$\underline{p}_{\text{Obs}}$: model parameters of the observation system

\underline{n} : observation noise vector

It is generally desirable that observables $\underline{z} (t)$ have small errors and have high sensitivity to the orbital motion \underline{r} and $\dot{\underline{r}}$ of a spacecraft, and have small sensitivity to errors of model parameters $\underline{p}_{\text{Obs}}$.

Observables

Fig. 2.1 shows an example of geometry of tracking a spacecraft from two earth stations. Let us show definitions of some typical orbital observables.

A range observable ρ_i is defined as

$$\rho_i = \|\underline{\rho}_i\| = \|\underline{r} - \underline{r}_{\text{Si}}\| \quad (2.10)$$

where

$\underline{r}_{\text{Si}}$: position vector of an earth station i

$\underline{\rho}_i$: range vector

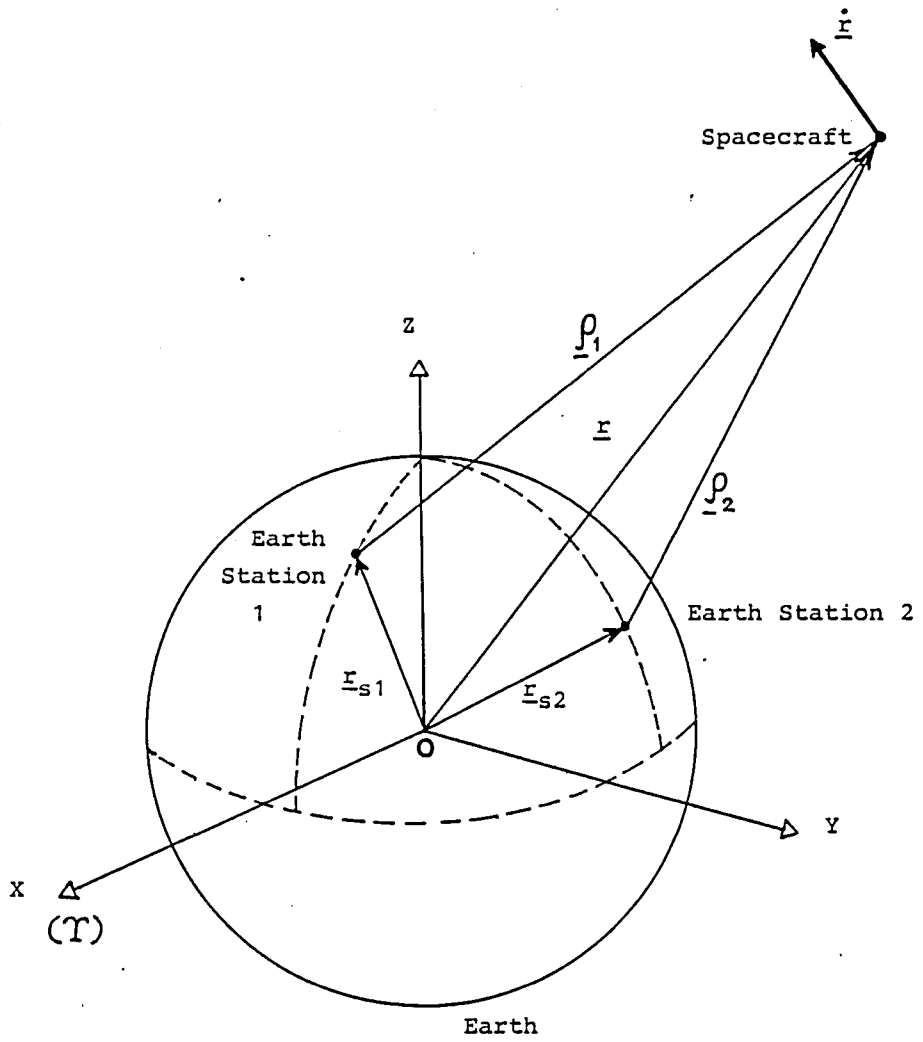


Fig.2.1 Geometry of spacecraft tracking from earth stations

A range rate observable $\dot{\rho}_i$ is defined as

$$\dot{\rho}_i = \frac{1}{\rho_i} \rho_i \cdot (\dot{\underline{r}} - \dot{\underline{r}}_{si}) \quad (2.11)$$

where

$\dot{\underline{r}}_{si}$: velocity vector of the earth station i

A differential range observable ρ_d is defined as

$$\rho_d = \rho_1 - \rho_2 \quad (2.12)$$

A summed range observable ρ_s is defined as

$$\rho_s = \rho_1 + \rho_2 \quad (2.13)$$

Inertial Coordinate System

In order to describe the motion of a satellite around the earth, it is common to use an inertial coordinate system of which the origin is the center of the earth. The x-axis is in the earth's equatorial plane and in the direction of the vernal equinox (Υ). The z-axis is aligned to the earth's spin axis and the y-axis is selected to make the right hand coordinate system.

However, the earth's equatorial plane and the spin axis is not fixed in the inertial space due to the precession and the nutation of the spin axis. Therefore, the mean or the true equatorial plane and spin axis at an epoch time are usually referred. The conversions between different coordinate systems are made using coordinate conversion matrices based on the models of the precession and the nutation of the earth⁽⁶⁾⁽⁷⁾.

Position of Earth Station

The position of an earth station is usually given using a reference ellipsoid of the earth. Fig. 2.2 shows a concept of station position description. The position of an earth station S is defined by, for example, (λ, ϕ, H) or (u, v, λ) , where

λ : geodetic longitude

ϕ : geodetic latitude

H : geodetic height

u : spin radius

v : height from the equatorial plane

In Fig. 2.2 the Z_E -axis which is the principal axis of the given reference ellipsoid does not always coincide with the actual spin axis of the earth. Because the latter moves irregularly around the Z_E -axis due to hydrodynamic effects of the surface and internal substance of the earth. This is called the polar motion. The polar motion is usually described by two angular parameters (x_p, y_p) (as shown in Fig. 2.3) which represent the deviation of the instant spin axis from the averaged axis obtained for the period from 1900 to 1906 (this averaged spin axis is called CIO: Conventional International Origin).

At an arbitrary time, the position of an earth station is given in the inertial coordinate system with the true equatorial plane at that time by using the geodetic station

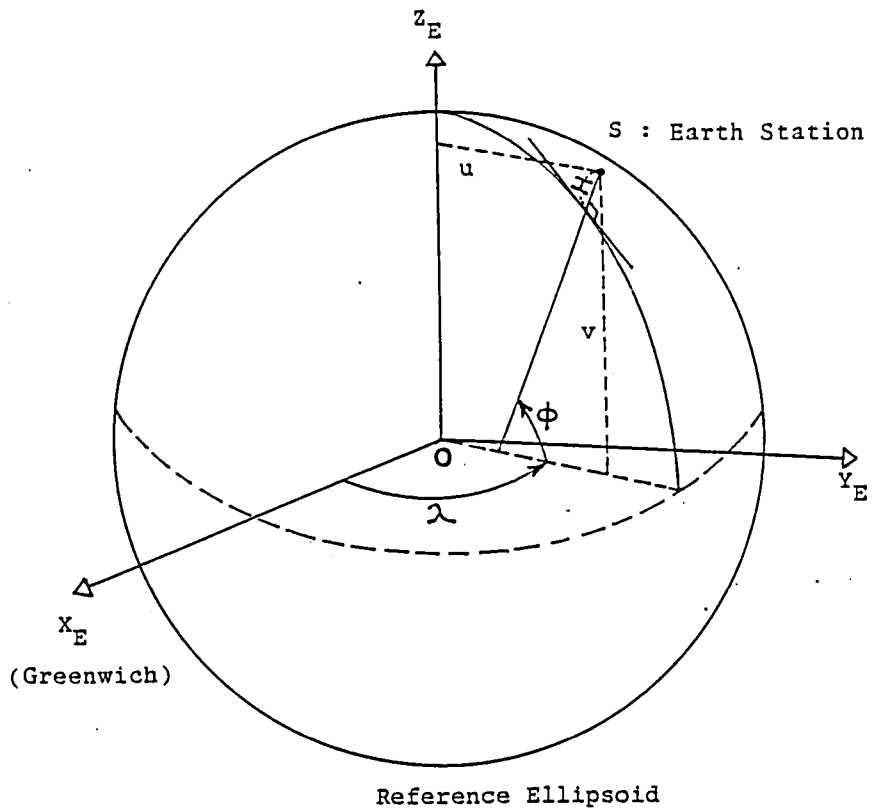
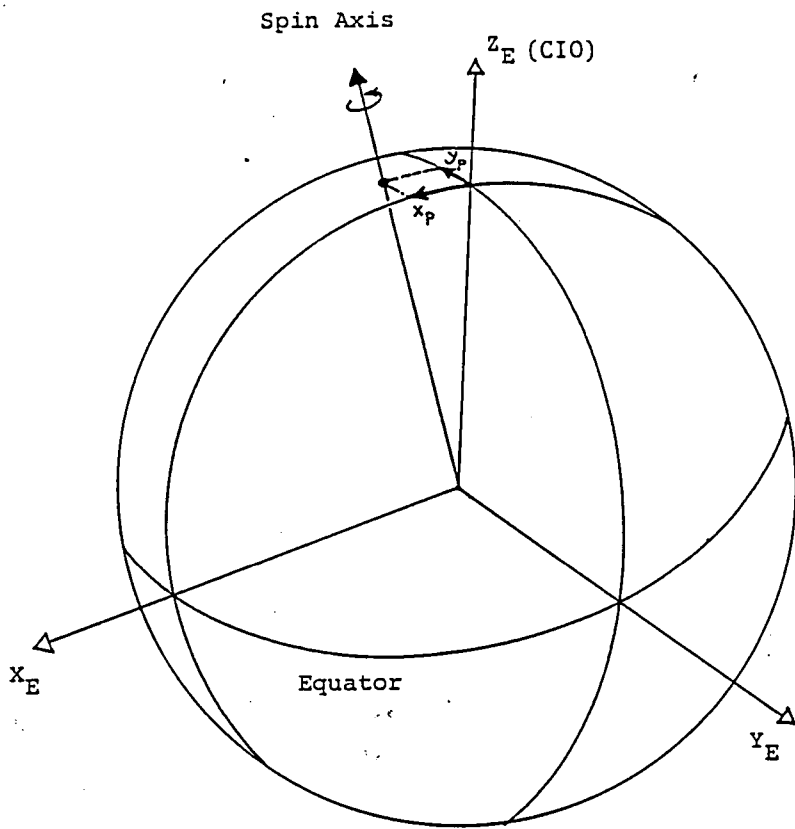


Fig.2.2 Station location description
 (X_E, Y_E, Z_E) : Coordinate system fixed to the earth



CIO: Conventional International Origin

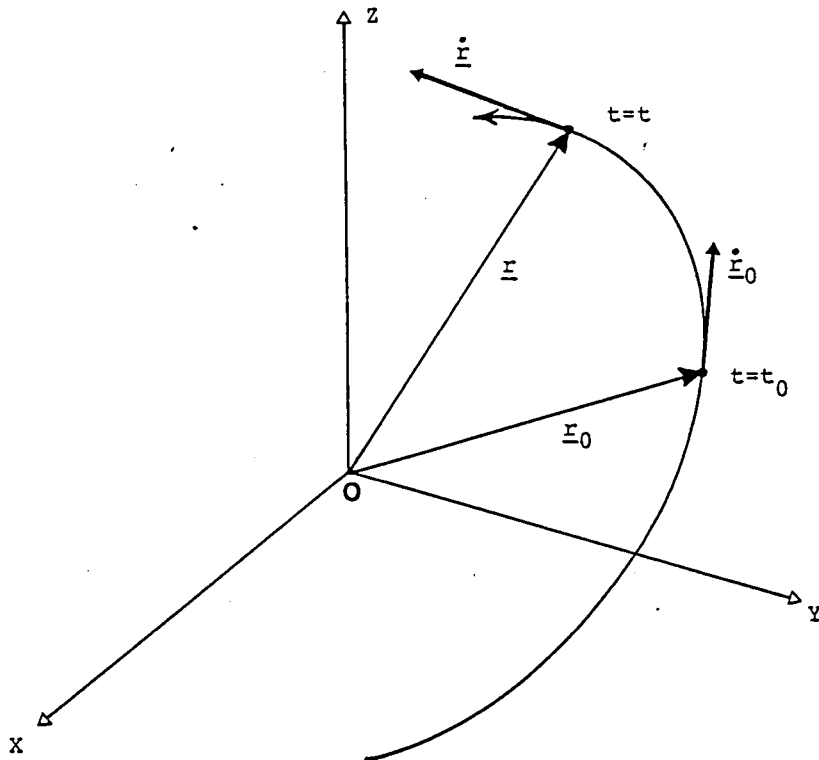
Fig.2.3 Polar motion

location data by considering the earth's spin (rotation) and the polar motion. However, since the angular velocity of the earth's spin is not constant we must use the universal time system UT1 instead of UTC which is a uniform time system and is used in our daily life. UT1 represents the actual rotation of the earth.

Consequently, in order to describe the position of an earth station in the inertial coordinate system, we convert the position vector from the earth-fixed (X_E, Y_E, Z_E) system using polar motion data and UT1 to the inertial system. If we need to convert a position vector from one inertial system to another one, we use coordinate conversion matrices based on the precession and nutation of the earth's spin axis between these epochs. The precession and nutation of the earth's spin axis are caused by the gravitational torque induced by the sun, the moon and the planets.

2.1.3 Orbit Determination

Suppose that model parameters p_{sc} in Eq.(2.1) and p_{obs} in Eq.(2.9) are given. The state vectors of the spacecraft \underline{r} and $\dot{\underline{r}}$ at an arbitrary time t are determined by Eq.(2.1) from initial state vectors \underline{r}_0 and $\dot{\underline{r}}_0$ at an epoch time t_0 (Fig.2.4). Then the observation vector $\underline{z}(t)$ is also given by Eq.(2.9) from \underline{r}_0 and $\dot{\underline{r}}_0$. It means that the \underline{r}_0 and $\dot{\underline{r}}_0$ can be obtained from



XYZ : Inertial coordinate system

Fig.2.4 Orbital motion of satellite

Eq.(2.9) when $\underline{z}(t)$ have independent components of which the dimension exceeds that of the state vectors. The orbit determination is a process in which spacecraft's state vectors \underline{r} and $\dot{\underline{r}}$ at a specified epoch time are estimated from observed data (tracking data) of the spacecraft's motion. It is usually the case that some of the model parameters of \underline{p}_{sc} and \underline{p}_{obs} are also simultaneously estimated in orbit determinations. It is at least theoretically possible to estimate such parameters from observed data which depend on them.

The most popular and fundamental method of orbit determination is the weighted least-square method⁽⁴⁾⁽⁵⁾. The state vector \underline{x}_0 at an epoch time t_0 are estimated as $\hat{\underline{x}}_0$ that minimizes a cost function $F(\underline{x}_0)$;

$$F(\underline{x}_0) = \sum_{i=1}^N \left\{ \underline{z}(t_i) - \underline{z}_c(t_i, \underline{x}_0, t_0) \right\}^T W_i \cdot \left\{ \underline{z}(t_i) - \underline{z}_c(t_i, \underline{x}_0, t_0) \right\} \quad (2.14)$$

where

t_i : observation time ($i=1,2,\dots,N$)

\underline{z}_c : observation vector calculated from the initial state vector \underline{x}_0 of the spacecraft at t_0

$()^T$: matrix transpose

W : weighting matrix

The weighting matrix is usually given by

$$W_i = (E x (\underline{n}_i \underline{n}_i^T))^{-1} \quad (2.15)$$

$$A_i = \left. \frac{\partial z_c}{\partial x_0} \right|_{\substack{x_0 = \tilde{x}_0 \\ t = t_i}}$$

: observation partial matrix

Using Eq.(2.17), Eq.(2.14) becomes

$$F(\Delta \underline{x}) = \sum_{i=1}^N (\Delta \underline{z}_i - A_i \Delta \underline{x})^T W_i (\Delta \underline{z}_i - A_i \Delta \underline{x}) \quad (2.18)$$

where

$$\Delta \underline{z}_i = \underline{z}(t_i) - \tilde{\underline{z}}_c(t_i) : \text{observation residual vector}$$

According to Eq.(2.18) we obtain an equation of $\Delta \underline{x}$ which makes

$F(\Delta \underline{x})$ minimum in a matrix form as

$$\begin{bmatrix} \sqrt{W_1} A_1 \\ \sqrt{W_2} A_2 \\ \vdots \\ \sqrt{W_i} A_i \end{bmatrix} \Delta \underline{x} = \begin{bmatrix} \sqrt{W_1} \Delta \underline{z}_1 \\ \sqrt{W_2} \Delta \underline{z}_2 \\ \vdots \\ \sqrt{W_i} \Delta \underline{z}_i \end{bmatrix}$$

or it is rewritten as

$$\sqrt{W} A \Delta \underline{x} = \sqrt{W} \Delta \underline{z} \quad (2.19)$$

where \sqrt{W} is the square-root matrix of W , that is, $W = \sqrt{W}^T \sqrt{W}$.

Eq.(2.19) is sometimes called normal equation. It is also

derived from a linearized observation equation

$$\Delta \underline{z} = A \Delta \underline{x} + \underline{n}$$

or generally this is written as

$$\underline{z} = A \underline{x} + \underline{n} \quad (2.20)$$

Eq.(2.19) is solved as

$$\Delta \underline{x} = (A^T W A)^{-1} A^T W \Delta \underline{z} \quad (2.21)$$

$\Delta \underline{x}$ is a correction to an initially assumed state vector $\tilde{\underline{x}}_0$, so we obtain $\tilde{\underline{x}}_0 + \Delta \underline{x}$ as a more accurate guess of the state vector at time t_0 . The above process is repeated to obtain an estimate of the state vector with a required accuracy. This is called a differential correction method of orbit determination. It is one of typical batch processing methods where all of the tracking data are processed at one time.

On the other hand, various sequential filtering methods have been developed⁽⁸⁾ to estimate the state vector at time t . One of them is Kalman filtering method which is theoretically equivalent to a least square method applied to a dynamical system. Those sequential filtering methods are effective in deep space navigations and various numerically stable algorithms have been developed⁽⁹⁾⁽¹⁰⁾⁽¹¹⁾. In the case of Earth orbiting satellites, however, batch processing methods are satisfactorily used.

We have several computer programs for orbit determination in Radio Research Laboratory (RRL). The Definitive Orbit Determination Operating System (DODS)⁽¹²⁾ was first introduced from NASA in 1974 in a satellite control experiment using ATS-1 (Applications Technology Satellite 1). After that RRL has

developed two operational orbit determination programs for Japan's experimental geosynchronous satellites CS(Experimental Communications Satellite⁽¹³⁾) and BSE(Experimental Broadcasting Satellite⁽¹⁴⁾). Another program was also developed for orbit determination studies. It is named KODS (Kashima Orbit Determination Software⁽¹⁵⁾⁽¹⁶⁾) with a small program size and a sufficient accuracy for a geosynchronous satellite. The author has developed DVODP (Delta-VLBI Orbit Determination Program) by improving KODS so that it can process VLBI observables in addition to range, range rate, angles and range-sum observables and it has functions to estimate not only satellite state vector but also observation biases and some of model parameters and to evaluate effects of model parameter errors (Appendix A).

2.2 Accuracy of Orbit Determination

2.2.1 Covariance Analysis and Simulations

We should know the accuracy of an orbit determination in order to correctly grasp the uncertainty of the obtained spacecraft state and to evaluate the efficiency of a tracking method by which the observation data are obtained. If the true state vector of a spacecraft is given by some other method, it is easy to evaluate the accuracy of an orbit determination. It

is, however, not usually given. So we use following two methods; covariance analyses⁽¹⁷⁾ and numerical simulations.

In a covariance analysis, we calculate an expected covariance of an estimated state vector as

$$C_x = \text{Ex} \left\{ (\hat{\underline{x}} - \underline{x}_0)(\hat{\underline{x}} - \underline{x}_0)^T \right\} \quad (2.22)$$

where

- C_x : covariance matrix
- $\hat{\underline{x}}$: estimated state vector
- \underline{x}_0 : true state vector

In the case of a least-square method of an orbit determination,

$\hat{\underline{x}} - \underline{x}_0$ is given by Eq.(2.21) as

$$\hat{\underline{x}} - \underline{x}_0 = \Delta \underline{x} = (A^T W A)^{-1} A^T W \Delta \underline{z} \quad (2.23)$$

Then Eq.(2.22) becomes

$$\begin{aligned} C_x &= \text{Ex}(\Delta \underline{x} \Delta \underline{x}^T) \\ &= (A^T W A)^{-1} A^T W \text{Ex}(\Delta \underline{z} \Delta \underline{z}^T) W A (A^T W A)^{-1} \end{aligned} \quad (2.24)$$

Suppose that the observation residual vector $\Delta \underline{z}$ contains only observation noises, then

$$\text{Ex}(\Delta \underline{z} \Delta \underline{z}^T) = \text{Ex}(\underline{nn}^T) = W^{-1} \quad (2.25)$$

Consequently we obtain a general expression of the covariance matrix

$$C_x = (A^T W A)^{-1} = \begin{pmatrix} \sigma_i & \sigma_j \end{pmatrix} \quad (2.26)$$

In many cases the estimated state vector \underline{x} behaves as a Gaussian random vector of which the probability density function $P_x(\underline{x})$ is written as

$$P_x(\underline{x}) = ((2\pi)^{N/2} (C_x)^{1/2})^{-1} \exp(-\frac{1}{2} \underline{x}^T C_x^{-1} \underline{x}) \quad (2.27)$$

where N is the dimension of the state vector \underline{x} . C_x represents an error ellipsoid, that is, a quadratic equation

$$\underline{x}^T C_x^{-1} \underline{x} = c, \quad c: \text{constant} \quad (2.28)$$

makes an equi-probability N -dimensional ellipsoid with respect to a vector \underline{x} . Fig.2.5 shows an example of two-dimensional error ellipsoid (ellipse). The diagonal components σ_1^2 , σ_2^2 , ..., σ_N^2 of C_x give rough measures of the size of the ellipsoid.

To evaluate the error ellipsoid more precisely, we can use the eigen values σ_{10}^2 , σ_{20}^2 , ..., σ_{N0}^2 of C_x , which correspond to the principal axes of the ellipsoid. The eigen values are obtained as the diagonal elements of a diagonalized covariance matrix. A covariance matrix can be diagonalized by a linear transformation of the state vector \underline{x} as

$$\underline{x} = K \underline{X} \quad (2.29)$$

where

\underline{X} : transformed state vector

K : orthogonal transformation matrix

The diagonalized covariance matrix C_X which corresponds to \underline{X} is

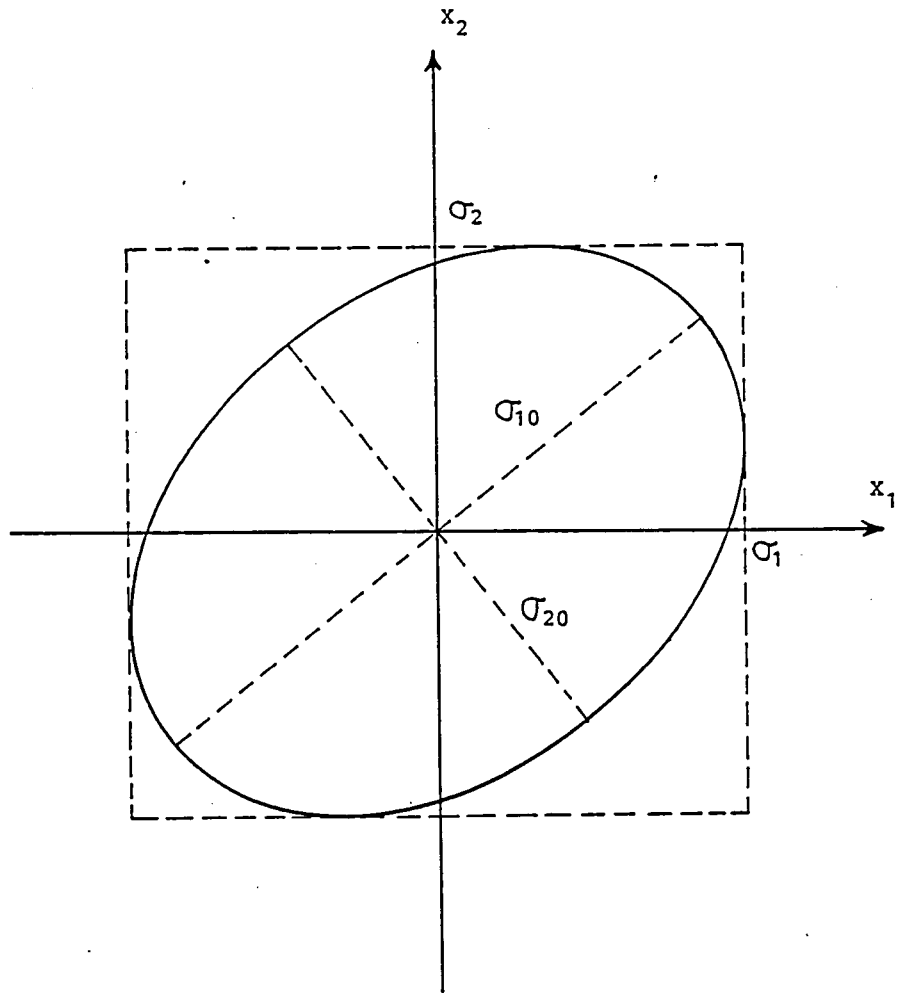


Fig.2.5 Two-dimensional error ellipsoid

actual observations are needed. The matrix A depends on a tracking strategy, that is, observation types and schedule. We will further look into this point in the next section.

Numerical simulation is another method to evaluate the accuracy. In this case we make simulated observation data which include possible observation errors of bias and random types. Though this method requires a process to create simulated observation data, it gives us more detailed information in specific orbit determination cases.

It would be recommended to use a covariance analysis method to obtain a general concept of the accuracy and to carry out a lot of simulations to get detailed information in a specified case.

2.2.2 Bias Errors and Model Parameter Errors

The covariance analysis described above can show the effect of random noises in observation data. Actually, however, observation data may have some bias errors. According to Eq(2.21) we can evaluate the effect as

$$\Delta \underline{x}_b = (A^T W A)^{-1} A^T W \Delta \underline{z}_b \quad (2.32)$$

where

$\Delta \underline{x}_b$: errors in the state vector due to
observation biases

$\Delta \underline{z}_b$: vector of observation biases

The observation biases are usually estimated as well as the

spacecraft state vector in an orbit determination.

Other important factors affecting the accuracy of an orbit determination are possible model errors in the orbit dynamics and observation systems. In the least-square orbit determination method, the state vector is estimated so that it gives the minimum difference between actual observation data and calculated values which are obtained using models of the orbit dynamics and the observation system (see Sec. 2.1.3). Consequently, model errors and calculation errors lead to erroneous estimates.

Observation equations which include errors in model parameters can be linearized around nominal values and written as

$$\underline{z} = A \underline{x} + B \underline{y} + \underline{n} \quad (2.33)$$

where

\underline{z} : linearized observation vector (\underline{z} in Eq.(2.20))

\underline{y} : vector of errors of model parameters
(errors in vectors \underline{p}_{sc} in Eq.(2.2) and \underline{p}_{obs} in Eq.(2.9))

A : observation partial matrix with respect to the state vector \underline{x}

B : observation partial matrix with respect to \underline{y}

\underline{n} : observation noise vector

If we assume that $\text{Ex}(\underline{y}) = 0$, then the vector $\hat{\underline{x}}$ given by

$$\hat{\underline{x}} = K_1 \underline{z}, \quad K_1 = (A^T W A)^{-1} A^T W \quad (2.34)$$

is an unbiased estimate vector. $\hat{\underline{x}}$ becomes the least square estimate vector in Eq.(2.21) when $\underline{y} = 0$. The covariance matrix C_c is calculated as

$$\begin{aligned} C_c &= \text{Ex} \left((\hat{\underline{x}} - \underline{x})(\hat{\underline{x}} - \underline{x})^T \right) \\ &= \text{Ex} \left\{ (K_1(A\underline{x} + B\underline{y} + \underline{n}) - \underline{x})(K_1(A\underline{x} + B\underline{y} + \underline{n}) - \underline{x})^T \right\} \\ &= \text{Ex} \left\{ K_1(B\underline{y} + \underline{n})(B\underline{y} + \underline{n})^T K_1^T \right\} \\ &= K_1 \text{Ex}(\underline{n}\underline{n}^T) K_1^T + K_1 B \text{Ex}(\underline{y}\underline{y}^T) B^T K_1^T \\ &= C_x + S C_y S^T \end{aligned} \quad (2.35)$$

where

$$\begin{aligned} C_x &= (A^T W A)^{-1} \quad (\text{already defined by Eq.(2.26)}) \\ S &= K_1 B = (A^T W A)^{-1} A^T W B \\ C_y &= \text{Ex}(\underline{y}\underline{y}^T) \end{aligned}$$

Eq.(2.35) means that the covariance matrix which includes model parameter errors has an additional term $S C_y S^T$ to the original C_x . The term $S C_y S^T$ represents the effect of model parameter errors. It is sometimes called "consider covariance", because the model parameter errors are not estimated but they are only considered in evaluation of covariance of the state vector.

Eq.(2.35) can be slightly generalized and written as

$$C_c = (A^TWA)^{-1}A^TW(Ex(\underline{nn}^T) + BC_yB^T + C_n)WA^T(A^TWA)^{-1} \quad (2.36)$$

where C_n represents a covariance due to errors such as numerical calculation errors which do not depend on observation noises nor model parameter errors. Therefore, by calculating C_c we can include effects of not only observation noises and modeling errors but also numerical errors in the evaluation of accuracies of various orbit determination systems⁽¹⁸⁾. From the viewpoint of the information content of the observation data, the terms BC_yB^T and C_n in Eq.(2.36) degrade the information contents. This concept is further discussed and studied in the next section.

2.2.3 Evaluation of Observation Residuals

In the least-square method of an orbit determination (see Eq.(2.21)), we expect that the observation residual $\Delta \underline{z}$ becomes random corresponding to the observation noises (see Eq.(2.25)) after the iterative correction $\Delta \underline{x}$ converges. In the estimation process, if we have not fully used the information contained in the observation data, the observation residuals would show a slightly different features. We can quantitatively evaluate the characteristics of the observation residuals by a chi-square (χ^2) test. It is well known that a set of random variables (x_1, x_2, \dots, x_N) with variance $(\sigma_1^2, \sigma_2^2, \dots, \sigma_N^2)$ show a chi-square statistics. That is,

if we define a χ^2 as

$$\chi^2 = \frac{x_1^2}{\sigma_1^2} + \frac{x_2^2}{\sigma_2^2} + \dots + \frac{x_N^2}{\sigma_N^2} \quad (2.37)$$

then we have

$$\text{Ex} (\chi^2) = k \quad (2.38)$$

where k is the degree of freedom of the set of random variables.

In our case, χ^2 of the observation residuals is defined as

$$\chi^2 = \sum_{i=1}^N \frac{\Delta z_i^2}{v_i} \quad (2.39)$$

where N is the total number of observation data, Δz_i is i -th observation residual and v_i is variance of i -th observation noise (or the i -th diagonal component of the matrix given by Eq.(2.25), where each Δz_i is assumed to be independent). Then we expect

$$\text{Ex} (\chi^2) = N-M \quad (2.40)$$

where M is the number of the estimated parameters, therefore $N-M$ is the degree of freedom of the observation residuals.

Usually we define a normalized chi-square σ_χ^2 by

$$\sigma_\chi^2 = \frac{1}{N-M} \sum_{i=1}^N \frac{\Delta z_i^2}{v_i} \quad (2.41)$$

If we fully used the information contained in the observation data by using a correct weighting matrix and appropriate physical models, σ_x reaches 1.0. But if we used, for example, wrong v_i^2 , that is, wrong weighting matrix W^{-1} , then σ_x exceeds 1.0 or becomes smaller than 1.0. Therefore, we can check σ_x after the least-square iterative estimation has converged in order to confirm whether we used a correct weighting matrix and whether we used appropriate physical models. This chi-square test of the observation residuals is useful to correct our erroneous a priori knowledge of the observation noise. Because it is usually the case that our a priori evaluation is an overestimate or underestimate of the observation noise when we start a least-square estimation with a weighting matrix based on these a priori knowledge.

2.3 Sensitivity and Information Contents of Observations

2.3.1 Sensitivity and Observability

In the covariance analysis described in Sec.2.2.1 it was shown that the observation partial matrix A plays an essential role. This matrix represents the sensitivity of observations with respect to the elements of a state vector. It is useful to define the column vectors $\underline{a}_1, \underline{a}_2, \dots, \underline{a}_N$ of the matrix A . Then linearized observation predictions are written as

$$\begin{aligned}\underline{z} &= (\underline{a}_1 \underline{a}_2 \cdots \underline{a}_N) \underline{x} \\ &= \underline{a}_1 x_1 + \underline{a}_2 x_2 + \cdots + \underline{a}_N x_N\end{aligned}\quad (2.42)$$

where N is the dimension of the state vector \underline{x} and x_1, x_2, \dots, x_N is the elements of \underline{x} . Eq.(2.42) means that the observation vector \underline{z} is represented as a linear combination of the column vectors. Therefore, if one of them, , for example, \underline{a}_i , is independent from the others and has a large magnitude in a certainly normalized sense, then the observation vector has a high sensitivity to the element x_i .

For example let us consider a case where an angular position of a deep space spacecraft is derived from a VLBI observation⁽¹⁹⁾. Fig.2.6 (a) shows a geometry of VLBI observations. By a VLBI observation the signal delay (or excess path d) is derived. The observation equation is

$$d = \underline{B} \cdot \underline{S} + n \quad (2.43)$$

where

\underline{B} : baseline vector

\underline{S} : unit vector in the direction to the spacecraft

n : observation noise (error)

Let us define a state vector \underline{x} which represents the angular position of the spacecraft as

$$\underline{x} = \begin{pmatrix} \Delta\alpha \cos\delta \\ \Delta\delta \end{pmatrix} \quad (2.44)$$

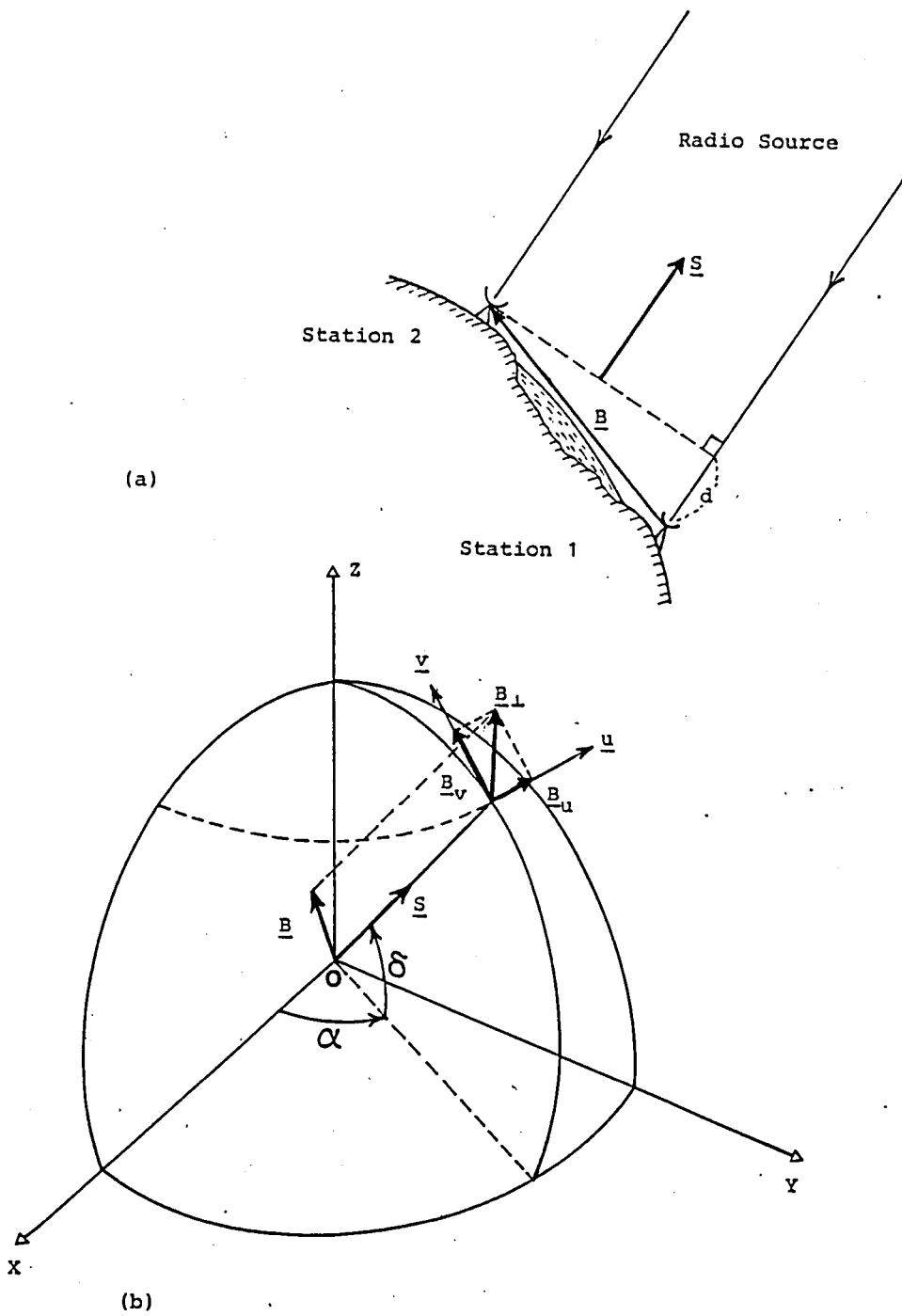


Fig.2.6 Geometry of VLBI observation(a), and sensitivity of observation(b)

where

$\Delta\alpha$: small deviation from a nominal right
ascension α of the spacecraft

$\Delta\delta$: small deviation from a nominal declination δ
of the spacecraft

then a linearized observation equation is

$$\Delta d = \underline{A}\underline{x} + n \quad (2.45)$$

where

Δd : deviation from a nominal observation d

$$A = \frac{\partial d}{\partial \underline{x}} = \underline{B}^T \cdot \frac{\partial \underline{S}}{\partial \underline{x}} = \underline{B}^T \cdot (\underline{u} \ \underline{v}) = (B_u \ B_v) \quad (2.46)$$

where \underline{u} , \underline{v} are unit vectors shown in Fig.2.6(b), and B_u , B_v are the components of the baseline vector \underline{B} in the u-v plane which is perpendicular to the line-of-sight or vector \underline{S} . Therefore, the component of the baseline vector perpendicular to the line-of-sight represents the sensitivity of VLBI delay observation with respect to the angular information of a radio source.

From the viewpoint of estimation of the state vector, another important concept is observability. The observation system (2.20) or (2.33) is said to have an observability if the state vector \underline{x} can be definitely determined from the observation vector \underline{z} . As is clear from Eq.(2.21) or Eq.(2.34) the system has an observability when the matrix A^TWA is normal or

$\det(A^TWA) \neq 0$. Because of the numerical instability or limitation to the accuracy of calculations, even if $\det(A^TWA) \neq 0$ the observability is not actually kept when one or some of eigen values of A^TWA reach zeros, or $\det(A^TWA)$ becomes very small. It corresponds that the error ellipsoid becomes very large in one or some directions in the N -dimensional space.

So it is practical to use various methods to evaluate system observability⁽²⁰⁾. One of them checks the eigen values of the matrix A^TWA . If some of them are less than a given threshold value, which is usually selected near zero, the corresponding elements of the state vector are quit to be estimated.

One of other methods evaluates the orthogonality of column vectors of weighted (normalized) observation partial vectors, that is, the column vectors of matrix \sqrt{WA} . Eq.(2.18) is rewritten as

$$F(\Delta \underline{x}) = \| \sqrt{WA} \Delta \underline{x} - \sqrt{W} \Delta \underline{z} \| \quad (2.47)$$

The estimates vector $\Delta \hat{\underline{x}}$ which makes $F(\Delta \underline{x})$ minimum is given by an orthogonal projection of vector $\sqrt{W} \Delta \underline{z}$ on to the plane which is spanned by the column vectors of $\underline{a}_{w1}, \underline{a}_{w2}, \dots, \underline{a}_{wN}$ of the matrix \sqrt{WA} (Fig.2.7). The i -th element x_i of the state vector \underline{x} corresponds to the column vector \underline{a}_{wi} . It means that the independency of each column vector is important to estimate each element separately, or if some of the column vectors are not independent from the others the corresponding state

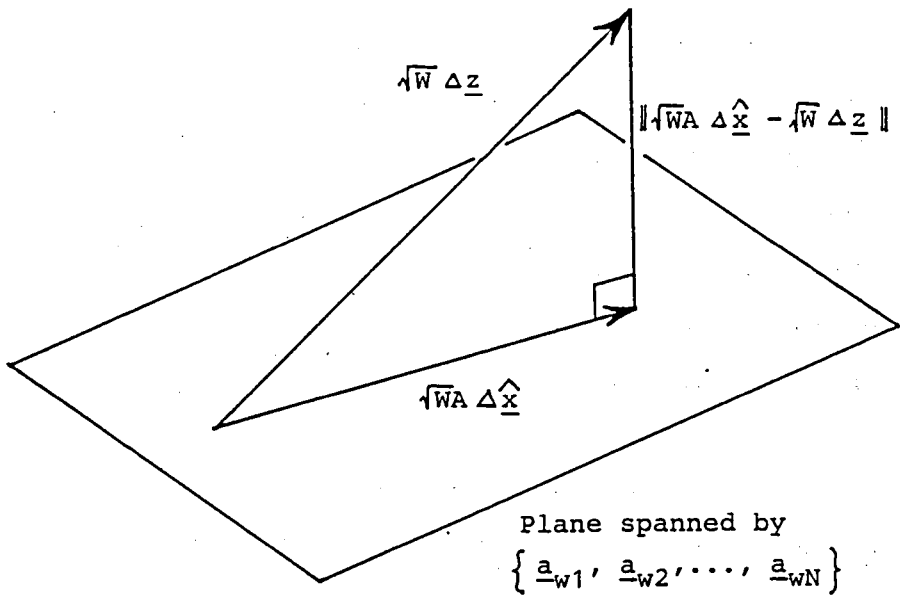


Fig.2.7 Parameter estimation by orthogonal projection

elements cannot be estimated. In an actual orbit determination program, the independency of the column vectors is tested through Schmidt's orthogonalization method⁽¹⁶⁾. If the orthogonal component of a column vector to the other vectors is less than a given threshold, the corresponding element of the state vector is rejected from the estimation process.

2.3.2 Information Contents of Observations

Through a least-square estimation process, uncertainty of a state vector is reduced by information which is brought by observation data. In other words, observations bring some information of the state vector. We can evaluate the quantity of the information by the mutual information defined as⁽²²⁾⁽²³⁾

$$I(\underline{x}; \underline{z}) = 1/2 \log \det(C_0 C^{-1}) \quad (2.48)$$

where

$I(\underline{x}; \underline{z})$: mutual information which is brought by observations \underline{z} with respect to the state vector \underline{x}

C_0 : covariance of \underline{x} before the observations

C : covariance of \underline{x} after the observations

In the right hand side of Eq.(2.48), the term $(\det(C_0 C^{-1}))^{1/2}$ represents the ratio of error ellipsoids before and after the observations. For example, in a simple case where

$$C_0 = \begin{bmatrix} \sigma_{01}^2 & & 0 \\ & \ddots & \\ 0 & & \sigma_{0N}^2 \end{bmatrix} \quad (2.49)$$

$$C = \begin{bmatrix} \sigma_1^2 & & 0 \\ & \ddots & \\ 0 & & \sigma_N^2 \end{bmatrix} \quad (2.50)$$

then the information content is given as

$$I(\underline{x}; \underline{z}) = \sum_{i=1}^N (\log \sigma_{0i} - \log \sigma_i) \quad (2.51)$$

Generally speaking, observations bring information and $\sum_{i=1}^N \log \sigma_i$ is less than $\sum_{i=1}^N \log \sigma_{0i}$, so $I(\underline{x}; \underline{z})$ is positive.

Using the concept of information content we can quantitatively evaluate the usefulness of observations, which is sometimes useful to optimize observation strategy (24).

It can be said that an estimation process is optimum when it completely utilizes the information which is brought by observations. If there are some errors in observation models used in an estimation process, we cannot fully use the information content. The effects of model parameter errors and numerical calculation errors are given in Eq.(2.36) by a covariance matrix which includes these effects. The degradation of the information is given by comparing the mutual information of erroneous model estimation with that of an error-free estimation. That is,

$$D_I = 1/2 \log \det(C_x C_c^{-1}) \quad (2.52)$$

shows information degradation by errors in the observation equation. Using C_x (Eq.(2.26)) and C_c (Eq.(2.36)), D_I becomes

$$\begin{aligned}
D_I &= 1/2 \log \det \left[C_x \left\{ C_x + C_x A^T W (B C_y B^T + C_n) W A^T C_x \right\}^{-1} \right] \\
&= 1/2 \log \det \left[\left\{ I_x + C_x A^T W (B C_y B^T + C_n) W A^T \right\}^{-1} \right] \\
&= 1/2 \log \left[\det \left\{ I_x + C_x A^T W (B C_y B^T + C_n) W A^T \right\} \right]^{-1}
\end{aligned}
\tag{2.53}$$

where I_x is unit matrix. Because of model parameter error covariance C_y and numerical calculation error covariance C_n , $\det \left\{ I_x + C_x A^T W (B C_y B^T + C_n) W A^T \right\}$ becomes larger than 1, which means that the information content D_I is negative, or in other words, the information is degraded by the model errors.

When there are errors in some model parameters, we should reweight the observations in order to optimally utilize the information content. In a system without model errors (Eq.(2.20)) it is optimum to select weighting matrix as $W = \left\{ \text{Ex}(\underline{nn}^T) \right\}^{-1}$ in the sense that the weight gives the minimum covariance of the estimates⁽²¹⁾. For a system which has model parameter errors (Eq.(2.33)), it is optimum to use a reweighting matrix as

$$W_R = W A (J_x + S_1 C_y S_1^T)^{-1} A^T W \tag{2.54}$$

where

$$\begin{aligned}
W_R &: \text{reweighting matrix} \\
J_x &= C_x^{-1} \\
S_1 &= A^T W B
\end{aligned}$$

The estimates vector $\hat{\underline{x}}$ is given by

$$\hat{\underline{x}} = K_2 \underline{z} ; \quad K_2 = (A^T W_R A)^{-1} A^T W_R \quad (2.55)$$

and

$$\begin{aligned} \text{Ex}(\hat{\underline{x}} - \underline{x}) &= \text{Ex} \left\{ K_2 (B \underline{y} + \underline{n}) \right\} \\ &= K_2 B \text{Ex}(\underline{y}) + K_2 \text{Ex}(\underline{n}) \end{aligned} \quad (2.56)$$

Therefore, if $\text{Ex}(\underline{y}) = \text{Ex}(\underline{n}) = 0$ then $\hat{\underline{x}}$ becomes unbiased estimate. The covariance is given as (Appendix B)

$$\begin{aligned} \text{Ex} \left\{ (\hat{\underline{x}} - \underline{x})(\hat{\underline{x}} - \underline{x})^T \right\} &= K_2 \text{Ex} \left\{ (B \underline{y} + \underline{n})(B \underline{y} + \underline{n})^T \right\} K_2^T \\ &= K_2 (B C_y B^T + W^{-1}) K_2^T \\ &= C_x + S C_y S^T \\ &= C_c \end{aligned} \quad (2.57)$$

The above reweighting process can be said optimum because it gives the same covariance matrix as is given by considering information degradation by model parameter errors (Eq.(2.35)).

In the above discussion we do not completely utilize the information content of the observations. If we successfully estimate all the model parameters and the state vector we can use all the information. However, it is practically difficult because of numerical instabilities. On the other hand we can stably estimate parts of the parameters alternatively. That is, first, half of the parameters are estimated with the other parameters fixed, then using the estimated parameters as known the other parameters are estimated, and so forth. By an analysis using the concept of information content, we can show that the alternative estimation process is theoretically

equivalent to the simultaneous estimation if the former process converges (Appendix C).

References

- (1) Thornton, C. L. and S. G. Finley, Square-root algorithm for evaluating mismodeled process noise, *J. Spacecraft*, 11, 4, April 1974.
- (2) Goddard Trajectory Determination Subsystem mathematical specifications, GSFC, X-552-72-244, March 1972.
- (3) Moyer, T. D., Mathematical formulation of the Double-Precision Orbit Determination Program (DPODP), TR32-1527, JPL, May 1971.
- (4) Escobal, P. R., *Methods of orbit determination*, John Wiley & Sons, Inc., 1965.
- (5) Gordon, R. A., G. D. Mistretta and J. S. Watson, A comparison of classical analytic theories for the motion of artificial satellite, *J. Guidance and Control*, 2, 3, May-Jun 1979.
- (6) Lieske, J. H., Precession matrix based on IAU(1976) system of astronomical constants, *Astron. Astrophys*, 73, 1979, pp. 282-284.
- (7) Seidelmann, P. K., 1980 IAU theory of nutation: The final report of the IAU working group on nutation, *Celestial Mechanics*, 27, 1982, pp. 79-106.
- (8) Thornton, C. L. and G. J. Bierman, A numerical comparison of discrete Kalman filtering algorithms: An orbit determination case study, IAF-76-015, Oct. 1976.

- (9) Schmidt, S. F., The Kalman filter: Its recognition and development for aerospace applications, J. Guidance and Control, 4, 1, Jan-Feb. 1981.
- (10) Sorenson, H. W., Kalman filtering techniques, "Advances in control systems-- Theory and applications", Academic Press, 1965.
- (11) Jazwinsky, A. H., "Stochastic processes and filtering theory", Academic Press, 1970.
- (12) Definitive Orbit Determination Operating System Description, X-544-71-296, GSFC, July 1971.
- (13) Tsukamoto, K., Y. Otsu, K. Kosaka, T. Shiomi and H. Sasaoka, Experimental program and performance of Japan's Communication Satellite (CS) and its first results, IEEE Trans. on Communications, COM-27, 10, 1979, pp. 1392-1405.
- (14) Imai, N., M. Matsushita and M. Kajikawa, Japan's BSE program, IEEE Trans. of Broadcasting, BC-28, 4, 1982, pp. 120-124.
- (15) Tanaka, T. and S. Kawase, A high-speed integration method for the satellite's ephemeris generation, J. Guidance and Control, 1, 3, May-June 1978.
- (16) Kawase, S. and T. Tanaka, A simple method for evaluating the system observability in satellite orbit determination, IEEE Trans. on Aerosp. and Electron. Systems, AES-15, 1, 1977, pp. 152-156.
- (17) Walter, H. G., Accuracy estimation for spacecraft

position and velocity, ESRO Science Report, SR-16, 1971.

(18) Shiomi, T., S. Kawase and S. Shimizu, Accuracy of orbit determination using tracking data via TDRS (in Japanese), Technical Paper of the Professional Group on Space and Aeronautics Navigation Electronics, Inst. Electronics Comm. Engrs. Japan, SANE78-5, 1978.

(19) Melbourne, W. G. and D. W. Curkendall, Radio metric direction finding: A new approach to deep space navigation, AAS/AIAA Astrodynamics Specialist Conference, Sept. 1977.

(20) Ham, F. M. and R. G. Brown, Observability, eigenvalues and Kalman filtering, IEEE Trans. on Aerospace and Electronic Systems, AES-19, 2, 1983, pp. 269-273.

(21) Luenberger, D. G., "Optimization by vector space method", John Wiley and Sons, Inc., 1969.

(22) Bucy, R. S. and P. D. Joseph, "Filtering for stochastic processes with applications to guidance", Interscience Publ., John Wiley and Sons, Inc., 1968.

(23) Omatsu, S., Y. Tomita and T. Soeda, An alternative expression of the mutual information for Gaussian processes, IEEE Trans. on Inf. Theory, Sept. 1976.

(24) Shiomi, T., Angle information of the measurements of range and Doppler from a Space Tracking Station (STS), JPL EM 314-311, June 1983.

3.1 Introduction to VLBI

3.1.1 General Concept and Brief History of VLBI

A VLBI uses two receiving stations which are usually separated over thousands kilometers. Each station has independent frequency standard (for example, a hydrogen maser frequency standard) which is used to make local frequency signals and various timing references in order to sample and record the received signal. Fig. 3.1 shows a general concept of VLBI. The received signal from a radio source is down-converted into a baseband signal of a bandwidth, for example, of 2 MHz and sampled, formatted (or coded by adding receiving time-tag, receiving frequency information, and so on), and recorded on a magnetic tape. The magnetic tapes of the recorded signals at the two stations are sent to a data processing center. By correlating the reproduced signals, delay and delay rate observables are derived. Through various calibration for receiving system delays, propagation media effects, clock errors and so on, geometric delay and delay rate observables are obtained. These observables contain information of radio source position and station locations (or baseline vector). Actually, observations at many frequency

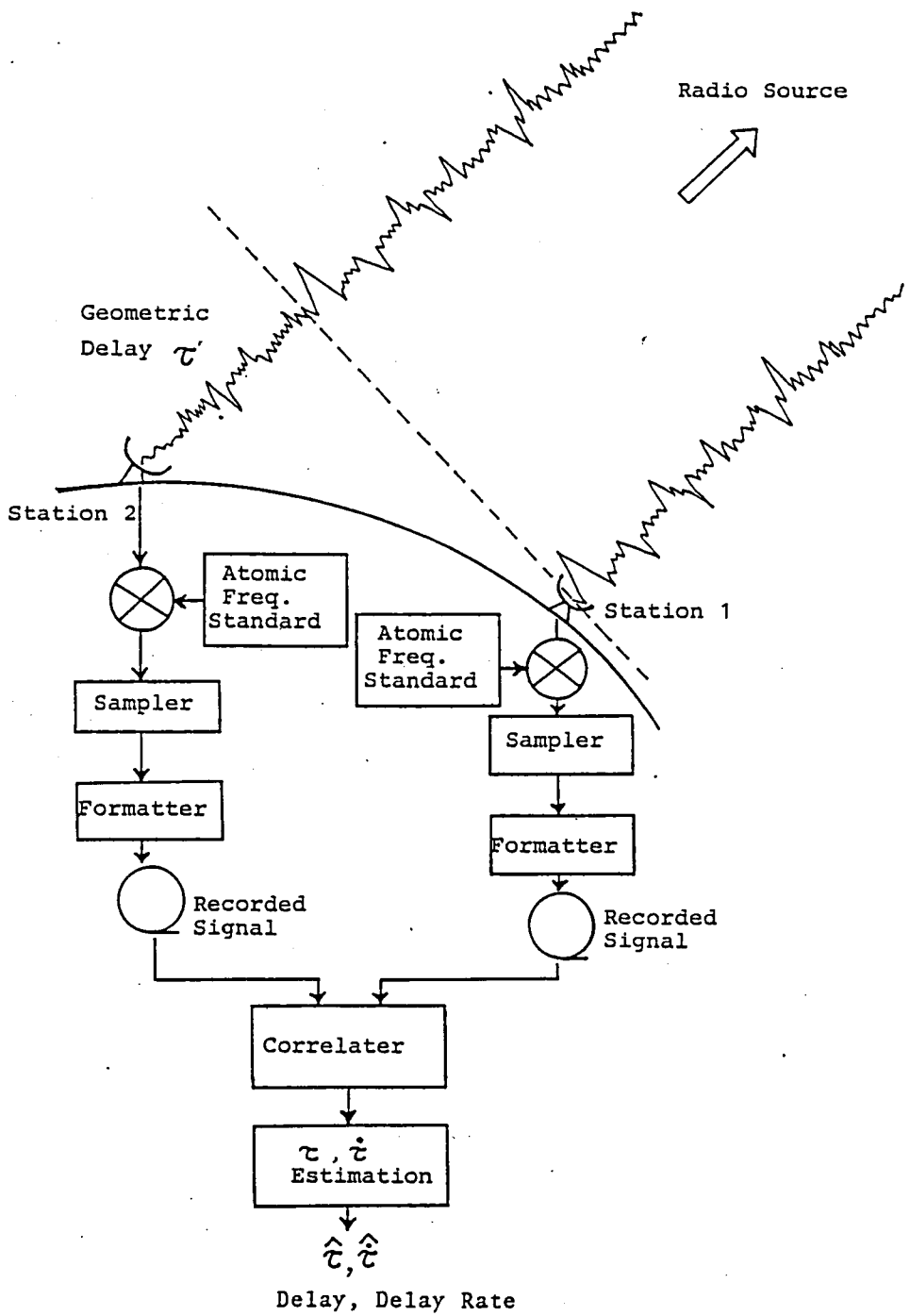


Fig.3.1 Concept of VLBI

channels (each of which has bandwidth of, for example, 2 MHz) are simultaneously conducted and the data are synthesized to lead to effectively wideband observations⁽¹⁾. The propagation delays through ionized media (ionosphere, earth's magnetospheric plasma, and interplanetary plasma) are corrected by observations at dual frequencies (usually 2 GHz and 8 GHz).

A VLBI system was first developed in 1967 in the east coast of the U.S.A. using so-called "Mark-I" digital recording system by groups in NRAO(National Radio Astronomical Observatory), MIT(Massachusetts Institute of Technology) and Cornell University⁽²⁾. After that a NRAO group improved the Mark-I recording system to a "Mark-II" system early in 1970's⁽³⁾. The most recently developed system is "Mark-III"⁽⁴⁾⁽⁵⁾ by the east coast group, which has been widely used since 1980 especially in earth's crustal dynamics projects.

In the west coast of the U.S.A., groups in JPL(Jet Propulsion Laboratory) and CALTECH(California Institute of Technology) have also developed VLBI systems named Block 0⁽⁶⁾ and Block I⁽⁷⁾. Their newest Block II correlater system⁽⁸⁾ is now under development. These systems have been used not only in astrometry and geodesy but also in clock synchronization between Deep Space Network stations, in measurements of polar motion and UT1⁽⁹⁾, and in navigation of spacecrafts especially in deep space orbits.

On the other hand, in Japan RRL developed an experimental

VLBI system "K-I" in 1976⁽¹⁰⁾ and a real-time VLBI system "K-II"⁽¹¹⁾ in 1980. RRL also developed the newest system "K-III"⁽¹²⁾ in 1983 which is compatible with Mark III system. The K-III system has been used since early 1984 in Japan-US joint experiments under the Crustal Dynamics Project (CDP), NASA.

3.1.2 Applications of VLBI for Tracking Spacecrafts

VLBI systems have been developed originally for astronomy, astrometry, and geodesy. However, the advantages of a VLBI which is a passive method and gives highly accurate observables of geometrical delay and delay rate have also been noticed in the field of spacecraft navigation. For example, in early 1970's, a geosynchronous satellite ATS-3 was observed by a VLBI method using baselines in the U.S.A. in addition to range and range-rate measurements⁽¹³⁾. Using the obtained VLBI observables, an accuracy of 70m . 100m in the satellite position was attained. In RRL, using K-I VLBI system a geosynchronous satellite ATS-1 was tracked in 1977 using a baseline 125 km long in Japan⁽¹⁴⁾. Those were, however, essentially experiments to show the possibility of VLBI in the navigation field.

With practical purposes to obtain highly accurate tracking data of spacecrafts, JPL has developed various VLBI techniques and demonstrated them especially in deep space navigation

field⁽¹⁵⁾. In the deep space navigation, the required accuracy of spacecraft's position determination has been growing as mission goals have become more and more sophisticated. However, the conventional radio tracking methods of ranging and Doppler (range rate) measurements have become insufficient, because they generally cannot supply highly accurate angular information (or position information in the plane perpendicular to the line-of-sight⁽¹⁶⁾⁽¹⁷⁾). Especially, angular information of spacecraft declination, which is derived from the amplitude of diurnal variation of Doppler measurements due to the earth's rotation, suffers serious errors when the declination becomes nearly zero (this is usually called a zero declination problem). In addition to that, it takes from several weeks to months to derive effective observables (angular position accuracy of 250 to 500 nano-radians) from Doppler measurements⁽¹⁵⁾⁽¹⁸⁾. Fig. 3.2 shows a concept of position determination accuracy of a spacecraft in deep space by range and Doppler measurements. In Fig. 3.2 an error ellipse in the plane perpendicular to the line-of-sight is shown. It is elongated in the direction of declination (or north-south) and has much larger size than the position error in the line-of-sight. The spacecraft position in the direction of the line-of-sight can be determined with an accuracy of less than hundreds meters because conventional range measurements can supply the accuracy.

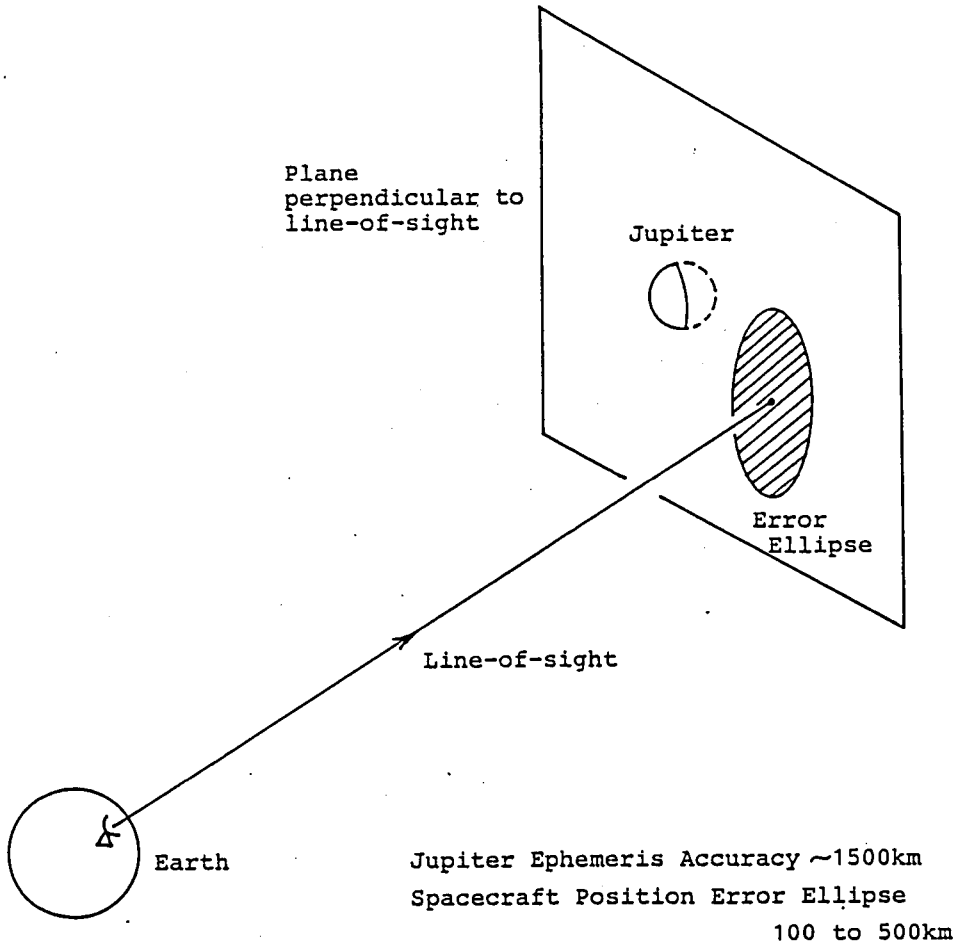


Fig.3.2 Accuracy of orbit determination with conventional radio tracking method (range and range rate measurements)

A VLBI can supply highly accurate angular information by much less period of observation (from several tens of minutes to hours) than that of Doppler measurements. Demonstrations of VLBI tracking of Voyager I and II spacecrafts proved an angular accuracy of about 50 nrad⁽¹⁵⁾⁽¹⁹⁾⁽²⁰⁾. In the field of geosynchronous satellite tracking by VLBI methods with a purpose of precise orbit determination, we made the first experiment⁽²¹⁾ on CS (Japan's Medium-Capacity Communication Satellite for Experimental Purposes, launched in 1977) by a DVLBI method (see Chapter 4) with a baseline 46 km long. A JPL group made an analysis on VLBI tracking method for geosynchronous satellite by assuming truly long baselines⁽²²⁾. In the case of VLBI observations of spacecraft signals, it is required to develop methods of processing narrowband signals. Because the spacecraft signals have not always so wideband characteristics as those of signals from natural radio stars. We study further on this point in the next section. After the CS experiment JPL and we carried out a joint experiment⁽²³⁾⁽²⁴⁾ of tracking a geosynchronous satellite by a DVLBI method with inter-continental baselines (Chapter 5).

3.2 VLBI Data Processing

3.2.1 Signal Analysis of VLBI

Here we describe basic concept of VLBI signal processing and signal-to-noise ratio which is important to evaluate the

accuracies of VLBI observables. Fig. 3.3 shows a concept of VLBI signal flow. Observed signals at the VLBI stations 1 and 2 are written in the frequency (ω) domain as⁽²⁾

$$\begin{aligned} \underline{x}_1(\omega) &= \sqrt{T_{a1}} \underline{S}(\omega) + \sqrt{T_{s1}} \underline{N}_1(\omega) \\ \underline{x}_2(\omega) &= \sqrt{T_{a2}} \underline{S}'(\omega) + \sqrt{T_{s2}} \underline{N}_2(\omega) \end{aligned} \quad (3.1)$$

where

$$\begin{aligned} \underline{S}'(\omega) &= \underline{S}(\omega) \exp \left[-i \left\{ \omega(\tau + \dot{\tau}t) \right\} - i\phi_0 \right] \\ \left| \underline{S} \right|^2 &= \left| \underline{S}' \right|^2 = \left| \underline{N}_1 \right|^2 = \left| \underline{N}_2 \right|^2 = 1 \end{aligned} \quad (3.2)$$

and

- $\underline{x}_i(\omega)$: observed signal at VLBI station i
- T_{ai} : radio source signal temperature at station i
- T_{si} : system noise temperature at station i
- $\underline{S}(\omega), \underline{S}'(\omega)$: normalized radio source signal
- $\underline{N}_i(\omega)$: normalized system noise at station i
- τ : signal delay time
- $\dot{\tau}$: delay rate
- ϕ_0 : fringe phase

Eq. (3.2) means that the signal observed at VLBI station 2 is delayed by $(\tau + \dot{\tau}t)$ from the signal observed at the other station. The fringe phase ϕ_0 is caused by the difference of phase shifts due to receivers at the VLBI stations. The delay

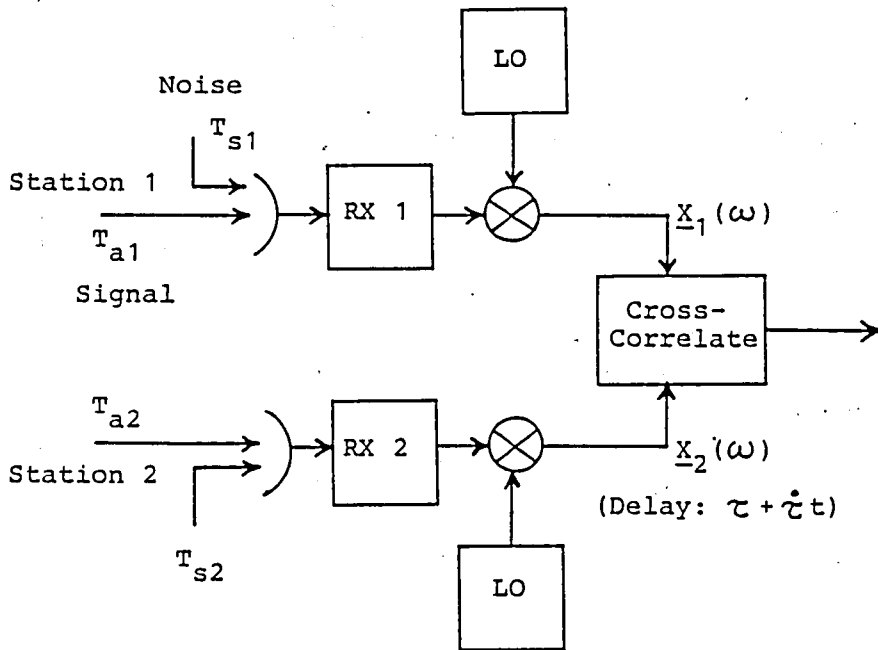


Fig.3.3 Signal flow in VLBI

model $(\tau + \dot{\tau}t)$, where a linear variation of the delay with respect to time is assumed, is usually valid for a short observation duration or for a short baseline. If necessary, however, we can use more accurate models of the delay.

We can obtain the delay and delay rate by correlation processing of the observed signals given by Eq.(3.1). First, we counter-rotate the phase of the signal $\underline{x}_2(\omega)$ by using predicted delay and delay rate. That is,

$$\begin{aligned}
 \underline{x}_2'(\omega) &= \underline{x}_2(\omega) \exp \left\{ i\omega(\tilde{\tau} + \tilde{\dot{\tau}}t) \right\} \\
 &= \sqrt{T_{a2}} \underline{S}(\omega) \exp \left[-i\omega \left\{ (\tau - \tilde{\tau}) + (\dot{\tau} - \tilde{\dot{\tau}})t \right\} - i\phi_0 \right] \\
 &\quad + \sqrt{T_{s2}} \underline{N}_2(\omega) \exp \left\{ i\omega(\tilde{\tau} + \tilde{\dot{\tau}}t) \right\} \\
 &= \sqrt{T_{a2}} \underline{S}(\omega) \exp \left\{ -i\omega(\Delta\tau + \Delta\dot{\tau}t) - i\phi_0 \right\} \\
 &\quad + \sqrt{T_{s2}} \underline{N}_2'(\omega) \\
 &= \sqrt{T_{a2}} \underline{S}(\omega) \exp(-i\phi_1) + \sqrt{T_{s2}} \underline{N}_2'(\omega) \quad (3.3)
 \end{aligned}$$

where

$\tilde{\tau}$: predicted delay
 $\tilde{\dot{\tau}}$: predicted delay rate

and we define $\Delta\tau$, $\Delta\dot{\tau}$, $\underline{N}_2'(\omega)$ and ϕ_1 as

$$\begin{aligned}\Delta\tau &= \tau - \tilde{\tau} \\ \Delta\dot{\tau} &= \dot{\tau} - \tilde{\dot{\tau}} \\ \underline{N}_2'(\omega) &= \underline{N}_2 \exp \left\{ i\omega (\tilde{\tau} + \tilde{\dot{\tau}} t) \right\} \\ \phi_1 &= \omega (\Delta\tau + \Delta\dot{\tau} t) + \phi_0\end{aligned}\tag{3.4}$$

Then the cross-correlated signal vector (or cross-spectral function) between $\underline{x}_1(\omega)$ and $\underline{x}_2'(\omega)$ is written as

$$\begin{aligned}\underline{R}(\omega) &= \underline{x}_1(\omega) \underline{x}_2'^*(\omega) \\ &= \sqrt{T_{a1} T_{a2}} \underline{S}(\omega) \underline{S}^*(\omega) \exp \left\{ i\omega (\Delta\tau + \Delta\dot{\tau} t) + i\phi_0 \right\} \\ &+ \sqrt{T_{s1} T_{a2}} \underline{N}_1(\omega) \underline{S}^*(\omega) \exp \left\{ i\omega (\Delta\tau + \Delta\dot{\tau} t) + i\phi_0 \right\} \\ &+ \sqrt{T_{a1} T_{s2}} \underline{S}(\omega) \underline{N}_2'^*(\omega) + \sqrt{T_{s1} T_{s2}} \underline{N}_1(\omega) \underline{N}_2'^*(\omega)\end{aligned}\tag{3.5}$$

where

* : complex conjugate

The last three terms in the last right-hand side of Eq.(3.5) vanish in a time-averaging (or we call this signal integration) process because they are correlated vectors between essentially independent (non-coherent) noise terms. The first term represents the cross-correlation of the coherently received

signals, where the amplitude is the coherent signal power and the phase is the correlated phase (sometimes it is called fringe phase). The correlated phase ϕ_1 (Eq.(3.4)) gives the corrections $\Delta\tau$ and $\Delta\dot{\tau}$ to the predicted VLBI observables $\tilde{\tau}$ and $\dot{\tilde{\tau}}$ through next equations

$$\Delta\tau = \frac{\partial\phi_1}{\partial\omega}, \quad t=0 \quad (3.6)$$

$$\Delta\dot{\tau} = \frac{1}{\omega} \frac{\partial\phi_1}{\partial t} \quad (3.7)$$

then we obtain $\tau (= \tilde{\tau} + \Delta\tau)$ and $\dot{\tau} (= \dot{\tilde{\tau}} + \Delta\dot{\tau})$ from Eq.(3.4).

The cross-correlated vector $\underline{R}(\omega)$ given by Eq.(3.5) is usually integrated both within a frequency bandwidth and a time period to reduce the contribution of the noises. The signal-to-noise ratio (SNR) of the integrated cross-correlated vector is given as⁽²⁾

$$\text{SNR} = \sqrt{\frac{T_{a1}T_{a2}}{T_{s1}T_{a2} + T_{a1}T_{s2} + T_{s1}T_{s2}}} 2BT \quad (3.8)$$

where

B : observation bandwidth

T : integration time.

Since 2B is a sample frequency, 2BT is the data number in the integration period. The variance of the correlated phase

estimate $\hat{\phi}_1$ is given as

$$\sigma_{\hat{\phi}}^2 = \left(\frac{1}{\text{SNR}} \right)^2 \quad (3.9)$$

In Eq.(3.8) it is assumed that the coherency of the received signals are completely kept through the VLBI signal processing. Actually, however, the received signals are converted into video signals and sampled and digitized. In the above processes some of the coherency is lost and the effect can be described by coherence loss coefficients L_1 and L_2 for the stations 1 and 2, respectively. Therefore, a more practical formulation of SNR is

$$\text{SNR}_L = \sqrt{\frac{L_1 L_2 T_{a1} T_{a2} 2BT}{L_2 T_{s1} T_{a2} + L_1 T_{a1} T_{s2} + T_{s1} T_{s2}}} \quad (3.10)$$

Using Eq.(3.10), we obtain a SNR formulation for quasar observations (where $T_{s1}, T_{s2} \gg T_{a1}, T_{a2}$) as

$$\text{SNR}_L(\text{quasar}) = \sqrt{L_1 L_2 \frac{T_{a1} T_{a2}}{T_{s1} T_{s2}} 2BT} \quad (3.11)$$

On the other hand, in the case of spacecraft signal observations where the relations $T_{s1}, T_{s2} \ll T_{a1}, T_{a2}$ are satisfied, we obtain

$$\text{SNR}_L(\text{spacecraft}) = \sqrt{\frac{1}{\frac{T_{s1}}{L_1 T_{a1}} + \frac{T_{s2}}{L_2 T_{a2}}} 2BT} \quad (3.12)$$

When we observe a tone signal transmitted from a spacecraft it

is effective to use a local phase model⁽⁶⁾ to raise SNR. That is, the observed tone at a VLBI station is correlated with predicted noise free tone model (local phase model). By differentiating the correlated phases at two VLBI stations the fringe phase between the spacecraft tones received at the two stations is obtained. In the process of the correlation using a local phase model, SNR is written as

$$\text{SNR}_L(\text{local phase model}) = \sqrt{\frac{LP_S}{P_N} 2BT} \quad (3.13)$$

where

- L : coherence loss coefficient
- P_S : spacecraft tone power
- P_N : noise power in the pass-band

3.2.2 Derivation of VLBI Observables

The geometric observables τ and $\dot{\tau}$ in VLBI are given as slopes of the phase of a cross-spectral function with respect to angular frequency and time (see Eqs.(3.6) and (3.7)). The cross-spectral function is obtained as a Fourier transform of a cross-correlation function in time domain. In a usual VLBI signal processing, the received signals at many observation frequencies are sampled and digitized, then they are cross-correlated in time domain with short integration time for

a few seconds. In the cross-correlation process, phase rotations by predicted delay and delay rate are applied. The obtained cross-correlation function is Fourier transformed into frequency domain to give a cross-spectral signal vector $\underline{S}_{jk}(\omega_j, t_k)$ at an angular frequency ω_j and time t_k . This is defined as

$$\underline{S}_{jk}(\omega_j, t_k) = \frac{1}{B'T'} \int_{\omega_j - B'/2}^{\omega_j + B'/2} \int_{t_k - T'/2}^{t_k + T'/2} \underline{R}(\omega) d\omega dt \quad (3.14)$$

where B' is a receiving bandwidth, and T' is a few second of integration time. Eq.(3.14) is rewritten in a form

$$\begin{aligned} \underline{S}_{jk}(\omega_j, t_k) &= S_{jk} \exp(i\phi_{jk}), \\ \phi_{jk} &= \phi_0 + \omega_j(\Delta\tau + \Delta\dot{\tau}t_k) + \phi_{njk} \end{aligned} \quad (3.15)$$

where

ϕ_0 : fringe phase at $(\omega_j, t_k) = (0,0)$

ϕ_{njk} : phase noise due to receiving system noise.

The delay and delay rate observables τ and $\dot{\tau}$ are derived by using cross-spectral vectors \underline{S}_{jk} at many ω_j and t_k . Two typical methods have been developed : one is a coherent phase method and the other is a phase tracking method.

(1) Coherent Phase Method⁽²⁾

In Eq.(3.15) it is expected that every \underline{S}_{jk} at various ω_j and t_k has the same phase ϕ_0 except random noise ϕ_{njk} when

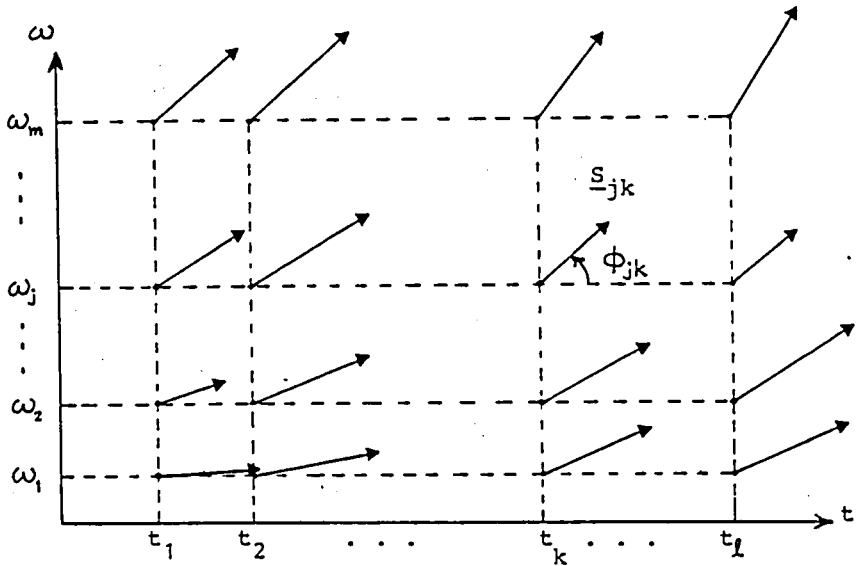
the predicted delay and delay rate coincide with the true values of them, that is, $\Delta\tau = \dot{\Delta\tau} = 0$ (see Eq.(3.4)). This means that a vector-sum of \underline{S}_{jk} becomes the largest when $\Delta\tau = \dot{\Delta\tau} = 0$. In order to get $\Delta\tau = \dot{\Delta\tau} = 0$, we can equivalently eliminate $\Delta\tau$ and $\dot{\Delta\tau}$ in Eq.(3.15) by counter-phase rotation using their estimates $\hat{\Delta\tau}$ and $\hat{\dot{\Delta\tau}}$ as

$$\underline{S}_{jk} \exp \left\{ -i \omega_j (\hat{\Delta\tau} + \hat{\dot{\Delta\tau}} t_k) \right\} = S_{jk} \exp \left[i \phi_0 + i \omega_j \left\{ (\Delta\tau - \hat{\Delta\tau}) + (\dot{\Delta\tau} - \hat{\dot{\Delta\tau}}) t_k \right\} + i \phi_{nj k} \right].$$

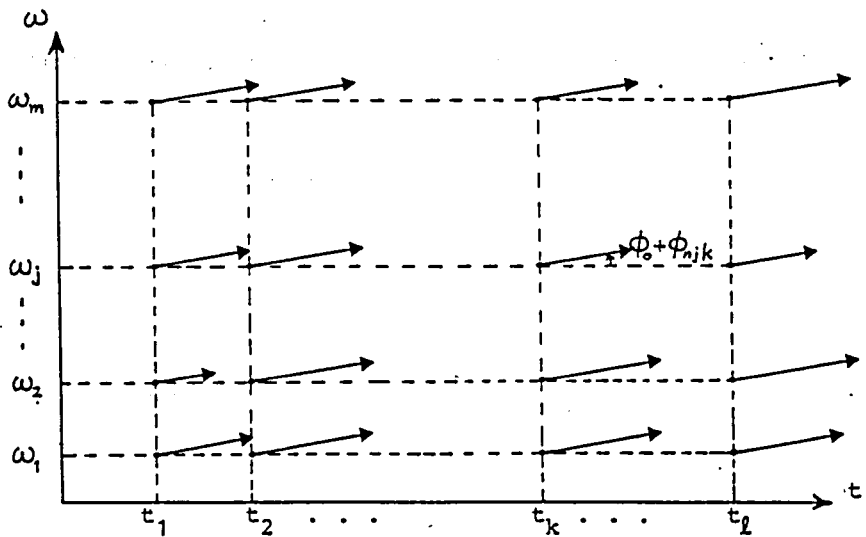
The coherent phase method gives optimum estimates of $\hat{\Delta\tau}$ and $\hat{\dot{\Delta\tau}}$ which eliminate the residual $(\Delta\tau - \hat{\Delta\tau})$ and $(\dot{\Delta\tau} - \hat{\dot{\Delta\tau}})$. This is done by searching $\hat{\Delta\tau}$ and $\hat{\dot{\Delta\tau}}$ which maximize the following summed cross-spectral vector \underline{S}_{Σ} ,

$$\begin{aligned} \underline{S}_{\Sigma} &= \sum_{j=1}^m \sum_{k=1}^{\ell} \underline{S}_{jk} \exp \left\{ -i \omega_j (\hat{\Delta\tau} + \hat{\dot{\Delta\tau}} t_k) \right\} \\ &= \exp(i \phi_0) \sum_{j=1}^m \sum_{k=1}^{\ell} S_{jk} \exp \left[i \omega_j \left\{ (\Delta\tau - \hat{\Delta\tau}) + (\dot{\Delta\tau} - \hat{\dot{\Delta\tau}}) t_k \right\} + i \phi_{nj k} \right] \end{aligned} \quad (3.16)$$

Fig. 3.4 shows the vectors \underline{S}_{jk} in (ω_j, t_k) plane. At first, \underline{S}_{jk} do not lie in the same direction because the predicted delay and delay rate do not coincide with the true counterparts of them (Fig.3.4(a)). The counter rotation of the phase by the optimum $\hat{\Delta\tau}$ and $\hat{\dot{\Delta\tau}}$ aligns the vector \underline{S}_{jk} in the direction of which the average phase is ϕ_0 (there still remains the effect of



(a)



(b)

Fig.3.4 Cross-spectral vectors in (ω, t) -plane
 (a) With residual delay and delay rate
 (b) Without residual delay nor delay rate

phase noise ϕ_{njk} , Fig.3.4(b)). From $\Delta\hat{\tau}$ and $\Delta\hat{\dot{\tau}}$ we obtain the estimates of delay $\hat{\tau}$ and delay rate $\hat{\dot{\tau}}$ as

$$\left. \begin{aligned} \hat{\tau} &= \tilde{\tau} + \Delta\hat{\tau} \\ \hat{\dot{\tau}} &= \tilde{\dot{\tau}} + \Delta\hat{\dot{\tau}} \end{aligned} \right\} \quad (3.17)$$

Let us discuss the accuracies of the estimates $\Delta\hat{\tau}$ and $\Delta\hat{\dot{\tau}}$. Define a vector \underline{S}_Δ as the right-hand side of Eq.(3.16) excluding the term $\exp(i\phi_0)$,

$$\underline{S}_\Delta = \sum_{j,k} S_{jk} \exp \left\{ -i\omega_j(x + yt_k) + i\phi_{njk} \right\} \quad (3.18)$$

where

$$\left. \begin{aligned} x &= \Delta\hat{\tau} - \Delta\tau \\ y &= \Delta\hat{\dot{\tau}} - \Delta\dot{\tau} \end{aligned} \right\} \quad (3.19)$$

When the $\Delta\hat{\tau}$ and $\Delta\hat{\dot{\tau}}$ are effectively estimated, both x and y approach to zeros and we can write

$$\begin{aligned} \|\underline{S}_\Delta\| &\doteq \sum_{j,k} S_{jk} \cos \left\{ -\omega_j(x + yt_k) + \phi_{njk} \right\} \\ &\doteq \sum_{j,k} S_{jk} \left[1 - \left\{ -\omega_j(x + yt_k) + \phi_{njk} \right\}^2 / 2 \right] \end{aligned} \quad (3.20)$$

Since $\Delta\hat{\tau}$ and $\Delta\hat{\dot{\tau}}$ are obtained as those which maximize Eq.(3.20), we obtain the equivalent relation which gives x and y as

$$\sum_{j,k} S_{jk} \left\{ -\omega_j(x + yt_k) + \phi_{njk} \right\}^2 \longrightarrow \text{minimum} \quad (3.21)$$

This is a weighted least-square method to solve x and y .

In other words, x and y are solved through a linear fitting to the data ϕ_{njk} . Eq.(3.21) is rewritten in a matrix form

$$(\underline{H}\underline{x} - \underline{z})^T \underline{S} (\underline{H}\underline{x} - \underline{z}) \rightarrow \text{minimum} \quad (3.21')$$

where

$$\underline{H} = \begin{bmatrix} \vdots & \vdots \\ \omega_j & \omega_j t_k \\ \vdots & \vdots \end{bmatrix} \quad (2 \times (mx \ell)) \quad (3.22)$$

$$\underline{x} = \begin{bmatrix} x \\ y \end{bmatrix} \quad (1 \times 2) \quad (3.23)$$

$$\underline{z} = \begin{bmatrix} \vdots \\ \phi_{njk} \\ \vdots \end{bmatrix} \quad (1 \times (mx \ell)) \quad (3.24)$$

$$\underline{S} = \begin{bmatrix} \cdot & \cdot & \cdot & 0 \\ \cdot & \cdot & \cdot & \cdot \\ \cdot & \cdot & S_{jk} & \cdot \\ 0 & \cdot & \cdot & \cdot \end{bmatrix} \quad ((mx \ell) \times (mx \ell)) \quad (3.25)$$

The covariance matrix C of the estimates \underline{x} is given by

$$C = (\underline{H}^T \underline{S} \underline{H})^{-1} \underline{H}^T \{ \text{cov}(\phi_{njk}) \}^{-1} \underline{H} (\underline{H}^T \underline{S} \underline{H})^{-1}, \quad (3.26)$$

$$\{ \text{cov}(\phi_{njk}) \}^{-1} = \begin{bmatrix} \cdot & \cdot & \cdot & 0 \\ \cdot & \cdot & \cdot & \cdot \\ \cdot & \cdot & (\text{SNR}_{jk})^2 & \cdot \\ 0 & \cdot & \cdot & \cdot \end{bmatrix}$$

where $\{ \text{cov}(\phi_{njk}) \}^{-1}$ is given by Eq.(3.9) and SNR_{jk} corresponds to cross-spectral signal vector \underline{S}_{jk} .

In Eq.(3.21) S_{jk} is used as a weighting factor. It should be, however, replaced by $(\text{SNR}_{jk})^2$ from the viewpoint of the optimum estimation where the covariance matrix is

minimized⁽²⁵⁾. That is, $\hat{\Delta\tau}$ and $\hat{\Delta\hat{\tau}}$ should be obtained by

$$\sum_{j,k} (\text{SNR}_{jk})^2 \exp \left\{ -i \omega_j (x + yt_k) \right\} \longrightarrow \text{minimum} \quad (3.27)$$

Then the covariance matrix of the estimates $\hat{\Delta\tau}$ and $\hat{\Delta\hat{\tau}}$ is given by

$$C_{\hat{\tau}\hat{\tau}} = \left[H^T \begin{bmatrix} \ddots & & 0 \\ & \text{SNR}_{jk}^2 & \\ 0 & & \ddots \end{bmatrix} H \right]^{-1} \quad (3.28)$$

As a simple application of Eq.(3.28), let us calculate the variance of $\hat{\Delta\hat{\tau}}$ where only $\Delta\tau$ is estimated with fixed $\Delta\hat{\tau}$. In this case we can use a linear fitting function ($\omega_j x + c_0$) in Eq.(3.21), where c_0 is a constant. Then we obtain

$$H = \begin{bmatrix} \omega_1 & 1 \\ \vdots & \vdots \\ \omega_m & 1 \end{bmatrix} \quad (3.29)$$

$$\underline{x} = \begin{bmatrix} x \\ c_0 \end{bmatrix} \quad (3.30)$$

According to Eq.(3.28), the covariance matrix becomes

$$C_{\hat{x}c_0} = \left[H^T \begin{bmatrix} \ddots & & 0 \\ & \text{SNR}_j^2 & \\ 0 & & \ddots \end{bmatrix} H \right]^{-1}, \quad j=1, \dots, m$$

$$= \frac{1}{\sum_j \omega_j^2 \text{SNR}_j^2 \sum_j \text{SNR}_j^2 - (\sum_j \omega_j \text{SNR}_j^2)^2} \cdot \begin{bmatrix} \sum_j \text{SNR}_j^2 & -\sum_j \omega_j \text{SNR}_j^2 \\ -\sum_j \omega_j \text{SNR}_j^2 & \sum_j \omega_j^2 \text{SNR}_j^2 \end{bmatrix} \quad (3.31)$$

When $\text{SNR}_j = \text{SNR}$ ($j=1,2,\dots,m$), we obtain a simple expression for the variance of the delay estimate $\Delta \hat{\tau}$ from the (1,1) element of matrix $c_{\hat{\tau}c_0}$ as

$$\sigma_{\Delta \hat{\tau}}^2 = \sigma_{\hat{\tau}}^2 = \frac{1}{\text{SNR}^2} \frac{1}{\sum_j \omega_j^2 - m (\sum_j \omega_j / m)^2}$$

or

$$\sigma_{\Delta \hat{\tau}}^2 = \frac{1}{\text{SNR}^2} \frac{1}{\omega_{\text{eff}}^2}, \quad (3.32)$$

$$\omega_{\text{eff}}^2 = \sum_j (\omega_j - \bar{\omega})^2, \quad \bar{\omega} = \sum_j \omega_j / m$$

where ω_{eff} is effective angular frequency distribution.

A similar expression for the variance of the delay rate estimate is derived as

$$\sigma_{\Delta \hat{\tau}}^2 = \frac{1}{\text{SNR}^2} \frac{1}{\omega_j^2 T_{\text{eff}}^2} \quad (3.33)$$

$$T_{\text{eff}}^2 = \sum_k \frac{\ell}{k} (t_k - \bar{t})^2, \quad \bar{t} = \sum_k t_k / \ell$$

Eqs.(3.32) and (3.33) agree with those which were obtained by other linear fitting methods to the cross-spectral phase with

respect to angular frequency and time⁽²⁾⁽²⁶⁾.

It should be noted, however, that the expression in Eq.(3.28) is more general for the covariance of simultaneous delay and delay rate estimates.

(ii) Phase Tracking Method

The phase of a cross-spectral vector $\underline{S}_{jk}(\omega_j, t_k)$ given in Eq.(3.15) rotates in time because of residual delay rate $\Delta\dot{\tau}$. In a phase tracking method the phase of \underline{S}_{jk} at an angular frequency ω_j is tracked and is fit by a sinusoidal function. As is clear from Eq.(3.15), the angular frequency of the fitted sinusoidal function is expected to be $\omega_j \Delta\dot{\tau}$. Fig.3.5 shows phase trackings at two angular frequencies ω_1 and ω_2 . The accuracy of the estimated $\Delta\dot{\tau}$ is equivalent to that obtained by coherent phase method.

A delay estimate is obtained in the phase tracking method, for example, from a fit pair of phases at ω_i and ω_j as

$$\hat{\Delta\dot{\tau}} = \frac{\phi(\omega_j, t_k) - \phi(\omega_i, t_k)}{\omega_j - \omega_i} + \frac{2\pi N}{\omega_j - \omega_i} \quad (3.34)$$

(N : integer)

where the second term means an ambiguity. We can also use

many angular frequency points $\omega_1, \omega_2, \dots, \omega_m$ to estimate $\hat{\Delta\dot{\tau}}$

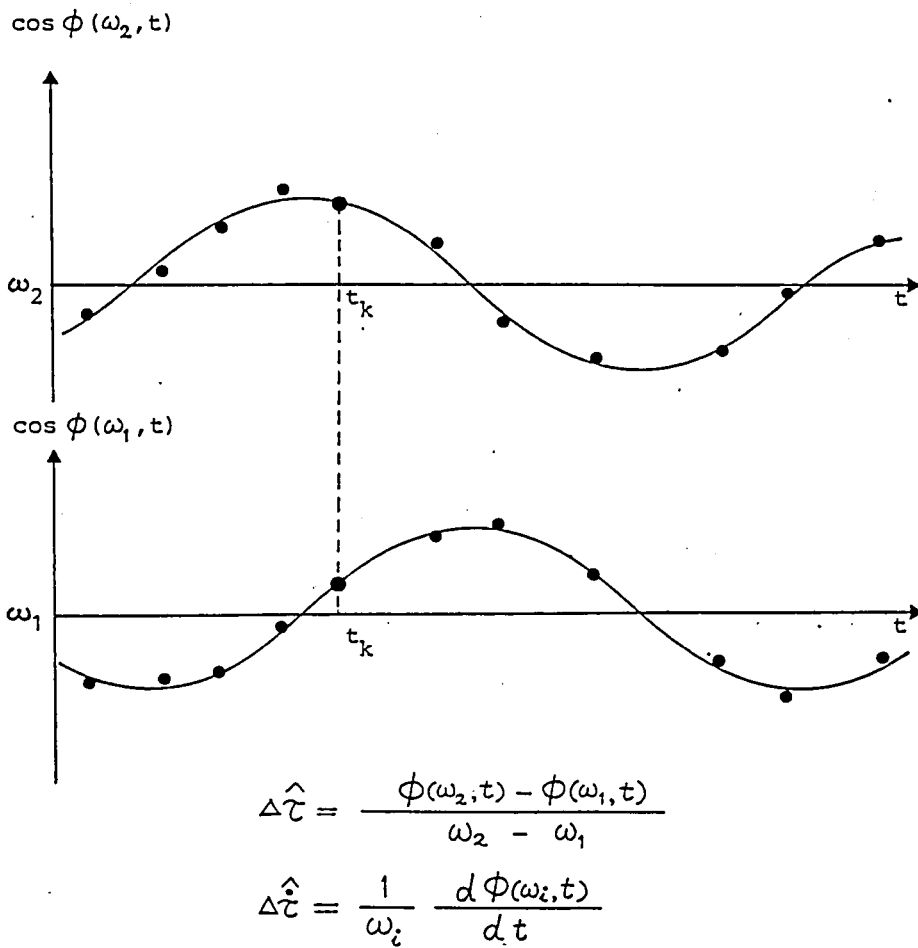


Fig.3.5 Correlated phases tracked at two frequencies

by a linear fitting to phases $\phi(\omega_j, t_k)$ by weighting according to the accuracy of each phase data. This process is fundamentally same as that in the coherent phase method.

The phase tracking method is essentially useful in a DVLBI data processing. Suppose that the DVLBI observations are made at two angular frequencies ω_1 and ω_2 , for example, in the case of a spacecraft which transmits two tones at these frequencies. Hereafter we only consider $\Delta\tau$ estimation. The cross-spectral phases(or fringe phases) at ω_1 and ω_2 are written for a satellite observation as

$$\left. \begin{aligned} \phi_{s1}(t) &= \phi_{s0} + \phi_{I1} + \omega_1 \Delta\tau_s + \phi_{sn1}(t) \\ \phi_{s2}(t) &= \phi_{s0} + \phi_{I2} + \omega_2 \Delta\tau_s + \phi_{sn2}(t) \end{aligned} \right\} (3.35)$$

where

$\phi_{si}(t)$: cross-spectral phase at ω_i

ϕ_{s0} : cross-spectral phase independent to
frequency

ϕ_{Ii} : phase rotation by the receiving instrument
at ω_i

$\Delta\tau_s$: satellite delay (residual delay from a
prediction)

ϕ_{sni} : phase noise at ω_i

We obtain similar expressions for a quasar observation as

$$\left. \begin{aligned} \phi_{q1}(t) &= \phi_{q0} + \phi_{I1} + \omega_1 \Delta\tau_q + \phi_{qn1}(t) \\ \phi_{q2}(t) &= \phi_{q0} + \phi_{I2} + \omega_2 \Delta\tau_q + \phi_{qn2}(t) \end{aligned} \right\} (3.36)$$

where the subscript "q" indicates quasar. A delay estimate $\hat{\Delta\tau}_s$ for the satellite observation is given by Eq.(3.34) as

$$\hat{\Delta\tau}_s = \Delta\tau_s + \frac{\Delta\phi_I + \Delta\phi_{sn}}{\omega_2 - \omega_1} \quad (3.37)$$

where

$$\left. \begin{aligned} \Delta\phi_I &= \phi_{I2} - \phi_{I1} \\ \Delta\phi_{sn} &= \phi_{sn2} - \phi_{sn1} \end{aligned} \right\} \quad (3.38)$$

A quasar delay estimate $\hat{\Delta\tau}_q$ is similarly given as

$$\hat{\Delta\tau}_q = \Delta\tau_q + \frac{\Delta\phi_I + \Delta\phi_{qn}}{\omega_2 - \omega_1} \quad (3.39)$$

where

$$\Delta\phi_{qn} = \phi_{qn2} - \phi_{qn1} \quad (3.40)$$

and $\Delta\phi_I$ is assumed to be the same as that in the satellite observation. A DVLBI delay observable $\hat{\Delta\tau}_0$, which is defined as the difference between $\hat{\Delta\tau}_s$ and $\hat{\Delta\tau}_q$, is

$$\begin{aligned} \hat{\Delta\tau}_0 &= \hat{\Delta\tau}_s - \hat{\Delta\tau}_q \\ &= \Delta\tau_s - \Delta\tau_q + \frac{\Delta\phi_{sn} - \Delta\phi_{qn}}{\omega_2 - \omega_1} \end{aligned} \quad (3.41)$$

The last term of Eq.(3.41) contains only random errors due to receiver system noises and so on, which can be reduced by attaining a sufficient SNR and a lot of observations.

The effect of $\Delta\phi_I$ vanishes, or in other words, systematic phase rotations in receiving equipment do not affect the DVLBI delay observable.

On the other hand, we obtain a different result in the coherent phase method. First, in the case of satellite observation, the residual phases $\Delta\phi_{s1}$ and $\Delta\phi_{s2}$ are defined using Eq.(3.35) as

$$\left. \begin{aligned} \Delta\phi_{s1} &= \phi_{s1}(t) - \phi_{s0} - \phi_{I1} - \omega_1 \Delta\hat{\tau}_s \\ &= \omega_1(\Delta\tau_s - \Delta\hat{\tau}_s) + \phi_{sn1}(t) \\ \Delta\phi_{s2} &= \phi_{s2}(t) - \phi_{s0} - \phi_{I1} - \omega_2 \Delta\hat{\tau}_s \\ &= \omega_2(\Delta\tau_s - \Delta\hat{\tau}_s) + \phi_{sn2}(t) + \Delta\phi_I \end{aligned} \right\} (3.42)$$

where

$$\begin{aligned} \Delta\phi_I &= \phi_{I2} - \phi_{I1} \\ \Delta\hat{\tau}_s &: \text{satellite delay estimate} \end{aligned} \quad (3.43)$$

In the coherent phase method, $\Delta\hat{\tau}_s$ is estimated by minimizing a weighted square-sum, that is,

$$\text{SNR}_{s1}^2 \Delta\phi_{s1}^2 + \text{SNR}_{s2}^2 \Delta\phi_{s2}^2 \longrightarrow \text{minimum} \quad (3.44)$$

Substituting Eq.(3.42) into Eq.(3.44) we solve $\Delta\hat{\tau}_s$ as

$$\Delta\hat{\tau}_s = \Delta\tau_s + \Delta\tau_{ns} + \Delta\tau_{Is} \quad (3.45)$$

where

$$\Delta\tau_{ns} = \frac{\text{SNR}_{s1}^2 \omega_1 \phi_{sn1} + \text{SNR}_{s2}^2 \omega_2 \phi_{sn2}}{\text{SNR}_{s1}^2 \omega_1^2 + \text{SNR}_{s2}^2 \omega_2^2} \quad (3.46)$$

$$\Delta\tau_{Is} = \frac{\text{SNR}_{s2}^2 \omega_2 \Delta\phi_I}{\text{SNR}_{s1}^2 \omega_1^2 + \text{SNR}_{s2}^2 \omega_2^2} \quad (3.47)$$

The quasar delay estimate $\hat{\Delta\tau}_q$ is obtained by a similar process as

$$\hat{\Delta\tau}_q = \Delta\tau_q + \Delta\tau_{nq} + \Delta\tau_{Iq} \quad (3.48)$$

$$\Delta\tau_{nq} = \frac{\text{SNR}_{q1}^2 \omega_1 \phi_{qn1} + \text{SNR}_{q2}^2 \omega_2 \phi_{qn2}}{\text{SNR}_{q1}^2 \omega_1^2 + \text{SNR}_{q2}^2 \omega_2^2} \quad (3.49)$$

$$\Delta\tau_{Iq} = \frac{\text{SNR}_{q2}^2 \omega_2 \Delta\phi_I}{\text{SNR}_{q1}^2 \omega_1^2 + \text{SNR}_{q2}^2 \omega_2^2} \quad (3.50)$$

Using Eqs.(3.45) and (3.48), DVLBI delay observable is written as

$$\hat{\Delta\tau}_o = \Delta\tau_s - \Delta\tau_q + \Delta\tau_{ns} - \Delta\tau_{nq} + \Delta\tau_{IS} - \Delta\tau_{Iq} \quad (3.51)$$

The term $(\Delta\tau_{ns} - \Delta\tau_{nq})$ is inherently random, but the term $(\Delta\tau_{IS} - \Delta\tau_{Iq})$ has usually a systematic component. The latter term only vanishes when SNR is independent to angular frequencies ω_1, ω_2 for both satellite and quasar observations.

In a DVLBI between a satellite and a quasar, it is usually the case where observed signals are completely different. Because satellite signals have usually narrowband characteristics and the power spectrum is not flat. It means that the SNR depends on frequency in a passband and the phase tracking method would be more effective than the coherent phase method.

3.3 Tracking a Geosynchronous Satellite by DVLBI Method

3.3.1 Principle of DVLBI Method

The delay observables obtained by a VLBI contain both systematic (or bias) errors and random errors. Random errors, for example, due to receiver noises and random fluctuations of propagation media, may be reduced by longer integration times and by smoothing of many observations. The systematic errors, however, must be corrected by suitable calibrations. A DVLBI calibrates systematic errors by eliminating them using radio sources with precisely known positions.

Figure 3.6 shows a geometry of DVLBI observations of a quasar and a satellite. The delay observable $\hat{\tau}_q$ obtained by a quasar observation is given as

$$\hat{\tau}_q = \tau_q + n_q \quad (3.52)$$

where τ_q is the geometrical delay and n_q is the error which consists of systematic and random errors. The τ_q is given as

$$c \tau_q = \underline{S} \cdot \underline{B} \quad (3.53)$$

where

c : velocity of light

\underline{S} : unit vector in the line-of-sight to the quasar

\underline{B} : baseline vector formed by two stations which receive the same phase of the radio wave emitted

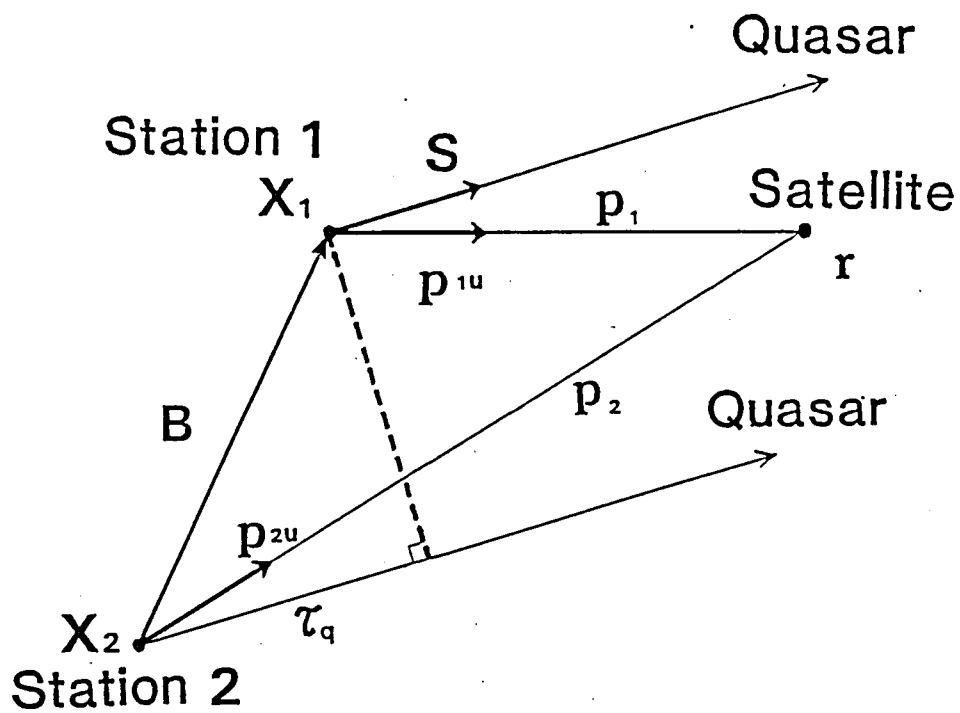


Fig. 3.6 Geometry of DVLBI observation

by the quasar

The delay observable for the satellite $\hat{\tau}_s$ is given by

$$\hat{\tau}_s = \tau_s + n_s \quad (3.54)$$

$$\tau_s = p_2 - p_1 \quad (3.55)$$

where p_1 and p_2 correspond to the propagation times which are required for the same phase of the radio wave transmitted by the satellite to arrive at the stations 1 and 2 respectively. The term n_s means errors of systematic and random for the satellite observation.

In the DVLBI method, we take the observable $\hat{\tau}_o$ which is the difference between $\hat{\tau}_q$ and $\hat{\tau}_s$, that is,

$$\hat{\tau}_o = p_2 - p_1 - \tau_q + n_s - n_q \quad (3.56)$$

When the observations of the quasar and the satellite are made under nearly same conditions (with small separation angle between radio sources and with small separation time between observations), the systematic errors in n_s and n_q are eliminated in $\hat{\tau}_o$. Since τ_q in the right-hand side of Eq.(3.56) is precisely known, we can obtain the geometrical delay observable $p_1 - p_2$ for the satellite. The remaining random errors are decreased by sufficient integration time and are smoothed out through many similar observations.

3.3.2 Sensitivity of DVLBI Observable

Let us study on the sensitivity of a DVLBI observable to geometrical parameters. In Eq.(3.56), the term $p_2 - p_1$ is

written as

$$p_2 - p_1 = \| \underline{r} - \underline{x}_2 \| - \| \underline{r} - \underline{x}_1 \| \quad (3.57)$$

where

\underline{r} : satellite position vector where the satellite transmitted the signal which is observed by VLBI

\underline{x}_i : position vector of station i which receives the signal transmitted by the satellite at \underline{r} .

Using Eqs.(3.53) and (3.57), the sensitivity equation of DVLBI delay observable $\hat{\tau}_0$ is given as

$$c \Delta \hat{\tau}_0 = (p_{2u} - p_{1u}) \cdot \Delta \underline{r} + (\underline{S} - p_{2u}) \cdot \Delta \underline{x}_2 - (\underline{S} - p_{1u}) \cdot \Delta \underline{x}_1 - \underline{B} \cdot \Delta \underline{S} \quad (3.58)$$

where

$\Delta \hat{\tau}_0$: variation of $\hat{\tau}_0$ due to variations (or errors) in geometrical parameters

p_{iu} : unit vector pointing to the satellite at station i

$\Delta \underline{r}$: variation of satellite position

$\Delta \underline{x}_i$: error in station(i) location

$\Delta \underline{S}$: error in quasar position

The first term of the right-hand side in Eq.(3.58) shows that a DVLBI delay observable is sensitive to the satellite position deviation in the direction of the differenced vector $(p_{2u} - p_{1u})$. Figure 3.7 shows $(p_{2u} - p_{1u})$. As is clear from Fig. 3.7 a DVLBI delay observable has information on position deviation in the plane which is nearly (completely in

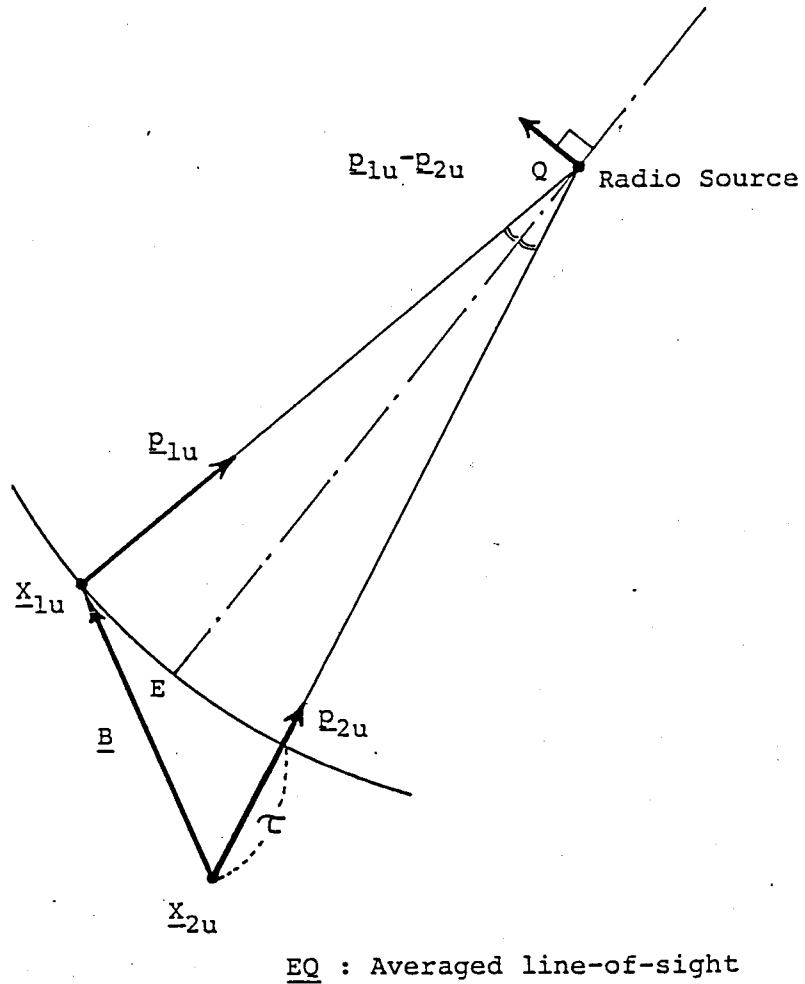
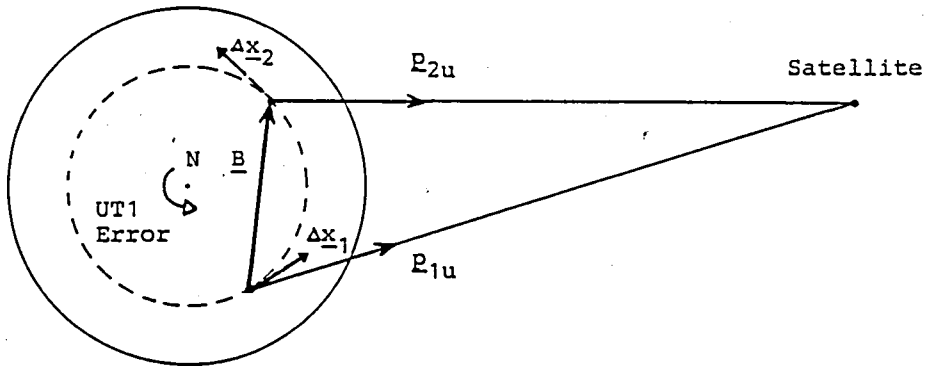


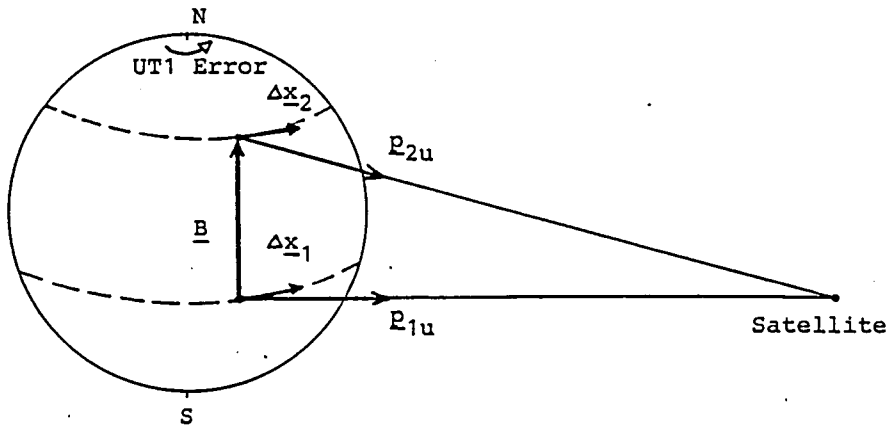
Fig.3.7 Sensitivity of delay observable with respect to radio source position

the case of infinite radio source) perpendicular to the line-of-sight. In other words, the DVLBI delay observable gives angle information as described in Sec. 2.3.1. If we need complete angle information on the radio source, another baseline vector which has component perpendicular to the plane spanned by \underline{B} and \underline{p}_{1u} (or \underline{p}_{2u}) is required.

The terms including $\Delta \underline{x}_i$ ($i=1,2$) show the sensitivity of $\hat{\tau}_0$ to station location errors. In DVLBI observations, since separation angle between a quasar and the satellite is selected small, the vector ($\underline{S} - \underline{p}_{iu}$) in Eq.(3.58) is nearly perpendicular to the line-of-sight to the quasar or the satellite at station i . Consequently, the components of station location errors projected on to that perpendicular plane may affect the DVLBI delay observable. Besides geodetic errors, we also treat modeling errors in UT1 and polar motion as factors which cause station location errors. Because those errors cause systematic errors in calculation of station positions in an inertial coordinate system. The UT1 error causes station location errors along with station motions by the earth's spin. That is, the sensitivity of $\hat{\tau}_0$ to UT1 error depends on orientation of a baseline. Figure 3.8 shows two cases of satellite observations, one is sensitive to UT1 error and the other is not. In the DVLBI geometry shown as the case (b) in Fig. 3.8, contributions by $\Delta \underline{x}_1$ and $\Delta \underline{x}_2$ eliminate each other.



(a) \underline{B} : perpendicular to the spin axis
 DVLBI delay observable is affected by $\Delta\underline{x}_1$ and $\Delta\underline{x}_2$



(b) \underline{B} : parallel to the spin axis
 DVLBI observable is insensitive to $\Delta\underline{x}_1$ and $\Delta\underline{x}_2$

Fig.3.8 Sensitivity of VLBI delay to UT1 correction error

The remaining term $\underline{B} \cdot \underline{\Delta S}$ shows the sensitivity to the quasar position error. It is clear that the position error in the direction of \underline{B}_\perp which is the perpendicular component of \underline{B} to the line-of-sight affects a DVLBI delay observable.

The delay observable has information on the parameters to which the observable has sensitivity. We are sometimes interested in estimating both satellite position (orbit) and station locations, because we are not always given exact station location data. According to the above sensitivity analysis, we can estimate station position components in the plane perpendicular to the line-of-sight. In other words, we hardly expect any information of station position components in the line-of-sight direction.

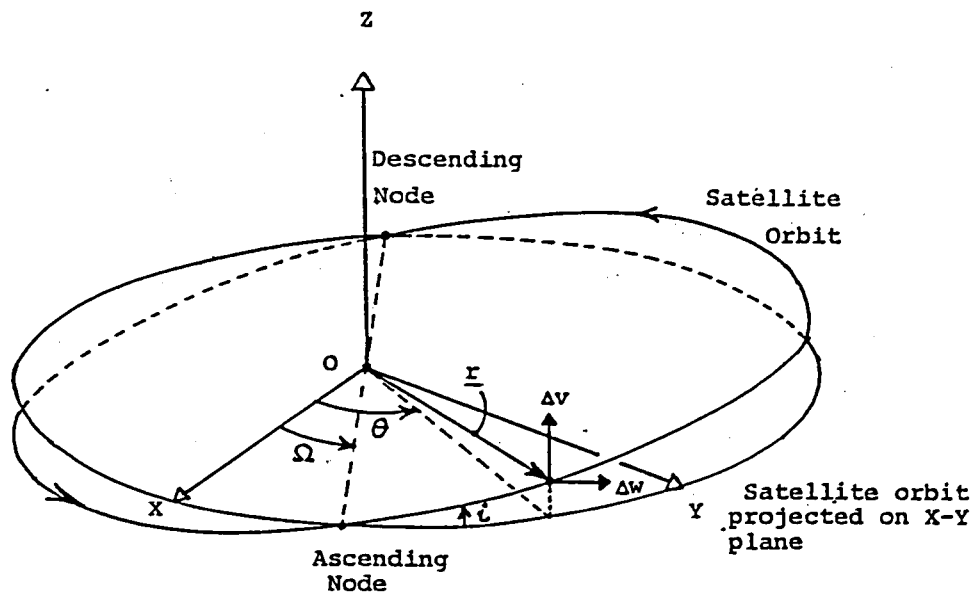
3.3.3 DVLBI as Tracking Method for Geosynchronous Satellite

As is shown in Sec. 3.3.2, a DVLBI delay observable has information on satellite position components in the plane nearly perpendicular to the line-of-sight. On the contrary, range or summed range observables defined in Sec. 2.1.2 have complementary sensitivity. That is, in Fig. 3.7 a range observable at station i has sensitivity to the satellite position component in the direction of \underline{p}_{iu} and a summed range obtained by observations at stations 1 and 2 has sensitivity to the satellite position component in the direction of $(\underline{p}_{1u} +$

p_{2u}). In the case of a geosynchronous satellite, a delay rate observable of a DVLBI is not so useful as a delay observable, because the delay rate is very small. Due to the same reason, the range rate observable is not used for a geosynchronous satellite.

A combination of DVLBI observations and range or summed range observations gives complete information on a satellite three dimensional position vector. Using these observables at different observation times we can determine the satellite orbit. However, from the viewpoint of highly accurate orbit determination, there are disadvantages to use various types of tracking data. Because, each type of tracking method contains errors in its observation model parameters. This fact leads to a large number of model parameters which have possible errors in an orbit determination process.

The DVLBI delay observables obtained by appropriate baselines can supply complete observability with respect to a geosynchronous satellite orbit. Let us discuss a basic concept of the observability. With two different baseline vectors, DVLBI delay observables supply position information of a geosynchronous satellite in the plane perpendicular to the radial vector. Because, an averaged line-of-sight (EQ in Fig.3.7) for a baseline on the earth is nearly in the direction of the satellite's radial vector. Figure 3.9 shows small position deviation vectors Δw and Δv which are



- XYZ : Inertial coordinate system
- \underline{r} : Satellite's radial vector
- Ω : Right ascension of ascending node
- θ : Satellite's longitude
- i : Orbital inclination
- $(\Delta v, \Delta w)$: Satellite position deviation

Fig.3.9 Geosynchronous satellite orbit and small position deviations observed by DVLBI

perpendicular to the radial vector and can be observed by DVLBI. Δw and Δv are parallel to the earth's equatorial plane and to the spin axis, respectively. Δw and Δv are given from a satellite's position deviation in the inertial frame (ΔX , ΔY , ΔZ) through a linear transformation as,

$$\begin{pmatrix} \Delta w \\ \Delta v \end{pmatrix} = \begin{pmatrix} -\sin\theta & \cos\theta & 0 \\ 0 & 0 & 1 \end{pmatrix} \begin{pmatrix} \Delta X \\ \Delta Y \\ \Delta Z \end{pmatrix} \quad (3.59)$$

where θ is the satellite's longitude in the inertial coordinate system.

On the other hand, the position of a geosynchronous satellite in the inertial frame is easily described by coordinate transformation from an orbit plane coordinate system as

$$\begin{pmatrix} X \\ Y \\ Z \end{pmatrix} = G \begin{pmatrix} x \\ y \\ 0 \end{pmatrix} \quad (3.60)$$

where (x, y) is the satellite position in an orbital plane coordinate system (see Fig. 3.10), and G is a transformation matrix given as

$$G = \begin{pmatrix} \cos(\omega + \Omega) & -\sin(\omega + \Omega) & i \sin \Omega \\ \sin(\omega + \Omega) & \cos(\omega + \Omega) & -i \cos \Omega \\ i \sin \omega & i \cos \omega & 1 \end{pmatrix} \quad (3.61)$$

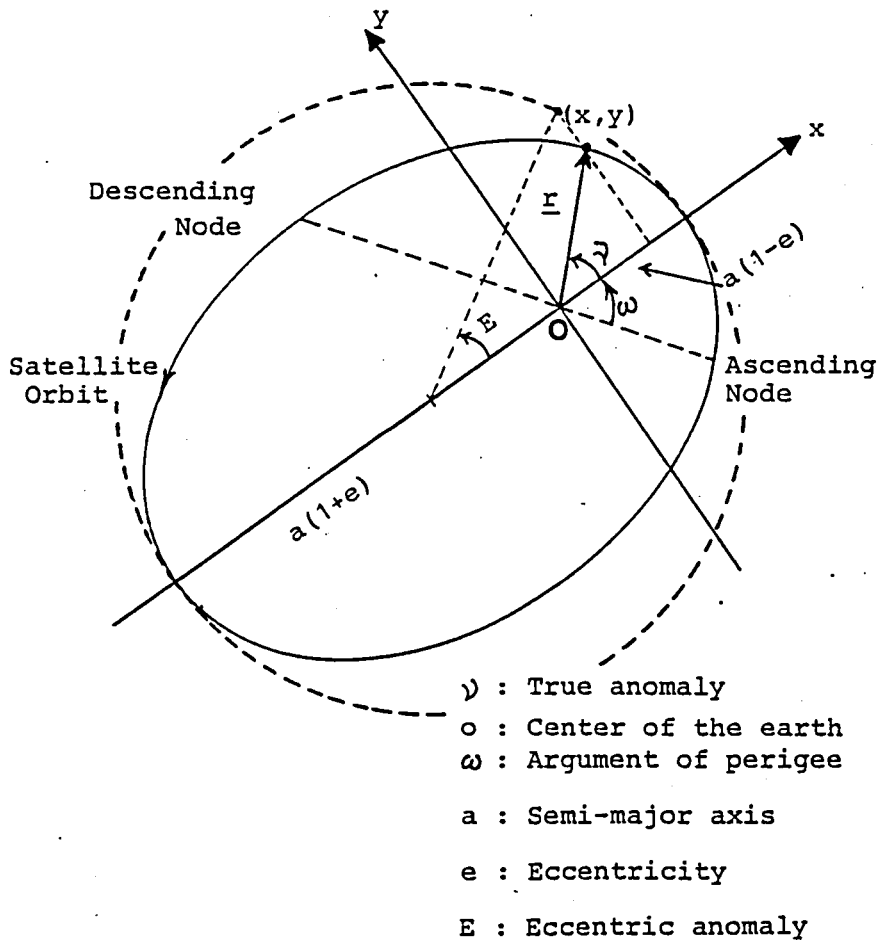


Fig. 3.10 Description of satellite position in orbital plane coordinate system

where

ω : argument of perigee

Ω : right ascension of ascending node

i : inclination (assumed to be small in the case of a geosynchronous satellite)

and they are three of six Keplerian orbital elements of the satellite. The satellite position (x, y) in the orbital plane are given by the remaining three Keplerian elements as

$$\left. \begin{aligned} x &= a(\cos E - e) \\ y &= a\sqrt{1 - e^2} \sin E \end{aligned} \right\} \quad (3.62)$$

where

a : semi-major axis

E : eccentric anomaly

e : eccentricity

In the case of a geosynchronous satellite, the eccentricity is also small. So θ is approximately written as

$$\theta \doteq \Omega + \omega + M \quad (3.63)$$

where M is the mean anomaly which has following relation with e and E,

$$M = E - e \sin E \quad (3.64)$$

Using Eqs.(3.61) and (3.62) in Eq.(3.60), (X, Y, Z) are written as functions of Keplerian elements. By partial differentiations of the (X, Y, Z) we obtain expressions for (ΔX , ΔY , ΔZ) in Eq.(3.59). Then we get finally

3.4 Errors in DVLBI Delay Observable

3.4.1 VLBI Hardware System Errors

A DVLBI delay observable has errors which are inherent to the hardware system. They are SNR error (or errors caused by system noises including sky noise, antenna noise and thermal noises in receiver system), system delay error, and clock error.

SNR Error

In the coherent phase method (Sec. 3.2.2) to estimate VLBI delay observables, SNR error of a delay observable is given by Eq.(3.32). SNR is given by Eq.(3.11) for a quasar observation, and by Eq.(3.12) or Eq.(3.13) for a satellite observation. Since these errors are independent, SNR error for a DVLBI delay observable is written as

$$\sigma_{\Delta\hat{\tau}D}^2 = \sigma_{\Delta\hat{\tau}Q}^2 + \sigma_{\Delta\hat{\tau}S}^2 \quad (3.66)$$

where

$\sigma_{\Delta\hat{\tau}D}$: SNR error of DVLBI delay observable

$\sigma_{\Delta\hat{\tau}Q}$: SNR error of quasar delay observable

$\sigma_{\Delta\hat{\tau}S}$: SNR error of satellite delay observable

In the phase tracking method (Sec. 3.2.2) to estimate a VLBI delay observable, the same discussion mentioned above is possible, except that in Eq.(3.32) the effective angular frequency ω_{eff} should be calculated using ω_i and ω_j in

Eq.(3.34). In the case of DVLBI tracking of a geosynchronous satellite, $\sigma_{\Delta\hat{\tau}_S}$ is usually much smaller than $\sigma_{\Delta\hat{\tau}_Q}$, because the signal power of a satellite is much stronger than those of quasars.

System Delay Error

Signal delays which are caused in equipment at VLBI stations are not the same nor time-invariant.

In a DVLBI a constant system delay is successfully removed. However, time-variable system delay remains due to a time difference between observations of a satellite and a quasar.

It is written as

$$\Delta\tau_{ST} = b \Delta T \quad (3.67)$$

where

$b = \dot{\tau}_{ST2} - \dot{\tau}_{ST1}$: rate of the system delay difference
between VLBI stations

$\Delta\tau_{ST}$: DVLBI delay error due to system delay rate

$\dot{\tau}_{STi}$: rate of system delay at station i

ΔT : observation time difference between satellite
and quasar

Since ΔT is about 10 to 15 minutes in typical DVLBI observations⁽²¹⁾⁽²³⁾, if $b = 0.1$ psec/sec (1 psec = 10^{-12} sec) then $\Delta\tau_{ST}$ is less than 0.1 nsec (3 cm of equivalent light pass).

Clock Error

Though a clock offset at a VLBI station directly causes a delay offset (delay bias), it is removed by a DVLBI method. However, a difference of clock rate between the VLBI stations remains as

$$\Delta\tau_f = \frac{\Delta f}{f} \Delta T \quad (3.68)$$

where

$\Delta\tau_f$: DVLBI delay error due to difference of station
clock rates difference

$\Delta f/f$: difference of clock rates

The clock rate ($\Delta f/f$) has the same effect as the geometrical delay rate in a VLBI, so it is usually estimated as well as the delay observable. If the delay rate is estimated with an accuracy of 10^{-13} , then $\Delta\tau_f$ becomes less than 0.1 nsec (3 cm).

3.4.2 Propagation Media Errors

Propagation media errors which are caused by calibration errors of delays due to the troposphere, the ionosphere and other ionized media such as the earth's magnetospheric plasma and the solar wind plasma. In order to satisfy an accuracy requirement of several centi-meters in delay measurements for geosynchronous satellite tracking, the effects of the troposphere and the ionosphere are significant.

Tropospheric Delay Calibration Error

The delay due to the troposphere (especially for a "dry" component, which means an ideal troposphere without water vapor) can be calibrated using a theoretical model of radio wave propagation⁽²⁷⁾ through the troposphere. The excess path due to water vapor ("wet" component of the troposphere) is sometimes measured with a water vapor radiometer⁽²⁸⁾⁽²⁹⁾. Calibration errors are caused in systematic (or bias) and random manners. The systematic error can be written as⁽²⁹⁾

$$\sigma_T^2 = \left(\frac{1}{\sin \tau_{s1}} - \frac{1}{\sin \tau_{q1}} \right)^2 \sigma_{Tz1}^2 + \left(\frac{1}{\sin \tau_{s2}} - \frac{1}{\sin \tau_{q2}} \right)^2 \sigma_{Tz2}^2 \quad (3.69)$$

where

σ_T : systematic calibration error in DVLBI delay
observable due to the troposphere

τ_{si} : satellite elevation angle at station i ($i=1, 2$)

τ_{qi} : quasar elevation angle at station i ($i=1, 2$)

σ_{Tzi} : systematic calibration error in the zenith
at station i ($i=1, 2$)

Eq.(3.69) means that a difference between elevation angles of satellite and a quasar causes delay error in DVLBI observable, and the error becomes larger as the elevation angles become lower. This should be considered in making an observation schedule of DVLBI measurements.

The random error caused by irregular structures of the troposphere is written as

$$\sigma_{Tr}^2 = \left\{ \left(\frac{1}{\sin \gamma_{s1}} \right)^2 + \left(\frac{1}{\sin \gamma_{q1}} \right)^2 \right\} \sigma_{Trz1}^2 + \left\{ \left(\frac{1}{\sin \gamma_{s2}} \right)^2 + \left(\frac{1}{\sin \gamma_{q2}} \right)^2 \right\} \sigma_{Trz2}^2 \quad (3.70)$$

where

σ_{Tr} : random error in DVLBI delay observable due to the troposphere

σ_{Trzi} : random tropospheric delay in the zenith at station i ($i=1,2$)

The effect of the random errors are reduced by an averaging effect by using many observations. Further considerations are made for an actual observation geometry in Chapter 5.

Ionospheric Delay Calibration Error

The ionospheric delay calibration error can similarly be divided into two types, systematic and random, errors. The systematic calibration error can be written as

$$\sigma_I^2 = \left[f(\chi_1) \left\{ g(\gamma_{s1}) - g(\gamma_{q1}) \right\} \right]^2 \sigma_{Iz1}^2 + \left[f(\chi_2) \left\{ g(\gamma_{s2}) - g(\gamma_{q2}) \right\} \right]^2 \sigma_{Iz2}^2 \quad (3.71)$$

where

σ_I^2 : systematic calibration error in DVLBI delay observable due to the ionosphere

f : solar-zenith angle factor

- χ_i : solar-zenith angle at station i (i=1, 2)
 g : elevation angle factor
 τ_{si} : satellite elevation angle at station i (i=1, 2)
 τ_{qi} : quasar elevation angle at station i (i=1, 2)
 I_{zi} : systematic calibration error in the zenith
 at station i (i=1, 2)

Eq.(3.71) is based on a simple model of the ionosphere where the total electron content in the line-of-sight to a radio source depends on elevation angle and solar-zenith angle at the station. The factor f and g are empirically given, for example, as⁽²⁹⁾

$$f(\chi) = 0.2 + 0.8(\cos \chi)^{2/3} \quad (3.72)$$

$$g(\tau) = \left[\left\{ (R_e + h_2)^2 - R_e^2 \cos^2 \tau \right\}^{1/2} - \left\{ (R_e + h_1)^2 - R_e^2 \cos^2 \tau \right\}^{1/2} \right] / (h_2 - h_1) \quad (3.73)$$

where R_e is the earth's mean radius, h_1 and h_2 are the lower and upper limits of a constant charged-particle density model of the ionosphere. The numerator of Eq.(3.73) approximates the ray path length in the modeled ionosphere, therefore $g(\tau)$ gives the excess-path ratio to the zenith path.

σ_I^2 becomes larger as elevation angle becomes lower and the separation angle between the satellite and a quasar becomes larger, which should also be considered to make a DVLBI observation schedule.

The random error caused by irregular structures of the

ionosphere is given as

$$\begin{aligned} \sigma_{Ir}^2 = & f^2(\chi_1) \left\{ g^2(\gamma_{s1}) + g^2(\gamma_{q1}) \right\} \sigma_{Irz1}^2 \\ & + f^2(\chi_2) \left\{ g^2(\gamma_{s2}) + g^2(\gamma_{q2}) \right\} \sigma_{Irz2}^2 \end{aligned} \quad (3.74)$$

where

σ_{Ir} : random error in DVLBI delay observable due to the ionosphere

σ_{Irzi} : random ionospheric delay in the zenith at station i ($i=1, 2$)

The ionospheric total electron content in the zenith at a station i is calculated using an ionospheric model or based on measurements such as Faraday rotation of the polarization angle with a beacon radio wave from a geosynchronous satellite. In order to directly obtain the ionospheric delay in the line-of-sight to a radio source, it is effective to make observations at two different frequency bands, such as 2 GHz and 8 GHz. The ionospheric delay at a frequency f_i is given as

$$\tau_{fi} = \frac{40.3}{c f_i^2} N_T \quad (3.75)$$

where

τ_{fi} : ionospheric delay (sec)

c : velocity of light (m/sec)

N_T : total electron content (m^{-2})

Using measured data of the ionospheric delay, for example, by VLBI observations at two frequencies f_1 and f_2 , N_T is obtained as

$$N_T = c (\tau_{f1} - \tau_{f2}) / 40.3 \left(\frac{1}{f_1^2} - \frac{1}{f_2^2} \right) \quad (3.76)$$

We can derive next relation for the accuracy of N_T ,

$$\sigma_{NT} = \frac{c}{40.3} \frac{f_1^2 f_2^2}{f_2^2 - f_1^2} (\sigma_{\tau f1}^2 + \sigma_{\tau f2}^2) \quad (3.77)$$

where $\sigma_{\tau fi}$ is the standard deviation of τ_{fi} . This means σ_{NT} becomes larger as the frequency difference becomes smaller. So we cannot practically obtain accurate N_T in the case of observations at frequencies which are close to each other.

Delay Errors Due to Other Ionized Media

The magnetospheric plasma, solar wind plasma and interstellar plasma cause errors in DVLBI delay observable, especially in quasar observations. However, in the case of tracking a geosynchronous satellite those errors can be neglected⁽²⁹⁾.

3.4.3 Geometric Errors

Here we discuss two geometric errors in DVLBI. One of them is station location error and the other is position error of reference radio sources (quasars). The station location error described as $\Delta \underline{x}_i$ in Sec. 3.3.2 contains geodetic station location error and modeling errors of UT1 and polar motion. It is written as

$$\Delta \underline{x}_i = A_i \Delta \underline{x}_{Si} \quad (3.78)$$

$$A_i = \begin{pmatrix} \cos \theta_i & -\sin \theta_i & 0 \\ \sin \theta_i & \cos \theta_i & 0 \\ 0 & 0 & 1 \end{pmatrix} \quad (3.79)$$

$$\Delta \underline{x}_{Si} = \begin{pmatrix} \Delta u_i \\ \Delta w_i \\ \Delta v_i \end{pmatrix} = \Delta \underline{x}_{gi} + \Delta \underline{x}_{ui} + \Delta \underline{x}_{pi} \quad (3.80)$$

where

$\Delta \underline{x}_i$: station(i) location error in the inertial coordinate system

A_i : coordinate conversion matrix

θ_i : longitude (right ascension) of station i

$\Delta \underline{x}_{Si}$: station(i) location error in the local coordinate system (Fig. 3.11).

$\Delta u_i, \Delta w_i, \Delta v_i$: components of $\Delta \underline{x}_{Si}$ in the local (u, w, v) coordinate system

$\Delta \underline{x}_{gi}$: geodetic station(i) location error

$\Delta \underline{x}_{ui}$: station(i) location error due to inaccurate UT1 model

$\Delta \underline{x}_{pi}$: station(i) location error due to inaccurate polar motion model

$\Delta \underline{x}_{gi}$ represents errors in station coordinates described using a reference ellipsoid of the earth. It has been reduced to the order of a meter or less using various satellite tracking data or VLBI observations, especially in the case of

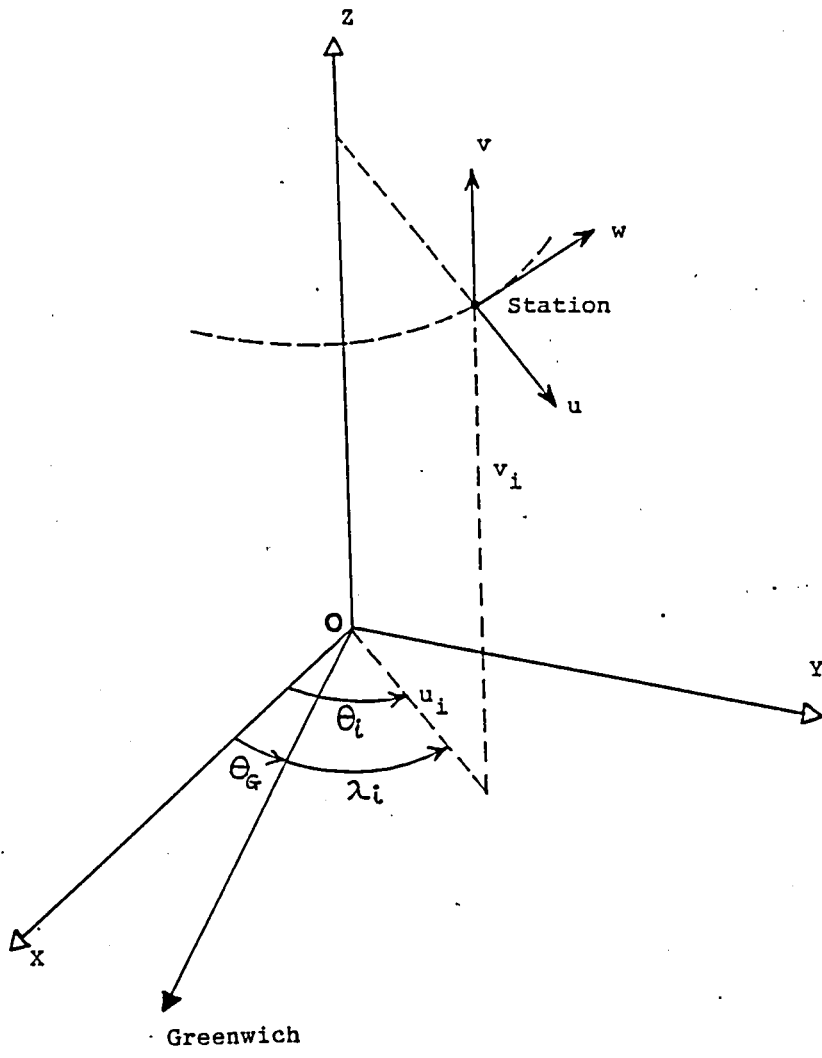


Fig.3.11 Local coordinate system to describe station location errors

important earth stations in the world. For example, positions of DSN (Deep Space Network, NASA-JPL) stations have been estimated using tracking data of deep space spacecrafts with such accuracies⁽³⁰⁾.

$\Delta \underline{x}_{ui}$ is written as

$$\Delta \underline{x}_{ui} = \underline{T}_u \Delta t_u \quad (3.81)$$

$$\underline{T}_u = \begin{pmatrix} 0 \\ \omega_e u_i \\ 0 \end{pmatrix} \quad (3.82)$$

where

\underline{T}_u : UT1 error conversion vector

Δt_u : UT1 error

ω_e : rotation rate of the earth

u_i : distance of station i from the earth's spin axis

The UT1 error is effective only in w-component (Fig. 3.11) of station location error.

$\Delta \underline{x}_{pi}$ is written as

$$\Delta \underline{x}_{pi} = P_i \Delta \underline{p} \quad (3.83)$$

$$P_i = \begin{pmatrix} -v_i \cos \lambda_i & v_i \cos \lambda_i \\ v_i \sin \lambda_i & v_i \cos \lambda_i \\ u_i \cos \lambda_i & -u_i \sin \lambda_i \end{pmatrix} \quad (3.84)$$

$$\Delta \underline{p} = \begin{pmatrix} \Delta x_p \\ \Delta y_p \end{pmatrix} \quad (3.85)$$

where

P_i : conversion matrix of polar motion errors
 Δp : polar motion modeling error with components
 Δx_p and Δy_p (see Fig.2.3 for definition)

v_i : height of station i from the earth's
 equatorial plane

The magnitude of Δp is less than tens of centimeters, but they directly cause station location errors.

DVLBI delay error due to a quasar position error is given in Eq.(3.58) (Sec. 3.3.2) and is written as

$$\begin{aligned}
 \Delta \tau_{qe} &= \underline{B} \cdot \Delta \underline{S} \\
 &= B_{\perp} \Delta \Upsilon
 \end{aligned}
 \tag{3.86}$$

where

$\Delta \tau_{qe}$: delay error due to quasar position error
 B_{\perp} : projection of baseline vector \underline{B} on the
 plane perpendicular to the line-of-sight to
 the quasar
 $\Delta \Upsilon$: error of quasar angular position (rad)

Eq.(3.86) can be rewritten in more general form as

$$\sigma_{qe} = B_{\perp} \sigma_{\Upsilon}
 \tag{3.87}$$

where

σ_{qe} : delay error due to quasar position error
 σ_{Υ} : quasar angular position error

For a numerical example, $\sigma_{qe} = 20$ cm when $B_{\perp} = 8000$ km and $\sigma_{\Upsilon} = 25$ nrad (5.2 arcsec).

References

- (1) Rogers, A. E., Very long baseline interferometry with large effective bandwidth for phase-delay measurements, *Radio Science*, 5, 10, 1970, pp. 1239-1247.
- (2) Whitney, A. R., Precision geodesy and astrometry via Very-Long-Baseline Interferometry, Doctoral Thesis, MIT, 1974.
- (3) Clark, B. G., The NRAO tape-recorder interferometer system, *Proc. IEEE*, 61, 9, 1973, pp. 1242-1248.
- (4) Ryan, J. W., Ma, C. and Vandenberg, N. R., The Mark III VLBI data analysis system, NASA X-945-80-25, 1980.
- (5) Ma, C., Very Long Baseline Interferometry applied to polar motion, relativity and geodesy, NASA TM-79582, 1978.
- (6) Thomas, J. B., An analysis of radio interferometry with the Block 0 system, JPL Publication 81-49, 1981.
- (7) Wilcher, J. H., Block I, Phase I very long baseline interferometry implementation, JPL TDA Progress Rep., May and June 1980.
- (8) Peterson, J. C., Developing new architectures for the Block II VLBI correlator system, JPL TDA Progress Rep., May and June 1981.
- (9) Fanselow, J. L., B. D. Mulhall, J. B. Thomas, G. H. Purcell, E. J. Cohen, D. H. Rogstad, P. F. MacDoran, L. J. Skjerve, W. G. Melbourne, and D. J. Spitzmesser, Determination of UT1 and polar motion by the Deep Space Network using Very

Long Baseline Interferometry, "Time and the Earth's rotation",
D. D. McCarthy and J. D. Pilkington (eds.), pp. 199-209, IAU
1979.

(10) Kawajiri, N., T. Ojima, N. Kawano, F. Takahashi, T.
Yoshino and K. Koike, The first VLBI experiment in Japan, J.
RRL, 26, 119, 1979, pp. 13-64.

(11) Kawano, N., F. Takahashi, T. Yoshino, K. Koike, H. Kumagai
and N. Kawajiri, Development of real-time VLBI and measurements
of scintillation, J. RRL, 29, 127, 1982, pp. 53-102.

(12) VLBI Research and Development Group, RRL, The first
US-Japan VLBI test observation by use of K-3 system at the
Radio Research Laboratories, J. RRL, 31, 132, 1984, pp. 31-37.

(13) Ramasastry, J., B. Rosenbaum, R. D. Michelini, D. Frost,
S. Ross and A. Boornazian, Tracking of the ATS-3 synchronous
satellite by the VLBI technique, GSFC X553-72-290, 1972.

(14) Kawase, S. and T. Tanaka, Orbit determination of
geosynchronous satellite by the VLBI technique, J. RRL, 26,
119, 1979, pp. 65-71.

(15) Hildebrand, C. E., J. S. Border, F. F. Donivan, S. G.
Finley, B. Moultrie and L. J. Skjerve, Progress in the
application of VLBI to interplanetary navigation, Conference on
VLBI Techniques, Toulouse, France, 1982.

(16) Ransford, G. A., C. E. Hildebrand and V. J. Ondrasik,
Orbit determination capability analysis for the
Mariner-Jupiter-Saturn 1977 mission, J. Spacecraft, 11, 9,
1974.

- (17) Campbell, J. K., S. P. Synott and G. J. Bierman, Voyager orbit determination at Jupiter, IEEE Trans. on Automatic Cont., AC-28, 3, 1983.
- (18) Curkendall, D. W. and R. P. Stepenson, Earth based tracking and orbit determination -- Backbone of the planetary navigation system, Astronautics and Aeronautics, May 1970.
- (19) Christensen, C. S., P. S. Callahan, B. Moultrie, F. F. Donovan and S. C. Wu, Results of a demonstration of the use of Δ VLBI data for precise navigation of interplanetary spacecraft, AIAA/AAS Astrodynamics Conference, Denvers, Mass., 1980.
- (20) Border, J. S., F. F. Donovan, S. G. Finley, C. E. Hildebrand, B. Moultrie and L.J. Skjerve, Determining spacecraft angular position with Delta VLBI: The Voyager demonstration, AIAA/AAS Astrodynamics Conference, San Diego, Calif., 1982.
- (21) Shiomi, T, S. Kozono, Y. Arimoto, S. Nagai and M. Isogai, Precise orbit determination of a geosynchronous satellite by Δ VLBI method, J. RRL, 31, 133, 1984, pp. 111-132.
- (22) Yunck, T. P. and S. C. Wu, Tracking geosynchronous satellites by Very-Long-Baseline Interferometry, J. Guidance, 6, 5, Sept.-Oct. 1983.
- (23) Border, J. S. and F. F. Donovan, Geosynchronous orbiter tracking by VLBI: Demonstration design, AIAA/AAS Astrodynamics Conference, Seattle, Wash., 1984.
- (24) Donovan, F. F., J. S. Border and B. Moultrie,

Geosynchronous orbiter tracking by VLBI: Demonstration results, AIAA/AAS Astrodynamics Conference, Seattle, Wash., 1984.

(25) Luenberger, D. G., "Optimization by vector space methods", John Wiley & Sons, Inc., 1969.

(26) Kawaguchi, N., Coherence loss and delay observation error in Very-Long-Baseline Interferometry, J. RRL, 30, 129, 1983, pp. 59-87.

(27) Marini, J.W. and C. W. Murray, Jr., Correction of laser range tracking data for atmospheric refraction at elevations above 10 degrees, NASA, X-591-73-351, 1973.

(28) Resch, G.M., Description and overview of an instrument designed to measure line-of-sight delay due to water vapor, JPL TDA Progress Rep., 42-72, Oct.- Dec. 1982.

(29) Wu, S. C., Error estimation for ORION baseline vector determination, JPL TDA Progress Rep., 42-57, Mar.-Apr. 1980.

(30) Ellis, J., Large scale state estimation algorithms for DSN tracking station location determination, AAS/AIAA Astrodynamics Specialist Conference, June 1979.

CHAPTER 4 CS TRACKING EXPERIMENT BY DVLBI
AND RANGE AND ANGLE MEASUREMENTS

4.1 Introduction

RRL was involved in satellite control experiments as well as research and development in satellite communication systems and studies on radio propagation by using Japan's first experimental communication satellite (CS, Fig.4.1)⁽¹⁾ from 1978 to 1985. In the CS program RRL developed a tracking station (at Kashima Space Research Center) which measures the slant range and viewing angles of the satellite⁽²⁾. In contrast to an established way of tracking a geosynchronous satellite by two or three earth stations which are geometrically apart from each other and are equipped with orbit measurement facilities, RRL's one-station tracking system was much more economical and easy to operate.

On the other hand, various differential tracking methods (including differential ranging and differential VLBI) had been tried by JPL in the field of deep space navigations⁽³⁾. We noticed that the differential VLBI (DVLBI) would also be effective to tracking of a geosynchronous satellite. In 1981 planning began for the first DVLBI experiment to be conducted in 1982 to measure the CS orbit more accurately than conventional

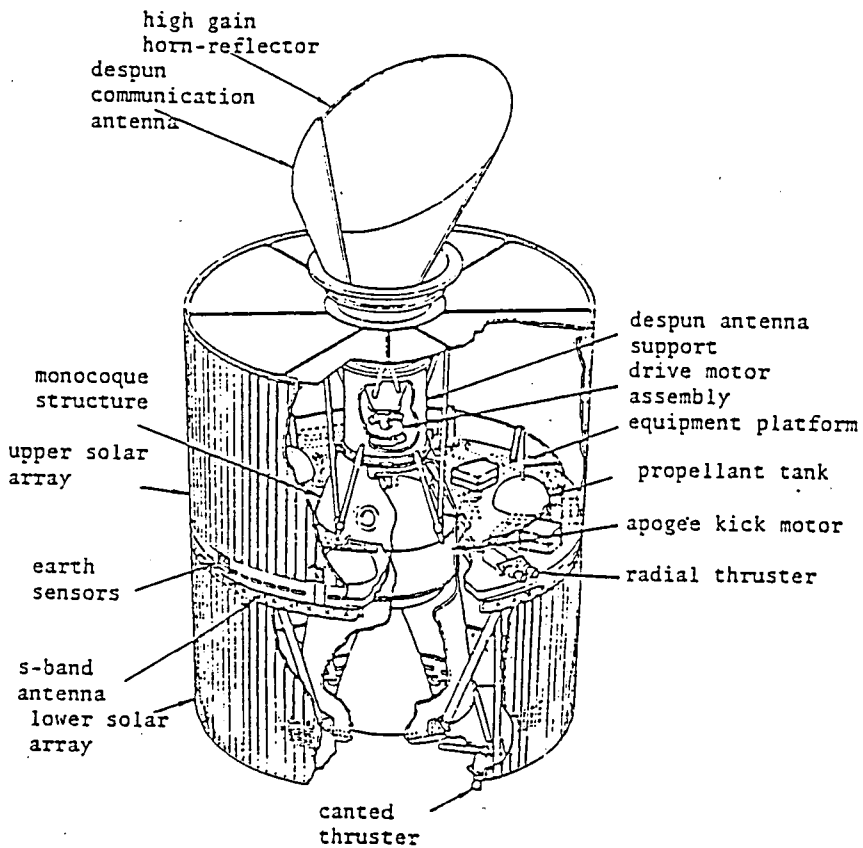


Fig.4.1 Structure of CS

radio tracking methods. The experiment had three goals: 1) to demonstrate the capability of DVLBI method applied to tracking a geosynchronous satellite, 2) to determine the orbit with higher accuracy than that obtained by ranging and angle measurements, 3) to study on VLBI techniques which would be useful as a passive monitoring methods of geosynchronous radio stations from a viewpoint of space monitoring techniques for the efficient usages of the orbital resources in space communication services.

The available VLBI system then was the real-time VLBI system K-II (Sec.3.1.1) with the baseline 46 km long between Kashima and Hiraiso stations, RRL. Though the baseline was not long, K-II system had a capability to detect the time delay with the highest accuracy of 0.1 nsec and it could receive the CS' transponder noise in the 4 GHz band. The differential VLBI observations of CS and several quasars were conducted⁽⁴⁾⁽⁵⁾ for 17 hours, while the ranging and angle measurements were made simultaneously.

In this chapter, we first describe the system of the experiment, then analyze sensitivities and accuracies of the tracking data (range, angle and DVLBI). After that the method of derivation of geometrical delay observables from the DVLBI data is shown and discussions of orbit determination based on the obtained observation data are given.

4.2 System of Experiment

4.2.1 Range and Angle Measurement System

Fig.4.2 shows the tracking (range and angle measurement) system for CS at Kashima station. The slant range between CS and the C-band antenna is measured by a conventional radio ranging method using a ranging tone of 100 kHz via 6/4 GHz TT&C (Tracking, Telemetry and Command) link. The range resolution is about 1 m. The viewing angles are obtained by the use of a 30/20 GHz band 13m dish antenna which can receive the CS K-band beacon (19.45 GHz) in an auto-tracking antenna driving mode. Fig.4.3 shows the frequency allocations of CS. In order to obtain a desired accuracy of orbit determination (satellite position determination accuracy of about 1 km) for satellite control experiments on station keeping, attitude keeping and despun antenna pointing, detailed calibrations of the tracking system and careful treatment of the observed data were needed. In particular, there were many problems to be solved concerning the angle measurements⁽⁶⁾. Because, the 13m dish antenna was installed on the top of a tower-like building (Fig.4.4) and the angle data were easily affected by thermal distortions not only of the antenna structure but also of the building as well as by the refractions due to the propagation media.

Through orbit determination studies using these radio tracking data, it was found that the azimuth angle data of CS

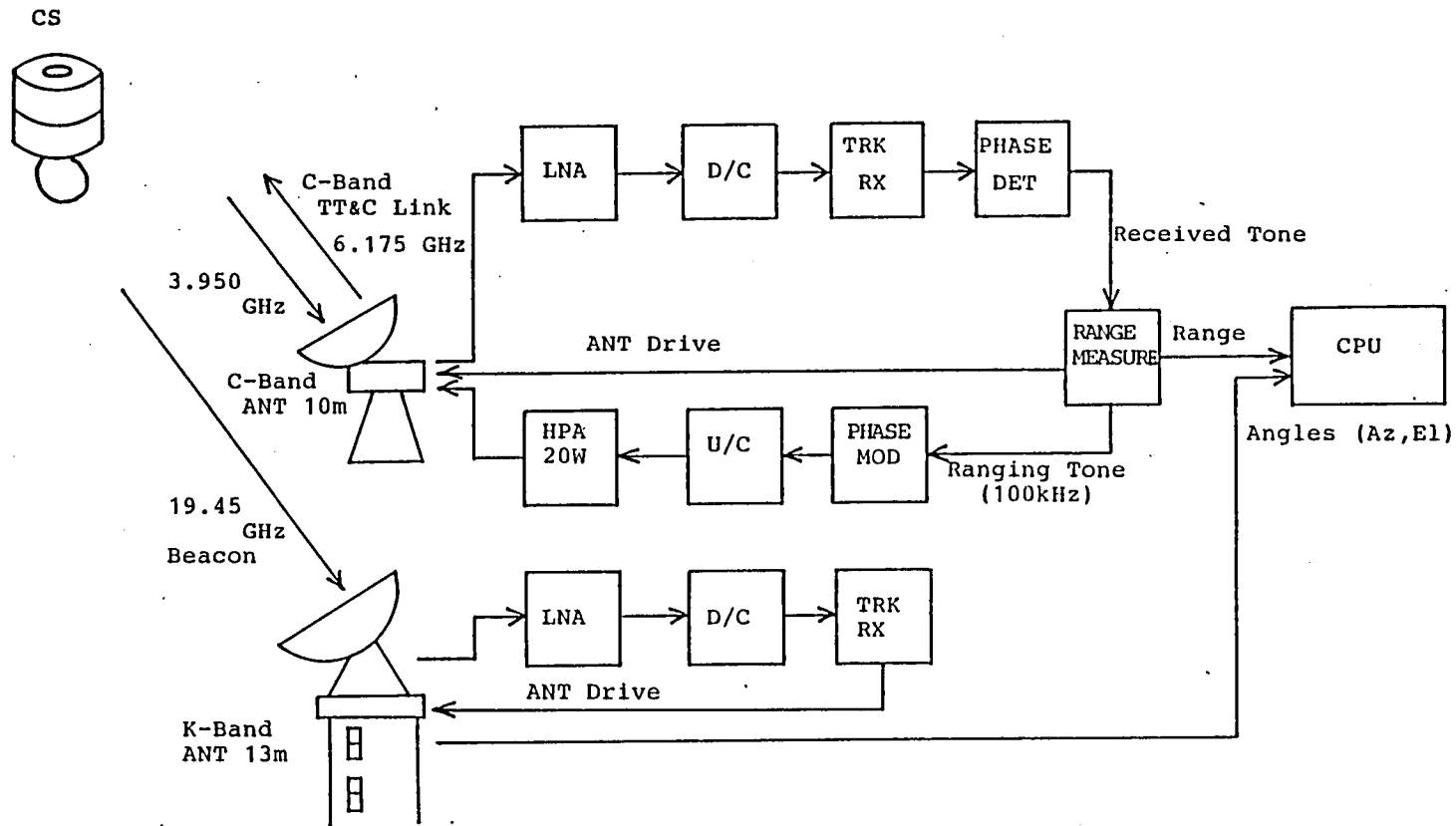


Fig.4.2 CS tracking system at Kashima Station (RRL)

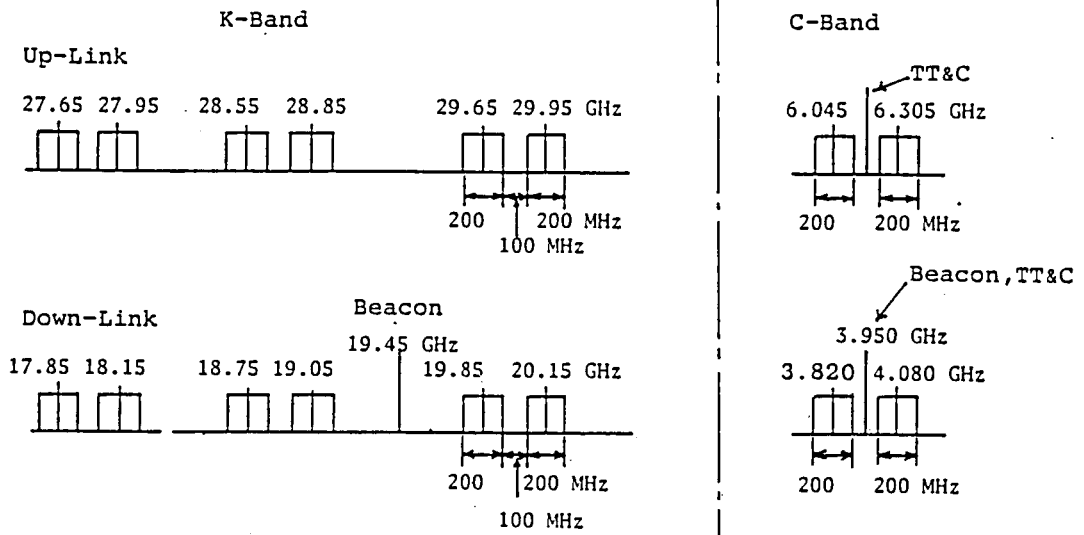


Fig.4.3 Frequency allocations of CS

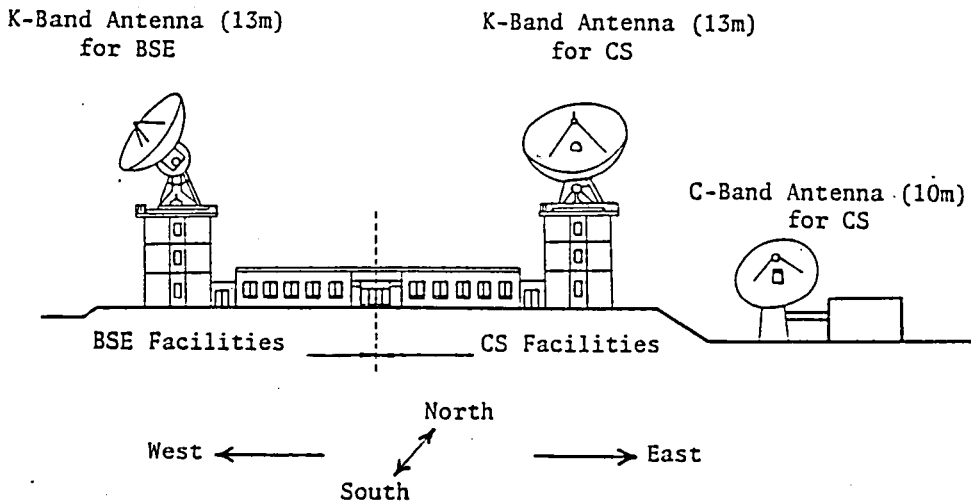


Fig.4.4 Antennas and facility building for CS at Kashima Station (BSE: Experimental Broadcasting Satellite)

during night time had quality with an accuracy of about $1.0 \times 10^{-3} \sim 0.5 \times 10^{-3}$ degrees⁽⁷⁾. That is, the angle errors became the smallest during night time, suffering from the least atmospheric refractions and thermal distortions due to the sunlight.

4.2.2 K-II VLBI System

The K-II real-time VLBI system⁽⁸⁾ was originally developed to measure the tropospheric phase scintillations of radio waves in the frequency bands 4 GHz and 32 GHz by the use of Japan's Experimental Communication Satellite (ECS)⁽⁹⁾. In our experiment we used the system with the observation frequency 4 GHz, because CS had the downlink channels in that band (Fig.4.3). Fig.4.5 shows the outline of the K-II system (4 GHz band) and Table 4.1 summarizes its main features. The two stations at Kashima and Hiraiso are connected via a microwave ground link, by which the digitized and formatted observed signal at Hiraiso are transmitted to Kashima. At Kashima station the raw data of the two stations are correlated on the real-time base and integrated for every 10 msec by using fringe stopping functions calculated based on the predicted delay rate. The obtained complex correlation function of every 10 msec are recorded on a computer tape with the time code, predicted delay and delay rate, bit-shifts number, and the other necessary information. The post data reductions to get delay and delay rate are conducted later.

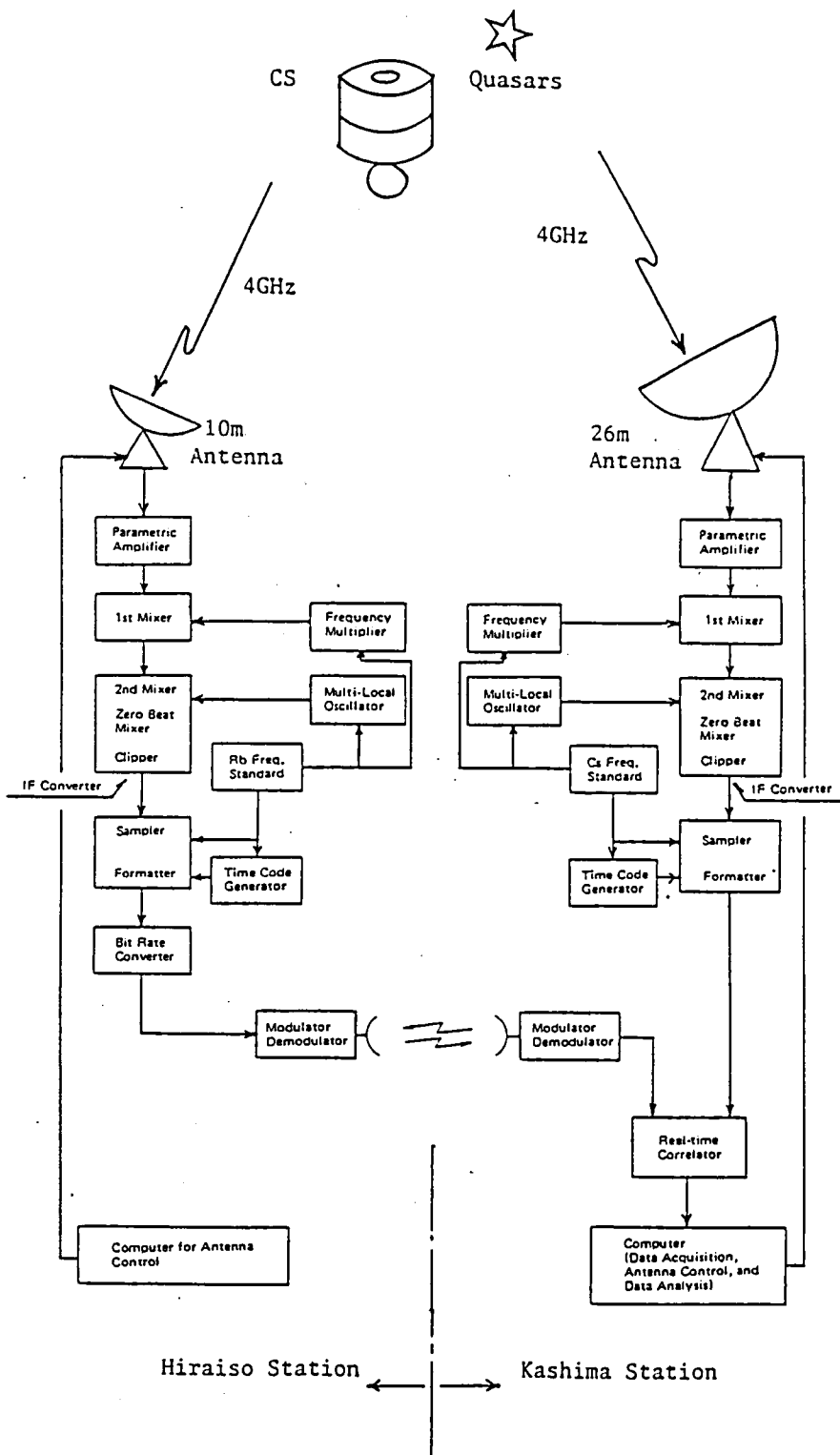


Fig.4.5 K-II VLBI System

Table 4.1 K-II VLBI system

Stations	Kashima	Hiraiso
Longitude (East, deg)	140.662675	140.621737
Latitude (North, deg)	35.9542028	36.3679429
Geodetic height (m)	77.1346	71.6750
Reference ellipsoid	SAO-C7 : Re = 6378.142 km f = 1/298.255	
Baseline length (m)	46057.433	

VLBI System	Kashima	Hiraiso
Receiving antenna	26 m	10 m
Antenna gain	58.9 dB	48.9 dB
System noise	111 K	130 K
Receiving frequencies (MHz)	CH1: 4031 , CH2: 4041 , CH3: 4061, CH4: 4091 , CH5: 4131	
Bandwidth	2 MHz/CH	
Sampling rate	4 Mbits/sec	
Frequency standard	cesium	rubidium
(stability 10 sec)	(2.5×10^{-12})	($< 1.6 \times 10^{-12}$)
Data transmission	Raw data of Hiraiso are transmitted to Kashima via a microwave data link	
Correlator	Real-time correlator, Lag 32 bits, Integration 10 msec	
Clock synchronization	using 1 sec pulses exchanged via the microwave link	
Clock calibration	using JJY with the accuracy ± 1 msec	

The observation bandwidth is 2 MHz per channel and the maximum number of observation channels is five. Each channel is sequentially alternated every 100 msec.

4.2.3 Observation Strategy

The experiment was scheduled on July 16 to 17, 1982.

Fig.4.6 shows the geometry of CS tracking by K-II VLBI and the conventional ranging and angle measurements. At Kashima we used three antennas, that is, the 26m antenna for K-II VLBI, the 10m antenna for ranging and the 13m antenna for angle measurements. CS was stationed at longitude 135 degrees east and it had orbital inclination of 0.27 degrees because the north-south station keeping maneuvers had been stopped to save fuels.

The DVLBI observations and range and angle measurements were planned to be conducted for at least 24 hours. Fig.4.7 shows the originally planned DVLBI observation schedule which intended to carry out 13 sets of observations using 11 quasars. The actual observations were successfully made for 17 hours using 7 quasars. Fig.4.8 shows the viewing angles of the quasars and CS at the center of each observation period at Kashima. Quasars with more than $1 J_y$ ($1 J_y = 10^{-26} \text{ W/m}^2\text{Hz}$) of correlation flux density were selected. Though some quasars were seen angularly apart from CS by more than 10 degrees, they were used because of their strong fluxes.

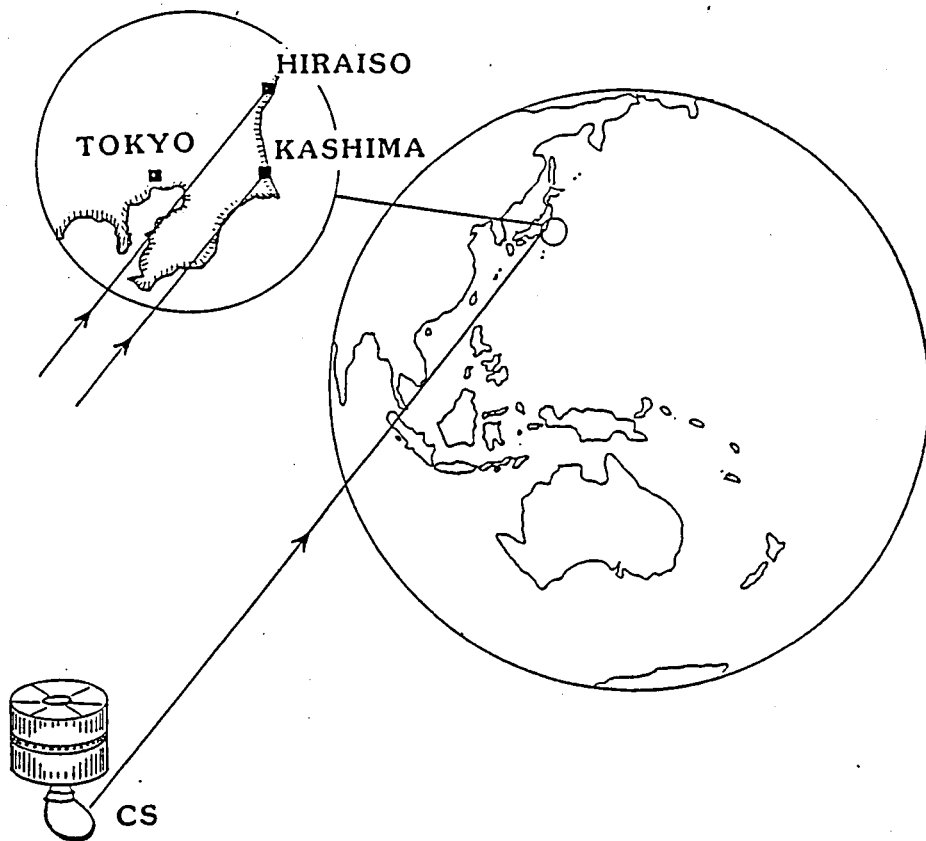


Fig.4.6 Geometry of CS tracking by K-II VLBI

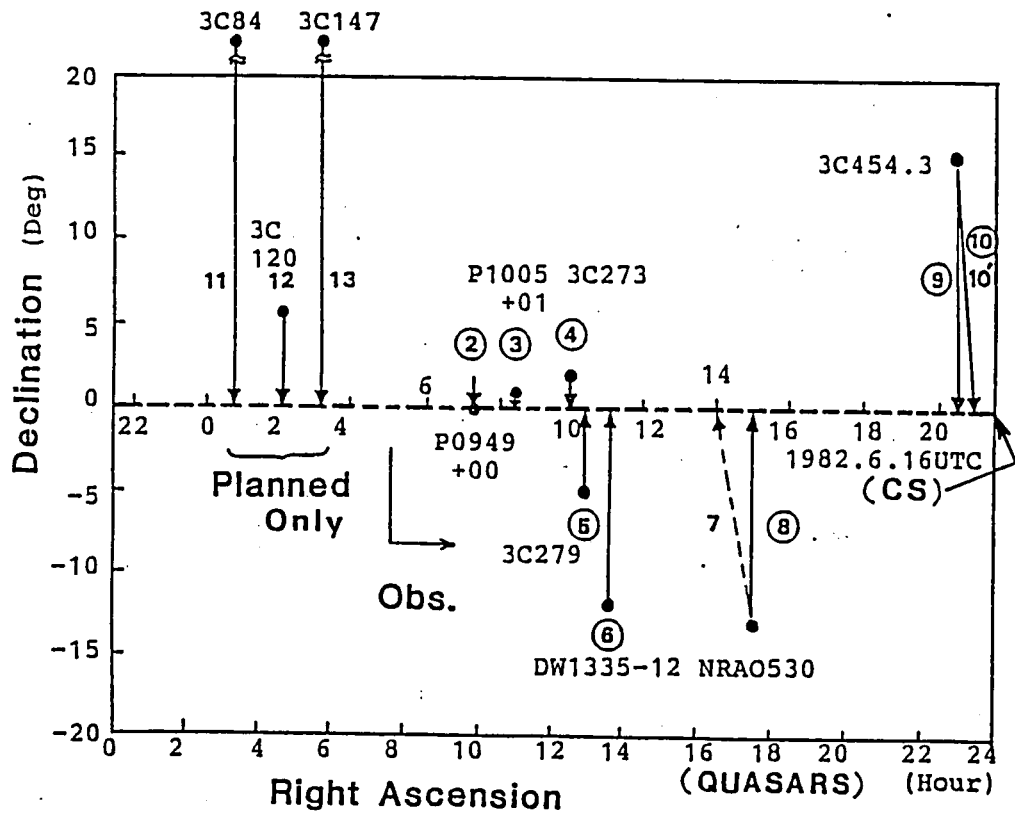


Fig.4.7 DVLBI observation schedule

- ②~⑩ : Observed by DVLBI method
- 7, 10^{*} : only CS was observed
- 11,12,13: planned only
- : differential observation between CS and a quasar
- - - : CS orbit

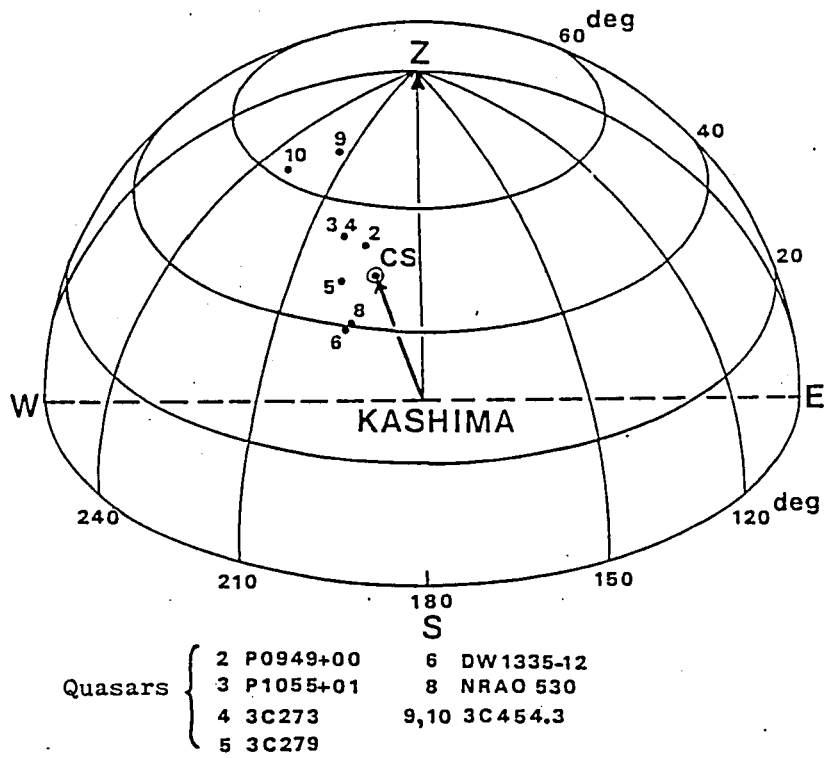


Fig.4.8 Viewing angles of CS and quasars at Kashima Station
 The figures correspond to the observation numbers in Fig.4.7

One set of observations consisted of three consecutive ten-minutes of observations, that is, first a quasar was observed, then CS, and again the quasar. It means that the CS observation was sandwiched between the quasar observations. This method was effective to calibrate the CS observation by using the quasar observations. The first few minutes in each ten minutes pass were kept to point the receiving antenna to the corresponding radio source. The VLBI observation data were recorded for 45 seconds in the case of a quasar observation, and for 20 seconds in the case of CS. The recordings were made during the last part of the ten-minutes pass, when the antennas completely tracked the radio source. We used two observation channels (CH2 and CH3 in Table 4.1) of K-II.

The real-time correlator controlled the bit-shifts of one of the signals received at the two stations and correlated them to produce cross-correlation function. Then it stopped the fringe phase rotation (which is caused by a delay rate due to the baseline vector change with the earth's rotation) using a quantized fringe-stopping function based on a predicted delay rate. The result is a complex cross-correlation function, which is then integrated for every 10 msec. In the case of quasar observations, the fringe-stopping function of 10-levels of quantization was used. In the case of CS observations, no fringe stopping was applied and the correlation function was directly integrated for every 10 msec, because the delay rate in a CS

observation was very small (less than $\pm 5 \times 10^{-11}$). This is due to the observation geometry in which the baseline is short and the difference between the longitude of the baseline vector and that of each object radio source (CS or a quasar) is small. Fig.4.9 shows the predicted delay and delay rate for the CS observations.

The cesium clock at Kashima station was calibrated by using Japanese broadcast standard time (JJY) to UTC within the error of ± 1 msec. The clock accuracy of ± 1 msec was sufficient for time-tagging of the DVLBI observables. Because the delay observable suffers no meaningful change in 1 msec since the delay rate is small as described above.

The clock synchronization between the stations Kashima and Hiraiso, which is needed for correlation processing, was conducted within the error of 0.1 micro-seconds by the method of transmitting pulses of 1 Hz via the microwave data link. This was sufficient to obtain a meaningful correlation in about 4 micro-seconds window of the real-time correlator.

4.3 Sensitivity and Accuracy of Observables

4.3.1 Sensitivity of Range, Azimuth Angle and DVLBI Observables

In the CS experiment, we obtained three different kinds of tracking data, range, angles (azimuth and elevation) and differential range (DVLBI). Here we show that these observables are complementary each other.

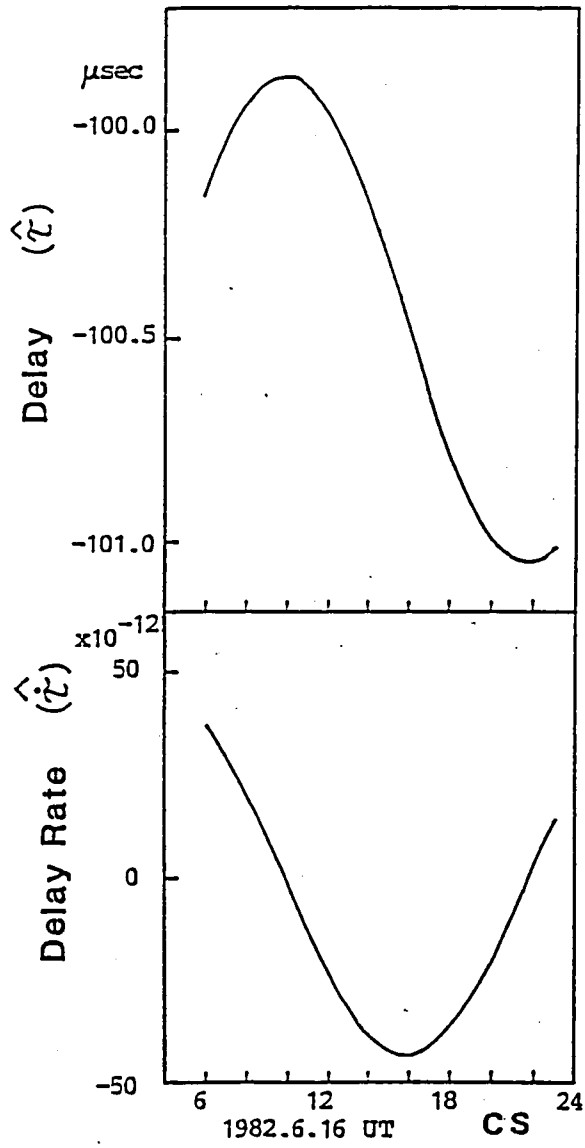


Fig.4.9 Predicted delay and delay rate for CS observations

Range

The range observable is defined in Eq.(2.10) (Sec.2.1.2). The range variation $\Delta\rho$ due to a small position deviation $\Delta\underline{r}$ of CS is easily derived from Eq.(2.10) as

$$\Delta\rho = \underline{\rho}_u \cdot \Delta\underline{r} \quad (4.1)$$

where $\underline{\rho}_u$ is the unit vector along the slant range vector $\underline{\rho}$ from Kashima station to CS. According to Eq.(4.1) $\underline{\rho}_u$ directly represents the sensitivity of the range observable with respect to the CS position deviation. Fig.4.10 shows the radial and cross-track components of $\underline{\rho}_u$, where the along-track (or in-track) component is negligible. The range data have the major sensitivity to a radial position deviation of CS, as is intuitively expected.

Azimuth Angle

Fig.4.11(a) shows the definition of azimuth angle (Az) in a topocentric coordinate system, where \underline{N} , \underline{E} and \underline{Z} stand for the unit vectors in the directions of north, east and zenith, respectively. The azimuth angle is defined as

$$Az = \tan^{-1} \left(\frac{\rho_E}{\rho_N} \right) \quad (4.2)$$

where

$$\begin{aligned} \rho_E &= \underline{\rho} \cdot \underline{E} \\ \rho_N &= \underline{\rho} \cdot \underline{N} \end{aligned}$$

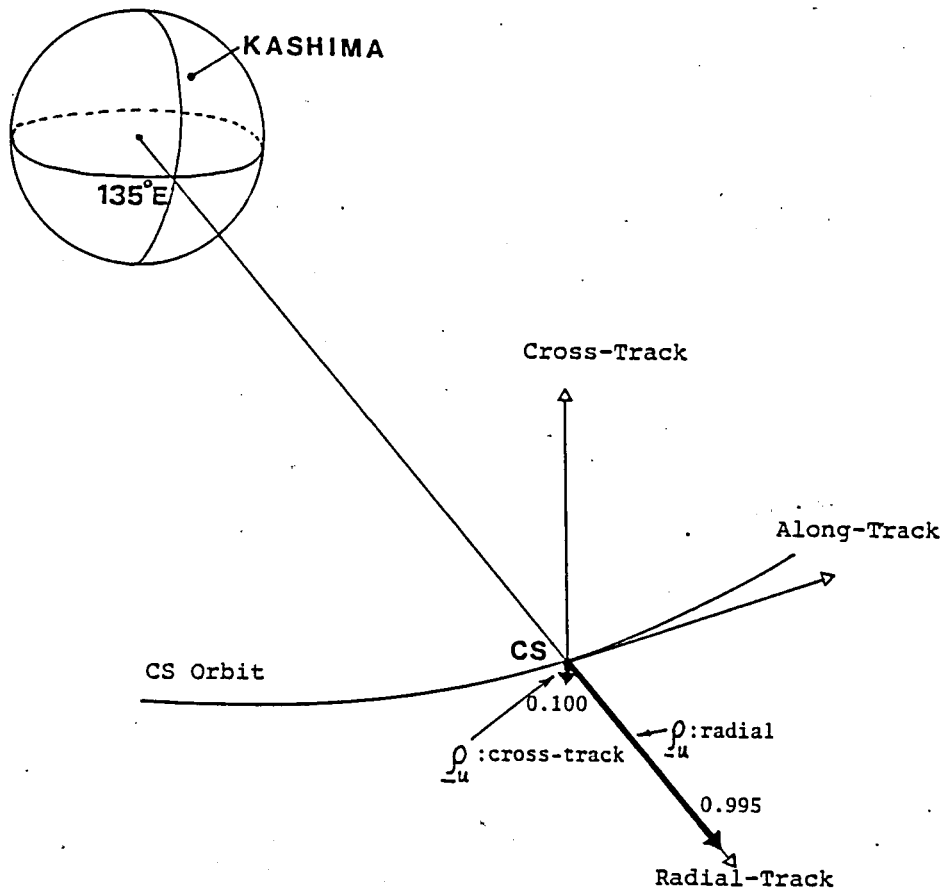


Fig.4.10 Sensitivity of range observable

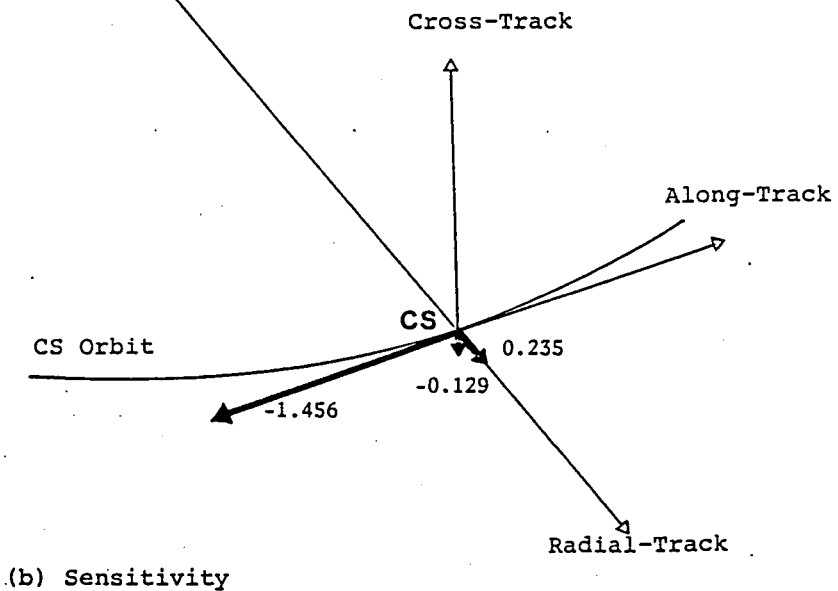
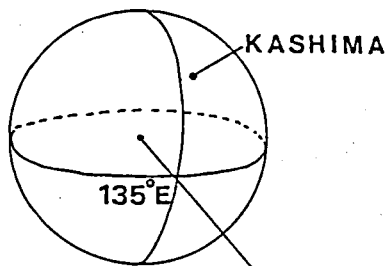
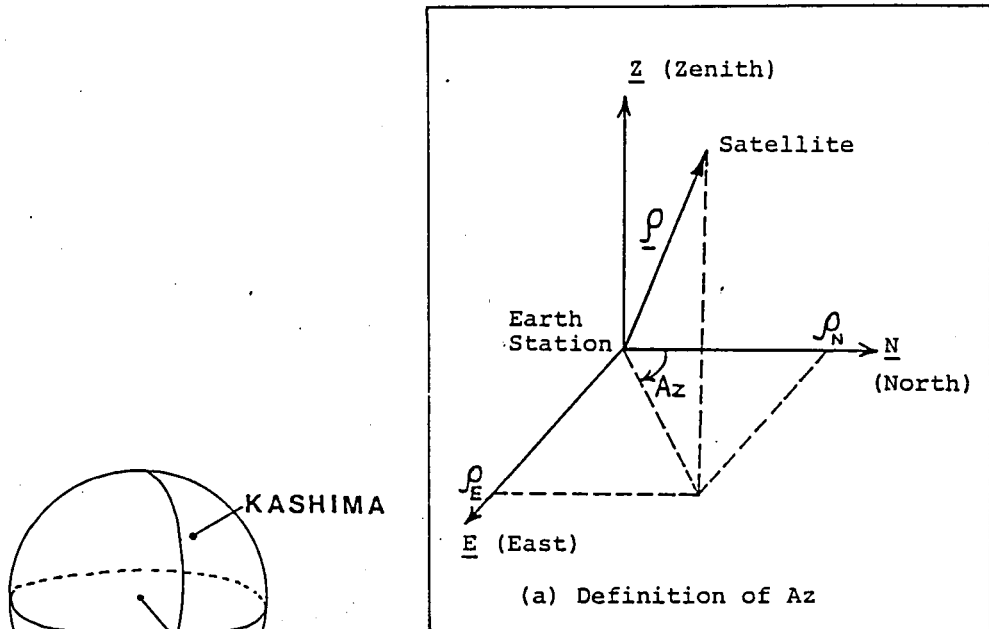


Fig.4.11 Sensitivity of azimuth angle observable

According to Eq.(4.2) we obtain

$$(1 + \tan^2 Az) \Delta Az = (\Delta \rho_E \rho_N - \rho_E \Delta \rho_N) / \rho_N^2 \quad (4.3)$$

where $\Delta \rho_E$ and $\Delta \rho_N$ are written as

$$\left. \begin{aligned} \Delta \rho_E &= \Delta \underline{\rho} \cdot \underline{E} = \underline{E} \cdot \Delta \underline{r} \\ \Delta \rho_N &= \Delta \underline{\rho} \cdot \underline{N} = \underline{N} \cdot \Delta \underline{r} \end{aligned} \right\} \quad (4.4)$$

where $\Delta \underline{r}$ is a small deviation vector of the satellite position. Substituting Eq.(4.4) into Eq.(4.3) we obtain

$$\rho \Delta Az = p_{az} \cdot \Delta \underline{r}, \quad (4.5)$$

$$p_{az} = \frac{1}{1 + \tan^2 Az} \left(\frac{\rho}{\rho_N} \underline{E} - \frac{\rho \rho_E}{\rho_N^2} \underline{N} \right)$$

where the slant range ρ is used to convert ΔAz into position deviation of the satellite in the left-hand side of Eq.(4.5). Fig.4.11(b) shows the components of the sensitivity vector p_{az} for CS observed at Kashima station. It is clear that the azimuth angle observable has the major sensitivity to the along-track position deviation of CS. Using an approximate value for the range $\rho = 37200$ km, an azimuth angle variation $\Delta Az = 0.5 \times 10^{-3}$ degrees corresponds to the along-track deviation $\Delta \underline{r} = -220$ m of CS.

DVLBI Observable

A general formulation for the sensitivity of a DVLBI delay observable (differential range) is already given in Sec.3.3.2

(Eq.(3.58)). Fig.4.12 shows the normalized sensitivity vector $\underline{p}_u = (\underline{p}_{1u} - \underline{p}_{2u}) / \|\underline{p}_{1u} - \underline{p}_{2u}\|$ for a CS observation by K-II VLBI system. Since K-II VLBI has only short baseline, the magnitude of the sensitivity vector is small, that is, $\|\underline{p}_{1u} - \underline{p}_{2u}\| = 9.36 \times 10^{-4}$. However, the VLBI observable has the major sensitivity to the remaining cross-track position deviation of CS. Denote the accuracy of the DVLBI delay observable as σ_τ , then corresponding satellite cross-track position deviation σ_{rc} is given as (see Eq.(3.58) and Fig.4.12)

$$\sigma_{rc} = \frac{1}{9.36 \times 10^{-4} \times 0.977} \sigma_\tau \approx 1100 \sigma_\tau \quad (4.6)$$

Eq.(4.6) means that we need an accuracy of about 10 cm (0.3 nsec) for the DVLBI observable with K-II VLBI system in order to obtain a resolution to a cross-track position deviation of 100 m for CS.

Figs.4.10, 4.11 and 4.12 show the complementary feature of sensitivity vectors for the range, azimuth angle and DVLBI observables. In other words, these observables as a whole have sensitivities to three-dimensional satellite deviation from a nominal position in the geosynchronous orbit. Therefore, we can determine the satellite orbit using several sets of these observables. The elevation angle data are less accurate than the azimuth angle data because they are easily affected by propagation media for which we have no highly precise calibration method.

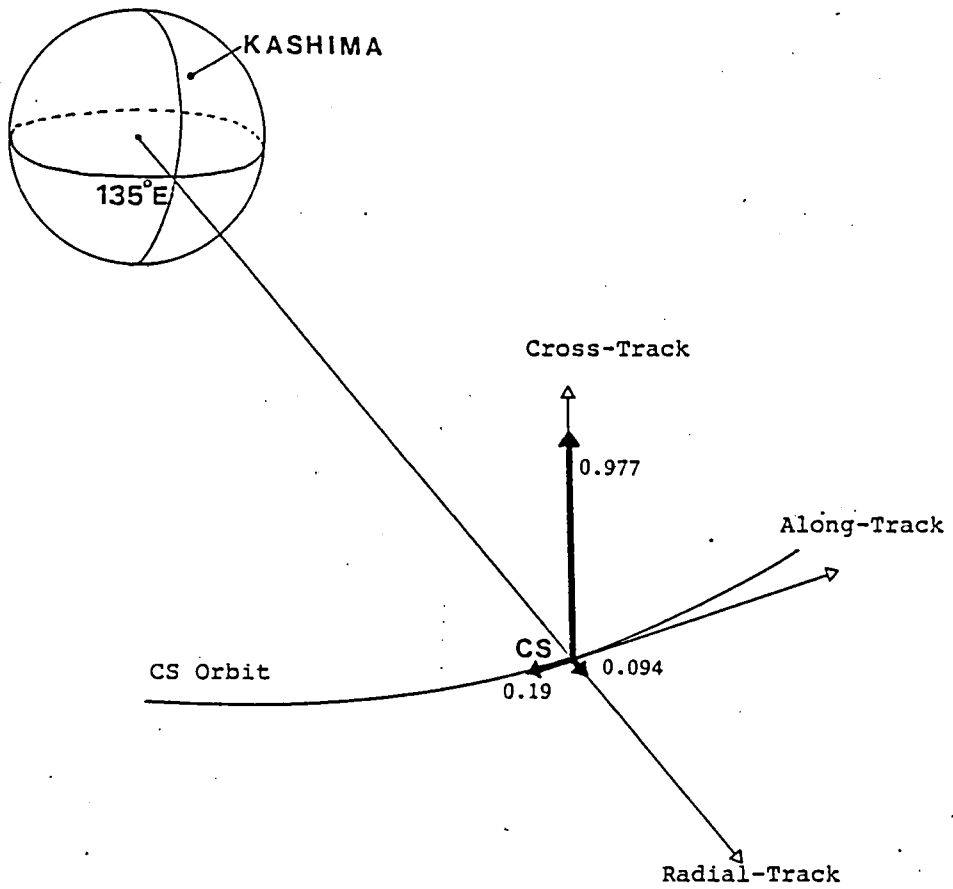


Fig.4.12 Sensitivity of DVLBI observable with K-II VLBI system

4.3.2 Accuracy of Range, Azimuth Angle and DVLBI Observables

Concerning the range and azimuth angle observables, we show fundamental performance of the tracking system at Kashima station under the nominal operational condition for CS. As for the DVLBI observable, we discuss SNR error and systematic errors in differential observations.

Range

Table 4.2 shows the nominal link parameters for ranging of CS in the C-band TT&C channel at Kashima station. The estimated range accuracy corresponding to signal to noise ratio is 0.17 m for the 100 kHz ranging tone. The practically obtained accuracy of the range data is about 0.5 to 1.0 m. The ranging system is frequently calibrated using a collimation facility 3.6 km apart from the station. However, the range data have errors due to the propagation media effects and the delay caused in the satellite transponder. We usually remove the former error using a physical models of the ionosphere and the troposphere. Concerning the latter error, we use the data obtained on the ground before the launch of the satellite.

Azimuth Angle

The 13 m dish antenna system has a pointing angle detection mechanism of which the measured performance is ± 0.0068 degrees

Table 4.2 Link parameters for CS ranging

Uplink	
Carrier frequency	6175 MHz
Earth station transmitter power	43 dBm
Feeder loss	2.0 dB
Antenna gain	53.5 dB
Propagation loss	200.6 dB
Polarization mismatching loss	0.5 dB
Satellite antenna gain	33 dB
Satellite down converter loss	15.2 dB
Receiver input power	-88.8 dBm
Receiver noise	-167.8 dB/Hz
C/N_0	79.0 dBHz
Downlink	
Carrier frequency	3950 MHz
Satellite transmitter power	16.4 dBm
Satellite antenna gain	29.7 dB
Propagation loss	196.6 dB
Polarization mismatching loss	0.3 dB
Earth station antenna gain	51.1 dB
Receiver input power	-99.7 dBm
Receiver noise	-179.3 dBm/Hz
C/N_0	79.6 dBHz
Modulation loss (Telemetry, Range tone, Noise)	-13.0 dB
Range tone demodulation bandwidth	-0.8 dBHz
Range tone S/N	65.8 dB
Range tone phase error	3×10^{-4} rad
Range accuracy (100 kHz tone)	0.17 m

and ± 0.0065 degrees for azimuth and elevation angles, respectively⁽¹⁰⁾. The electrical tracking performance of the auto-tracking system is about 0.001 deg(rms) for both azimuth and elevation angles with the signal input power higher than -110 dBm at the receiver input⁽¹⁰⁾. Since the nominal signal level of the 19.45 GHz CS beacon at Kashima is about -90 dBm to -95 dBm, the auto-tracking system electrically supplies the incident angle information with an accuracy of 0.001 degrees(rms). The actually obtained angles are not necessarily the same as the geometrically defined angles due to refractions through the propagation media, to angle offsets of the driving axis and to deformations of the antenna beam caused by the gravitational and thermal effects.

DVLBI Observable

(i) SNR Error in CS Observations

In a VLBI observation, estimated delay has a random error due to SNR (defined in Sec.3.2.1). The radio source signal temperature (it is also called antenna temperature) T_{ai} in Eq.(3.8) is given as

$$T_{ai} = \frac{\lambda^2}{8\pi k} S G_i C_i \quad (4.7)$$

where

λ : wavelength of the receiving signal

k : Boltzmann's constant

S : flux density of a radio source

G_i : receiving antenna gain of the station i ($i=1,2$)

C_i : polarization matching coefficient at the station i

$$(0 \leq C_i \leq 1)$$

Eq.(4.7) is applied to the case where one of the orthogonal polarizations is received. Suppose 4 GHz of the receiving frequency and assume $C_i=1$, then T_{ai} is written in decibel form as

$$T_{ai} \text{ dB(K)} = -67.9 + G_i \text{ dB} + S \text{ dB}(J_y) \quad (4.8)$$

The effective radiation power of the 4GHz transponder noise (with no communication signals) of CS is approximately 46.7 dBm. It gives the flux density of 31.0 dB(J_y) at the earth stations. Therefore, let $S=31.0$ in Eq.(4.8) and consider that the receiving polarizations are matched to that of the CS radio wave at the VLBI stations (plus 3 dB in Eq.(4.8)), we obtain the antenna temperature T_c of the CS observation as

$$T_c \text{ dB(K)} = -33.9 + G \text{ dB} \quad (4.9)$$

The antenna temperatures of Kashima and Hiraïso are given by Eq.(4.9) using the antenna gains for those stations (Table 4.1). That is, T_c (Kashima) =25.0 dB(K) and T_c (Hiraïso) =15.0 dB(K). The SNR of CS observations is given by Eq.(3.8) using these antenna temperatures, the system noise temperatures of the two stations (Table 4.1), and the channel bandwidth $B = 2$ MHz, as

$$\text{SNR dB} = 25.2 + \frac{1}{2} T \text{ dB(sec)} \quad (4.10)$$

where we assumed 60% loss of SNR due to K-II hardware system from

the theoretical value given by Eq.(3.8).

Suppose 10 sec of the integration T, then SNR is 30.2 dB. This gives the delay estimation accuracy $\hat{\sigma}_\tau = 0.30$ nsec (9.0 cm) with the effective bandwidth (ω_{eff}) of 0.5 MHz by Eq.(3.32). Since the flux of the radio wave from CS is strong, we obtain the desired accuracy of delay estimate (recall the description just after Eq.(4.6)) with the integration for 10 sec when we only consider the system noise error.

(ii) SNR Error in Quasar Observations

In the case of quasars, using the antenna gains in Table 4.1, the antenna temperatures given in Eq.(4.8), and the bandwidth B = 2 MHz, SNR is calculated as

$$\text{SNR dB} = -5.8 + S \text{ dB}(J_y) + \frac{1}{2} T \text{ dB}(\text{sec}) \quad (4.11)$$

Since the correlation flux density of a quasar is mostly a few Janskies, we need much longer integration time than that of CS observations and much wider observation bandwidth to improve the SNR.

As an example, we take the quasar 3C273 of which the correlation flux density is fairly strong, that is, in Eq.(4.8) S is approximately 13 dB(J_y). If we take 30 sec of integration time, SNR becomes 14.6 dB, which gives $\hat{\sigma}_\tau = 11$ nsec (3.3 m) with the effective bandwidth of 0.5 MHz. In order to obtain the

higher accuracy of the delay estimation, we should integrate the correlation function for a longer time and obtain a wider effective bandwidth.

Fig.4.13 shows SNR and accuracies of delay and delay rate estimates. Using Fig.4.13 we obtain SNR from the correlation flux density of a quasar for an integration time T . The accuracy of a delay estimate is evaluated by the SNR for an effective bandwidth ω_{eff} . The accuracy of a delay rate estimate is evaluated by the SNR for an effective integration time T_{rms} . For example, an observation of 3C273 with an effective bandwidth of 20 MHz gives $\hat{\sigma}_\tau = 0.3$ nsec with the integration for 30 sec.

(iii) Errors due to System Delay, Clock and Propagation Media

As described in Sec.3.4.1, errors due to the system delay variation and the drift in clock rate between observations of the satellite and a quasar are negligible for our goal to obtain delay observable with an accuracy of a few centimeters.

In differential VLBI observations using K-II VLBI, delay due to propagation media (ionosphere and troposphere) are also negligible, because the baseline is so short that those effects are eliminated with an accuracy of a few centimeters.

(iv) Geometric Errors

Quasar position errors are negligible in the case of K-II VLBI system due to its short baseline. As for the station

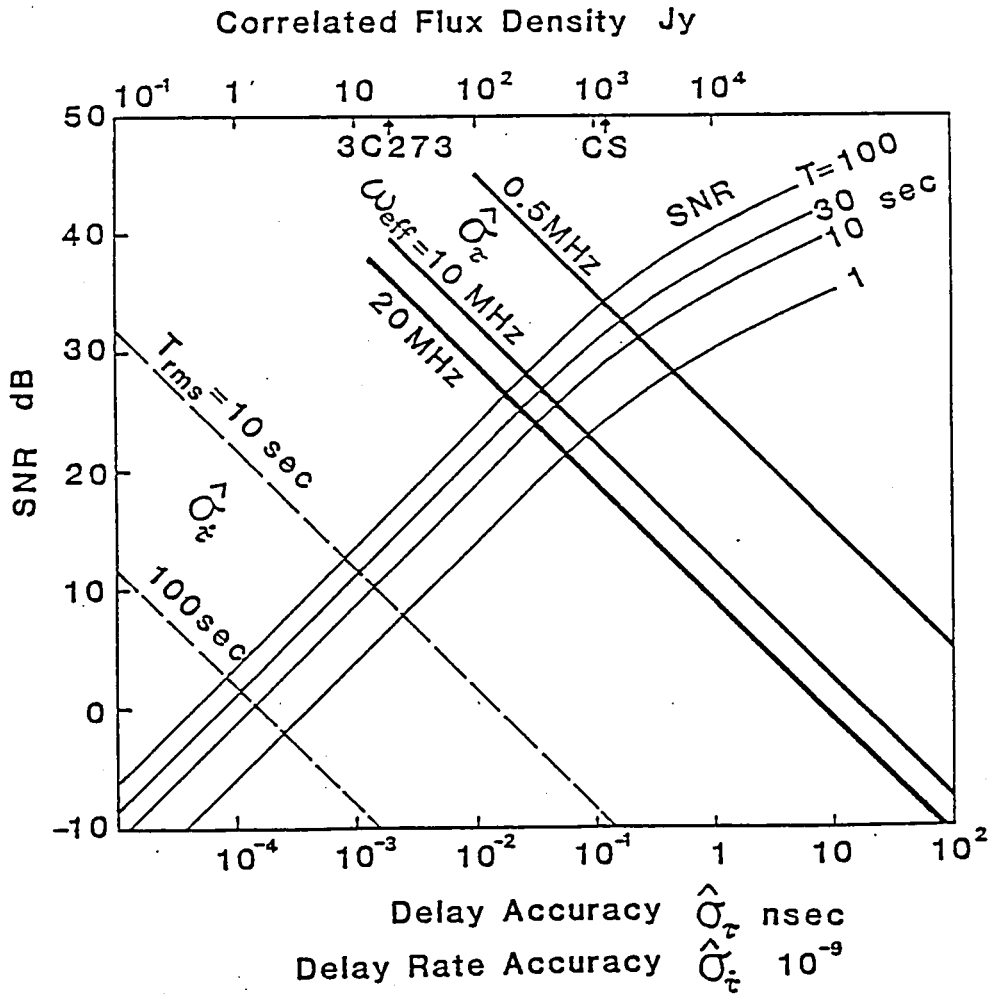


Fig.4.13 Accuracy of VLBI delay and delay rate estimates. Read SNR from given flux density of a radio source, then obtain the accuracies.

location errors described in Sec.3.4.3, the contributions of UT1 errors and polar motion errors are again negligible due to the shortness of the baseline. The remaining station location errors is due to uncertainty of the geodetic station location data. Denote the station location errors $\Delta \underline{x}_1$ and $\Delta \underline{x}_2$ for the stations 1 and 2, respectively. The angles between the line-of-sight of CS and the station location error vectors $\Delta \underline{x}_1$, $\Delta \underline{x}_2$ are defined as θ_1 and θ_2 , respectively, and the separation angles between CS and a quasar at the two station are $\Delta \theta_1$ and $\Delta \theta_2$, respectively (Fig.4.14). Then the delay observation error $\Delta \tau_s$ is written according to Eq.(3.58) as

$$\begin{aligned}
 c\Delta \tau_s &= \left\{ \cos(\theta_2 + \Delta \theta_2) - \cos \theta_2 \right\} \Delta x_2 \\
 &\quad - \left\{ \cos(\theta_1 + \Delta \theta_1) - \cos \theta_1 \right\} \Delta x_1 \\
 &\doteq \Delta x_2 \sin \theta_2 \cdot \Delta \theta_2 - \Delta x_1 \sin \theta_1 \cdot \Delta \theta_1 \quad (4.12)
 \end{aligned}$$

where the separation angles $\Delta \theta_1$ and $\Delta \theta_2$ are assumed to be small in the DVLBI observations. In the most conservative evaluation of $c\Delta \tau_s$, we treat Δx_1 and Δx_2 as random errors with standard deviations σ_{g1} and σ_{g2} , respectively. Then the delay error σ_{τ_s} due to station location errors Δx_1 and Δx_2 is written as

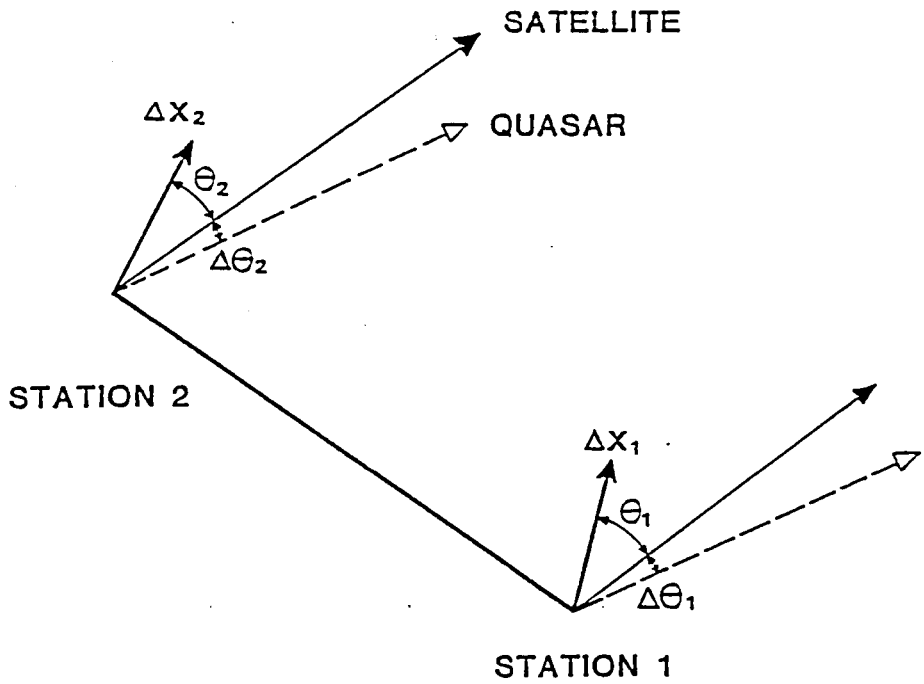


Fig.4.14 Station location errors and their effects on DVLBI observable

$$c^2 \sigma_{\tau_s}^2 = \Delta\theta_1^2 \sigma_{g1}^2 + \Delta\theta_2^2 \sigma_{g2}^2 \quad (4.13)$$

As a numerical example, suppose $\Delta\theta_1 = \Delta\theta_2 = 10$ degrees and $\sigma_{g1} = \sigma_{g2} = 20$ cm, then we get $c \sigma_{\tau_s} = 4.9$ cm ($\sigma_{\tau_s} = 0.16$ nsec).

4.4 DVLBI Data Processing

4.4.1 Method and Results of Delay Estimation

Typical two methods to derive VLBI observables are described in Sec.3.2.2. In the K-II VLBI experiment, we adopted the coherent phase method, because we observed wideband radio signals from both CS and quasars and aimed to utilize the whole information in the observation bandwidth.

The complex correlation function which is integrated by the real-time correlator of K-II system for every 10 msec and recorded on a magnetic tape (Raw Data Tape) is written as,

$$R_{oxy}(t_i, \tau) = C_i \sum_{t_i}^{\Delta t} \left\{ C_2 x(t+\tau)y(t-\tau_b)f(t) \right\} \quad (4.14)$$

where

R_{oxy} : complex correlation function at the time t_i

C_i : a coefficient multiplied to the complex correlation function when it is recorded on a magnetic tape

- C_2 : coherence loss by infinite clipping ($=2/\pi$)
 $x(t)$: received signal at Kashima station
 $y(t)$: received signal at Hiraiso station
 τ_b : delay by bit-shifts (1 bit = 250 nsec)
 $f(t)$: fringe-stopping function ($\doteq \exp \left\{ -i \omega_{RF} \tilde{\tau}_i (t-t_i) \right\}$)
 ω_{RF} : observation radio frequency (4 GHz band)
 $\tilde{\tau}_i$: predicted delay rate at t_i
 $\sum_{t_i}^{\Delta t}$: integration for Δt ($= 10$ msec) from t_i

Denote the normalized complex correlation function $R_{xy}(\tau)$, it is described as

$$R_{xy}(\tau) = R_{oxy}(\tau) C_3 / (\Delta t C_1 C_2) \quad (4.15)$$

where C_3 is the correction factor for quantization of the fringe-stopping function. The normalized cross-spectral function is obtained by integration of the Fourier-transformed and phase-rotated cross-correlation function as

$$S_{xy}(\omega_k, t_i) = \frac{1}{\Delta T} \sum_{t_i}^{\Delta T} F \left[R_{xy}(t, \tau) \right] e^{-i \omega_k (\tilde{\tau} - \tau_b)} \quad (4.16)$$

where

- $\omega_k = 2\pi Bk/32$: video frequency, $B = 2$ MHz, $k = 0, 1, \dots, 31$
 t_i : start time of the integration
 $F \left[R_{xy}(\tau) \right]$: Fourier transform of $R_{xy}(\tau)$
 $\tilde{\tau}$: predicted delay

$e^{-i\omega_k(\tilde{\tau} - \tau_b)}$: phase rotation for a fractional bit correction which is necessary to correct a quantization error of bit-shift τ_b

$\sum_{t_i}^{\Delta T}$: integration for ΔT from t_i ($\Delta T=1$ sec)

The cross-spectral data are obtained and recorded on another magnetic tape using an offline software (program "FTAPE" in Fig.4.15).

Denote the delay residual $\Delta\tau$, the delay rate residual $\Delta\dot{\tau}$ and the delay acceleration residual $\Delta\ddot{\tau}$, then the estimates for them are given as those which make the following coherence function (or normalized correlation amplitude) X_c maximum, that is,

$$(\hat{\Delta\tau}, \hat{\Delta\dot{\tau}}, \hat{\Delta\ddot{\tau}}) = \left[\Delta\tau, \Delta\dot{\tau}, \Delta\ddot{\tau} \mid \max(X_c) \right] \quad (4.17)$$

$$X_c = \left\| \frac{1}{T\omega_B} \sum^T \sum^{\omega_B} S_{xy}(\omega, t) \exp \left[-i \left\{ \omega\Delta\tau + \omega_0(\Delta\dot{\tau}t + \frac{1}{2}\Delta\ddot{\tau}t^2) \right\} \right] \right\| \quad (4.18)$$

where (Eq.(4.18) corresponds to Eq.(3.16))

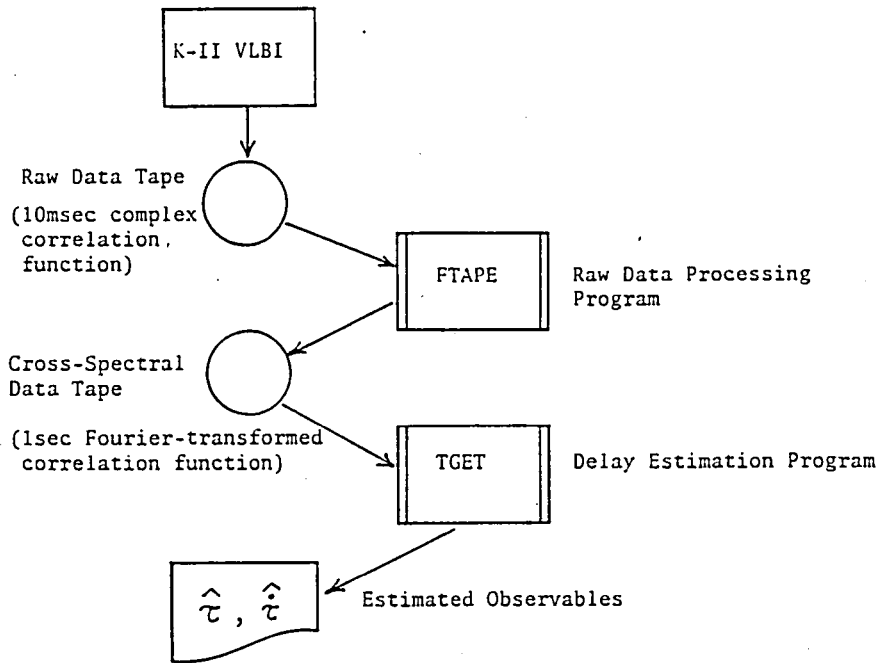
T ; integration time

ω_B : bandwidth

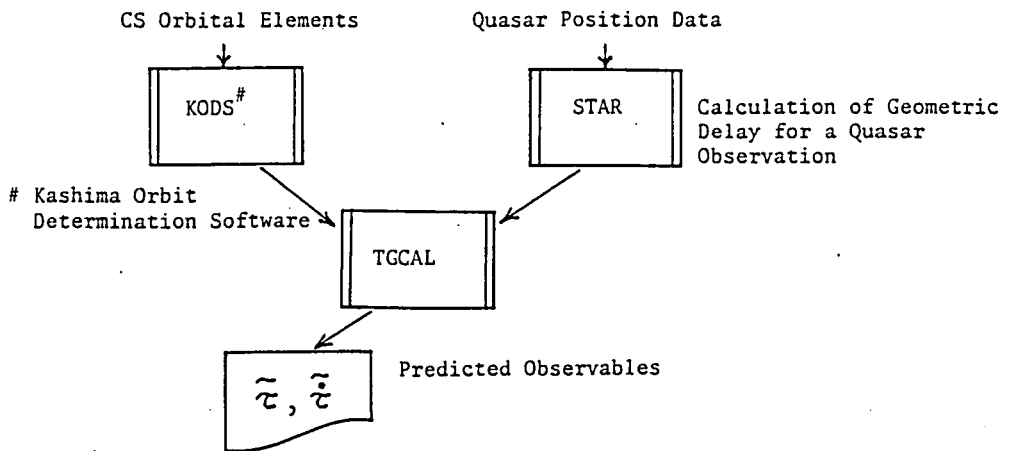
ω_0 : observation frequency (CH2: 4041 MHz, CH3: 4061 MHz)

ω : video frequency (0~2 MHz)

\sum^T : integration over the time span T



(a) Delay and delay rate estimation



(b) Predictions

Fig.4.15 Flow of data processing of DVLBI experiment using K-II VLBI system

\int^{ω_B} : integration with respect to the video frequency
bandwidth ω_B

The optimum delay and delay rate are obtained using the program "TGET" shown in Fig.4.15. In our data reductions, T is 30 sec for quasars and 20 sec for CS. In fact, the effective integration time for each channel is the half of T, because the observations were alternated every 100 msec between Channels 2 and 3. In the case of CS observations, since the correlated flux density is strong enough, the above integration time is sufficient. It is better to integrate the quasar signals for longer time, but there exists practically a limit to it due to the instabilities of the frequency standards at the two stations.

We processed all the data by the above mentioned method and obtained the delay and the delay rate estimates $\tau = \tilde{\tau} + \Delta\hat{\tau}$ and $\dot{\tau} = \tilde{\dot{\tau}} + \Delta\hat{\dot{\tau}}$ for CS and quasars. Typical cross-spectral in the CS and quasar observations are shown in Figs.4.16 and 4.17. The delay estimates for CS and quasars in terms of residuals from the corresponding predictions are shown in Fig.4.18. Table 4.3 summarizes the coherences (X_c in Eq.(4.18)) and the accuracies of the delay estimates. As is expected by the evaluation in Sec.4.3.2, the accuracy of the CS delay estimates is 0.3 nsec. In the case of quasars, it is in the range of 10 ~ 140 nsec.

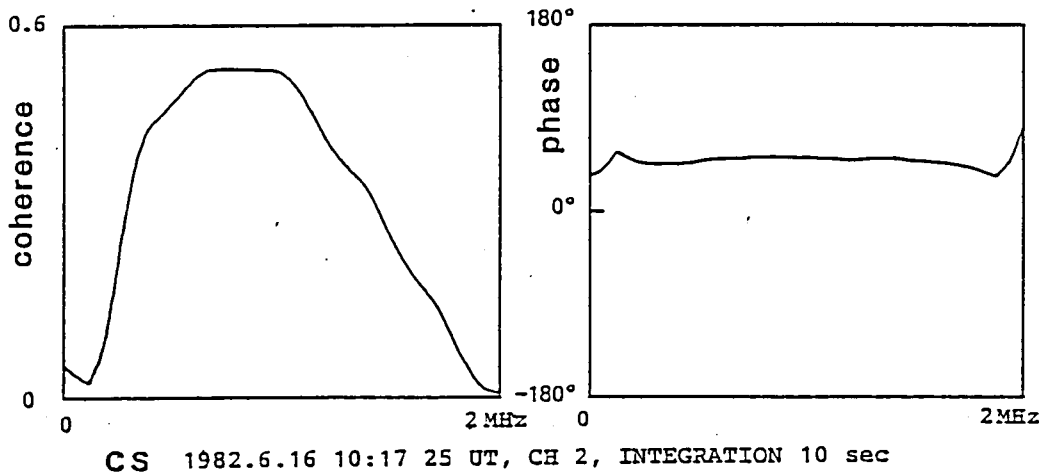


Fig.4.16 Cross-spectral amplitude and phase of a CS observation

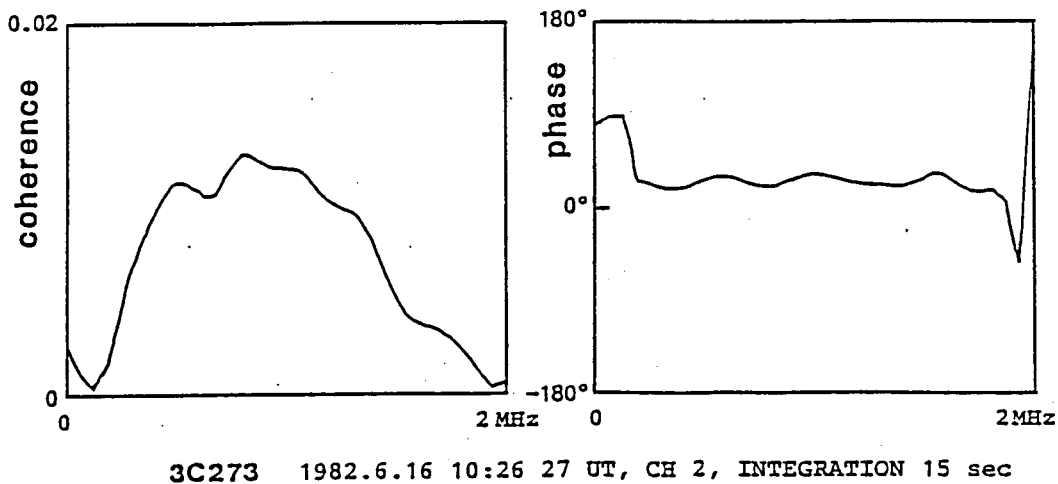


Fig.4.17 Cross-spectral amplitude and phase of a quasar observation

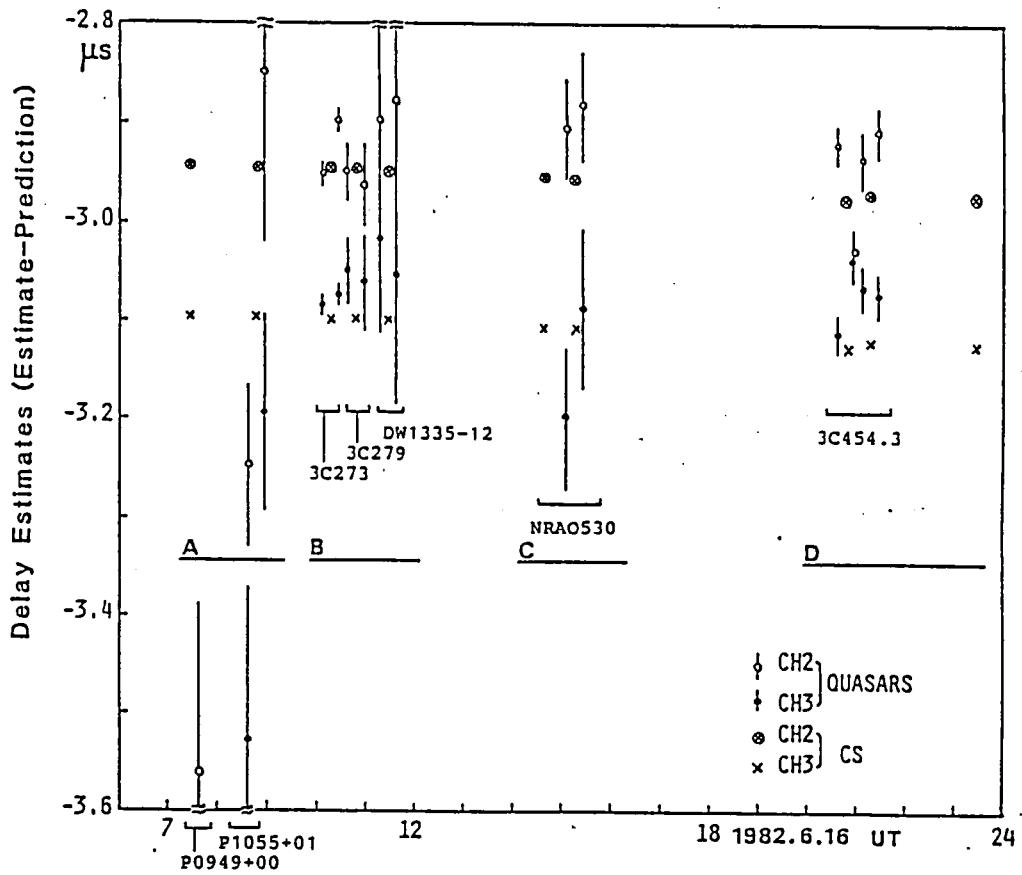


Fig. 4.18 Estimated delays
 The residuals from the predictions are shown. The bars are standard deviations, and A~D mean the observation periods.

Table 4.3 Accuracy of delay estimates

Observation number	Objects	Position of objects (1950.0)		Coherence (flux Jy)	Delay accuracy (nsec)
		right ascension	declination		
2-10	CS	_____	_____	0.412 (1240)	0.3
2	P0949+00	09 49 24.800	0 12 24.00	0.00078 (2.3)	140
3	P1055+01	10 55 55.330	1 50 03.35	0.00092 (2.8)	130
4	3C273	12 26 33.248	2 19 43.26	0.0093 (28)	11
5	3C279	12 53 35.835	-5 31 08.03	0.0029 (8.7)	38
6	DW1335-12	13 35 00.200	-12 42 10.00	0.00086 (2.6)	130
8	NRA0530	17 30 13.538	-13 02 45.93	0.0017 (5.1)	63
9,10	3C454.3	22 51 29.521	15 52 54.30	0.0046 (14)	23

4.4.2 Estimation of System Delay

Fig.4.18 shows the differences of the delay estimates between Channels 2 and 3, which are caused by the difference between the hardware performances of these channels. In the case of CS observations, they are pretty stable. The averages of them in the four time periods A, B, C and D in Fig.4.18 are 152.46 nsec, 151.32 nsec, 151.56 nsec and 149.68 nsec, respectively.

We assume that these delay differences for CS can be also applied to the quasars. Using these channel differences we can convert Channel 3 delay estimates to those which are equivalent to Channel 2 delay estimates. They are shown in Fig.4.19. We consider that the predicted delays for quasar observations are error free, then Fig.4.19 gives the estimates for the differential system delay between the two stations in Channel 2. Excluding the time period A which contains few data points, the differential system delays τ_B , τ_C and τ_D for the time periods B, C and D, respectively, are obtained by averaging the data shown in Fig.4.19. The results are summarized in Table 4.4.

Correcting the estimated delay using the differential system delays which were obtained above, we finally obtained the DVLBI delay observables for CS. The derived delay observables may have some bias error. Because the system delays in the observations of CS and quasars were not actually the same due to the difference between the power spectra of those signals. Suppose that the differences of the system delays between a CS

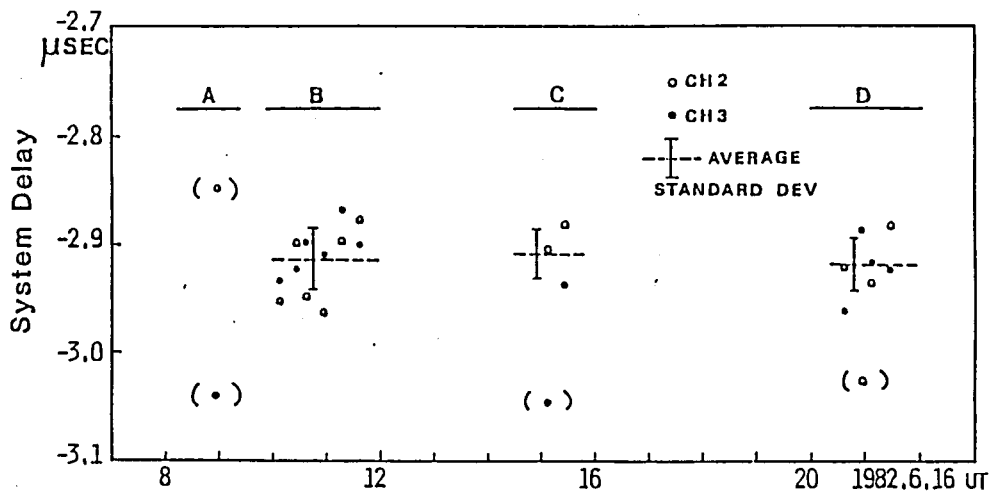


Fig.4.19 System delay estimates for Channel 2
 The data which are converted using the differential delay between the two channels are added. The broken line stand for the average in each period. (•): not used in averaging.

Table 4.4 System delay of Channel 2

Time period	System delay (nsec)	RMS (nsec)
A*	$\tau_A = \tau_B$	—
B	$\tau_B = -2913.51$	29
C	$\tau_C = -2907.96$	23
D	$\tau_D = -2918.18$	25

* τ_B is used in the period A.

observation and a quasar observation are denoted d_2 and d_3 for Channels 2 and 3, respectively. The error d_s of the differential system delay estimate of Channel 2 is given by

$$d_s = (d_2 + d_3)/2 \quad (4.19)$$

That is, the system delay estimate from the data shown in Fig.4.19 has the error d_s . This problem would be solved using, for example, phase tracking method if we had obtained much higher SNR of the observations. In our experiment, however, SNR was limited due to mainly instabilities of the clocks at both observation stations. Therefore, the possible bias error should be estimated in the orbit determination by the aid of other tracking data.

4.5 Orbit Determination and Accuracy Analysis

4.5.1 Orbit Determination

Orbit determinations were carried out using the tracking data obtained in the CS tracking experiment. Fig.4.20 shows the finally derived data points. The angle data in the night time were used (see Sec.4.2.1). In the orbit determination, the observation bias of the DVLBI observables and the solar radiation reflection coefficient of the satellite (the satellite cross-section multiplied with this coefficient is effective to the solar radiation pressure) were also estimated simultaneously. The bias of the DVLBI observables was introduced because of the reason mentioned in Sec.4.4.2. The range and angle measurements had been calibrated using an optical observation method⁽⁶⁾. We used the system parameters which have been updated through orbit determinations which were operationally performed in the CS project since then.

Table 4.5 summarizes the results of orbit determination with four accuracy models of DVLBI observables, Case 1 to Case 4. The same weights for the range and angles observables were used in all cases, which agreed with their actual characteristics. Cases 2 and 3 show that the estimated satellite position approaches to that of Case 1 as the assumed DVLBI delay accuracy becomes worse, while the estimates of the delay bias and the solar radiation reflection coefficient

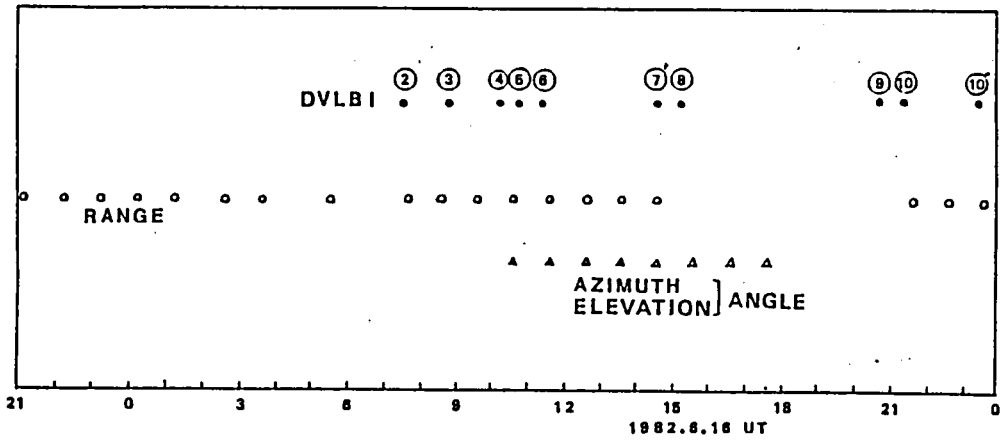


Fig. 4.20 Tracking data of CS
 The figures ②~⑩ corresponds to those in Fig.4.7.
 ⑦ and ⑩ mean that these were obtained by VLBI observations
 of CS only (not DVLBI).

Table 4.5 Result of orbit determination

	Orbit Determination			
	Case 1	Case 2	Case 3	Case 4
Observation Weight				
Range	0.52 m			
Azimuth Angle	0.98 x 10 ⁻³ deg			
Elevation Angle	0.85 x 10 ⁻² deg			
DVLBI Delay	not used	16.7 nsec (5.0 m)	3.33 nsec (1.0 m)	1.0 nsec (0.3 m)
Estimated Parameters				
DVLBI Delay Bias (nsec)	—	-83.79	-83.82	-83.66
Solar Radiation Reflection Coefficient	1.5084	1.5083	1.5071	1.5060
Satellite Position at Epoch Time				
		Deviation from Case 1		
X (km)	41918.261	-0.002	-0.030	-0.055
Y (km)	-4528.804	0.013	0.188	0.409
Z (km)	-194.197	-0.037	-0.496	-0.992

change only slightly. In other words, the DVLBI observables become almost meaningless if their accuracy is lower than about 3 nsec. Fig.4.21 shows the observation residuals of the range and the DVLBI delay data for Case 4, where the standard deviation of DVLBI delay residuals is about 1 nsec (0.3 m). Therefore it appears that the DVLBI observables obtained in our experiment might be effective to improve the orbit determination accuracy. However, the expected accuracy of the DVLBI observables was about 25 nsec as is shown in Fig.4.19. So it would be reasonable to consider that the small residuals in Fig.4.20 are obtained because of the small amount of DVLBI observables and that our DVLBI data are not useful for a precise orbit determination. Significant causes of the insufficiency of the DVLBI data are; 1) low accuracy of the delay data due to small SNR in the quasar observations, and 2) low sensitivity of the DVLBI delay observable to the satellite orbit due to shortness of the baseline. In the next section, covariance analyses show effects of some improvement in these two points.

4.5.2 Accuracy Analysis

Table 4.6 summarizes the results of the covariance analysis using six models. The DVLBI data were not used in Case a, DVLBI data with different models of accuracy were used

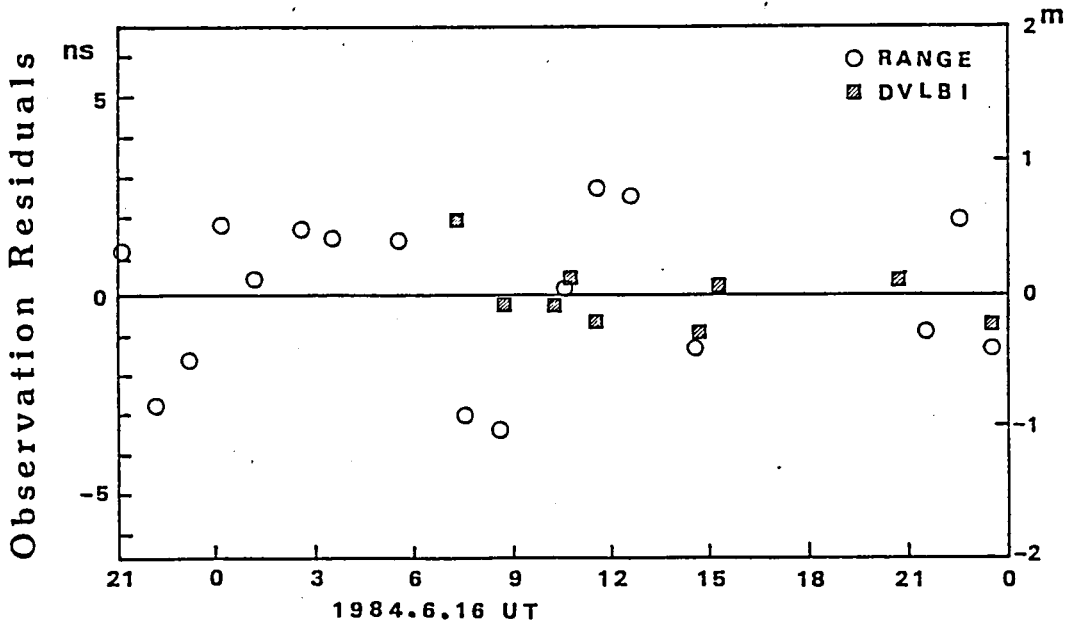


Fig.4.21 Observation residuals (range and DVLBI) corresponding to Case 4 in Table 4.5

Table 4.6 Result of covariance analysis

Covariance Analysis						
	Case a	Case b	Case c	Case d	Case e	Case f*
Observation Weight						
Range			0.52 m			
Azimuth Angle			0.98×10^{-3} deg			
Elevation Angle			0.85×10^{-2} deg			
DVLBI Delay (nsec) (m)	none	16.7 (5.0)	3.33 (1.0)	1.0 (0.3)	1.0 (0.3)	3.33 (1.0)
Parameter Uncertainty						
Solar Radiation Reflection Coefficient			0.003			
Earth's Gravity Constant			$0.04 \text{ km}^3/\text{sec}^2$			
Station Location (m)	1.0	1.0	1.0	1.0	0.5	1.0
Satellite Position Accuracy						
Parameter uncertainties are not considered						
σ_x (m)	47	46	33	18	18	2.9
σ_y (m)	158	158	146	128	128	17
σ_z (m)	455	446	318	129	129	20
Parameter uncertainties are considered						
σ_{xc} (m)	47	46	54	96	51	8.8
σ_{yc} (m)	173	172	170	367	220	65
σ_{zc} (m)	469	459	463	510	278	28
Information Content of DVLBI Observables						
	0	0.13	2.09	6.74	6.74	23.6

* DVLBI delay observables are replaced by those obtained by two baselines shown in Fig.4.22

in Cases b, c, d, and a model with smaller uncertainties in station locations was used in Case e. Simulated DVLBI data obtained by two baselines by three stations shown in Fig.4.22 (Kashima, Wakkanai and Yamagawa; they are all in Japan) were used in Case f.

Case d means that if we truly obtain the DVLBI data with an accuracy of 1 nsec, we can expect nearly 100 m accuracy of the orbit determination except the effect of the uncertainties in model parameters. In that case, we can expect 300 m accuracy, considering the effect of uncertainties in the model parameters including 50 cm uncertainties in the station locations, which is shown in Case e. In Case d, the satellite position accuracy which considers the effect of the parameter uncertainties is not improved from Cases a, b and c, in spite that the better accuracy of the DVLBI data is assumed. This is because the uncertainties in the VLBI station locations affect more in Case d than in the other cases. Case f shows a possibility of precise orbit determination with an accuracy of nearly 70 m by a combination of the conventional radio tracking and DVLBI with two baselines nearly 1000 km long.

The information content I_c which is defined by (see Eq.(2.48))

$$I_c = 1/2 \cdot \log_2(|P_0| / |P|)$$

is also shown in Table 4.6, where P is the 6-dimensional covariance matrix of the estimated position and velocity of CS,

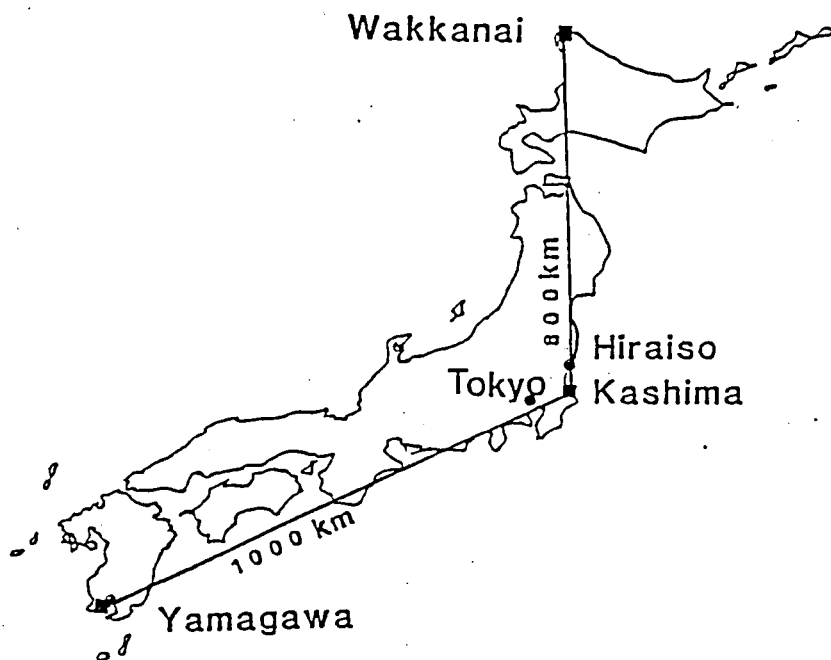


Fig.4.22 . Example of two, long baselines assumed in Japan

and $| \quad |$ denotes the determinant of a matrix. P_0 stands for the covariance with no DVLBI observables in the orbit determination. I_c is a measure of the information content of the DVLBI observables, because it represents the reduction of an error ellipsoid by the information brought by them. It is quantitatively clear that the more information is brought by DVLBI as its observables are the more accurate. Case f shows that DVLBI delay observables with longer baselines contain much larger amount of information even if the delay accuracy is about 3.3 nsec than that in a short baseline with a higher delay accuracy.

We used the range and the angle data obtained by the conventional radio tracking method as well as DVLBI data. In such a case, many types of tracking methods involved increase the number of parameters, such as calibration factors and observation system parameters, of which the uncertainties easily degrade the orbit determination accuracy. On the other hand, the DVLBI observables have an advantage that they are essentially free from bias errors or they can be calibrated by themselves. The station locations are also obtained by appropriate VLBI observations of quasars. So it would be better to use only DVLBI observables using truly long baselines to determine the orbit of a geosynchronous satellite with a high accuracy.

In our experiment, the insufficient quality of the DVLBI

delay observables is mainly due to the low accuracy of delay estimates in the observations of quasars. In order to obtain much better quality of quasar delays, some improvement which is effective to increase SNR would be required in the VLBI system. For example, a hydrogen maser frequency standard would be effective to achieve much longer integration time. It would also be important to use a phase calibration system which make possible to perform a bandwidth synthesis with observations in different frequency channels.

4.6 Conclusion

The geosynchronous satellite CS was tracked using a differential VLBI method. Since the baseline was short and the data quality of quasar observations were not sufficient, the obtained DVLBI delay observables were not actually useful to improve the orbit determination accuracy. However, orbit determinations and covariance analysis using various error models showed the possible effectiveness of DVLBI with a delay accuracy of better than 1 nsec, even with a short baseline 46 km long, in accurate orbit determination of geosynchronous satellites. A covariance analysis also shows that a DVLBI with long and independent baselines is very effective for an accurate orbit determination. Therefore, the goal 1) was fully

reached. Though the goal 2) was not completely attained, we obtained many fundamental points for an effective DVLBI. The goal 3) was also achieved by showing the possible effectiveness of a DVLBI method which can be applied to noise emissions from a geosynchronous satellite and supplies information to determine the orbit.

References

- (1) Tsukamoto, K., Y. Otsu, K. Kosaka, T. Shiomi, and H. Sasaoka, Experimental Program and Performance of Japan's Communication Satellite (CS) and Its First Results, IEEE Trans. on Comm, COM-27, 10, 1979.
- (2) Arimoto, Y., T. Shiomi, T. Nishigaki, S. Kawase and H. Murakami, Orbit Control of a Communication Satellite Based on One-Station Tracking, 13th International Symposium on Space Technology and Science, Tokyo, 1982.
- (3) Christensen, C. S., P. S. Callahan, B. Moultrie, F. F. Donovan and S. C. Wu, Results of a Demonstration of the Use of Δ VLBI Data for Precise Navigation of Interplanetary Spacecraft, AIAA/AAS Astrodynamics Conference, Danvers, Mass., 1980.
- (4) Shiomi, T., S. Kozono, Y. Arimoto, S. Nagai and M. Isogai, Precise orbit determination of a geosynchronous satellite by Δ VLBI method, J. RRL, 31, 133, July 1984.
- (5) Shiomi, T., S. Nagai, S. Kozono, Y. Arimoto and M. Isogai, Differential interferometry for precise tracking of a geosynchronous satellite, J. Guidance, Control and Dynamics, 9, 2, March-April 1986.
- (6) Kawase, S., N. Kawaguchi, T. Tanaka and T. Tomita, Optical Calibration of Geostationary Satellite Tracking System, IEEE Trans. on A. E. S., AES-17, 2, 1981.
- (7) Shiomi, T., S. Kawase, T. Nishigaki, K. Hayasaka and K. Hirai,

Satellite Control Experiments Via the CS, Review of the Radio Res. Labs., 26,140,1980(in Japanese).

(8) Kawano,N,F.Takahashi,T.Yoshino,K.Koike,H.Kumagai,and N.Kawajiri, Development of Real-Time VLBI and Measurements of Scintillation, J. Radio Res. Labs.,29,127,1982.

(9) Fugono,N,K.Yoshimura and R.Hayashi, Japan's Millimeter Wave Satellite Communication Program, IEEE Trans. on Comm.,COM-27,10,1979.

(10) Ojima,T.,N.Kawaguchi and Y.Hashimoto, K-band Facilities for CS Experiments, Review of the Radio Res. Labs.,24,131,1978(in Japanese).

CHAPTER 5 RRL-JPL DVLBI EXPERIMENT TO TRACK A GEOSYNCHRONOUS SATELLITE

5.1 Introduction

The effectiveness of a DVLBI method to track a geosynchronous satellite was shown in the CS experiment (Chapter 4). However, in that experiment there were some problems which hampered the thorough proof of the advantages of the DVLBI method. They were the shortness of the baseline, the poor quality of the DVLBI delay observables, the insufficiency of observability of DVLBI due to the single baseline, and additional model errors (including observation bias errors) due to the inclusion of other tracking methods (that is, ranging and angle measurements). The necessity to use truly long baselines which supply sufficient observability and data quality was seriously recognized.

On the other hand, a group in JPL had also applied a DVLBI method to tracking a US geosynchronous satellite (DSCS-II), which is above the Pacific Ocean, with three baselines spanned by earth stations at Goldstone in California, Canberra in Australia and Guam Island (1)(2). They attained nearly 30 m position accuracy of the satellite. The accuracy was limited mainly by the high system noise temperature and the

instability of the frequency standard at Guam station.

Under those background, a planning of a joint experiment between RRL and JPL began in late 1982 while the author had stayed at JPL. The goal of the experiment was mainly to demonstrate the capability of the DVLBI method to attain an accuracy of a few meters of satellite position determination. The technical agreement on the joint experiment was negotiated and signed by both RRL and JPL in 1984.

In this chapter, the system of the experiment is described first, then the sensitivity of the DVLBI observables and observation strategy are discussed. Following the description on the data processing, we discuss in detail the orbit determination and its accuracy⁽³⁾⁽⁴⁾.

5.2 System of Experiment

5.2.1 Earth Stations and VLBI System

The observation geometry of the RRL-JPL joint experiment to track the geosynchronous satellite DSCS-II is shown in Fig.5.1. The VLBI stations are at Kashima (RRL, Japan), Goldstone (DSN:Deep Space Network, USA), Canberra (DSN, Australia) and Owens Valley (OVRO:Owens Valley Radio Observatory, California Institute of Technology, USA). Among the baselines spanned by these stations, three baselines with

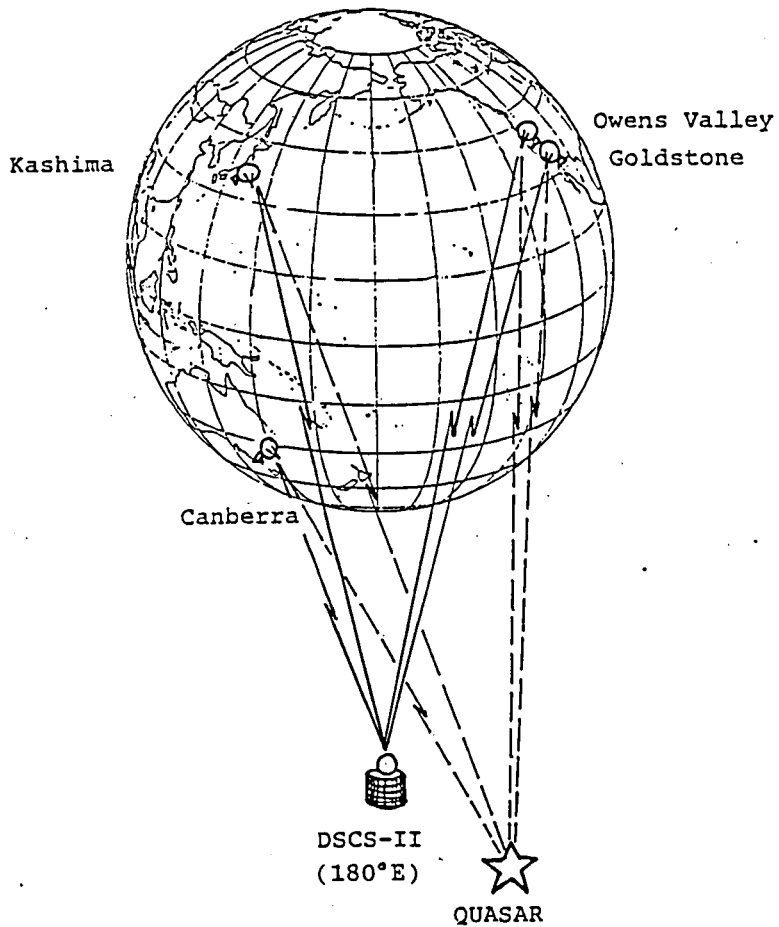


Fig. 5.1 Geometry of RRL-JPL experiment on DVLBI tracking of DSCS-II, June 1984

Kashima, Canberra and Goldstone (or Owens Valley) are important because they are not only long (7000 to 10000 km) but also different each other in directions. This means we can fully take advantages of the DVLBI to measure the orbital motion of the satellite (see also Sec. 3.3.2). The main features of the VLBI stations are shown in Table 5.1.

The Block-0 VLBI backend system⁽⁵⁾ which was developed by JPL was used in the experiment. The observation bandwidth is 2 MHz per channel and two channels with nearly 8 MHz apart in frequency were used to observe the satellite and quasar signals alternatively in a 2 GHz frequency band. The two channels were alternated every 1 second and the received signals were sampled, digitized and formatted, and recorded on a video tape at each station.

At Kashima station, RRL, we used 26 m antenna and K-III VLBI system, both of which were controlled by a computer HP-1000, for signal reception and down-conversion into an intermediate frequency band. A set of Block-0 backend system shipped from JPL was used to digitize and record observation signals. As shown in Fig.5.2, we also used a frequency counter to measure the carrier frequency of the satellite. The carrier frequency information was used to construct a phase model of the satellite tone signal in the correlation processing of the satellite signal (see Sec. 5.4.1).

Table 5.1 VLBI receiving station specifications

Station	Spin Radius km	Location		Z-Height km	Antenna m	Aperture Efficiency	System Temp. K
		East Long. deg					
Kashima RRL, Japan	5169.055	140.6627		3724.118	26	0.57	125
Canberra DSN, Australia	5205.251	148.9813		-3674.749	64	0.55	35
Goldstone DSN, USA	5215.484	243.2051		3660.957	26	0.55	35
Owens Valley OVRO, USA	5085.449	241.7173		3838.603	40	0.55	120

DSN: Deep Space Network, NASA

OVRO: Owens Valley Radio Observatory, California Institute of Technology

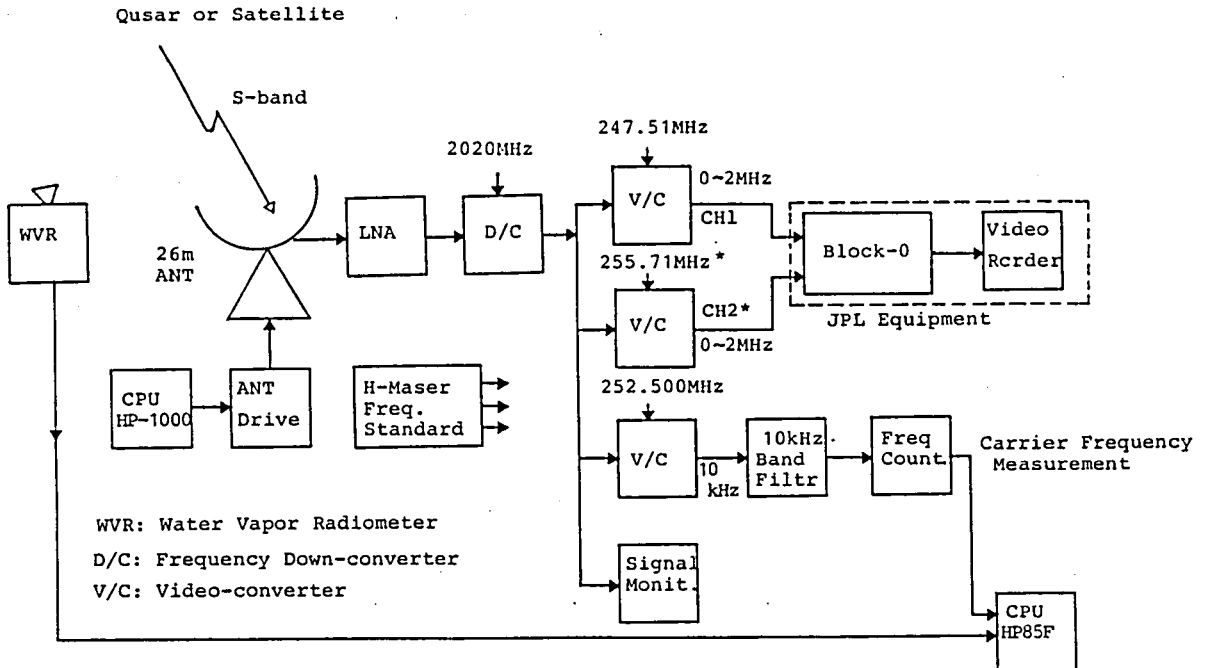


Fig. 5.2 VLBI system at Kashima station

The CH2 local signal frequency was changed to 249.56 MHz for two and half hours in the mid of 24-hour observation period (see also Fig.5.3) in order to make the frequency separation between the two channels narrower.

We also obtained the ionospheric total electron content data at Tokyo from a section at RRL. The data were derived from the Faraday rotation measurements of the 136 MHz beacon from a geosynchronous satellite ETS-II (Engineering Test Satellite Type II, Japan).

5.2.2 Geosynchronous Satellite and Its Signal

We needed a geosynchronous satellite which could be seen at all stations and transmitted signals in the 2 GHz and/or 8 GHz bands to which the VLBI system could be applied. The DSCS-II is the only satellite which satisfies the condition. It transmits 2 GHz signal and is stationed at the longitude 180 degrees east with an orbital inclination angle of about 3.5 degrees. Fig.5.3 shows the signal spectrum in the 2 GHz frequency band of DSCS-II and the receiving channel assignment. In order to make easy to resolve an ambiguity (the ambiguity is decreased as the frequency separation becomes small between the two observation channels; see Eq.(3.34) and also Sec.5.4.1), Channel 2 was assigned to observe the - 2nd harmonic tone for about two and a half hours during the total 24 hour observation span. The satellite has a subcarrier with the frequency 1.024 MHz, which is modulated by telemetry signal. The subcarrier modulated the phase of the main carrier of the frequency 2277.5 MHz. The satellite signal $S(t)$ is written as⁽¹⁾

$$S(t) = A \cos(\phi_c(t) + b a_t \sin \phi_s(t)) \quad (5.1)$$

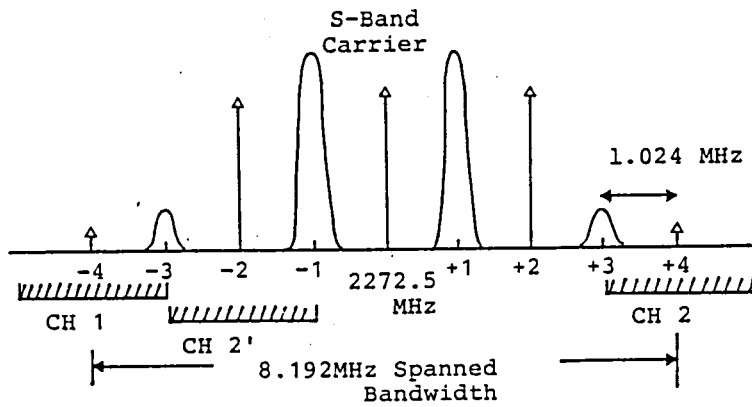


Fig.5.3 S-band spectrum of DSCS-II and VLBI observation channel assignment
 (CH 1 and CH 2; CH 2 used instead of CH 2 during a part of the observation period for ambiguity resolution)

Table 5.2 Receiving power estimation of the ± 4 th harmonic tones at Kashima station

DSCS-II		
Transmitter Power	31.27	dBm
Antenna Gain	4	dB
Feeder Loss	-5	dB
EIRP	30.27	dBm
Modulation Loss	-36.48	dB
± 4 th Harmonic Power	-6.48	dB
<hr/>		
Propagation Loss (Free Space)	-191.3	dB
Atmospheric Attenuation	-1	dB
<hr/>		
Kashima Station		
Antenna Gain	53	dB
Receiver Input Power	-145.8	dBm

where

$$\phi_c(t) = \omega_c t + \phi_0 \quad : \text{ carrier phase}$$

$$\omega_c \quad : \text{ carrier angular frequency}$$

$$\phi_s(t) = \omega_s t \quad : \text{ subcarrier phase}$$

$$\omega_s \quad : \text{ subcarrier angular frequency}$$

b : modulation index (a constant $0 \leq b \leq \pi/2$)

a_t : telemetry signal bit (+1 or -1)

The rate at which the telemetry bit transition is occurred is much less than the subcarrier frequency. So over a time interval where the telemetry bit is fixed at some value a , the signal can be described as

$$S(t) = AJ_0(ba) \cos \phi_c(t) + 2A \cos \phi_c(t) \sum_{n:\text{even}} J_n(ba) \cos n \omega_s t - 2A \sin \phi_c(t) \sum_{n:\text{odd}} J_n(ba) \sin n \omega_s t \quad (5.2)$$

The function $J_n(n:\text{even})$ assumes only positive values over the range of argument value allowed here. On the other hand, the function $J_n(n:\text{odd})$ is an odd function. Therefore, even when there exist telemetry transitions, the even harmonics experience only a change in amplitude. So we can call them tones which can be observed by VLBI stations and are correlated with phase models which are created for each stations (we call these as local phase models). Table 5.2 shows the receiving power of the ± 4th harmonic tones at Kashima station.

5.2.3 Quasars and Observation Window

In order to fully take advantage of a DVLBI method, we should use quasars which are viewed angularly close to the satellite. However, quasars which have enough correlation flux density and can be used as reference radio sources are limited in numbers and do not necessarily distribute uniformly in the sky. Therefore, we must use several quasars, even though their separation angles from the satellite were not small enough, as long as they came into the observation window. Fig.5.4 shows the observation window with respect to the major three VLBI stations (Kashima, Canberra and Goldstone) and quasar candidates for the reference sources. The observation window moves with the period of 24 hours along the axis of right ascension in Fig.5.4. Since the satellite has finite distance from each VLBI station, it is viewed at each station in slightly different angular position in the observation window. In Table 5.3 are summarized the quasars which were actually used in the experiment. We discuss the optimization of the observation schedule in Sec. 5.3.3.

5.3 Observation Strategy

5.3.1 Sensitivity of Delay Observables

As shown in Sec.3.3.2 the sensitivity of a DVLBI delay

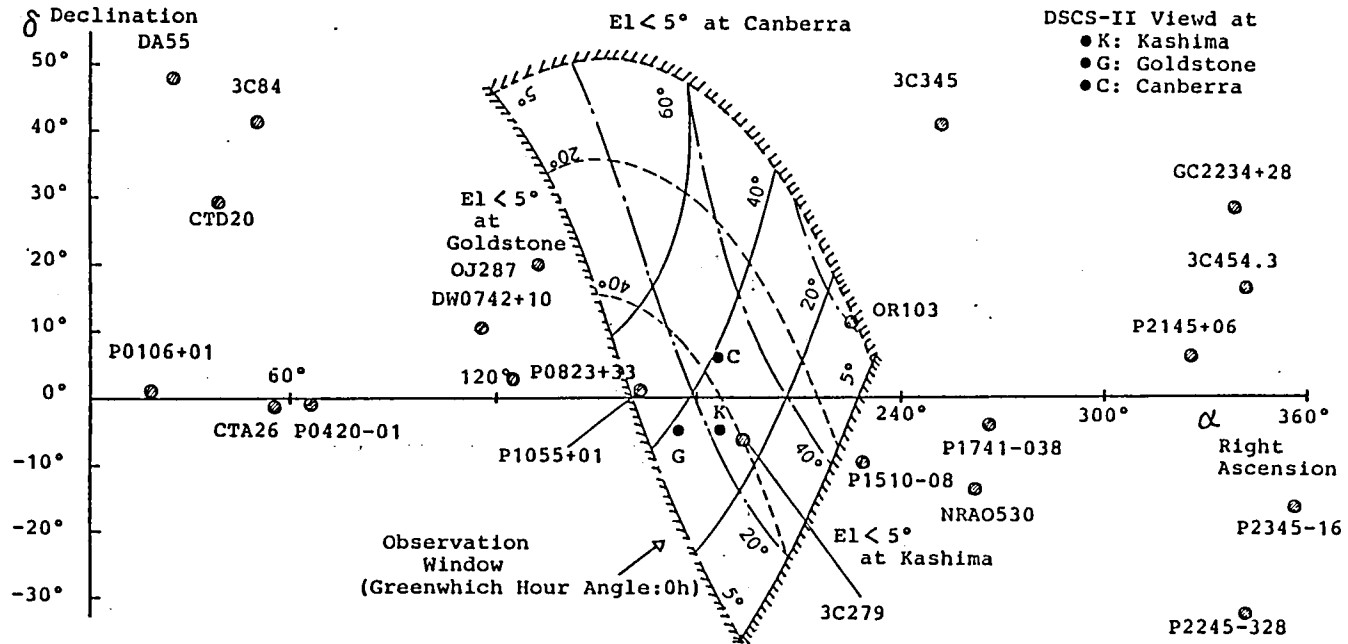


Fig. 5.4 Observation window for the three VLBI stations (Kashima, Canberra and Goldstone) and candidate quasars for DVLBI observations

Table 5.3 Quasar position in the J2000 coordinate system (JPL catalog)

Quasar	Right ascension			Declination		
	Hour	Min	Sec ^s	Deg	Arc min	Arc sec
P0106+01	01	08	38.77103	01	35	00.3199
CTA26	03	39	30.93767	- 01	46	35.7970
P0420-01	04	23	15.80076	- 01	20	33.0648
DW0742+10	07	45	33.05976	10	11	12.6891
P0823+033	08	25	50.33862	03	09	24.5159
OJ287	08	54	48.87516	20	06	30.6377
P1055+01	10	58	29.60529	01	33	58.8205
3C279	12	56	11.16656	- 05	47	21.5271
OR103	15	04	24.97976	10	29	39.1975
P1741-038	17	43	58.85607	- 03	50	04.6162
P2145+06	21	48	05.45869	06	57	38.6060
3C454.3	22	53	57.74794	16	08	53.5627

observable with respect to a satellite position is evaluated using the sensitivity vector (vector difference between unit vectors which direct to the satellite at a pair of VLBI stations). Table 5.4 shows the sensitivity vectors for the three major baselines in our experiment. These vectors are described in the earth's body-fixed coordinate system (X_b , Y_b , Z_b), where Z_b is in the earth's spin axis and X_b is in the intersection of the equatorial plane with the Greenwich meridian plane. Though the satellite DSCS-II has an orbital inclination of about 3.5 degrees, the sensitivity vectors were evaluated neglecting it (the inclination has not large effect on our sensitivity evaluation). As is clear in Fig.5.5, the sensitivity in the X_b -axis, Y_b -axis and Z_b -axis corresponds to the satellite position change in the radial, along-track and cross-track directions, respectively. The three baselines have the major sensitivities in the along-track and the cross-track directions with the magnitude of about 0.2. In other words, a satellite motion of 5 m in one of those directions gives a DVLBI delay observable change of 1 m for the corresponding baseline. As is discussed in the next section, it would be possible to attain an DVLBI delay accuracy of 1 m, so we can expect to determine the satellite orbital position with a few meters accuracy (we already discussed in Sec.3.3.3 that the radial component of the satellite position can also be determined by VLBI delay observables).

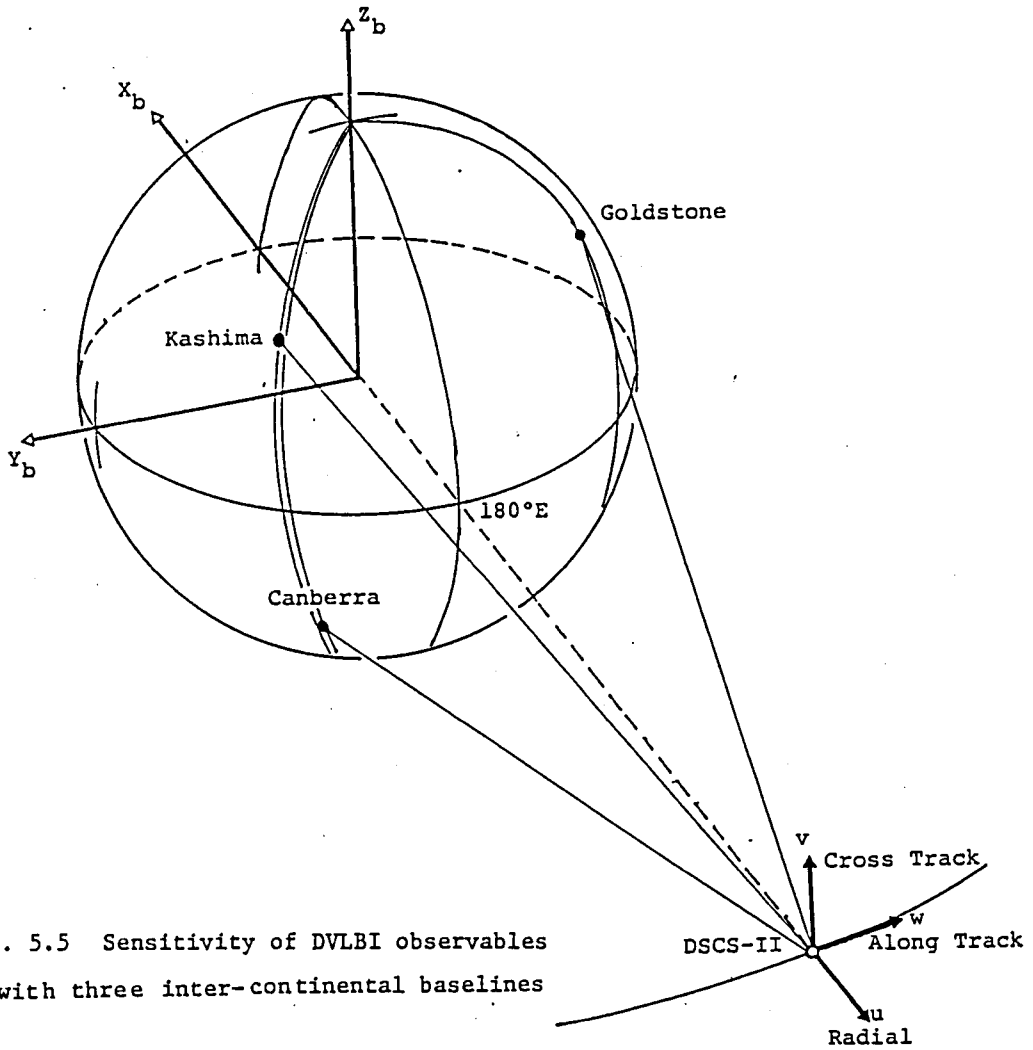


Fig. 5.5 Sensitivity of DVLBI observables with three inter-continental baselines

Table 5.4 Sensitivity vectors of DVLBI delay observable

Components of the sensitivity vector	Baselines		
	Kashima - Goldstone	Goldstone - Canberra	Kashima - Canberra
x_b	0.003	- 0.004	0.001
y_b	<u>0.201</u>	<u>- 0.187</u>	- 0.014
z_b	0.006	<u>0.188</u>	<u>- 0.194</u>

Underlines show major components

5.3.2 Observation Model and Errors

A general description on errors in a DVLBI delay observable is already given in Sec.3.4. Here we evaluate some significant errors in the RRL-JPL DVLBI observation system. As is described in Sec.5.3.1, each baseline spanned by the VLBI stations in Japan, Australia and USA has almost the same sensitivity of the delay observables to the spacecraft position change. For example, about 20 cm of delay change corresponds to 1 m in the spacecraft position change. Therefore, it is required to use a precise observation model which gives the delay observable with the total accuracy of less than 1 m in order to fit the spacecraft orbit within a few meters error.

(i) SNR Error

Concerning the three baselines formed by stations Kashima, Canberra and Goldstone, we can evaluate SNR error in the DVLBI delay observable as shown in Table 5.5. The error in the DVLBI delay observable is mainly determined by a reference quasar with a low correlation flux density.

(ii) System Delay and Clock Errors

These errors are removed in a DVLBI delay observable and negligible in our experiment.

Table 5.5 SNR error in DVLBI delay observable

Observation Condition			
Bandwidth (1 channel)		B = 2 MHz	
Effective Bandwidth (2 channels)		5.8 MHz	
Integration Time		T = 600 sec	
Coherence Loss Factor		L = 0.5	
DSCS-II Observation			
Station	Kashima	Goldstone	Canberra
S/C Signal (dBm)	-145.8	-146.0	-138.0
System Noise (dBm)	-114.6	-120.0	-120.0
SNR	956	1770	4360
Delay Error(cm) (with respect to model tone)	0.86	0.47	0.19
	Baseline		
	Kashima -Goldstone	Goldstone -Canberra	Canberra -Kashima
Delay Error (cm)	0.98	0.51	0.88
Quasar Observation (Flux density : S J _y)			
SNR	40.0 S	182.0 S	98.3 S
Delay Error(cm)	21/S	4.5/S	8.4/S
(S=0.2 J _y :	105	22.5	42)
(S=5.0 J _y :	4.2	0.9	1.7)
DVLBI Delay Error (cm)			
S=0.2 J _y :	105	22.5	42
S=5.0 J _y :	4.3	1.0	1.9
1 J _y = 10 ⁻²⁶ watt m ⁻² Hz ⁻¹			

(iii) Propagation Media Errors

The tropospheric delay errors can be evaluated using Eqs.(3.69) and (3.70) if an observation geometry is given. Here we use a model of typical quasars set, which is shown in Fig.5.6. In Fig.5.6, three quasars a, b and c have different declinations. Table 5.6 shows the calculated DVLBI delay errors due to the tropospheric delay corrections (where the tropospheric delay correction errors in the zenith are assumed 4 cm for a systematic delay and 2 cm for a random delay). The errors for the baselines which include Goldstone station become large, because of the low elevation angle of the satellite at Goldstone, which consequently leads to the large separation angle between a quasar (cases a and b in Fig.5.6) and the satellite.

The ionospheric delay errors can be evaluated using Eqs.(3.71) and (3.74). Let us take the case a in Fig.5.6 (or in Table 5.6) with the Kashima-Goldstone baseline. In this case, the source separation angles at both stations are large and the satellite's elevation angle at Goldstone is low, so we can evaluate a conservative delay error. If we use the solar-zenith angles $\chi_1 = \chi_2 = 40^\circ$, then we obtain a DVLBI ionospheric delay systematic error $\sigma_I = 33$ cm (with a zenith systematic delay correction error $\sigma_{IZ} = 50$ cm) and a random error $\sigma_R = 93$ cm (with a zenith random delay correction error $\sigma_{RZ} = 20$ cm).

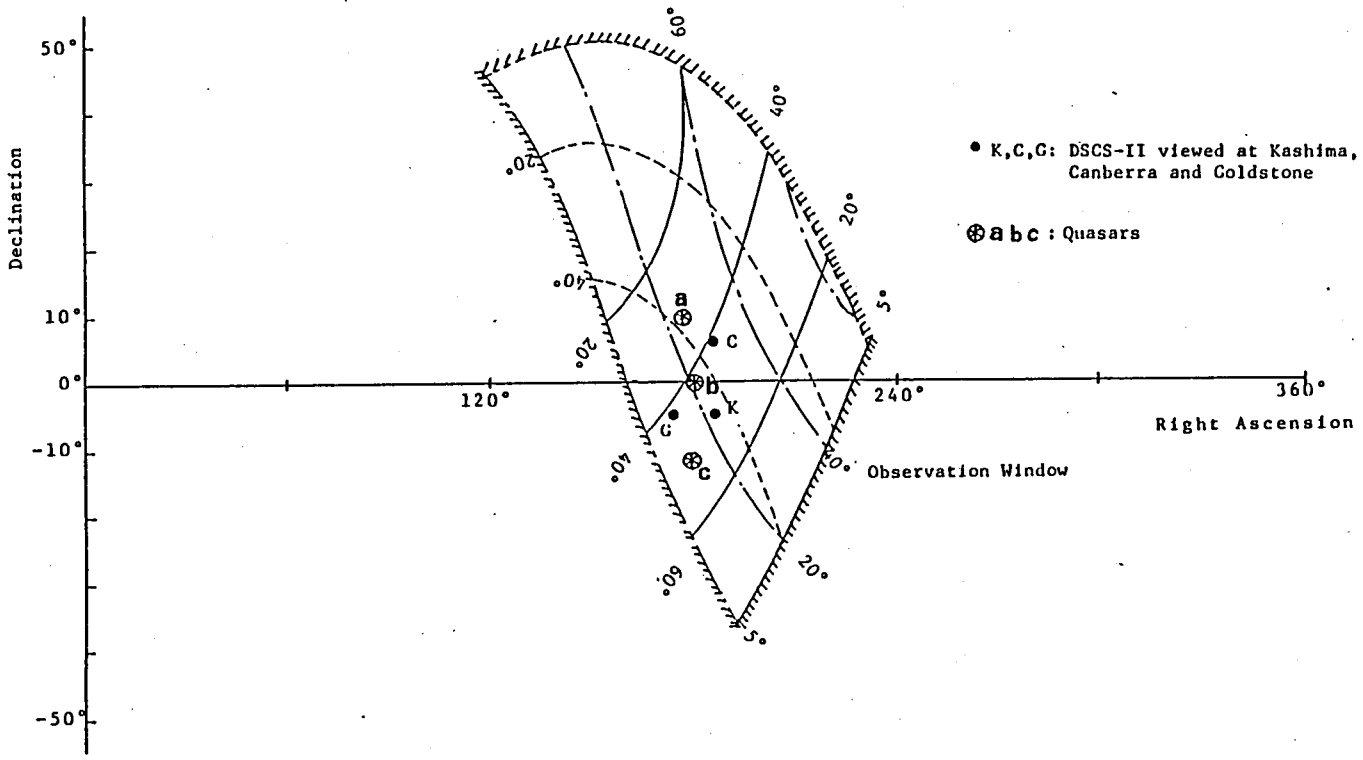


Fig. 5.6 Typical quasars in the observation window

Table 5.6 DVLBI observations with a typical quasars set and tropospheric delay correction errors

DVLBI observation model

Sources	Elevation angle (Elevation difference between quasar and satellite, degree)		
	Kashima	Goldstone	Canberra
Quasars			
a (OR103)	48 (17)	23 (10)	38 (1)
b (P1055+1)	38 (7)	21 (8)	44 (7)
c (P1510-08)	30 (1)	12 (1)	52 (15)
Satellite	31	13	37

Tropospheric delay correction errors

Quasar	Delay correction error (cm)		
	Systematic error (Random error)		
	Kashima-Goldstone	Goldstone-Canberra	Canberra-Kashima
a	7.9 (11.3)	7.5 (11.3)	2.4 (6.6)
b	6.7 (11.7)	6.7 (11.4)	1.5 (6.7)
c	1.5 (14.2)	2.1 (13.8)	1.6 (7.0)

(iv) Station Location Error, UT1 Error and Polar Motion Error

In the Table E.1 (Appendix E), we used two models for station location errors which are 1 m in model 1 and 10 m in model 2. In our experiment, however, we can expect small station location errors (about 10~20 cm) for all the stations. Because all the stations have been used as base stations in geodesic and astrometric observations using VLBI and their coordinates have been precisely determined.

A typical model of errors in UT1 and polar motion is also given in Table E.1. The UT1 correction error of 0.6 msec corresponds to a station location error of about 23 cm assuming 5200 km for the spin radius of the station. Polar motion correction error of 47 nrad corresponds to a station location error of about 30 cm.

(v) Quasar Position Error

The DVLBI delay error due to a quasar position error is not negligible when the baselines are long. As is described in Sec.3.4.3, the error is about 20 cm for the intercontinental baselines in the RRL-JPL experiment.

5.3.3 Observation Schedule

Three 24-hour DVLBI observations of DSCS-II were planned in late June 1984 considering the availability of the sensitivity stations. We carried out two rehearsals prior to

the actual observations. Fig.5.7 shows a summarized schedule of the experiment. It is desirable to perform observations of the satellite and of a reference quasar in a short period. However, it takes a certain time to slew antennas between radio sources. In our experiment the satellite and quasar observations were alternated every 15 minutes, where nearly 10 minutes of effective observation period for each source was obtained.

Since the number of quasars which can be used as reference radio sources is limited and the quasars do not distribute uniformly in the sky, we have to make an optimum observation schedule. In order to select the best quasar from those in the observation window at an each observation epoch, we should take into consideration the following errors which are dependent on a quasar selection as; the SNR error, the propagation media error, the station location error and the quasar position error. Fig.5.8 shows an example of error evaluations for a candidate set of quasars, where the SNR errors, the tropospheric delay correction errors and the station location errors are shown by bar graphs at the beginning time of each observation. The SNR errors were calculated using the same parameters which were used in Table 5.5 except that the coherent loss coefficient $L=0.7$, the integration time $T=300$ sec and the 34 m antenna at Canberra station were assumed. The tropospheric delay correction errors were calculated using

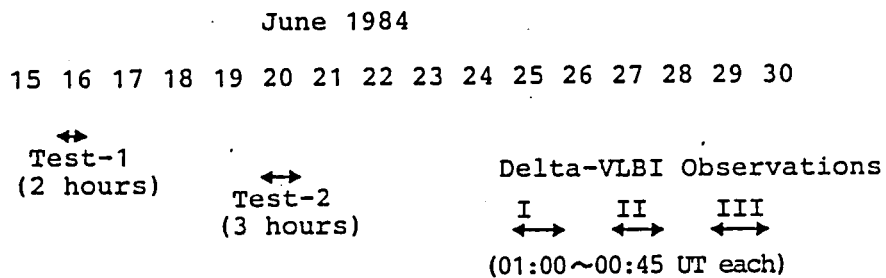


Fig. 5.7 Tests and three 24-hour DVLBI observations

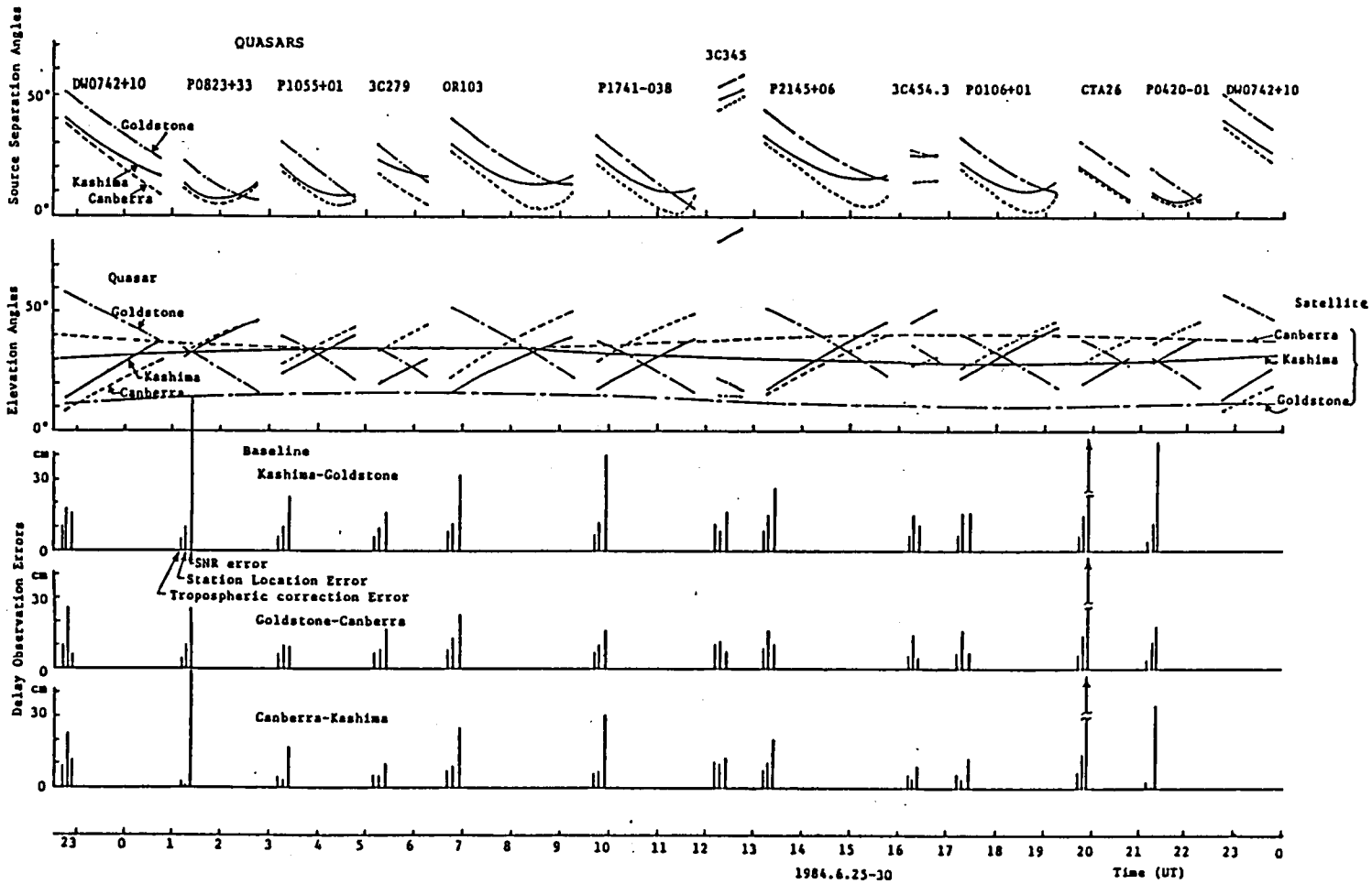


Fig. 5.8 An example of quasar set and evaluation for delay errors

$\sigma_{TZ1} = \sigma_{TZ2} = 4$ cm in Eq.(3.69) and the station location errors were calculated using $\sigma_{g1} = \sigma_{g2} = 10$ cm in Eq.(4.13). Fig.5.9 shows the finally selected quasars for the 24-hour observations.

5.4 Data Processing

5.4.1 Derivation of Delay and Delay Rate Observables

The recorded signal at a pair of VLBI stations were processed by Block 0 correlator at California Institute of Technology (CALTECH). In the case of a quasar observation, the recorded signals with 2 MHz bandwidth were directly correlated. The correlated phase at the center of the passband and the correlated amplitude were obtained every 1 second for each observation channel. The correlated phases were tracked, or were fit, to give smoothed phase data at every 60 seconds for each channel (see Fig.3.5 in Sec.3.2.2 (ii) phase tracking method). We obtained the delay rate observable from the phase rotation rate in time, and we obtained the delay observable from the differenced phase of the two channels (see Eq.(3.34)).

The delay rate observable has no ambiguity, but the delay observable may have cycle ambiguities which correspond to the spanned bandwidth of the two channels (that is, about 8 MHz in the ordinary observation mode, and 2 MHz in the special

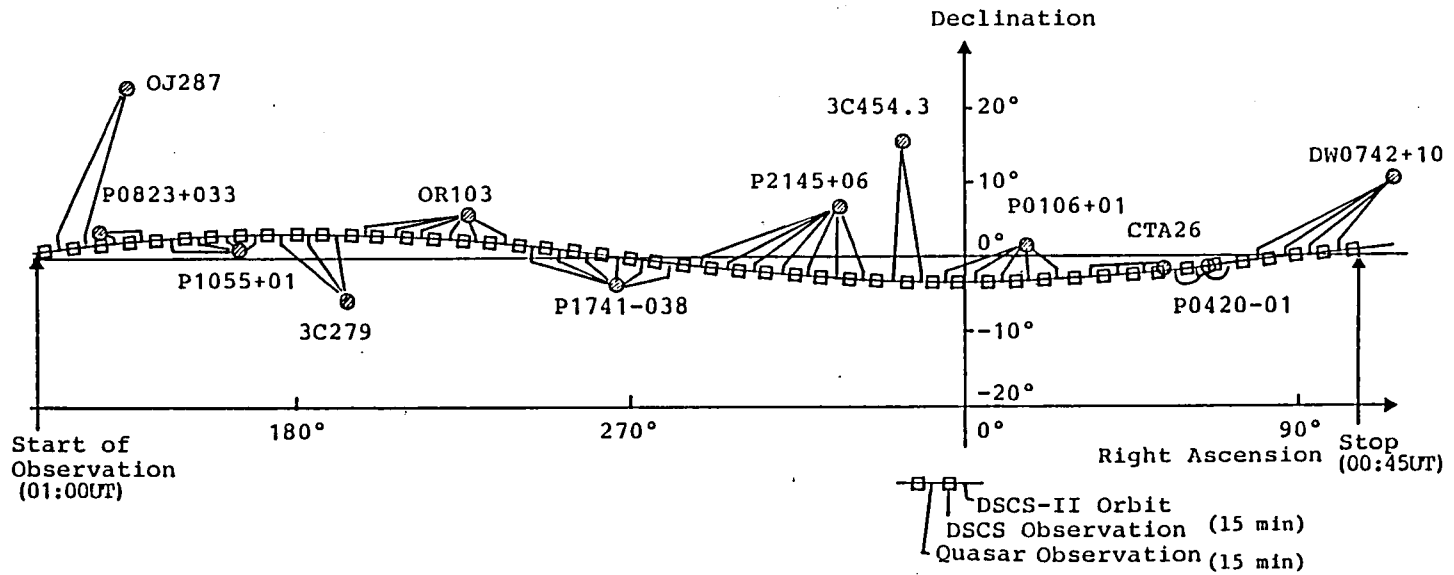


Fig. 5.9 DVLBI observation schedule (June 25-30, 1984)

observation mode; see Fig. 5.3). The both observables have some systematic bias caused by instrumental phase delays and clock errors. They were corrected by using a priori knowledge of the quasar position and the baseline vector (Sec.5.4.2 (v)).

In the case of a DSCS observation, the spacecraft signal consists of tones. Therefore, the recorded signal at each station and a numerically constructed tone based on the predicted frequency for each station (local phase model) were correlated (see Sec.3.2.1). The local phase model for each station was constructed by using an approximation with 2 nd order polynomials in time based on the measured carrier frequency at Kashima station. That is, the observed tone frequency was approximated by

$$f(t) = f_0 + f_1t + f_2t^2 \quad (5.3)$$

where $f(t)$ is the frequency at time t . The coefficients f_0 , f_1 and f_2 were derived from the measured frequency of the satellite carrier signal. The Doppler frequency-shift were taken into consideration for each station by using an initial knowledge for the state vector of DSCS. Fig. 5.10 shows the measured frequency of the carrier signal received at Kashima station. The difference between the observation and the prediction was caused by the instability of the satellite's oscillator. The phase of the received spacecraft tone was measured every 1 second with respect to the local phase model through the correlation processing. Then the difference of the

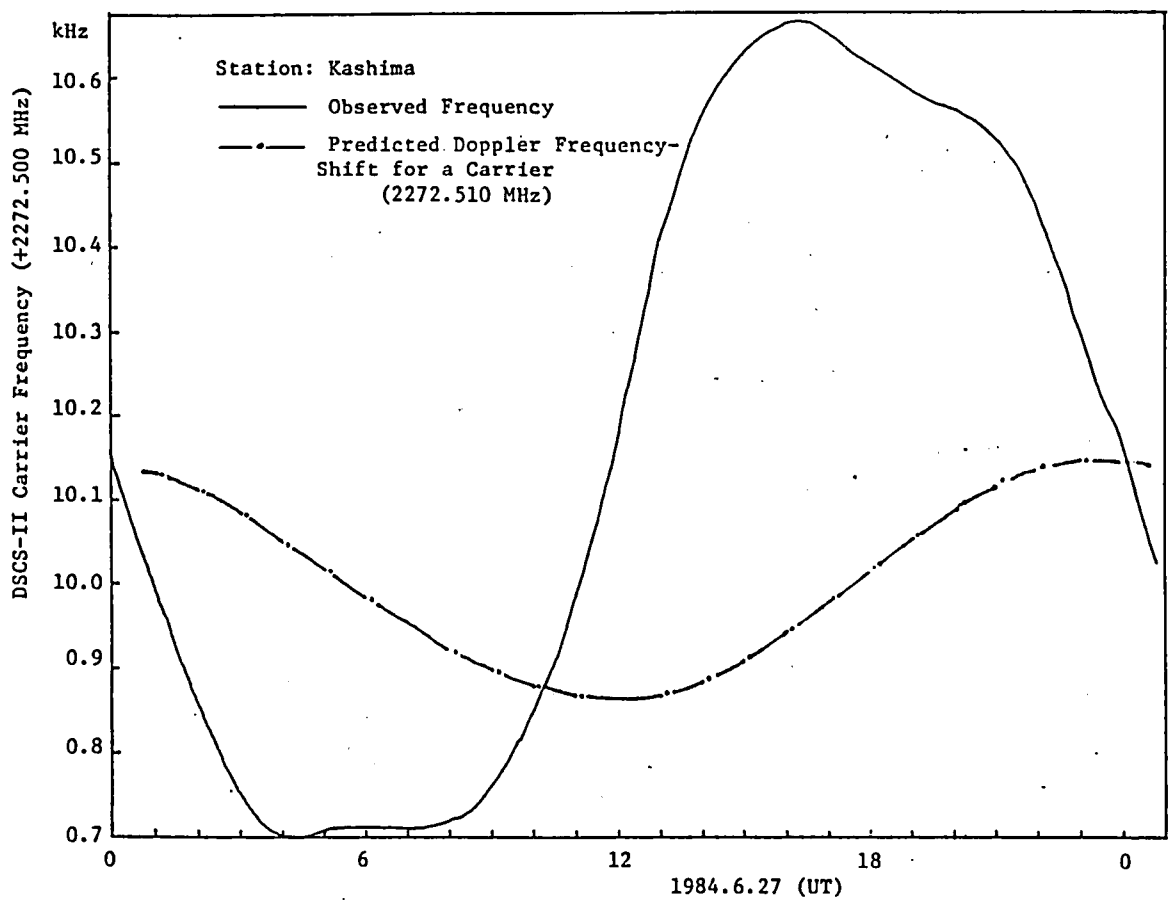


Fig. 5.10 DSCS-II carrier frequency measured at Kashima

measured phases at the two receiving stations gave the correlated phase which is written as

$$\begin{aligned} \varphi(\omega_i, t) &= \int_{t_0}^{t-p_1} \omega_i(s) ds - \int_{t_0}^{t-p_2} \omega_i(s) ds + \phi_i \\ &\doteq (p_2 - p_1) \cdot \omega_i \left(t - \frac{p_1 + p_2}{2} \right) + \phi_i \end{aligned} \quad (5.4)$$

where

$\varphi(\omega_i, t)$: difference of measured tone phases

ω_i : tone angular frequency of the observation channel i

p_i : propagation time of a radio signal between the satellite and station i (see Fig.3.6)

ϕ_i : differential phase due to instruments at the stations

The satellite delay observable τ_s is obtained from $\varphi(\omega_1, t)$ and $\varphi(\omega_2, t)$ by the same process given in Eq.(3.34) as

$$\begin{aligned} \tau_s &= \frac{\varphi(\omega_2, t) - \varphi(\omega_1, t)}{\omega_2(t^*) - \omega_1(t^*)} \\ &= (p_2 - p_1) + \frac{\phi_2 - \phi_1}{\omega_2(t^*) - \omega_1(t^*)} + \frac{2m\pi}{\omega_2(t^*) - \omega_1(t^*)} \end{aligned} \quad (5.5)$$

where

$$t^* = t - \frac{p_1 + p_2}{2} \quad (5.6)$$

and m is an integer. The first term of Eq.(5.5) means the propagation delay of the satellite signal, the second term

instrumental delay which is the same as that in quasar observations, and the third term ambiguity. The delay rate observables were derived in the same process as Eq.(5.5) replacing $\varphi(\omega_i, t)$ with its rate $\dot{\varphi}(\omega_i, t)$. The delay and delay rate observables were obtained every 30 seconds for each baseline.

5.4.2 Pre-Processing of Raw VLBI Observables

By using the Block 0 correlator and the related phase tracking software, we obtained the raw VLBI observables. They consisted of delay and delay rate data at every about 30 seconds for the satellite, and at every about 60 seconds for a quasar. Prior to the usage of these observation data in an orbit determination program, we performed the pre-processing of the raw data, which smoothed and compressed them into much smaller number of data. Then we made various corrections (for example, propagation media delay corrections), resolved the ambiguity, and derived the differential observables (that is, calibrated the DSCS data by the quasar data). The pre-processing and the orbit determination were carried out independently at RRL and JPL by using the different software systems. We describe the pre-processing at RRL. Fig.5.11 shows the outline of the pre-processing.

(i) Smoothing

Each 10 minute-observation period has 10~20 points of raw data (every 30 or 60 seconds). These data points were

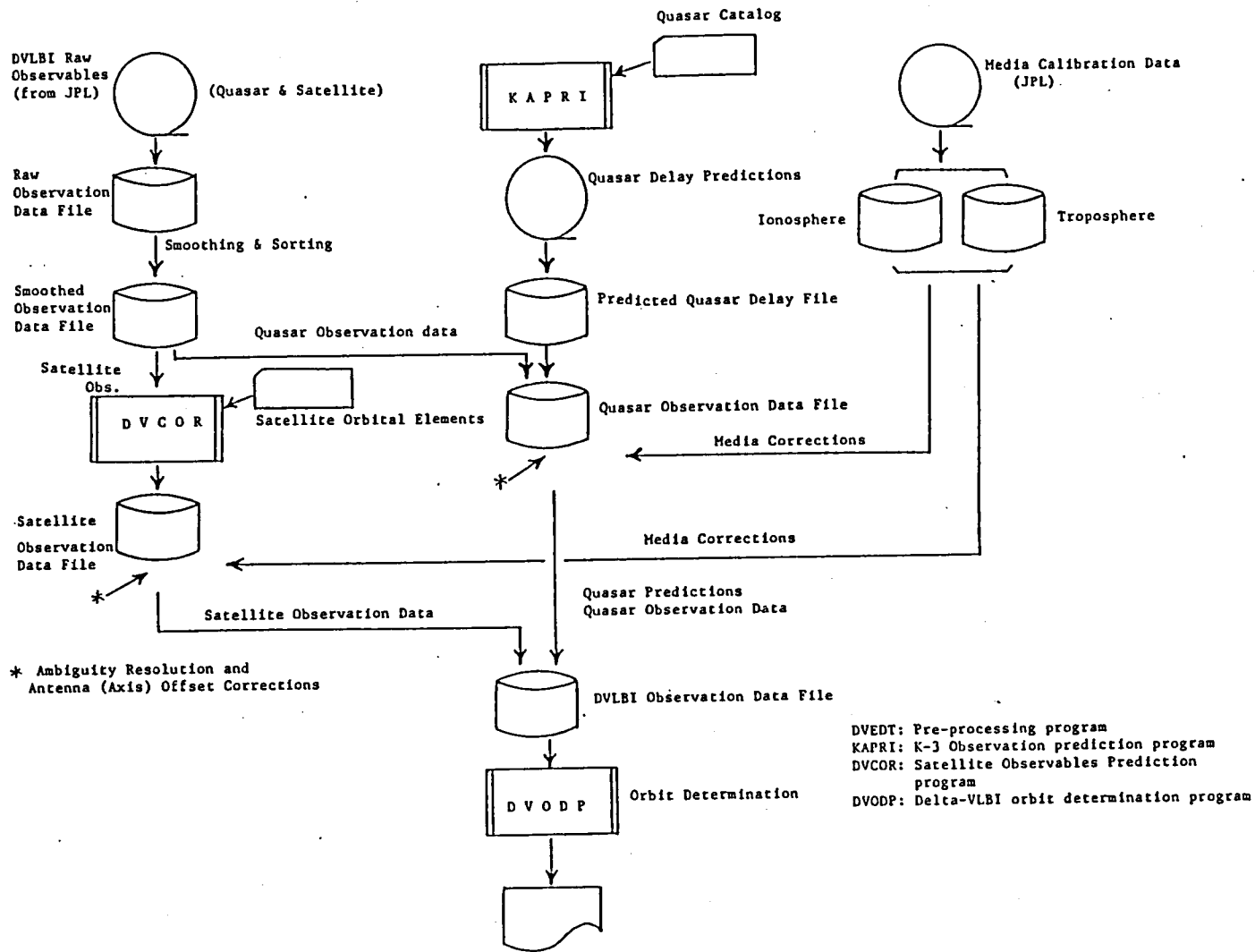


Fig. 5.11 Outline of pre-processing of the DVLBI observables for orbit determination

smoothed by the program "DVEDT" using 2nd order polynomial fitting function and compressed into one observable at the center of the period. Bad data points which had large deviation from the fit data were rejected in the smoothing process. The standard deviations of the raw delay data with respect to the fit data were about 1 nsec for the DSCS delays, and 1~10 nsec for the quasar delays. As is described in Sec.5.3.2, the SNR error depends on the correlation flux density of the observed radio source and the performance of the VLBI system. So the raw data have a wider range of deviations in the quasar observations than those in the satellite observations.

(ii) Media Corrections

If we can observe the satellite and quasars with the same viewing angles at every VLBI stations, we do not need any corrections of the propagation media (ionosphere and troposphere). Because these effects are cancelled by taking differential observables. However, it was not the actual case in our experiment.

We corrected the ionospheric effect by using the total electron content data. They were obtained at the VLBI stations, or at observation sites located nearby to them, by Faraday rotation measurements of the beacon signals in the 136 MHz band from three geosynchronous satellites (ETS-II at Tokyo, Japan, ATS-1 at Canberra and ATS-3 at Goldstone). The zenith

total electron contents, which were derived from the Faraday rotation measurements, were mapped into the actual viewing directions of DSCS satellite and quasars⁽⁶⁾. Fig.5.12 (a)~(d) show the delays caused by the ionosphere in each observation pass at the four VLBI stations. These ionosphere calibration data were provided by JPL.

The tropospheric delay consists of the delays caused by the "dry" component of the troposphere which has no water vapor and the "wet" component, that is, water vapor in the troposphere. For Kashima and Owens Valley, the predicted zenith delays for both the components based on the meteorological data were used. For the other stations, the empirically obtained seasonal models were used to calculate the zenith delays. The zenith delays were mapped to the line-of-sight directions using the following formula developed by C.C.Chao⁽⁷⁾.

$$P = \frac{P_z}{\sin E\ell + \frac{0.00143}{\tan E\ell + 0.0445}} \quad (5.7)$$

where P is the delay in the line-of-sight, P_z is the zenith delay, and $E\ell$ is the elevation angle of the line-of-sight. The tropospheric delays are also shown in Fig.5.12 (a)~(d).

In the actual pre-processing by the program DVEDT, the satellite observation data file and the quasar observation data

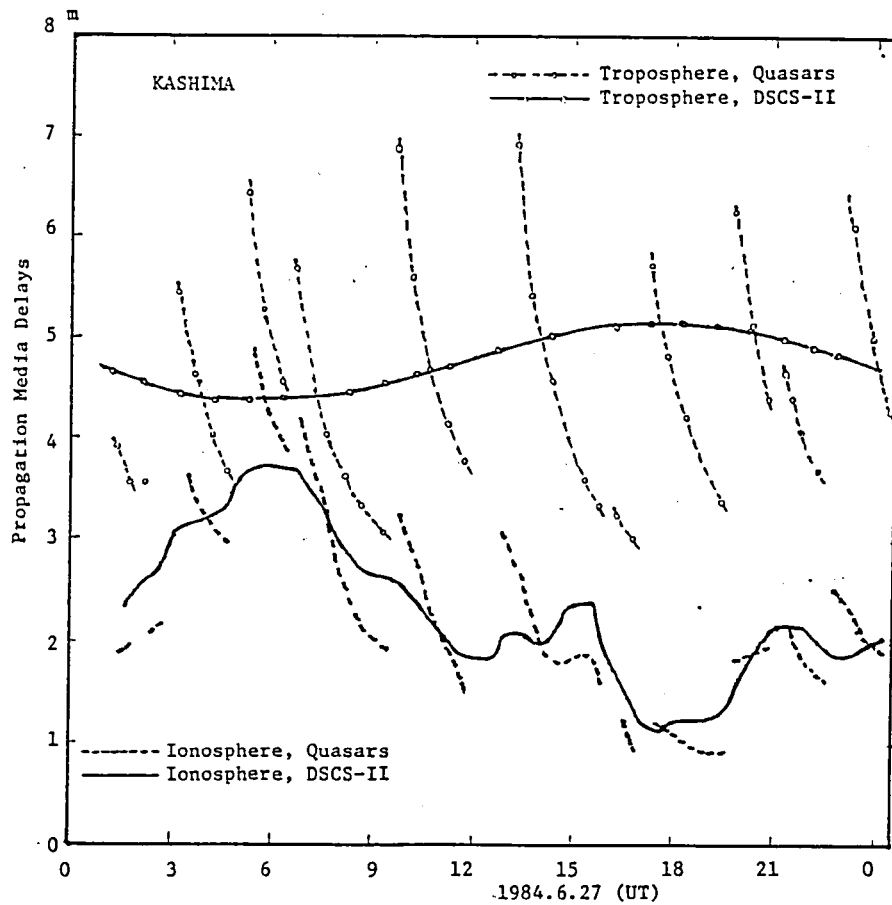


Fig. 5.12 (a) Propagation media delays at Kashima

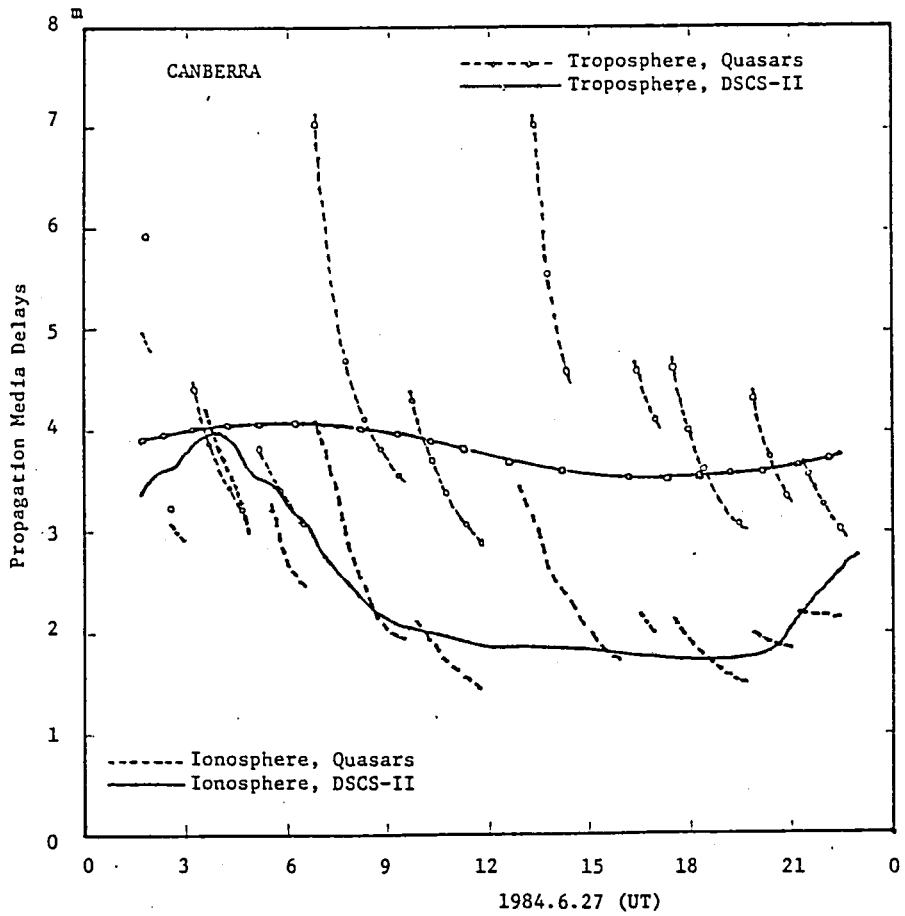


Fig. 5.12 (b) Propagation media delays at Canberra

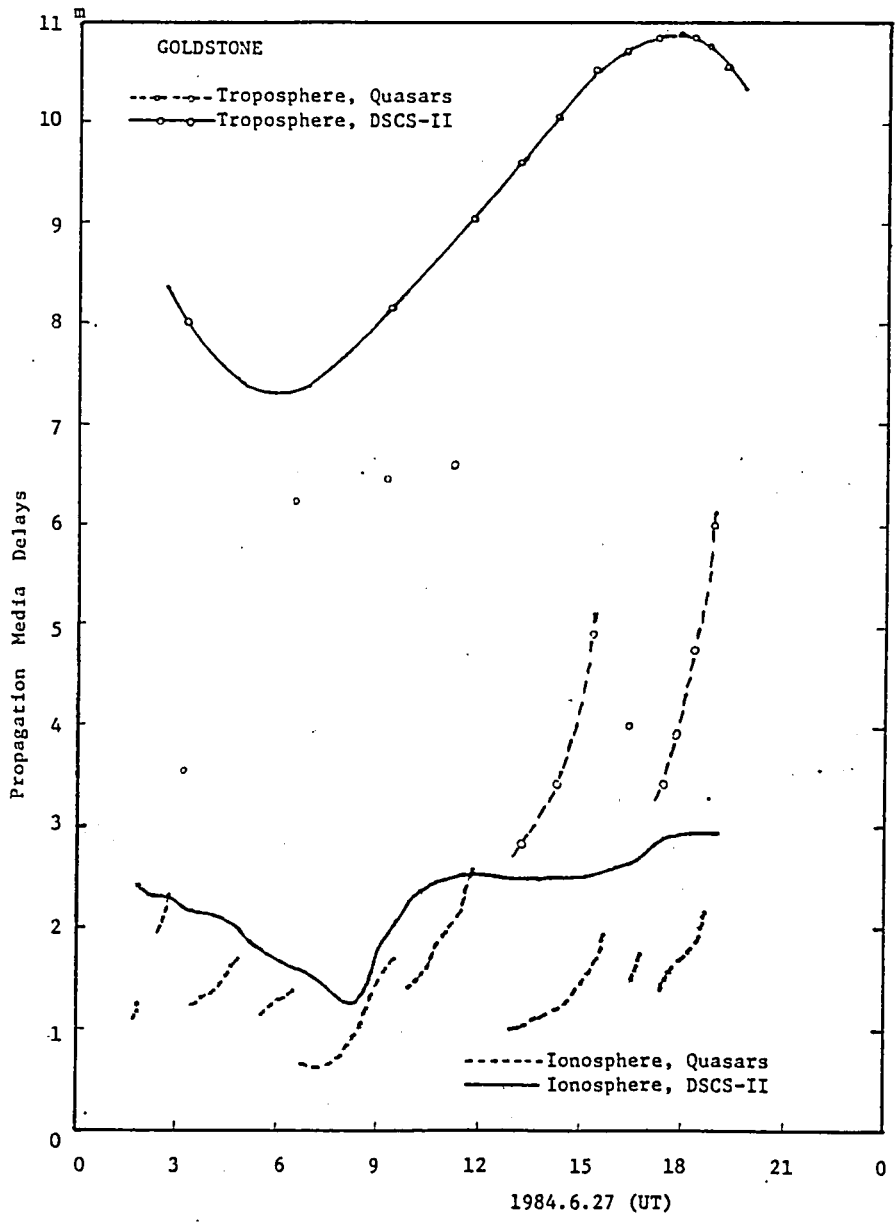


Fig. 5.12 (c) Propagation media delays at Goldstone

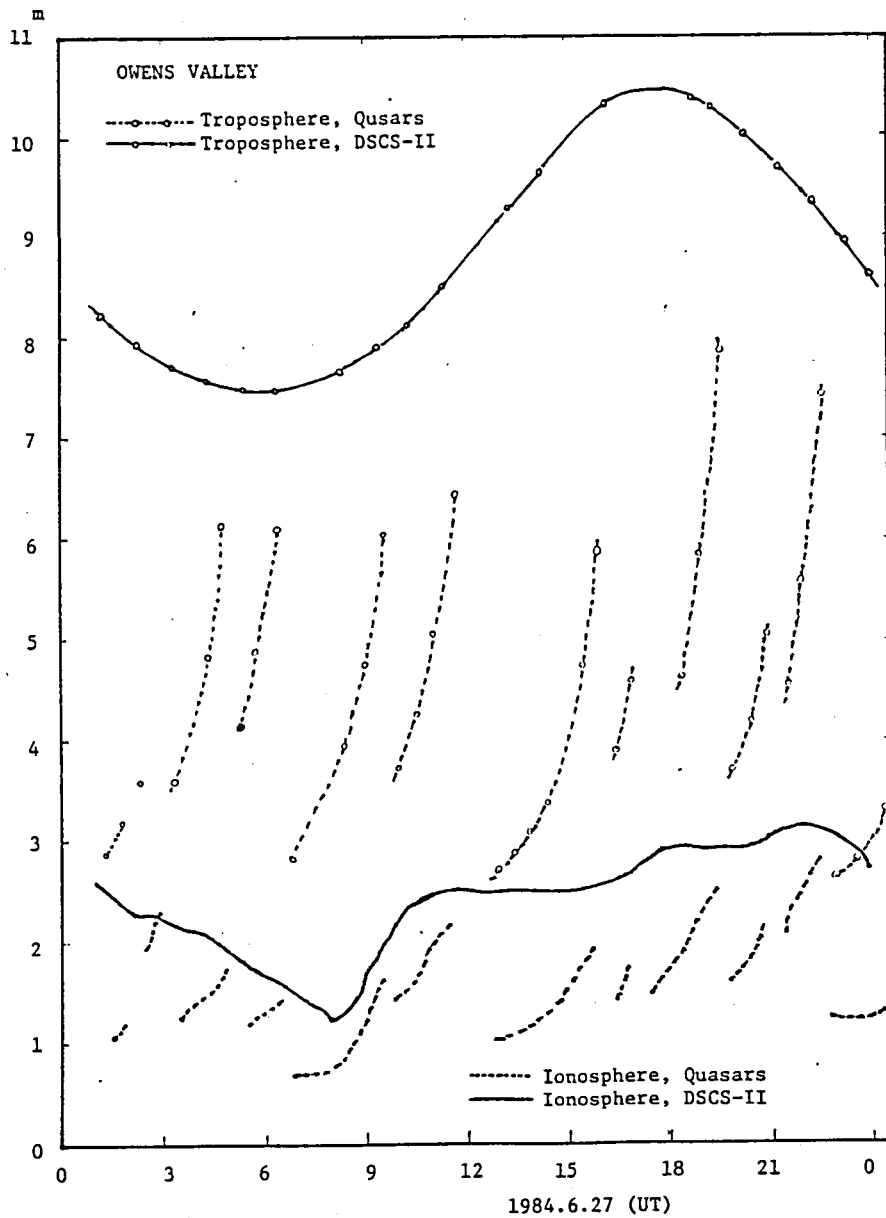


Fig. 5.12 (d) Propagation media delays at Owens Valley

file were created first from the smoothed and sorted observation data file (Fig.5.11). These observation data files contain not only observation data, but also calculated (or predicted) observation values and other informations such as elevation angles at each stations, standard deviations of the raw data, and so on.

The predicted observables for quasars were calculated by the program KAPRI in the K-III VLBI system⁽⁸⁾. The station coordinates (Table 5.1) and the quasar catalog (Table 5.3), were used in KAPRI.

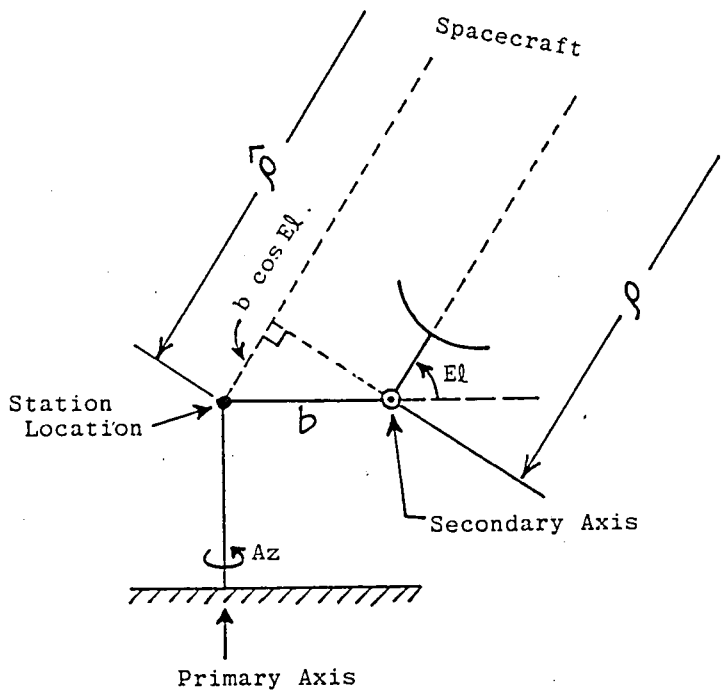
(iii) Station Antenna Axis Offset Correction

We corrected the VLBI delay observation data obtained by the baselines which include Goldstone station. Because, the two driving axes (elevation and azimuth driving axes) of the 26 m antenna do not intersect as shown in Fig.5.13.

(iv) Spacecraft Antenna Offset Correction

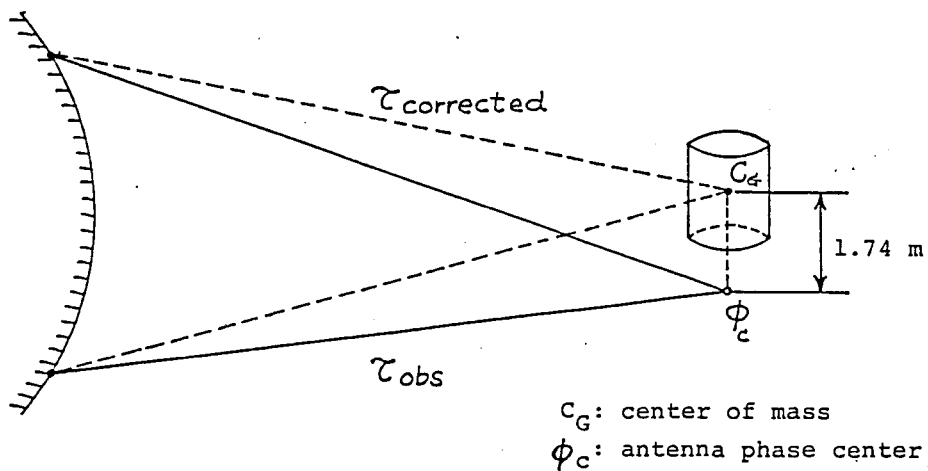
The phase center of the S-band antenna of DSCS-II satellite is 1.74 m apart from the center of mass (Fig.5.14). Therefore, the observed delay data were corrected in order to derive the delay data with respect to the center of mass. That is,

$$\tau_{\text{obs}} = \tau_{\text{corrected}} + 1.74 C \quad (5.8)$$



b : offset between two axes ($=0.9144\text{m}$)
 $b \cos El$: correction

Fig. 5.13 Antenna correction for the 26 m antenna at Goldstone station



C_G : center of mass
 ϕ_c : antenna phase center

Fig. 5.14 DSCS-II antenna correction

where τ_{obs} is the observed delay, $\tau_{\text{corrected}}$ is the corrected delay, and C is the correction coefficient given for each baseline as

- C = -0.64 nsec/m for Kashima/Canberra baseline,
- = -0.64 nsec/m for Owens Valley/Canberra baseline,
- = 0.00 nsec/m for Kashima/Owens Valley baseline,
- = -0.62 nsec/m for Goldstone/Canberra baseline,
- = 0.02 nsec/m for Goldstone/Owens Valley baseline.

The coefficient C can be considered as a constant, because the observation geometry changes little since the satellite antenna offset is very small compared with the distance between the satellite and each VLBI baseline on the earth.

(v) Derivation of System Delay and Formation of DVLBI Delay Observables

The system delay τ_{sys} , which is caused by clock offset and instrumental delays at VLBI stations, was derived from the difference between corrected observation delay τ_{obs} and predicted delay τ_{prd} , both for a quasar observation. However, the observed delay may have cycle ambiguity. So we have

$$\tau_{\text{sys}} = \tau_{\text{obs}} - \tau_{\text{prd}} + \frac{n}{B} \quad (5.9)$$

where n is an integer for the ambiguity, B is the frequency

separation between the two channels at which the VLBI observation were performed. Figs.5.15 (a)~(e) show raw ($\tau_{\text{obs}} - \tau_{\text{prd}}$) data, where τ_{obs} means the raw observation delay corrected with only dry part of the tropospheric delay. The observations were carried out with narrower (about 2 MHz) inter-channel frequency separation from 12:30 to 14:30 UTC, so the SNR decreased to result in larger delay data fluctuations in that period. Figs.5.16 (a)~(e) show the system delays for the five baselines, where the ambiguity is resolved, the antenna axis offset of Goldstone station is corrected, and all the propagation media delays are corrected.

The DVLBI delay observables of the satellite were formed by subtracting the system delays from the satellite delay observables. The data points of the quasars and the satellite did not coincide, so the system delays at the satellite data points were obtained by a linear interpolation. Fig.5.17 shows all the DVLBI observable points obtained.

(vi) Ambiguity Resolution

In the case of the quasar observations, it is easy to resolve cycle ambiguities. Because, the quasar delay was roughly estimated without ambiguity by correlating a single channel observation signal which spreads over the whole 2 MHz bandwidth.

On the other hand, ambiguities in the satellite delay

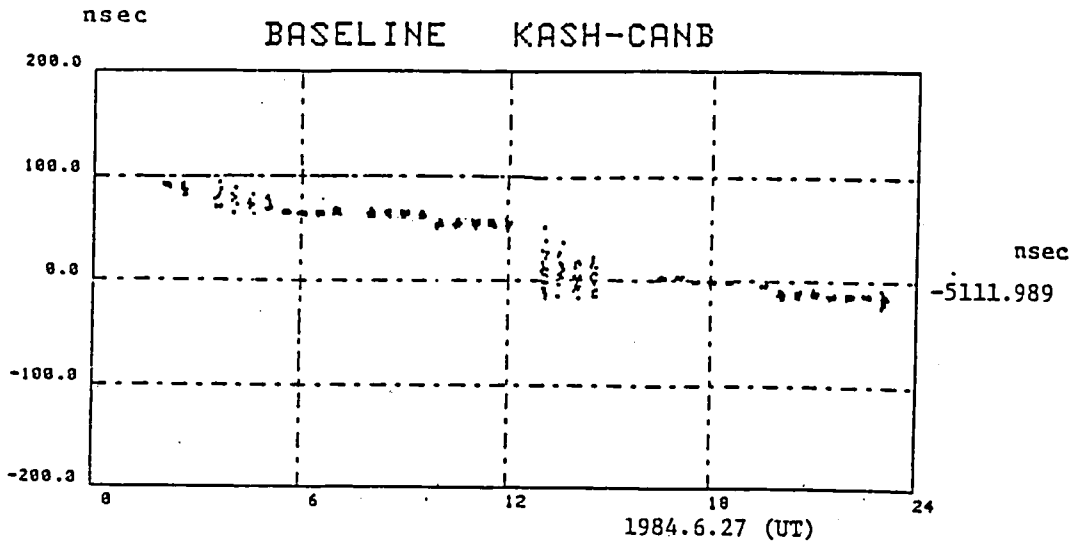


Fig. 5.15 (a) Raw quasar delay observations for Kashima-Canberra baseline

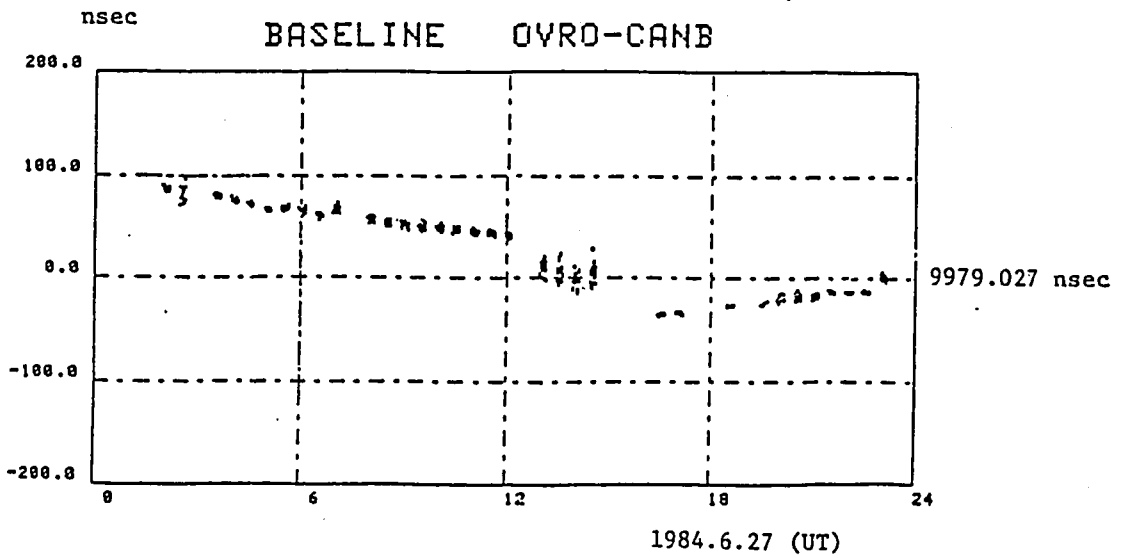


Fig. 5.15 (b) Raw quasar delay observations for Owens Valley-Canberra baseline

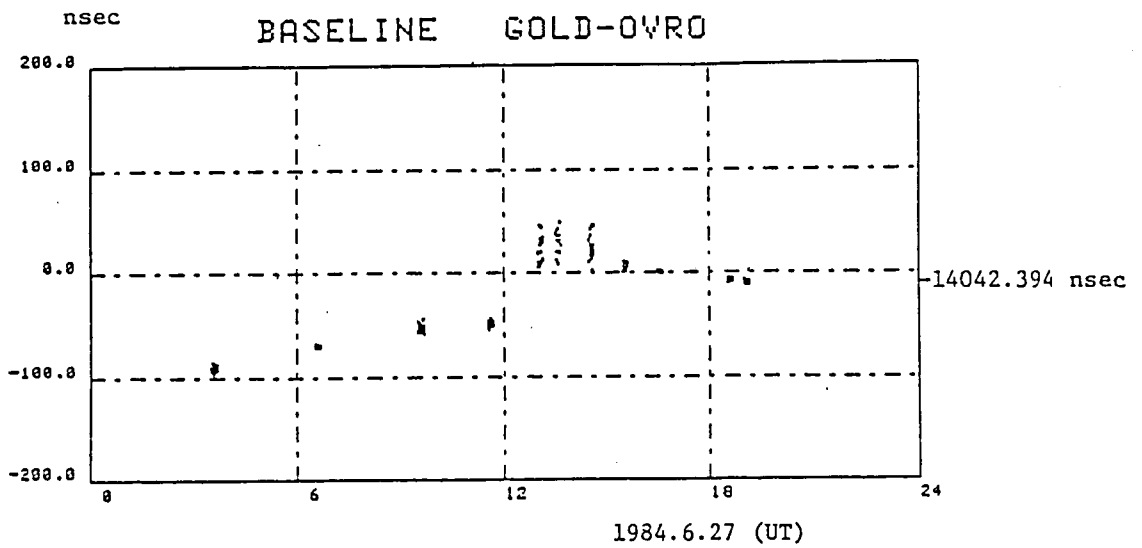


Fig. 5.15 (c) Raw quasar delay observations
for Goldstone-Owens Valley baseline

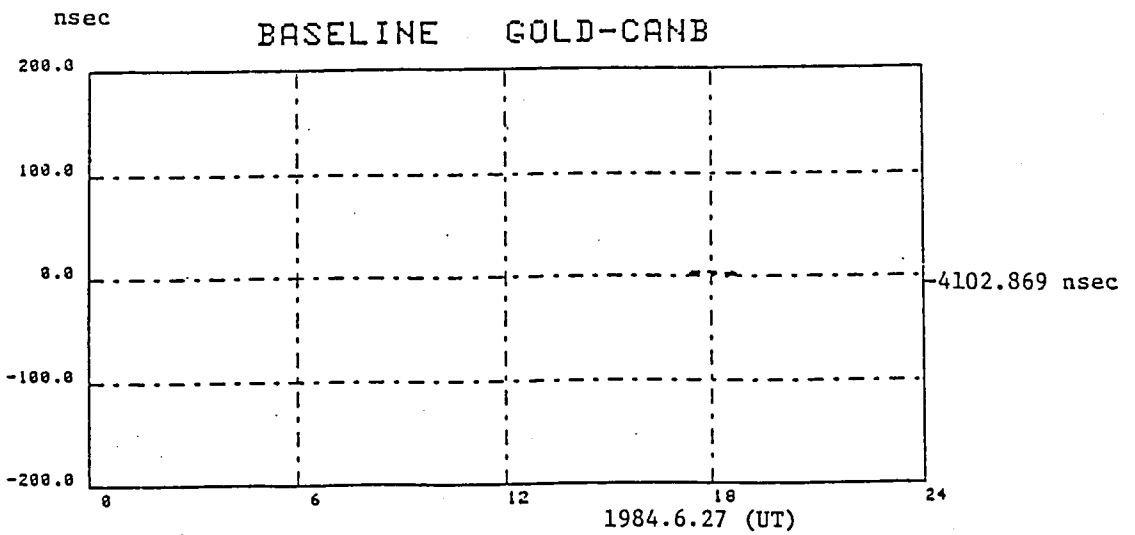


Fig. 5.15 (d) Raw quasar delay observations
for Goldstone-Canberra baseline

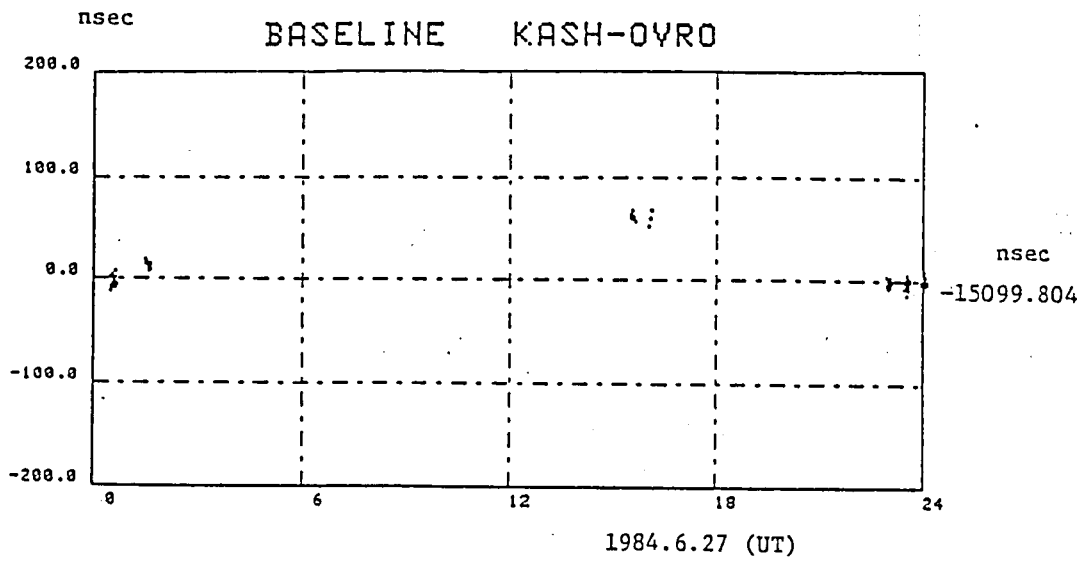


Fig. 5.15 (e) Raw quasar delay observations
for Kashima-Owens Valley baseline

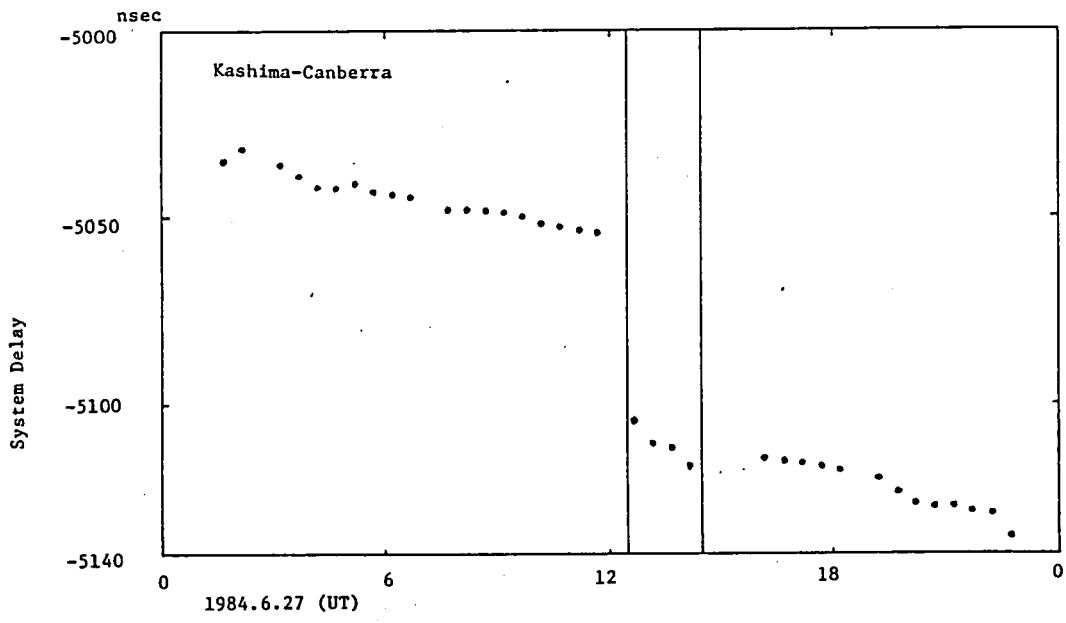


Fig. 5.16 (a) System delay for Kashima-Canberra baseline

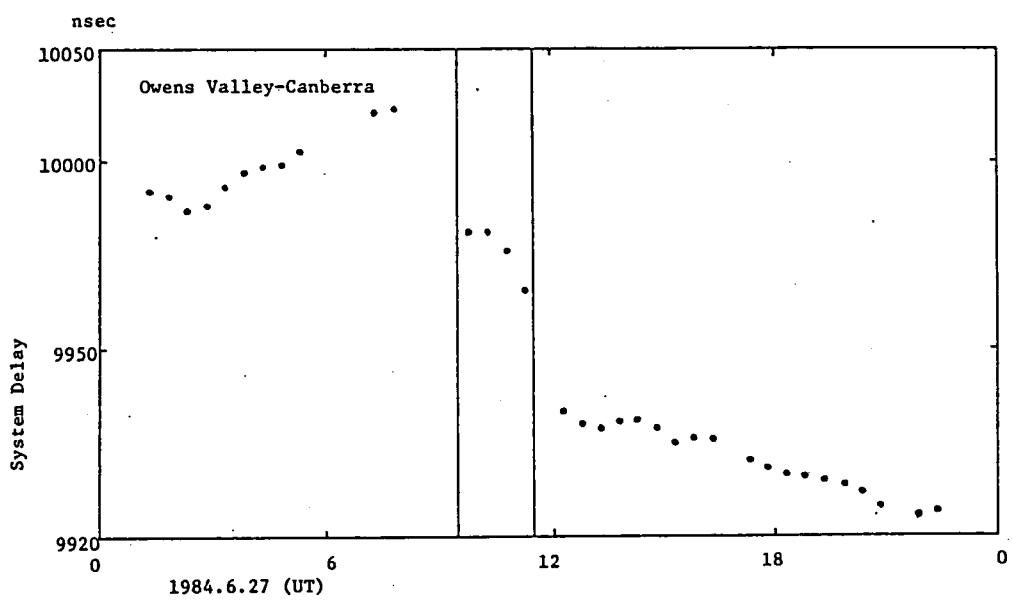


Fig. 5.16 (b) System delay for Owens Valley-Canberra baseline

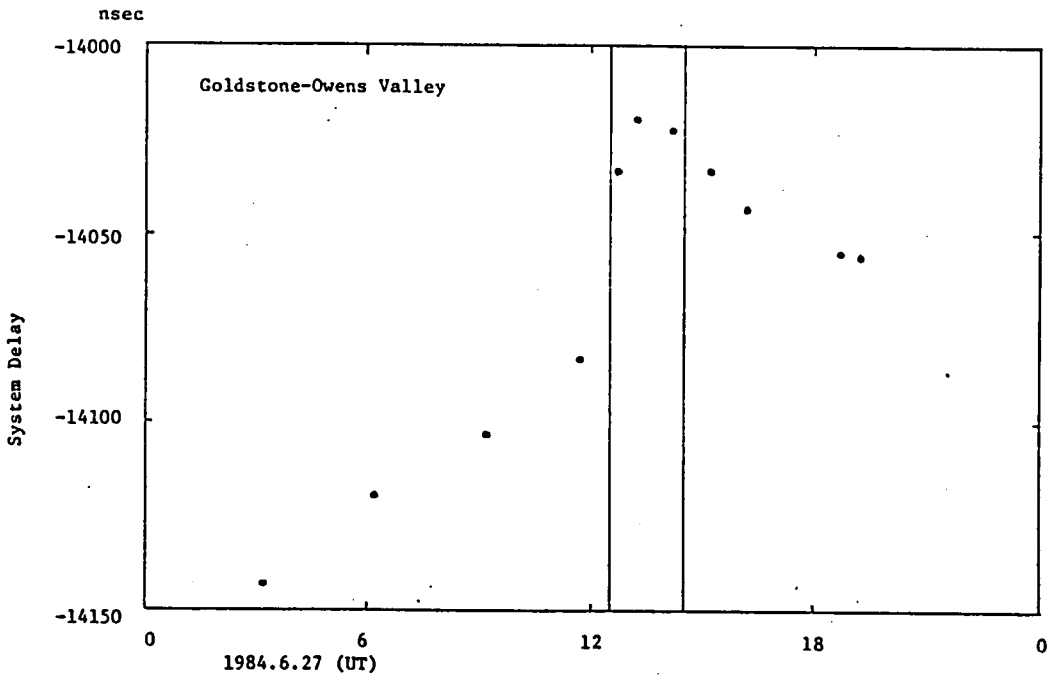


Fig. 5.16 (c) System delay for Goldstone-Owens Valley baseline

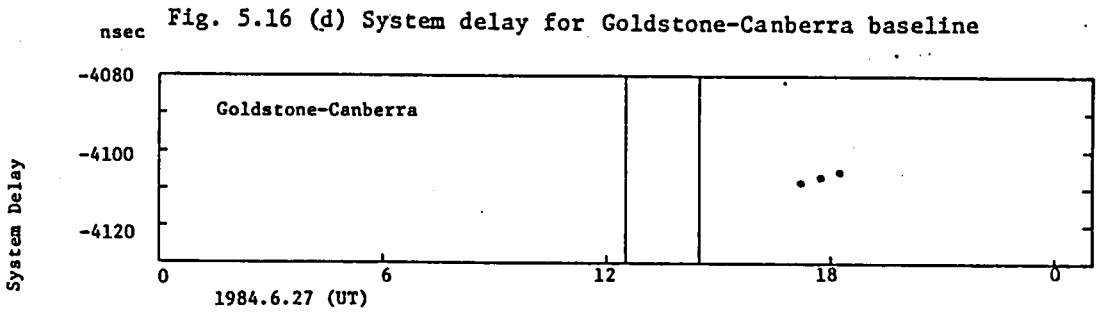


Fig. 5.16 (d) System delay for Goldstone-Canberra baseline

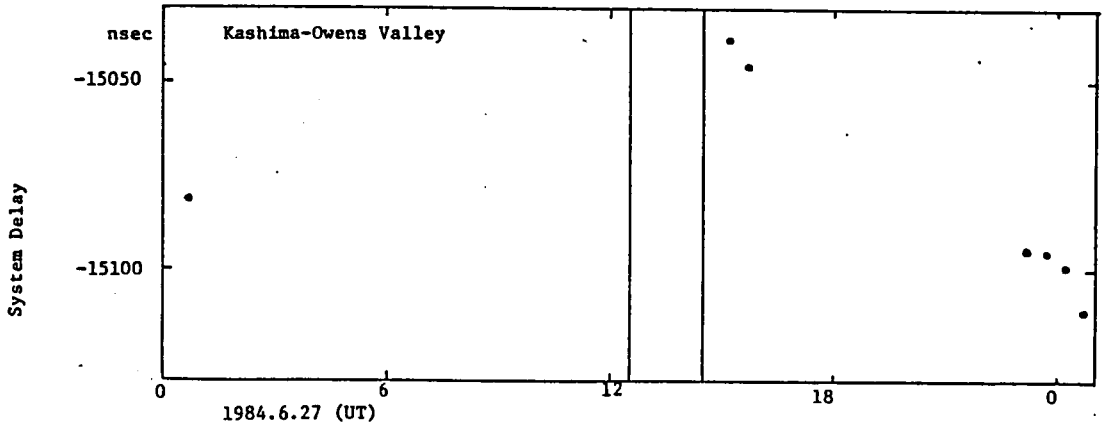


Fig. 5.16 (e) System delay for Kashima-Owens Valley baseline

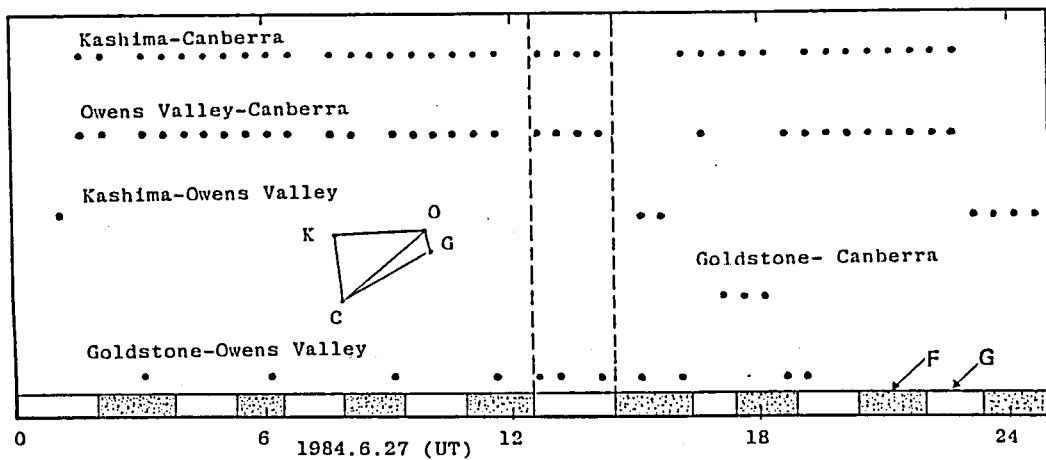


Fig. 5.17 DVLBI delay observable data points

estimates should be resolved carefully. Because, the delay estimates derived from the satellite tones (see Eq.(5.5)) are totally ambiguous and we are not necessarily given an accurate predictions. Therefore a few consecutive steps were taken to resolve the ambiguities. Fig.5.18 shows the process. First, we estimated the satellite orbit using unambiguous delay-rate observables, with an initially given satellite state vector which was predicted by the DSCS-II control center based on an orbital elements obtained by routinely performed with conventional radio tracking data.

An simulation had revealed the expected accuracy of the orbit obtained at each step⁽¹⁾. They are also shown in Fig.5.18. At each step, the DVLBI delay observables of which the ambiguity is larger than the accuracy of the orbit obtained at the previous step are added. It should be noted that the DVLBI data of the short baseline of Goldstone and Owens Valley stations had a significant role not only to resolve the ambiguity of the long baseline data, but also to raise the orbit accuracy from a few km to nearly 100 m, even though the number of the observables was small.

The data obtained with narrower separation of observation frequencies (during 12:30 to 14:30 UTC) were also useful to make sure the correct resolution of ambiguities. Because those data had four-times larger ambiguity for every baseline and they had smaller difficulties in ambiguity resolution at each

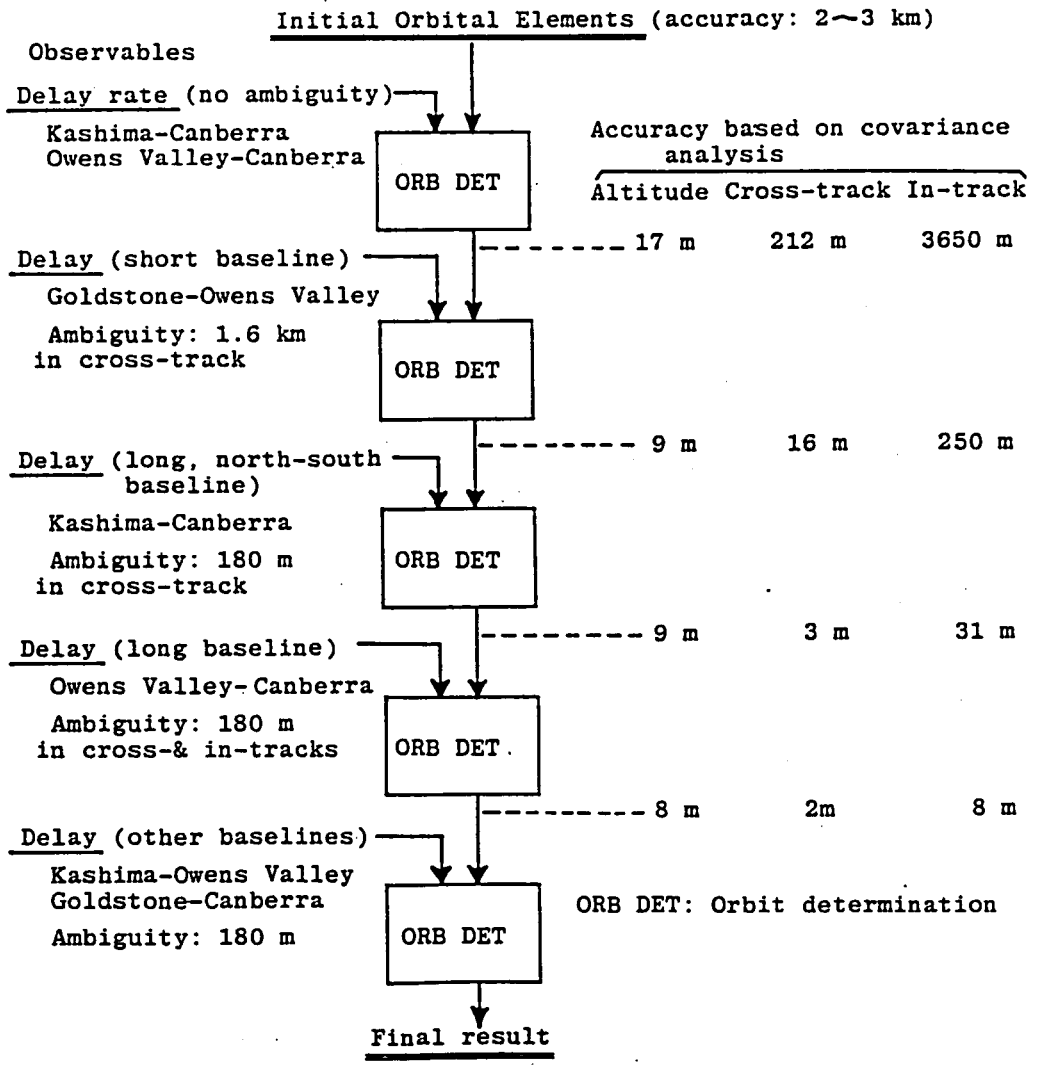


Fig. 5.18 Consecutive ambiguity resolution of DVLBI delay observables for DSCS-II

step. Fig.5.19 shows ambiguous (O-C) and ambiguity-resolved (O-C) for Kashima-Canberra baseline with respect to the initially given orbit.

We tried to resolve the ambiguity directly from the initially given orbit using the data during 12:30 to 14:30. In that case, the ambiguous data points were tried to be connected smoothly to the points with larger ambiguity $\tau_{amb} = 448$ nsec (see Fig.5.19). The connected data points may have a certain bias which is $m\tau_{amb}$ (where m is an integer). The number is to be estimated in the orbit determination. It is, however, not only a tedious process but also full of risk to connect incorrectly some of data points.

5.5 Orbit Determination

5.5.1 Satellite Dynamic Model

In order to determine a geosynchronous satellite orbit with an accuracy of a few meters, we should use a dynamic model precise enough. That is, the satellite orbit which is calculated based on the model must have an accuracy of less than 1 meter at least within 24 hour-period (one orbital revolution). Table 5.7 shows accelerations acting on a geosynchronous satellite and their approximate effects on the satellite position during an orbital revolution. We considered

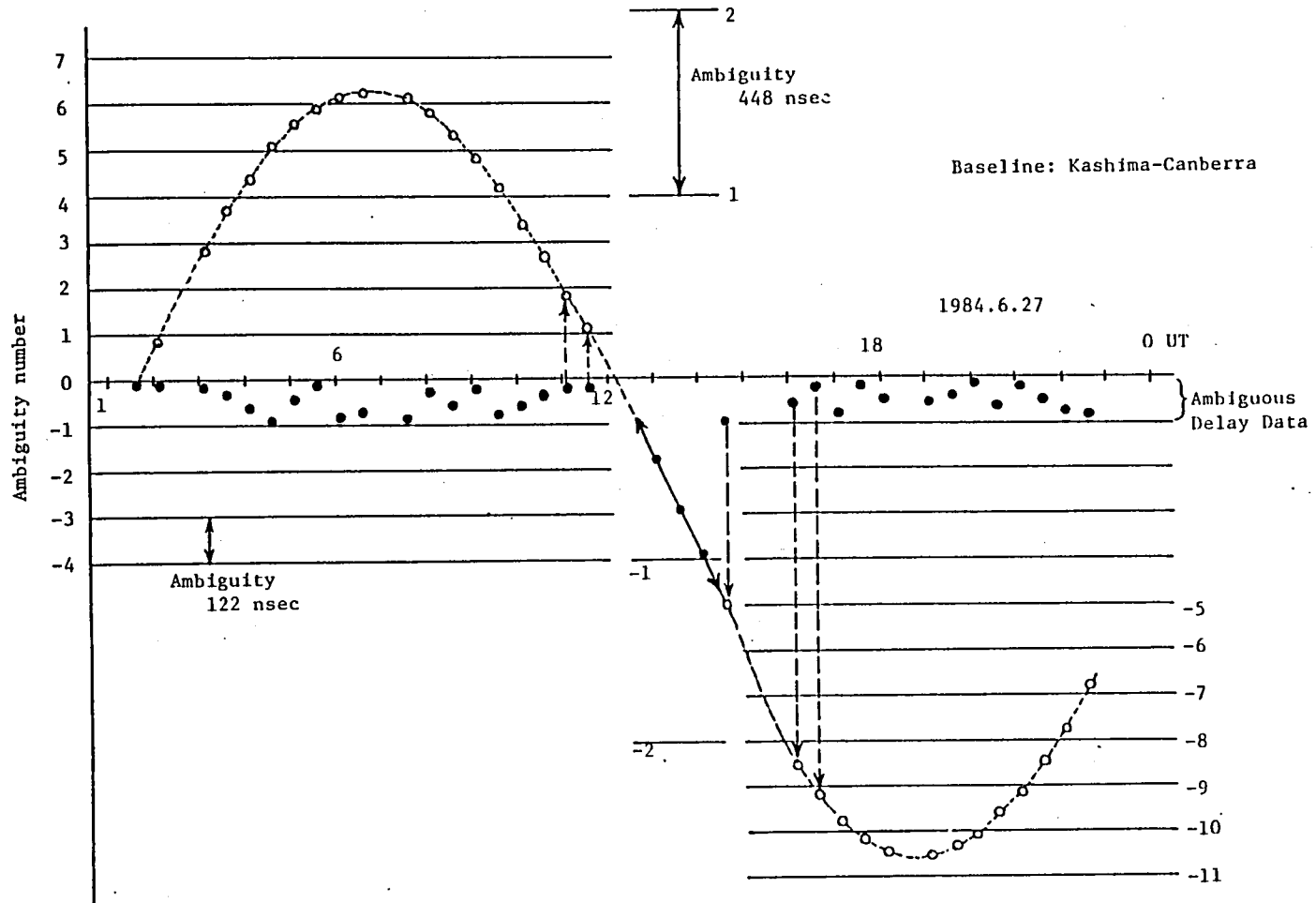


Fig. 5.19 Ambiguity resolution for the DSCS-II delay observables connecting the data points to those in the period with larger ambiguity (448 nsec)

Table 5.7 Significant accelerations on a geosynchronous satellite

Force	Acceleration km/sec ²	Approximate effect
* Earth's point mass gravitation	2×10^{-4}	Nominal orbit.
Earth's non-spherical gravitation		
* Harmonic components lower than or equal to the 8th order	10^{-8}	30 km
Harmonic components higher than 8th order	10^{-13}	20 cm
* Sun's gravitation	3×10^{-9}	3 km
* Moon's gravitation	6×10^{-9}	6 km
* Solar radiation pressure	10^{-10}	1 km
+ Earth's tidal effect	10^{-13}	20 cm
+ Large planet (Jupiter)	10^{-14}	2 cm
+ Relativity effect	10^{-11}	1 m

* Forces considered in both programs of DPODP (JPL) and DVODP (RRL).

+ Forces considered only in DPODP.

all the perturbative accelerations which result in at least 1 m position deviation of the satellite during 24 hours. There are two significant factors which should be evaluated carefully. The first, the earth's gravitational constant is directly effective to the earth's gravitational acceleration. The effect of the possible uncertainty of its value on the orbit determination was taken into consideration in a covariance analysis. The other is the solar radiation pressure acceleration. The acceleration can be modeled using an appropriate solar radiation reflection model whose parameters can be estimated in an orbit determination.

5.5.2 Precise Orbit Determination with DVLBI Delay Observables

(i) Data Weighting

Each DVLBI observable has an error which is a combination of SNR errors of quasar and satellite observations, propagation correction errors, station location errors, UT1 and polar motion errors, and quasar position errors. In order to obtain a minimum variance estimates, we use the standard deviation of the error as a weighting factor in an orbit determination. We can most probably evaluate the standard deviation of the delay observables by a following formula,

$$\sigma_i^2 = \sigma_{s/c}^2 + \sigma_q^2 \quad (5.10)$$

where σ_i is the standard deviation of the i-th delay

observable, $\sigma_{s/ci}$ is noise of the satellite observation, σ_{qi} is noise of the quasar observation. $\sigma_{s/ci}$ and σ_{qi} may be calculated by a formula,

$$\sigma_{s/ci \text{ or } qi}^2 = \sigma_{SNR}^2 + \sigma_p^2$$

for the satellite or a quasar (5.9)

where σ_{SNR} is the SNR error of the delay observable (given by Eq.(3.32)), and σ_p^2 represents the propagation media effects at the corresponding stations.

It is not easy to make a theoretical formulation of σ_p^2 , because this must reflect the systematic and random conditions of the troposphere and the ionosphere for all the stations involved. Therefore, we used practically useful two formulations, one of which considers σ_p^2 as a constant which is adjusted to the actual observation data (RRL method), and the other considers the low elevation effect (JPL method) using an elevation scaling factor. The JPL's formulation, which considers $\sigma_{s/ci}$ and σ_{qi} in Eq.(5.10) as a whole, is written as

$$\sigma_i = \sigma_0 \left(1 + \frac{18}{(1 + E_{\min})^2} \right) \quad (5.11)$$

where σ_0 is a constant which is determined based on the actual observation fluctuations, and E_{\min} is the minimum elevation angle given in degree in the observation scan.

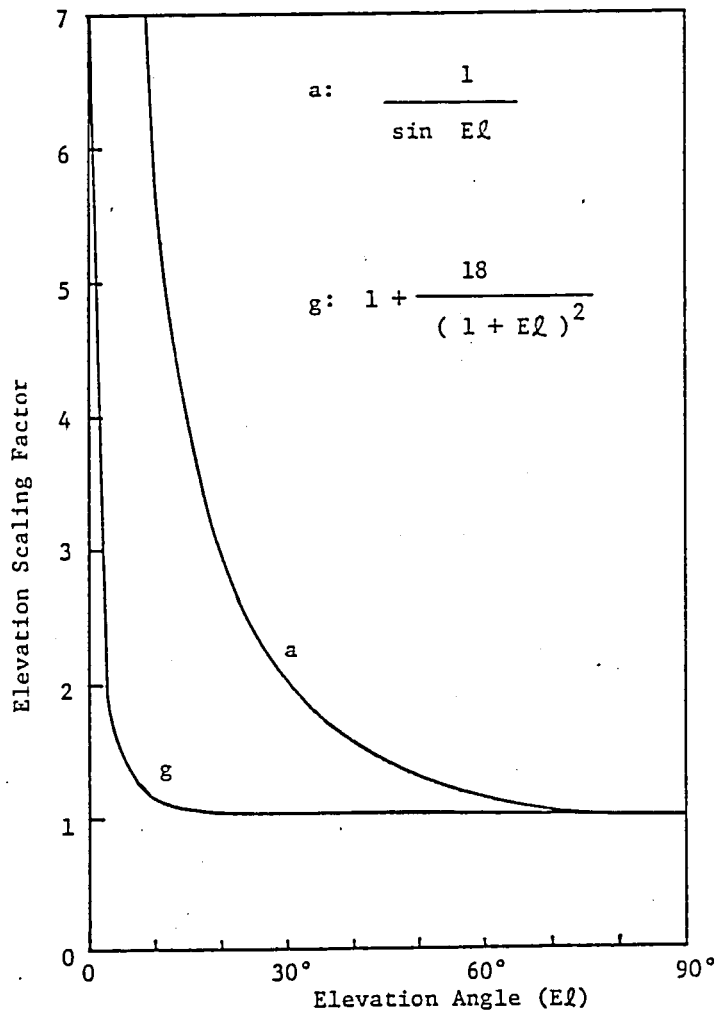


Fig.5.20 Elevation scaling factor for weighting the DVLBI delay observable
 a: Horizontal layer model
 g: JPL empirical model

These two formulations are not practically so different, because the elevation factor of JPL's formulation shows little elevation dependence except at elevations lower than 10 degrees as shown in Fig.5.20. As is described later, we found that $\sigma_0 = 1.0$ m is appropriate for the DVLBI delay observables obtained in our experiment.

(ii) Results of Orbit Determination

Orbit determination were carried out with the DVLBI data by using independent orbit determination programs DVODP (RRL) and ODP (JPL). Fig.5.21 shows typical observation residuals in a RRL's orbit determination. The delay observation residuals are almost within 3 nsec (about 1 m of differential path residuals). This indicates about 2 m of standard deviation of estimated satellite position by a covariance analysis where effects of model uncertainties are not included.

Orbit determinations with different conditions with respect to solve-for parameters, UT1 and polar motion data, observation weights, and satellite dynamic model were carried out to evaluate these effects. Table 5.8 summarizes the conditions of these orbit determinations and Fig.5.22 shows estimated satellite positions at the epoch time (01:00 ET July 27, 1984, the beginning edge of the observation period) for these orbit determination cases.

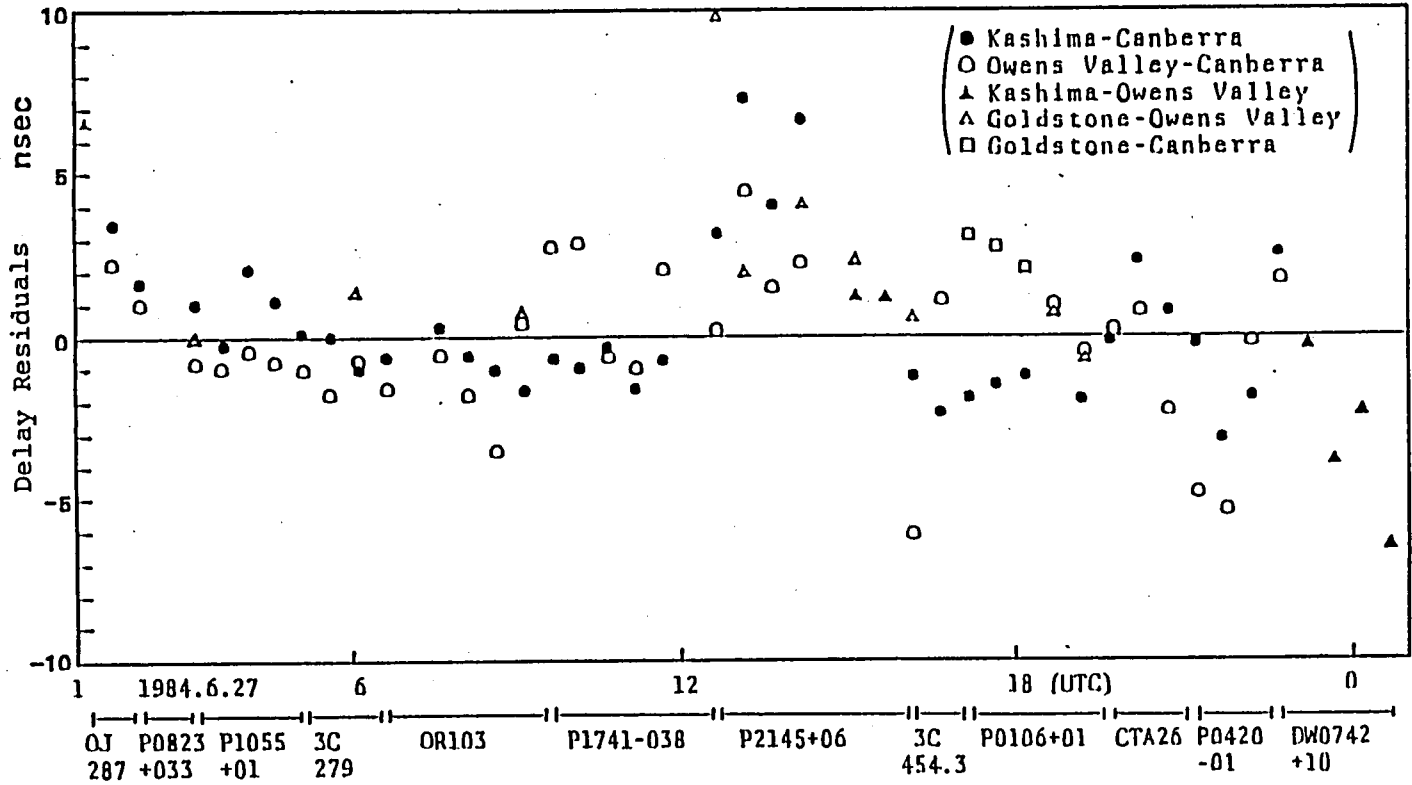
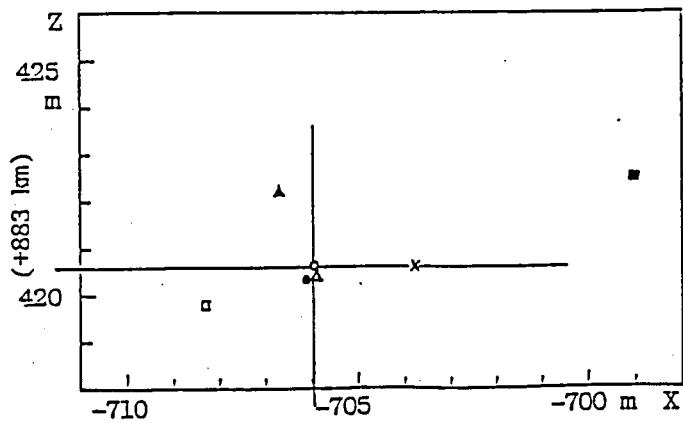
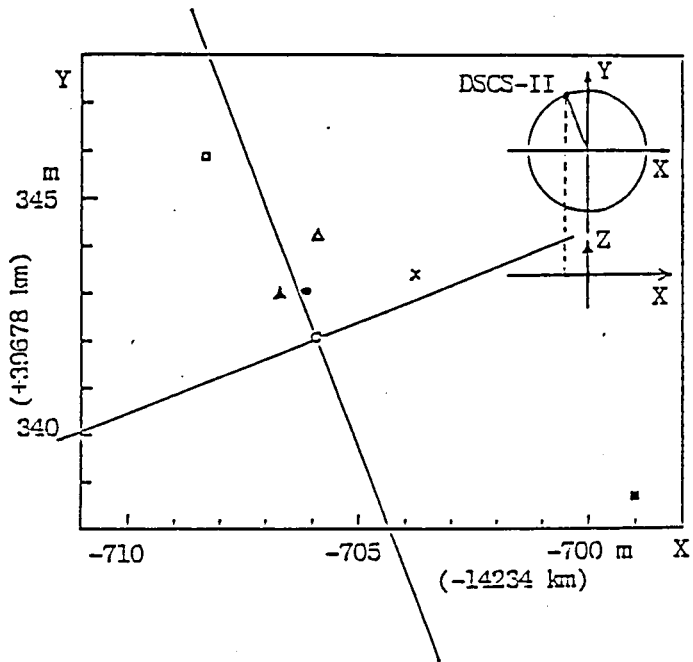


Fig. 5.21 Typical observation residuals of the DVLBI delay observables

Table 5.8 Orbit determinations with a variety of conditions

Case	Solve-for Parameters	Note
A	State vector G_r	Orbit Determination Program:DVODP (RRL) UT1 & Polar Motion : IRIS Data weight: Observation Data SNR No relativity
B	State vector G_r	Orbit Determination Program:ODP (JPL) UT1 & Polar Motion : BIH rapid service Data Weight: $g \sigma_0$ ($\sigma_0 = 1$ m) No relativity
C	State Vector	Orbit Determination Program:ODP (JPL) UT1 & Polar Motion : BIH smoothed Data Weight: $g \sigma_0$
D	State vector G_r, G_x, G_y	Same as Case C
E	State vector Station Coordinates*	Same as Case C * Only z-heights (four stations) estimated Solar Radiation Reflection Factors: nominal values ($G_r = 0.797, G_x = G_y = 0.0$)
F	State vector G_r, G_x, G_y	Same as Case C Observation Data: data set F
G	State vector G_r, G_x, G_y	Same as Case C Observation Data: data set G



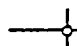
 DSCS-II Position Uncertainty
 ▲ : A △ : B ● : C ○ : D (Case D)
 × : E ■ : F □ : G

Fig. 5.22 Estimated satellite position at the beginning edge of the data arc. The bars show the position uncertainties evaluated by a covariance analysis (see Fig.5.23).

DVODP weighted the observation data according to SNR errors and ODP weighted them based on the observation accuracy evaluation $\sigma = g \sigma_0$, where $\sigma_0 = 1 \text{ m}$ and g is a factor shown in Fig.5.20.

Solve-for parameters were satellite state vector and solar radiation pressure factor (G_r for one dimension parallel to the sun-to-satellite vector, G_x and G_y for the other dimensions) in almost all cases. Station coordinates (heights from the equatorial plane) were also estimated in Case E. Cases F and G are orbit determinations with independent data sets which were obtained by dividing the data points as shown in Fig.5.17.

Fig.5.22 shows that the scattered estimated satellite positions are almost within several meters, which indicates the satellite position accuracy including the model errors is almost several meters at the epoch time.

(ii) Covariance Analysis

A more general evaluation of orbit determination accuracy was conducted by a covariance analysis which consider modeling errors as well as observation errors. Table 5.9 shows the error model and effect of each component on the determined satellite position. Fig.5.23 shows the over-all satellite position uncertainties over the observation period. The position uncertainties at the edge of the observation period is consistent with the results shown in Fig.5.22, which indicate

Table 5.9 Significant factors for an orbit determination with meter-order accuracy of a geosynchronous satellite

Factors	Noise or errors	S/C position error at the center of the observation arc
Earth's gravitational constant (nominal: 398600.448 km ³ /sec ²)	0.02 km ³ /sec ² (5x10 ⁻⁸)	70 cm
Solar radiation pressure model nominal G _r : 0.9 G _r ^x : 0.0 G _r ^x : 0.0 y	0.1 0.1 0.1	230 cm
Station location +Errors uncorrelated in three components for the 4-stations +UT1 and polar motion errors included	50 cm	40 cm
Troposphere correction (zenith)	Dry: 0.2 cm Wet: 4 cm	50 cm
Ionosphere correction (zenith)	Day: 50 cm Night: 10 cm	160 cm
Observation noise + Following components included: SNR error Propagation media inhomogeneities Quasar position error	100 cm	230 cm
RSS		375 cm

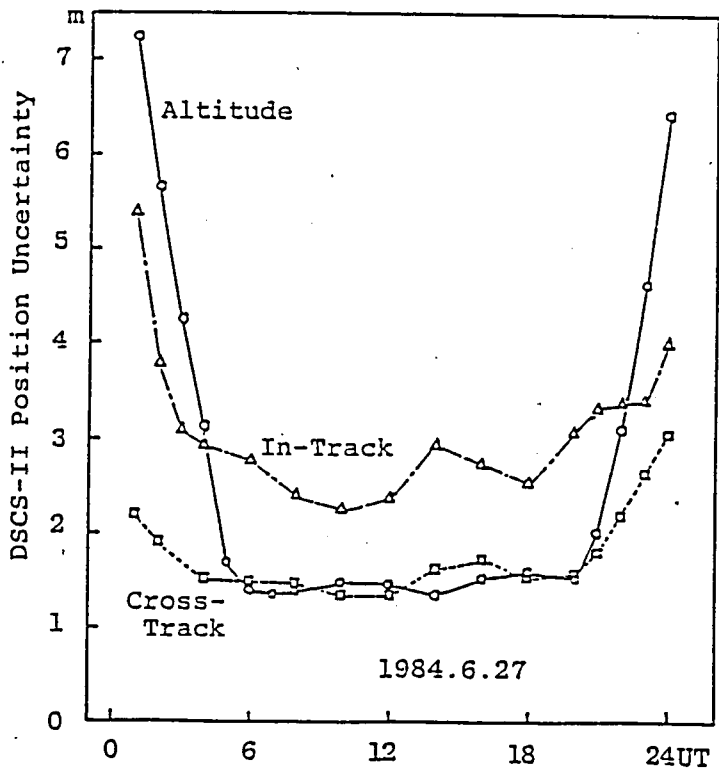


Fig. 5.23 Uncertainties of the estimated satellite position due to data noises and model errors

that we used a reasonable error models in the covariance analysis.

Considering the model errors, the satellite position was estimated with an accuracy of about 4 m at the center of the observation period. It should be noted that the position is absolutely referred to the extra-galactic reference frame.

The significant error sources are modeling error of the solar radiation pressure factor, ionospheric correction error and observation error including the quasar position errors. In order to attain higher accuracy, for example 1 m accuracy of the satellite position, we have to improve at least these three sources. The ionospheric delay would be corrected precisely if we can observe dual frequency signals as is usually conducted in geodesic VLBI observations. The observation errors would be much reduced by wideband observations, if a wideband satellite signal is available. The solar radiation pressure model would be improved by using more precise observation data obtained by dual-frequency and wideband observations.

The effects of general relativity and the solid earth tide are the order of about or less than 1 meter. Therefore, we cannot neglect these effects if we aim at the orbit determination accuracy of 1 m or higher.

5.6 Conclusion

An orbit determination with an accuracy of a few meters on a geosynchronous satellite was successfully performed by using a DVLBI method. We took an advantage of the high observability obtained by the inter-continental, orthogonal baselines including one short baseline for resolving ambiguities in delay observables. We also used the accurate knowledge of station coordinates which have been obtained through previous VLBI observations and spacecraft trackings.

Since the satellite was not designed to be tracked by DVLBI, the observations were conducted with single frequency (2 GHz band), which caused ionospheric delay calibration error, one of the major error sources. The effective observation bandwidth was also limited to about 8 MHz, which caused the insufficient observation accuracy, especially in quasar observations. By improving these factors, we can expect a satellite position determination accuracy of about 1 m or better, assuming that the solar radiation pressure model is improved by using high quality observation data.

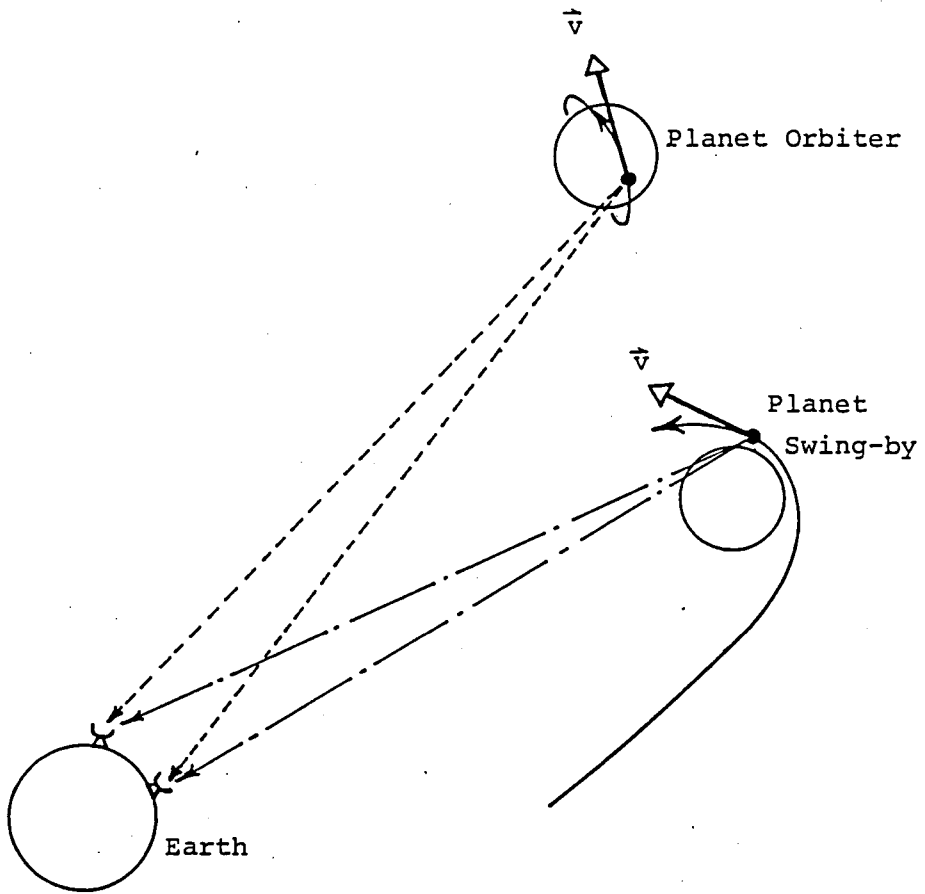
References

- (1) Border, J.S. and F.F. Donivan, Jr., Geosynchronous orbiter tracking by VLBI: Demonstration design, AIAA/AAS Astrodynamics Conference, Seattle, 1984.
- (2) Donivan, F.F., Jr., J.B. Border and B. Moultrie, Geosynchronous orbiter tracking by VLBI: Demonstration results, AIAA/AAS Astrodynamics Conference, Seattle, 1984.
- (3) Border, J.S., F.F. Donivan, T. Shiomi and N. Kawano, Precise interferometric tracking of the DSCS geosynchronous orbiter, AIAA 24th Aerospace Sciences Meeting, Reno, Nevada January 1986.
- (4) Shiomi, T., N. Kawano, J.S. Border and F.F. Donivan, Precise orbit determination of a geosynchronous satellite with differential very-long-baseline interferometry, 15th International Symposium on Space Technology and Science, Tokyo May 1986.
- (5) Thomas, J.B., An analysis of radio interferometry with the Block 0 system, JPL Publication 81-49, 1981.
- (6) Mulhall, B.D., V. J. Ondrasik and K.L. Thuleen, The ionosphere, JPL Technical Report 32-1499.
- (7) Chao, C.C., A preliminary estimation of tropospheric influence on the range and range rate data during the closest approach of the MM71 Mars Mission, JPL Technical Memorandum, 1970.
- (8) Takahashi, Y., A priori model calculation software (KAPRI), Review of the Radio Res. Lab., Vol. 30, Special Issue No. 1, Nov. 1984.

6.1 Tracking of Satellites in Various Orbits

The DVLBI is a useful tracking method for spacecrafts not only in the geosynchronous orbit but also in various other orbits. We already mentioned advantages of DVLBI in deep space navigations in Sec.3.1.2, where delay observables were used to determine the angular position of a spacecraft. A wideband spacecraft signal is desirable for the DVLBI to obtain precise delay observables. For example, the spacecraft GALILEO, which is to be launched in 1986 by USA to explore Jupiter and its satellites, will transmit coherent tones at the X-band with the maximum frequency separation of 38.25 MHz⁽¹⁾. On the other hand, even a narrowband signal can give useful information of the angular velocity of a spacecraft. That is, the delay rate observable obtained by DVLBI observing a narrowband signal represents the spacecraft velocity which is perpendicular to the line-of-sight⁽²⁾. Fig.6.1 shows two typical orbits with large angular velocities which can be detected by a narrowband DVLBI.

The DVLBI method can also be applied to highly elliptical earth orbits⁽³⁾. In this case, satellites reach so high



\vec{v} : Velocity Vector

Fig. 6.1 Typical orbits with large angular velocity perpendicular to the lone-of- sight

altitude that differential VLBI observations with quasars are possible with similar conditions as the case of a geosynchronous satellite. Generally speaking, when the altitude of a satellite becomes the higher, the smaller becomes the relative angular velocity of the satellite with respect to quasars. As was already mentioned, the differential observations give a full advantage when the satellite and a quasar are observed under the same conditions of VLBI stations and propagation paths. Therefore, the DVLBI with quasars as reference radio sources would be the optimum for deep space orbits in the above mentioned sense, if there exists an appropriate quasar which is angularly near to the satellite.

In the case of low-altitude orbits, for example altitude of 1000 km \sim 2000 km, a satellite passes through the sky in several tens of minutes. A VLBI with rather short baselines which provide mutual visibilities can be applied to a satellite in such orbits. However, in low-altitude orbits the conventional range and Doppler measurements with much simpler facilities than those of a VLBI give a sufficient accuracy in the orbit determination.

The VLBI method would be also useful to calibrate an conventional tracking system. For example, in an ordinary tracking system for a geosynchronous satellite, the observation biases due to tracking equipment both in the satellite and in

the earth stations can be estimated using precise orbit ephemerides obtained by a DVLBI method. A DVLBI can take advantages that it is a receive-only method without any transmitting facility and can basically be applied to various satellites as long as they radiate signals within the frequency bands which can be observed by the VLBI system.

6.2 Differential Tracking Methods with Navigation Satellite System

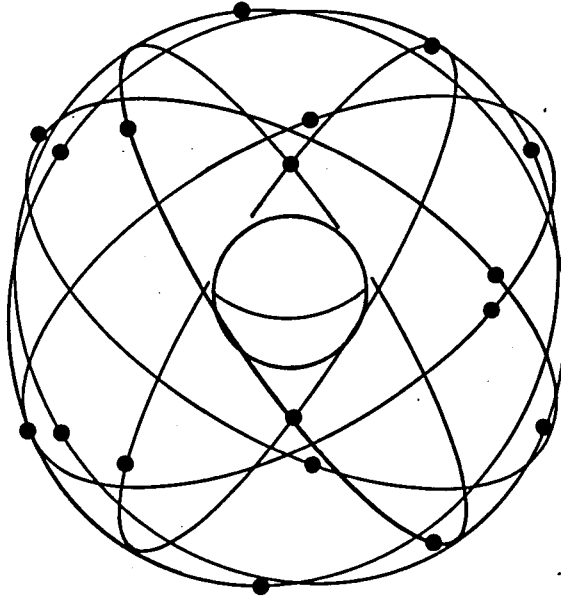
In our DVLBI experiments to track geosynchronous satellites, we used quasars as reference radio sources, because their angular positions are precisely known and because they radiate wideband noise which can be observed by VLBI. The radiation power of a quasar, however, is very weak (it is usually a few Jansky, 1 Jansky = 10^{-26} watt/m²Hz). Therefore, we need a large and effective antenna with low-noise receiver system and a highly stable frequency standard at each VLBI station to obtain sufficient signal-to-noise ratio (see Sec.3.2.1).

On the other hand, if there are spacecrafts transmitting radio signals from precisely known orbits we may also use them as reference radio sources. In this case a small antenna would be sufficient to receive satellite's strong signals and we do

not necessarily need a hydrogen maser frequency standard because a short integration time is sufficient to give a necessary signal-to-noise ratio.

The Global Positioning System (GPS)⁽⁴⁾ can be used for such purpose, because 18 navigation satellites are to be put on six different orbits (Fig.6.2) and several navigation satellites can be seen at any time from any point on the earth. Since the GPS satellites transmit navigation signals, we can use the satellites as reference radio sources in a differential tracking method similar to DVLBI. Fig.6.3 shows a concept of a differential GPS method applied to tracking of a high-altitude earth satellite⁽⁵⁾. Using a pair of GPS receivers, we can measure a differential range of each GPS satellite and of high-altitude satellite, where the latter satellite is assumed to have equipment to transmit the same signal as the GPS satellites. If the orbits of the GPS satellites are precisely known, we can calibrate the differential range measurements by them. Therefore, we can determine the high-altitude satellite orbit using the calibrated differential ranges with an accuracy equivalent to that of the GPS satellites.

Various types of GPS receivers have been developed especially in USA⁽⁶⁾. Many of them can derive the differential range (or differential phase) observables through a signal processing without decoding the modulated navigation information of GPS. That is, such receivers can derive



● GPS Satellite

Fig. 6.2 Navigation satellites of Global Positioning System (GPS) in fully operational phase

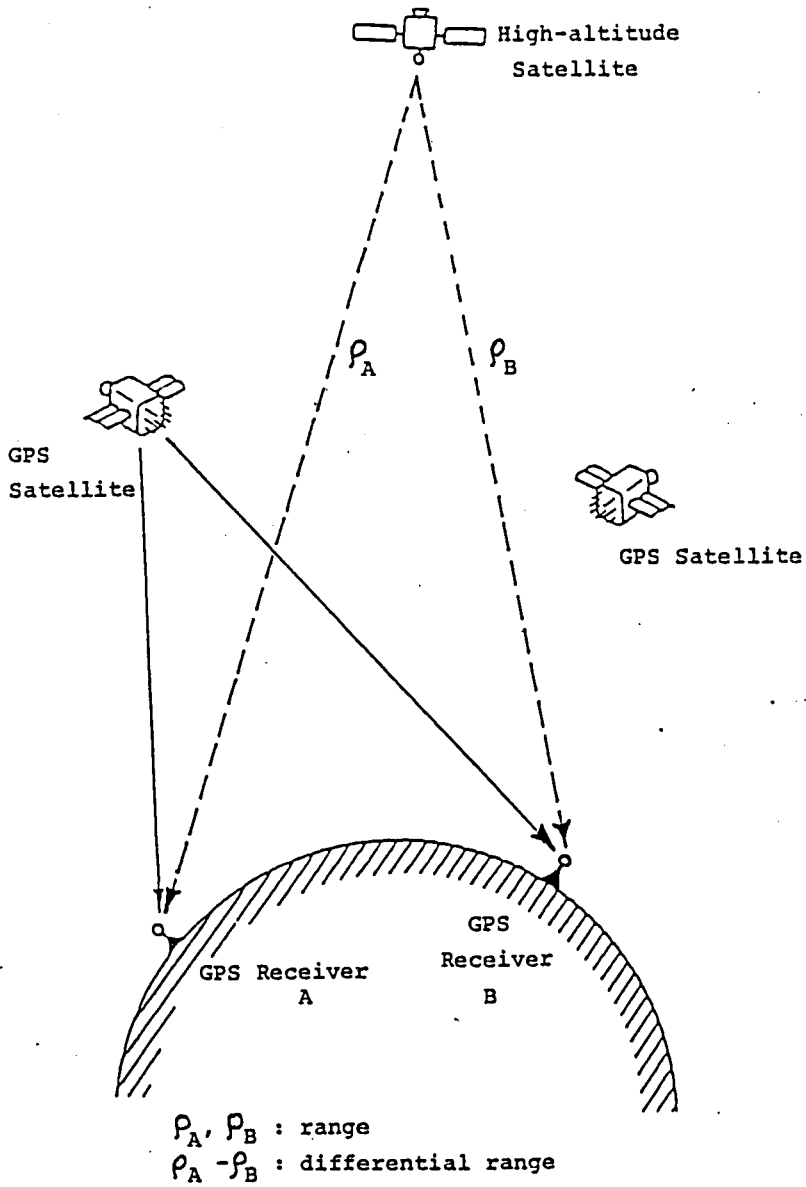


Fig. 6.3 Differential GPS tracking of a high-altitude earth satellite

observables independently to the navigation information being broadcasted from the GPS satellites. Some of them reproduce carrier tones and clock phase without decoding the navigation signals modulated by a pseudo-noise code (GPS uses a spread-spectrum modulation with PN-code).

Fig.6.4 shows a concept of differential tracking of a low-altitude earth satellite by the use of GPS. In this case, the low-altitude satellite has a GPS receiver and differential ranges with respect to a fixed GPS receiver on the earth were obtained. Using precisely known GPS satellites orbits and the receiver position on the ground, we can determine the low-altitude satellite orbit by the differential range observables. In other words, the low-altitude satellite orbit is determined with respect to GPS receivers on the ground. Though the receivers exist on the ground and on the satellite, the tracking geometry of Fig.6.4 is the same as that of DVLBI. The GPS satellites correspond to VLBI stations, and a GPS receiver on the ground corresponds to a reference radio source (quasar).

The accuracy of the GPS satellite orbit determination plays an important role in this tracking concept. For example, if we would like to determine the low-altitude satellite position with an accuracy of 10 cm, we need GPS satellite position with an accuracy of better than about 1 m⁽⁷⁾.

When a pair of GPS receivers are located on the ground, we

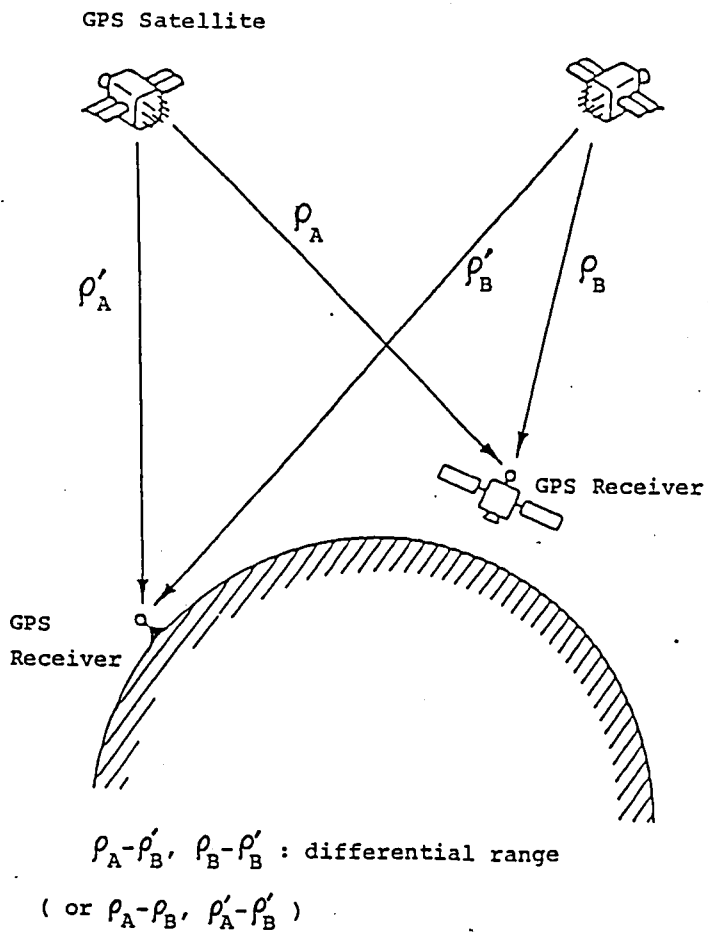


Fig. 6.4 Differential GPS tracking of a low-altitude earth satellite

can obtain relative positions of these receivers using differential measurements (Fig.6.5)⁽⁸⁾. This means that we can obtain the position of one of the GPS receivers if the other one's position is known. This differential measurement method is useful for geodesy, navigations and for other practical purposes. We can obtain a precise position data (for example, an accuracy of a few centimeters in the case of less than 100 km distance between the receivers) by using only small and handy GPS receivers with a short observation time.

The high accuracy (about 1m ~ 10m) of GPS satellite positions are also necessary in this system. In order to attain the required accuracy of the GPS satellites, we need many tracking stations globally distributed all over the earth at precisely known locations⁽⁷⁾. The differential observables obtained by GPS receivers can also be used to determine the orbit of the GPS satellites.

6.3 Radio Monitoring by Interferometric Methods

We can use an interferometric method such as a VLBI to monitor radio emissions from both the earth's surface and the space, because such method can passively receive various types of radio signals and gives information of the location of the radio sources. The radio monitoring techniques are necessary

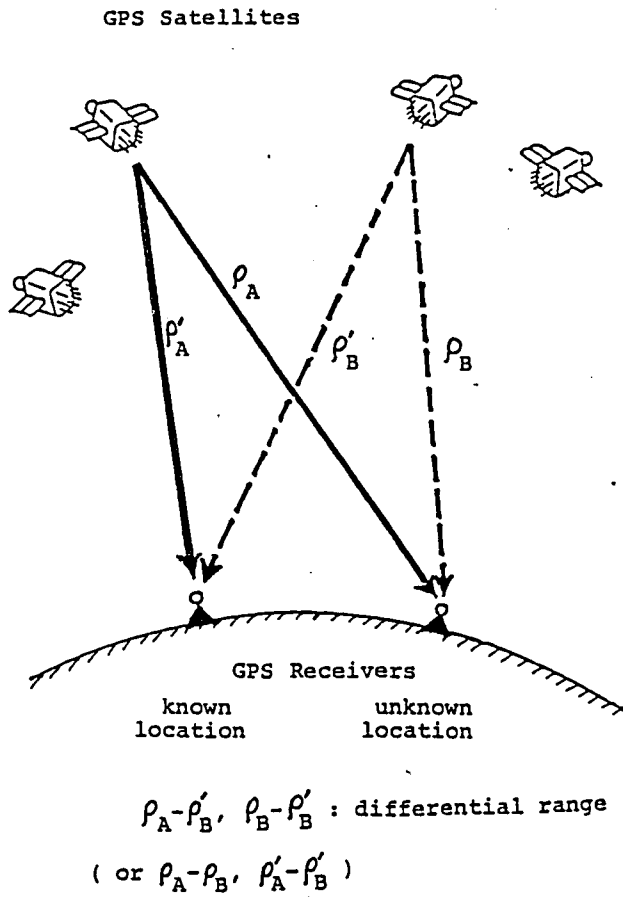


Fig. 6.5 Differential geodetic measurement by GPS

and useful not only for locating harmful interference radio sources in various radio communication systems, but also for detecting some kind of distress or emergency signals from mobile radio stations including airplanes, ships, cars, and so on. As quasars in our DVLBI observations, some reference radio sources would be also useful in such monitoring system for calibration of the system or for a differential estimation processing.

Fig.6.6 shows a concept of a radio monitoring system for space from the ground by DVLBI method. In order to cover wide range of orbits and frequency bands, the monitoring system should have too much capability to be practically implemented. Therefore, it would be necessary to select some important orbits and frequency bands. Fig.6.7 shows a concept of an interferometric radio monitoring system with satellites including space stations or geosynchronous space platforms. In this case, some reference radio sources on the ground would also be useful to locate interference or emergency signals from the surface of the earth or from low-altitude satellites.

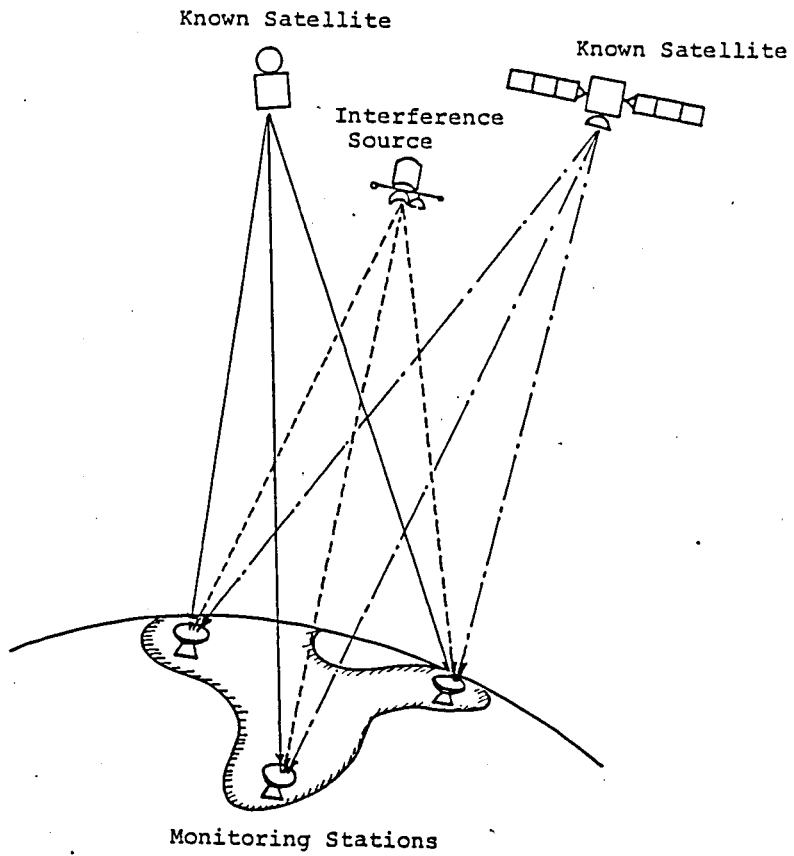


Fig. 6.6 Space radio monitoring system with DVLBI method

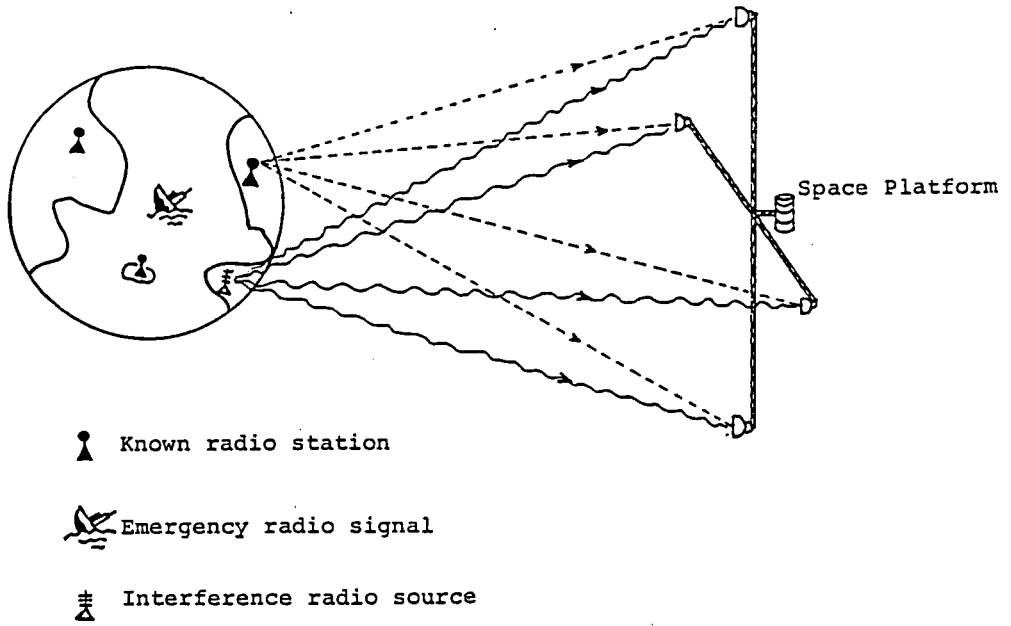


Fig. 6.7 Radio monitoring from space with interferometric method

References

- (1) Thomas, J.B., An error analysis for Galileo position measurements with the Block I Δ DOR system, JPL Engineering Memorandum, 335-26, 1981.
- (2) Poole, S.R., M. Ananda and C.E. Hildebrand, Radio interferometric measurements for accurate planetary orbiter navigation, AAS/AIAA Astrodynamics Specialist Conference, 1979.
- (3) Frauenholz, R.B. and J. Ellis, Determining highly elliptical earth orbits with VLBI and Δ VLBI, J. Astronaut. Sci., 32, 2, 1984.
- (4) Wooden, W.H., NAVSTAR Global Positioning System: 1985, First International Symposium on Precise Positioning with the Global Positioning System, Rockville, Maryland, 1985.
- (5) Wu, S.C., Orbit determination of high-altitude earth satellites: differential GPS approaches, First International Symposium on Precise Positioning with the Global Positioning System, Rockville, Maryland, 1985.
- (6) Goad, C.C., M.L. Sims and L.E. Young, A comparison of four precise Global Positioning System geodetic receivers, IEEE Trans. on Geosci. and Remote Sens., GE-23, 4, 1985.
- (7) Yunck, T.P. and S.C. Wu, Ultra-precise orbit determination by GPS, AAS/AIAA Astrodynamics Specialist Conference, 1983.
- (8) Yunck, T.P., A GPS measurement system for precise satellite

tracking and geodesy, Conference on Precision Electromagnetic Measurements, Delft, Netherlands, 1984.

CHAPTER 7 CONCLUSION

A new precise tracking method for a geosynchronous satellite was analyzed and proved through experiments. The method is a differential very-long-baseline interferometry (DVLBI) using quasars as reference radio sources. The analysis showed not only the observability and the sensitivity of the DVLBI observables in determination of a geosynchronous satellite orbit but also significant errors in the process of observations and in the models of satellite dynamics and observations. Computer programs for precise orbit determination and for pre-processing the observation data were newly developed.

In the first DVLBI experiment, a Japan's geosynchronous satellite CS was tracked. Since the baseline was short and the data quality of quasar observations were not sufficient, the obtained DVLBI delay observables were not actually useful to improve the orbit determination accuracy from that attained by conventional range and angle measurements. However, orbit determinations and covariance analysis using various error models showed the possible effectiveness of a DVLBI with a delay accuracy of better than 1 nsec, even with a short baseline in accurate orbit determination of geosynchronous satellites. A simulation shows that DVLBI with two baselines

1000 km long will furnish a prospective method of precise tracking of a geosynchronous satellite for an orbit determination with an accuracy of several tens of meters.

The next DVLBI experiment with much better observation geometry, that is, with inter-continental baselines was performed with collaboration of RRL and JPL aiming to determine a geosynchronous satellite orbit with a few meters position accuracy. The accuracy of the derived delay data was better than 1 nsec for the satellite, and was 1~10 nsec for the quasars. The differential VLBI observables were derived by subtracting systematic observation biases from the raw satellite VLBI observation data, where the systematic observation errors were obtained from the raw quasar VLBI data and the corresponding calculated values. In order to correct remaining systematic errors, which were caused by the propagation media, we used the ionosphere total electron content data and a tropospheric delay model for each station.

Orbit determinations with the DVLBI observables were performed by independent programs of RRL and JPL. A typical delay residuals were almost within 3 nsec (1 m) for all inter-continental baselines and obtained satellite positions at an epoch time agreed within a few meters. A covariance analysis shows that a formal error of the satellite position at the center of the 24-hour observation period is about 2.5 m. A more realistic evaluation of the accuracy was obtained by a

consider-covariance, where uncertainties in the satellite dynamic model and the observation model were considered. The consider-error of the satellite position is about 10 m and 4 m at the edges and the center of the observation period, respectively. It should be noted that the satellite position was determined with respect to the quasar frame without any biases by the DVLBI.

The attained accuracy of an orbit determination of a geosynchronous satellite is much better than that of conventional methods. A position estimation accuracy with an error of less than 1 m for a geosynchronous orbit can be attained if an optimization, especially in satellite signal transmitting system, is made. That is, if a satellite has a transmitting capability of signals with wider bandwidth in dual frequency bands, we can obtain much more precise observables which can be used to solve satellite dynamic parameters such as solar radiation pressure model more accurately, and consequently we can determine the satellite orbit with a better accuracy.

The differential VLBI technique is important not only for direct applications to precise tracking of spacecrafts in various orbits and to precise calibrations of conventional tracking systems, but also for indirect effect for development of various differential observation systems, for example, differential GPS systems for navigation and geodesy. The passive interferometry is also a prospective technique for

radio monitoring systems to detect harmful interference radio signals or distress (emergency) signals which are transmitted not only from the earth's surface but also from the space.

APPENDIX A Development of Precise Orbit Determination Program for DVLBI (DVODP)

A.1 Background

RRL had already developed a compact and precise orbit determination program (KODS) mainly for a geosynchronous satellite. It has an enough accuracy for orbital calculations for station and attitude keeping maneuvers of geosynchronous satellites and for antenna pointing controls both of the satellites and earth stations in ordinary space communication systems. However, we need a more accurate orbit determination program in an experiment (see Chap.5) where one of goals is to attain an accuracy of a few meters in satellite position determination by using a differential VLBI (DVLBI).

Therefore the author developed a new, highly precise orbit determination program for the DVLBI experiment (DVODP: DVLBI Orbit Determination Program) by revising KODS.

A.2 Main Features of DVODP

Fig.A.1 shows the computation flow in DVODP which has two modes of calculations. The OD mode is for orbit determination and the EG mode is for ephemeris generation, that is, predictions of satellite position, orbital elements, viewing angles, range and range rate, and so on. Table A.1 summarizes main features of DVODP. The improvements were made mainly in

three parts. First, the accuracy of orbit generation was improved. This is essentially done by using double-precision variables for calculation of perturbative accelerations which are treated with single-precision variables in KODS. Second, the functions in parameter estimation were improved. In DVODP we can estimate arbitrary combination of solve-for parameters up to 20. Finally, the function of covariance analysis were improved to include the effect of errors in model parameters (consider-parameters).

A.3 Validation and Utilization of DVODP

DVODP was validated by comparison with results calculated by JPL's highly accurate orbit determination program⁽²⁾. DVODP was effectively used in orbit determinations for DVLBI experiments on CS (see Chap.4) and on DSCS (see Chap.5).

References

- (1) Tanaka, T. and S. Kawase, A high-speed integration method for the satellite's ephemeris generation, J. Guidance and Control, 1, 3, 1978.
- (2) Moyer, T.D., Mathematical formulation of the Double-Precision Orbit Determination Program (DPODP), Technical Report 32-1527, JPL, 1971.

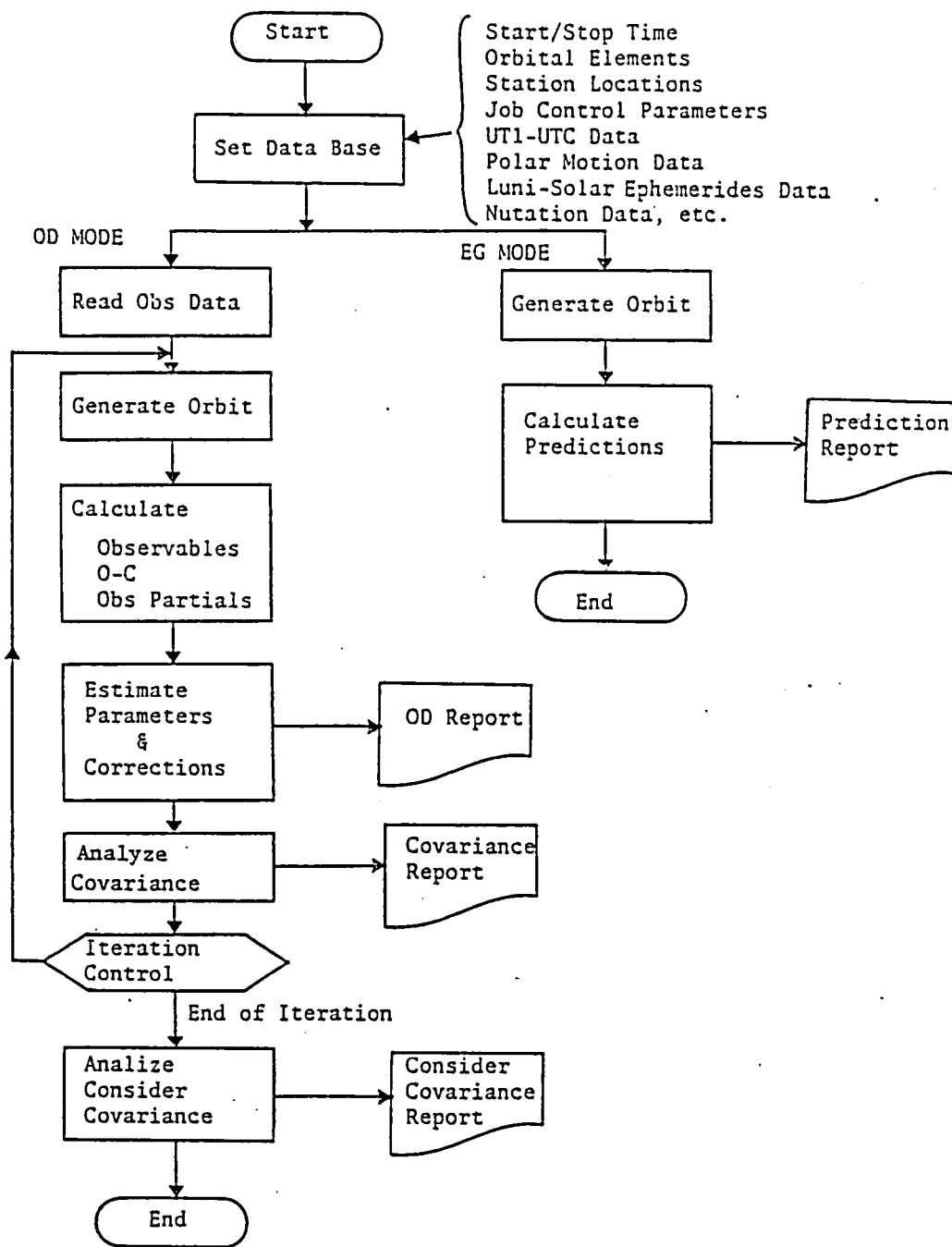


Fig. A.1 Computation flow in Delta-VLBI Orbit Determination Program (DVODP)

Table A.1 Main features of DVODP

Item	DVODP
Coordinate System	
Coordinate system for orbit generation	Epoch-true sidereal system
Time system for orbit generation	UTC
Input orbital elements	Keplerian elements or state vector
Conversion between true-of-date and body-fixed systems	With UTL and polar motion
Orbit Generation	
Integration method	Modified special perturbation method ⁽¹⁾
Perturbations	Earth's non-sphericity, Sun and moon's gravity Solar radiation pressure (calculated in double precision)
Accuracy of orbit generation Luni-solar ephemerides	Less than 1m in satellite position error Double precision
Orbit Determination	
Tracking station number	Less than 10
Number of observation data	Less than 300
Tracking data types	Range, Range rate, Azimuth and Elevation Angles, Summed range, Differential range and Differential range rate (with arbitrary baseline)
Estimated (solve-for) parameters	Orbital elements, Solar radiation reflection coefficient, Earth's gravitational constant, Observation biases (for range, Azimuth angle, Summed range, Differential range), Station locations (less than 3 stations)
	Arbitrary combinations of these solve-for parameters
Covariance Analysis	
Covariance of solve-for parameters	Covariance matrix
Covariance including the consider parameters' errors	Covariance matrix including consider covariance

APPENDIX B Reweighting the Observables

It is optimum to use a reweighting matrix W_R for a system which has errors in model parameters, because a reweighting matrix correctly evaluate the information of the observables degraded by the parameter errors. Using W_R given in Eq.(2.54), we can derive Eq.(2.57) as follows:

$$\begin{aligned} E \left\{ (\hat{\underline{x}} - \underline{x})(\hat{\underline{x}} - \underline{x})^T \right\} &= K_2 (BC_y B^T + W^{-1}) K_2^T \\ &= (A^T W_R A)^{-1} A^T W_R (BC_y B^T + W^{-1}) W_R A (A^T W_R A)^{-1} \end{aligned} \quad (B.1)$$

where

$$\begin{aligned} (A^T W_R A)^{-1} &= \left\{ A^T W A (J_x + S_1 C_y S_1^T)^{-1} A^T W A \right\}^{-1} \\ &= J_x^{-1} (J_x + S_1 C_y S_1^T) J_x^{-1} \\ &= J_x^{-1} + S C_y S^T \\ &= C_x + S C_y S^T = C_c \end{aligned} \quad (B.2)$$

and

$$\begin{aligned} A^T W_R &= A^T W A (J_x + S_1 C_y S_1^T)^{-1} A^T W \\ &= J_x (J_x + S_1 C_y S_1^T) J_x^{-1} A^T W \end{aligned}$$

$$\begin{aligned}
&= (C_x + SC_y S^T)^{-1} J_x^{-1} A^T W \\
&= C_c^{-1} J_x^{-1} A^T W \tag{B.3}
\end{aligned}$$

$$\begin{aligned}
W_R A &= WA (J_x + S_1 C_y S_1^T)^{-1} A^T WA \\
&= WA J_x^{-1} (C_x + SC_y S^T)^{-1} \\
&= WA J_x^{-1} C_c^{-1} \tag{B.4}
\end{aligned}$$

Substituting (B.2), (B.3) and (B.4) into (B.1) we obtain the desired result as

$$\begin{aligned}
E \left\{ (\hat{\underline{x}} - \underline{x})(\hat{\underline{x}} - \underline{x})^T \right\} &= C_c C_c^{-1} J_x^{-1} A^T W (BC_y B^T + W^{-1}) \\
&\quad \cdot WA J_x^{-1} C_c^{-1} C_c \\
&= J_x^{-1} (S_1 C_y S_1^T + J_x) J_x^{-1} \\
&= SC_y S^T + J_x^{-1} \\
&= C_x + SC_y S^T \\
&= C_c \tag{B.5} \text{ or } (2.57)
\end{aligned}$$

APPENDIX C Alternative Estimation of Large Dimensional
Parameters

There is an idea to alternatively estimate one of divided parts of a large dimensional parameters in order to avoid numerical instabilities. Here we show that the alternative method is equivalent to the other method where the whole parameters are simultaneously estimated from the viewpoint of the mutual information.

Let us start from the observation equation (2.33) (Sec.2.2.2).

$$\underline{z} = A \underline{x} + B \underline{y} + \underline{n} \quad (\text{C.1})$$

In this equation, we treat parameter vector \underline{x} and \underline{y} as two parts of parameters which are to be estimated. First, estimate \underline{x} with \underline{y} fixed. Then we obtain covariance matrix as (see Eq. (2.35))

$$C_{\underline{c}\underline{x}} = C_{\underline{x}} + S_{\underline{x}} C_{\underline{y}}' S_{\underline{x}}^T \quad (\text{C.2})$$

where

$$C_{\underline{x}} = (A^T W A)^{-1} = J_{\underline{x}}^{-1}$$

$$S_{\underline{x}} = J_{\underline{x}}^{-1} A^T W B$$

$C_{\underline{y}}'$: covariance matrix of errors in \underline{y}

and using \underline{y}^T instead of $(\hat{\underline{x}} - \underline{x})^T$ in Eq.(2.35) we obtain

$$E_{\underline{x}} \left\{ (\hat{\underline{x}} - \underline{x}) \underline{y}^T \right\} = E_{\underline{x}} \left\{ K_1 (B \underline{y} + \underline{n}) \underline{y}^T \right\} = S_{\underline{x}} C_{\underline{y}}' \quad (C.3)$$

Second, estimate \underline{y} with \underline{x} fixed. The covariance matrix with respect to \underline{y} is, similarly obtained as

$$C_{\underline{c}y} = C_{\underline{y}} + S_{\underline{y}} C_{\underline{x}}' S_{\underline{y}}^T \quad (C.4)$$

where

$$C_{\underline{y}} = (B^T W B)^{-1} = J_{\underline{y}}^{-1}$$

$$S_{\underline{y}} = J_{\underline{y}}^{-1} B^T W A$$

$C_{\underline{x}}'$: covariance matrix of errors in \underline{x}

and we also obtain

$$E_{\underline{x}} \left\{ (\hat{\underline{y}} - \underline{y}) \underline{x}^T \right\} = S_{\underline{y}} C_{\underline{x}}' \quad (C.5)$$

If the alternative estimation is repeated and converges, then Eqs.(C.2) and (C.4) should come to be

$$C_{\underline{c}x} = C_{\underline{x}} + S_{\underline{x}} C_{\underline{c}y} S_{\underline{x}}^T \quad (C.6)$$

$$C_{\underline{c}y} = C_{\underline{y}} + S_{\underline{y}} C_{\underline{c}x} S_{\underline{y}}^T \quad (C.7)$$

and Eqs.(C.3) and (C.5) should become

$$E_x \left\{ (\hat{\underline{x}} - \underline{x}) \underline{y}^T \right\} = E_x \left\{ (\hat{\underline{x}} - \underline{x}) (\hat{\underline{y}} - \underline{y})^T \right\} = S_x C_{cy} \quad (C.8)$$

$$E_x \left\{ (\hat{\underline{y}} - \underline{y}) \underline{x}^T \right\} = E_x \left\{ (\hat{\underline{y}} - \underline{y}) (\hat{\underline{x}} - \underline{x})^T \right\} = S_y C_{cx} \quad (C.9)$$

Eqs.(C.8) and (C.9) also lead the relation

$$S_x C_{cy} = C_{cx} S_y^T \quad (C.10)$$

Using Eqs.(C.6) ~ (C.9) we obtain the covariance matrix $C_{(xy)}$ of \underline{x} and \underline{y} after the convergence of the alternative estimation as

$$\begin{aligned} C_{(xy)} &= E_x \left\{ \begin{bmatrix} \hat{\underline{x}} - \underline{x} \\ \hat{\underline{y}} - \underline{y} \end{bmatrix} \begin{bmatrix} (\hat{\underline{x}} - \underline{x})^T & (\hat{\underline{y}} - \underline{y})^T \end{bmatrix} \right\} \\ &= \begin{bmatrix} C_{cx} & S_x C_{cy} \\ S_y C_{cx} & C_{cy} \end{bmatrix} = \begin{bmatrix} C_{cx} & C_{cx} S_y^T \\ C_{cy} S_x^T & C_{cy} \end{bmatrix} \end{aligned} \quad (C.11)$$

On the other hand, if we simultaneously estimate \underline{x} and \underline{y} , we obtain covariance matrix C_{xy} as

$$C_{xy} = \left[\begin{pmatrix} A^T \\ B^T \end{pmatrix} W (A \ B) \right]^{-1} = \begin{bmatrix} J_x & J_x S_x \\ J_x S_y & J_y \end{bmatrix}^{-1} \quad (C.12)$$

This is easily obtained by replacing A with $(A \ B)$ in, for example, Eq.(2.26).

From the viewpoint of information content, the determinant of a covariance matrix is important. The determinant of $C_{(xy)}$ is calculated as

$$\begin{aligned} |C_{(xy)}| &= \begin{vmatrix} C_{cx} & C_{cx} S_y^T \\ C_{cy} S_x^T & C_{cy} \end{vmatrix} = \begin{vmatrix} C_{cx} - C_{cx} S_y^T S_x^T & C_{cx} S_y^T \\ 0 & C_{cy} \end{vmatrix} \\ &= |C_{cx}| \cdot |I_n - S_y^T S_x^T| \cdot |C_{cy}| \end{aligned} \quad (C.13)$$

where I_n means the unit matrix with the same dimension as C_{cx} . We obtain the determinant in another way as

$$|C_{(xy)}| = \begin{vmatrix} C_{cx} & 0 \\ C_{cy} S_x^T & C_{cy} - C_{cy} S_x^T S_y^T \end{vmatrix}$$

$$= |C_{cx}| \cdot |I_m - S_x^T S_y^T| \cdot |C_{cy}| \quad (C.14)$$

where I_m means the unit matrix with the same dimension as C_{cy} . We can define a constant c according to the Eqs.(C.13) and (C.14) as

$$c = |I_n - S_y^T S_x^T| = |I_m - S_x^T S_y^T| \quad (C.15)$$

Using Eqs.(C.6) and (C.10) we obtain

$$C_{cx} = C_x + C_{cx} S_y^T S_x^T$$

then

$$C_{cx} = C_x (I_n - S_y^T S_x^T)^{-1} \quad (C.16)$$

Similarly, using Eqs.(C.7) and (C.10) we obtain

$$C_{cy} = C_y (I_m - S_x^T S_y^T)^{-1} \quad (C.17)$$

Substituting Eqs.(C.16) and (C.17) into Eq.(C.14) and using Eq.(C.15), Eq.(C.14) becomes

$$|C_{(xy)}| = |C_x| \cdot |C_y| \cdot c^{-1} = (|J_x| \cdot |J_y| \cdot c)^{-1} \quad (C.18)$$

Next, the determinant of C_{xy} is calculated as

$$\begin{aligned}
|C_{xy}| &= \begin{vmatrix} J_x & J_x S_x \\ J_y S_y & J_y \end{vmatrix}^{-1} = \begin{vmatrix} J_x - J_x S_x S_y & J_x S_x \\ 0 & J_y \end{vmatrix}^{-1} \\
&= (|J_x| \cdot |J_y| \cdot |I_n - S_x S_y|)^{-1} \\
&= (|J_x| \cdot |J_y| \cdot c)^{-1} \tag{C.19}
\end{aligned}$$

where the relation $|I_n - S_y^T S_x^T| = |(I_n - S_x S_y)^T| = |I_n - S_x S_y|$ is used.

Eqs.(C.18) and (C.19) show that the determinants of $C_{(xy)}$ and C_{xy} are the same, that is, the mutual information is the same in both methods of alternative and simultaneous estimation of large dimensional parameters.

It should be noticed, however, that the above derivations were based on an assumption that the alternative estimation method successfully gives converged estimates.

APPENDIX D Sensitivity of DVLBI Delay Observable to

Keplerian Orbital Elements of a Geosynchronous Satellite

Typical DVLBI delay observables (w,v) shown in Fig.3.9 are related with the satellite position coordinates (X,Y,Z) by Eq.(3.59), where they are expressed in small deviation form. The satellite position in the orbital plane is expressed in the (x,y) coordinates (Eq.(3.62)) and they are converted into the inertial coordinate system by the conversion matrix G (Eqs.(3.60) and (3.61)) which contains three orbital elements to determine the orientations of the orbital plane and the apsides.

By differentiating the related equation, though the process is tedious, we obtain the expression (3.65) as follows:

Differentiating Eq.(3.60), we obtain

$$\begin{bmatrix} \Delta X \\ \Delta Y \\ \Delta Z \end{bmatrix} = \Delta G \begin{bmatrix} x \\ y \\ 0 \end{bmatrix} + G \begin{bmatrix} \Delta x \\ \Delta y \\ 0 \end{bmatrix} \quad (D.1)$$

where the first term is calculated using Eq.(3.61) as

$$\Delta G \begin{bmatrix} x \\ y \\ z \end{bmatrix} = \begin{bmatrix} -x \sin(\omega + \Omega) - y \cos(\omega + \Omega) \\ x \cos(\omega + \Omega) - y \sin(\omega + \Omega) \\ i (x \cos \omega - y \sin \omega) \end{bmatrix}$$

$$\begin{pmatrix} -x \sin(\omega + \Omega) - y \cos(\omega + \Omega) \\ x \cos(\omega + \Omega) - y \sin(\omega + \Omega) \\ 0 \end{pmatrix} + i \begin{pmatrix} x \sin \omega \sin \Omega + y \cos \omega \sin \Omega \\ -x \sin \omega \cos \Omega - y \cos \omega \cos \Omega \\ x \sin \omega + y \cos \omega \end{pmatrix} \begin{pmatrix} \Delta \omega \\ \Delta \Omega \\ \Delta i \end{pmatrix}$$

(D.2)

and $(\Delta x, \Delta y)$ in the second term are calculated using Eqs.(3.62) ~ (3.64) as

$$\left. \begin{aligned} \Delta x &= \Delta a \cos E - a \sin E \cdot \Delta E - a \cdot \Delta e \\ \Delta y &= \Delta a \sin E - a \cdot e \sin E + a \cos E \cdot \Delta E \end{aligned} \right\} \quad (D.3)$$

where

$$\Delta E = \Delta e \sin E + \Delta M_0 - \frac{3}{2a} nt \quad (D.4)$$

and we used a condition $e \ll 1$ which generally holds for a geosynchronous satellite. In Eq.(D.4), n is the mean motion and M_0 is the mean anomaly at the epoch time ($t=0$), that is,

$$M = nt + M_0 \quad (D.5)$$

Using Eqs.(D.3) and (D.4) we obtain

$$\begin{bmatrix} \Delta x \\ \Delta y \end{bmatrix} = \begin{bmatrix} \cos M + \frac{3}{2}nt \sin M & -(1+\sin^2 M) & -\sin M \\ \sin M - \frac{3}{2}nt \cos M & -\sin M (e - \cos M) & \cos M \end{bmatrix} \begin{bmatrix} \Delta a \\ a \Delta e \\ a \Delta M_0 \end{bmatrix} \quad (D.6)$$

Substituting Eqs. (D.2) and (D.6) into (D.1) we obtain the desired expression (3.65).

APPENDIX E Nondynamic Analysis of the Position Estimation
Accuracy of a Geosynchronous Satellite

In order to grasp a general idea on the accuracy of satellite's position estimation by DVLBI delay observations, we can use a simple, nondynamic model of the DVLBI observation geometry. That is, in the observation window, we neglect the satellite's position deviations from the geosynchronous position due to the orbital inclination, to the eccentricity and to various perturbations, as long as we aim roughly to obtain a general concept of the determination accuracy of the satellite angular position in the observation window (or in the (v,w) -plane in Fig.5.5). In actual observations, quasar observations were carried out every 30 minutes over 23 and a half hours, so the total of 47 points of quasar observations were performed (see 5.3.3). However, we take a simple model of eight quasars which enter into the observation window. Fig.E.1 shows the quasar positions in the observation window for this sampled observation model. Using these quasars we obtain DVLBI delay observables with three baselines spanned by Kashima, Canberra and Goldstone stations. Strictly speaking, simultaneously obtained VLBI observables by these three baselines are redundant, but we assume to obtain independent observables by processing the observation signals received at

different time for each baselines.

The linearized observation equation is given by Eq.(3.58) where the station location error is given by Eq.(3.78). Based on the observation equation we can evaluate the estimation error including the effect of model parameter errors using Eq.(2.35)⁽¹⁾. The results are shown in Fig.E.2, where error ellipses of the satellite position estimation in the (v,w)-plane, are depicted for several models for model parameter errors. Table E.1 summarizes the models of observation errors and model parameter errors. We used a very simple model of the observation error σ_{DVLBI} consisting of two components; one corresponds to the system noise error (σ_{SNR} : SNR error) and the other constant one (σ_{const}) corresponds to propagation media errors, clock errors, and so on. That is,

$$\sigma_{DVLBI}^2 = \sigma_{SNR}^2 + \sigma_{const}^2 \quad (E.1)$$

As is expected from the baseline geometry and the observation accuracy, the error ellipsoids tend to be elongated in the direction perpendicular to the Goldstone-Canberra baseline. In other words, the satellite position can be determined the most accurately in the direction of that baseline.

Fig.E.2 shows results of accuracy evaluation for station location estimation for Kashima by the use of the same

observations given in Fig.E.1. In this case the satellite position uncertainty is considered as one of model parameter errors (a model of satellite position uncertainty is included in Table E.1). According to the observation equation Eq.(3.58), the sensitivity vector of the DVLBI delay observable to a position change, $\Delta \underline{x}_i$ of the VLBI station i is given by $(\underline{S} - \underline{p}_{iu})$. In a usual DVLBI observation geometry, however, this sensitivity vector is small and nearly perpendicular to the line-of-sight. In other words, the DVLBI delay observables have only a little information of station position components in the plane perpendicular to the line-of-sight, and have little information of the component in the direction of the line-of-sight. Therefore, it is not necessarily effective to estimate station locations using DVLBI delay observations. In Fig.E.2, case (d) shows some degradation of the accuracy due to removal of quasars which have a little larger sensitivity vectors than those of other quasars. That is, in the case (d), quasars 5 and 8 in Fig.E.1 are removed and two quasars which are at the same point as 1 are included (without change in the total quasar number). Therefore, the error ellipse (d) becomes a little larger than (b).

Reference

(1) Shiomi, T., Analysis on Δ VLBI navigation on a geosynchronous spacecraft, JPL Engineering Memorandum 314-314, July 1983.

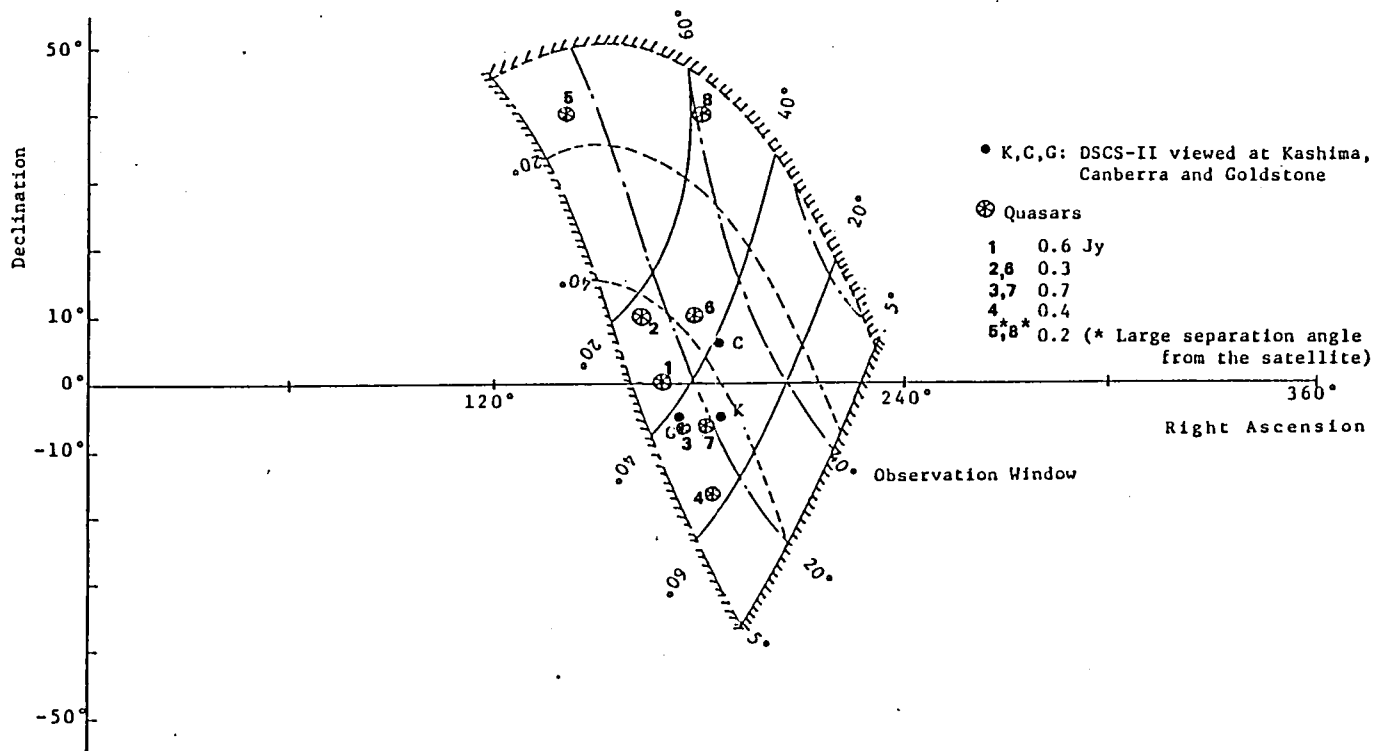


Fig. E.1 A model of quasars set in the observation window

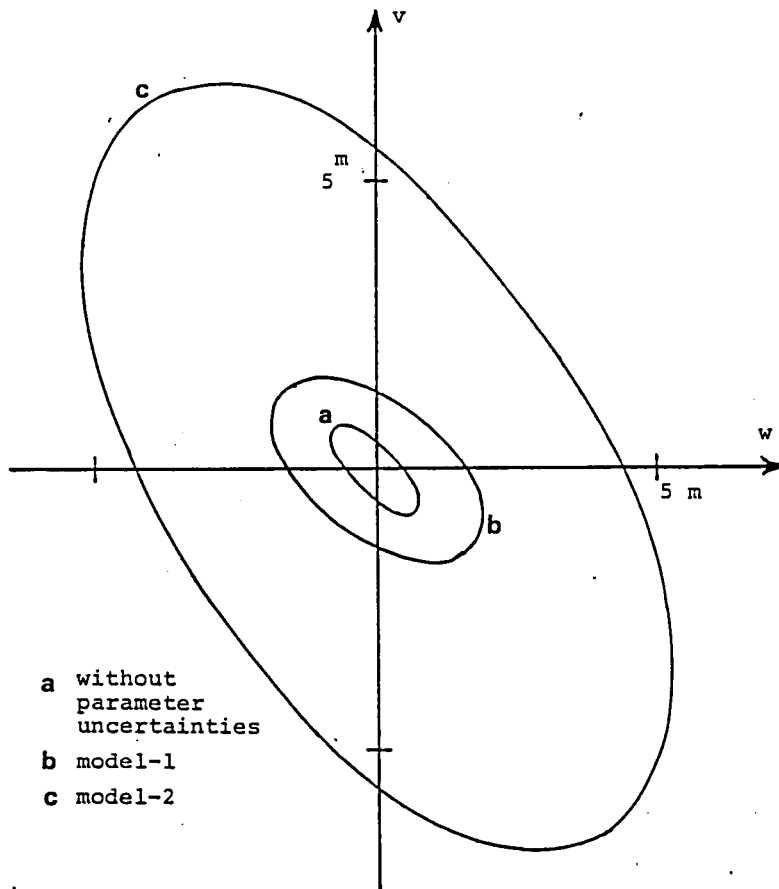


Fig. E.2 Error ellipses of satellite position estimation

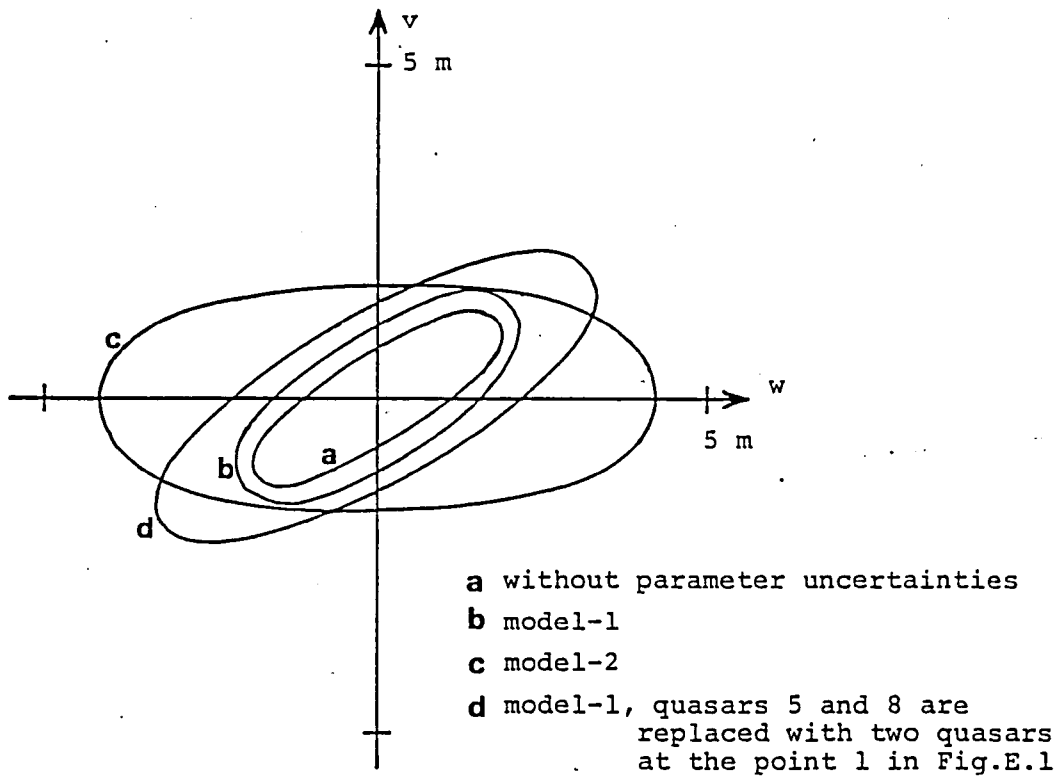


Fig. E.3 Error ellipses of station location estimation for Kashima